DESIGN, DEVELOPMENT, AND CONTROL OF A ROBOTIC GRIPPER FOR ACTIVITIES OF DAILY LIVING (ADL) ASSISTANCE.

by

Jaime Hernandez

A Thesis Submitted in

Partial Fulfillment of the

Requirements for the Degree of

Master of Science

in Engineering

at

The University of Wisconsin-Milwaukee

December 2022

ABSTRACT

DESIGN, DEVELOPMENT, AND CONTROL OF A ROBOTIC GRIPPER FOR ACTIVITIES OF DAILY LIVING (ADL) ASSISTANCE.
by

Jaime Hernandez

The University of Wisconsin-Milwaukee, 2022
Under the Supervision of Professor Mohammad Habibur Rahman

This research contributes to developing a robotic gripper designed to improve the object-handling capabilities of assistive robots manipulators. As developed in this research, the gripper for assistive robots (GAR) can be an alternative solution to the existing robotic grippers increasing the benefits in different ways, including the cost/benefits ratio and the range of graspable objects.

The GAR has been designed with simplicity in mind with a minimum viability approach. The design, construction, control, and operation of this robotic gripper have been simplified with a minimal number of custom-made components, resulting in better performance. In addition, GAR's rigidity allows it to hold objects weighing up to 5 kilograms without deforming or compromising its internal mechanism.

Various experiments mimicking real-world application scenarios have been performed to measure in quantitative and qualitative ways the performance of GAR to evaluate the proposed design.

Keywords: Gripper, Robotic hand, Assistive Robot, Rigid links, Design.

TABLE OF CONTENTS

LIST OF FIGURES

LIST OF TABLES

ACKNOWLEDGMENTS

First, I want to thank my mother for the strength, patience, and bravery she instilled in me. Second, I want to thank my fiancé for her support and patience over the years and for encouraging me to complete my education. After that, Dr. Mohammad Rahman for his help and advice during this project. The impact of his counsel and direction on the quality of the work accomplished for this thesis is incalculable.

AGRADECIMIENTOS

En primer lugar, quiero agradecer a mi madre por la fuerza, paciencia y valentía que me inculcó. En segundo lugar, quiero agradecer a mi prometida por su apoyo y paciencia a lo largo de los años y por animarme a completar mi educación. Después de eso, al Dr. Mohammad Rahman por su ayuda y asesoramiento durante este proyecto. El impacto de su consejo y dirección en la calidad del trabajo realizado para esta tesis es incalculable.

CHAPTER 1

INTRODUCTION

1.1 Statement of the Problem:

The human hand is an essential extension available to perform the activities of our daily lives. The human hand's capability to perform complex motion and tasks with high precision and control enable humans to perform most of the functions necessary for living. The human hand has approximately 38 muscles comprising its intricate musculoskeletal system, which controls its movement [1]. With this system, the hand can grab objects in particular ways, such as: cylindrical, tip, hook, palmar, spherical, and lateral grips [2]. Unfortunately, many live with full or partial loss or impairment of their arms, hands, or general mobility [135]. Movement impairments can range from minor deficiencies in motor control of the body to complete mobility loss. Various geriatric disorders, stroke, and trauma are the primary reason behind such impairments [7]. Apart from stroke, trauma from sports injuries, workplace accidents, and other orthopedic injuries result in the loss of mobility of the upper limb [8]. In the US, there are 61 million persons who live with a disability, of whom 3.6% have trouble getting dressed or bathing and 13.7% have mobility issues [147]. Over 6.8 million Americans use mobility devices to aid in their mobility; 1.7 million of these people use wheelchairs, and over one-third of those using mobility aids require assistance from another person for one or more ADLs[148]. The number of people who use wheelchairs has expanded [149] and is continuing growing at an average yearly rate of 5.9%. Users using wheelchairs report significant limitations in both instrumental and basic ADLs (BADLs) [150]. The inability to

do necessary ADLs may result in dangerous situations and a low quality of life. ULED sufferers must be capable of doing things on their own without major assistance from others.

1.1.1 Current Solutions

For this reason, focusing on dependent people with highly reduced mobility, an attempt has been made to help them through robotics with well-known assistive robots [9]. In order to perform activities of daily living, robots need to generate human-like movements, including the ability to grasp and carry objects with different shapes and weights from one side to another [9]. Inspired by the human hand, multiple mechanisms have been developed (Table 5) like the Kinova gripper GEN3 [139], that try to recreate, simulate, or enhance the abovementioned capabilities [136]. Those kinds of mechanisms are called Grippers or Manipulators [3] which will be discussed in the chapter reviewing the state of the art. The ability to grip and manipulate objects has been central to the advancement of robots. Manufacturers can use end-effector tooling for picking, placing, and packing objects using advances in gripper technology to reap the benefits of precision, performance, and productivity [4]. Different types of grippers are also classified depending on their design, power supply, and application [5], as explained later. Some of these grippers have been specially developed for activities of daily living, increasing their performance in tasks such as feeding, changing shoes, and taking objects from a shelf [10, 137, 138].

1.1.2 Limitations

However, a single type gripper cannot perform all the tasks of daily life. For example, some grippers perform better in holding square objects (like Kinova Gen3 lite gripper [140]) than spherical objects, and others can handle only light weights [3] like the gripper presented on

[141]. Thus, some recent research focuses [10, 137, 138, 142, 143, 144, 145, 146] on increase the number of tasks (Table 2) a gripper can perform (Like Picking/ Placing objects from Table or Opening & closing drawers), the number of differently shaped objects it can grasp (Table 5), and the maximum weight it can hold [11]. However, grippers are insufficient for active tasks like opening doors and refrigerators or working close to the users' faces [29]. In addition, reasonably performing grippers are highly intricate and bulky, making them difficult to manufacture, assemble, and repeat laboratory test findings; for example, the gripper found in [30]. Furthermore, their expenses make them unavailable to most individuals who need them the most [31].

1.1.3 Proposed solution:

The research under this project contributes to developing a robotic gripper for activities of daily living assistance. In order to contribute to this field, this research focuses on developing a three-finger, simple robotic gripper with a minimally feasible design that can grasp various objects of different shapes and weights. Furthermore, the gripper for assistive robots (GAR) is designed to increase the general performance of assistive robotic arms and provide users with a better experience when using them.

The GAR is comprised of three fingers. Each finger has two degrees of freedom. One of these degrees of freedom is active, and the other is passive. It is also designed to be mounted in any assistive robotic arm with a standard protocol. This thesis focuses mainly on the GAR's mechanical design, development, and control. However, the kinematic and dynamic model of the GAR is also included and developed based on a quasi-static analysis, especially proposed for underactuated systems. During the modeling, gripper parameters, such as

mechanism link lengths, masses of different link segments, and inertia, were estimated according to the CAD model made during the design stage. This research concentrated only on the mechanical design, been the mechatronic design, instrumentation, and control algorithm a secondary part of this research.

Therefore, as a first step, a state-of-the-art review was performed to understand better the advantages and disadvantages of most of the recent robotic grippers. As the second step, to compare the existing robotic grippers for assistive robots with the proposed research, a search of current commercial grippers was conducted, classifying their characteristics and evaluating their performance.

We conducted our study on the most recent developments and studies done in the academy regarding grippers. We analyzed the mechanisms, pros, and cons of the existing grippers to identify the best possible mechanisms, actuation, and control. Finally, proceed to design and mathematically analyze the selected mechanism before creating a prototype and evaluating its functionality. The proposed GAR is designed to handle essential activities of daily living (ADL) as criteria. Objects of various sizes and shapes are parameterized, and this information is used to design and select the optimal components that meet the proposed requirements.

After preparing the theoretical bases, the modeling, construction, and assembly of the gripper proposed in this thesis were carried out, and finally, according to the activities of the daily living list, the GAR was evaluated, first through simulation using 3D models, and then, through a series of experiments on expected environments.

1.2 Specific Aim:

The specific aim of this research project is to develop a simplistic and minimum viable robotic gripper to handle essential ADL objects.

1.3 Contribution:

A study is conducted on the most recent developments and studies done in the academy regarding grippers. Then, the mechanisms, pros, and cons of the existing grippers on the market are analyzed. Next, the possible best mechanisms, actuation, and control types are cataloged based on these two investigations. Finally, proceed to design and mathematically analyze the selected mechanism before creating a prototype and evaluating its functionality.

To make the suggested GAR concept more feasible and replicable, GAR is designed based on activities of daily living as criteria. In that order, objects of various sizes and shapes are parameterized, and this information is used to design and select the optimal components that meet the proposed requirements.

This thesis is organized into chapters as described below:

CHAPTER 2: BACKGROUND AND THEORETICAL FRAMEWORK

This chapter overviews how the human hand works, how humans grab objects, and how current grippers do those tasks.

CHAPTER 3: LITERATURE REVIEW

This chapter provides a comprehensive overview of the research undertaken on robotic grippers, covering earlier advances in assistive robot-based grippers.

CHAPTER 4 DESIGN OF THE GRIPPER

This chapter addresses the first design processes for the proposed robotic gripper based on simplicity and adaptability. Along with the gripper's specs, design details, and physical limitations, the gripper's design restrictions and innovations are described.

CHAPTER 5: KINEMATICS AND DYNAMIC MODELING

This chapter shows how kinematic and dynamic models of the proposed robotic gripper were developed. Kinematic modeling employs quasi-static modeling, especially for underactuated systems.

CHAPTER 6: EXPERIMENTS AND RESULTS

This chapter discusses the experimental setup and process used to assess the performance of the Robotic Gripper, as well as its mode of operation and control approach. This chapter also contains a graphical depiction of the test results and thorough explanations, as well as particular remarks on how each set of tests evaluates the performance of the gripper base on ADLs.

CHAPTER 7: CONCLUSIONS AND FUTURE WORK

In this chapter, a summary of the study's findings is offered, along with a discussion of prospective future research areas. Finally, the future horizons section shows the possibilities of this specific study when it is developed further.

CHAPTER 2:

BACKGROUND AND THEORETICAL FRAMEWORK

2.1 How Do Humans Grab Objects?

In order to design and construct a gripper that can manipulate objects in a manner comparable to the human hand, it is crucial first to comprehend how people interact with, hold, and move objects during everyday tasks.

For this, a study by the Max Planck Institute for Intelligent Systems trained computers to understand, model, and synthesize human grasping [12]. The study includes in its analysis complex 3D object shapes, detailed contact information, hand pose and shape, and 3D body motion. Similar analyses were conducted in [13] and [14], where grips are classified according to the object's nature, form, and weight. The categorization is proposed as follows: The suggested taxonomy has three categories at the highest level: power, intermediate, and precision grasp. In addition, circular and prismatic varieties of power and precision grasp exist. Finally, additional classes are discussed in more depth, bringing the total to 15 (Table 1)

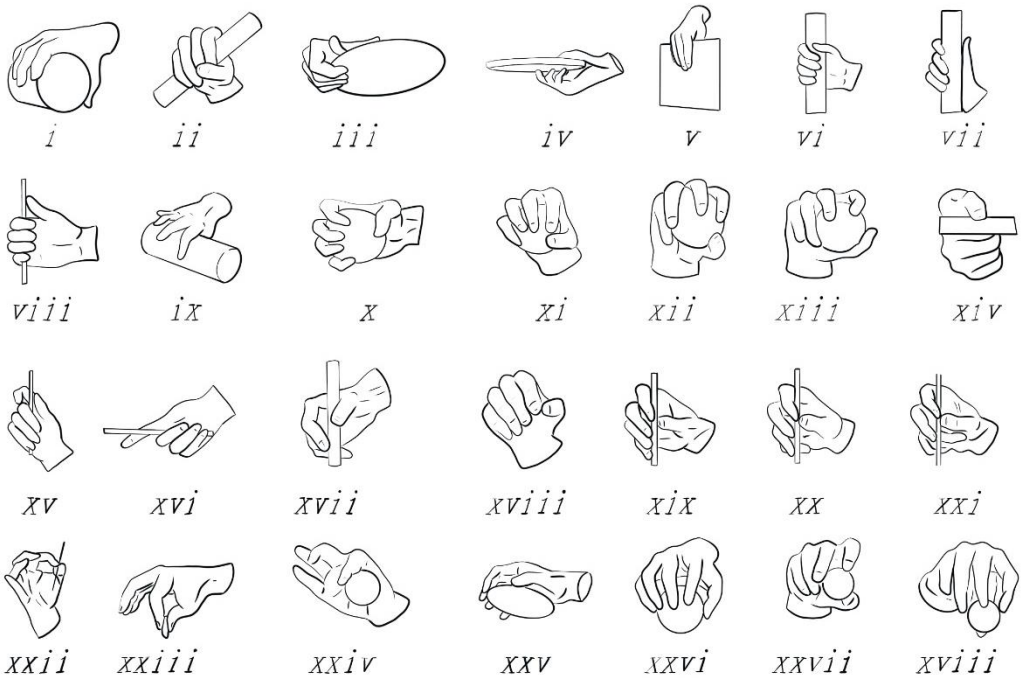

Figure 1 Grips modes classification.

Table 1 How humans grab objects

Grabs Type	Shape	Wrap Type	Geometrical Condition	Description
Power	Prismatic	Heavy Wrap	I. Large Diameter	Cylindrical or prismatic-shaped objects with a diameter greater than 50 mm. 5-finger grip. Orient the object horizontally.
			II. Small Diameter	Cylindrical or prismatic-shaped objects with a diameter of less than 50 mm. 5-finger grip. Orient the object horizontally
		Palmar Wrap	III. Palmar	Disc-shaped objects with a thickness-to-diameter ratio are more than 1/20. The 4-finger grip is on one side of the disc. Object orientation: Z axis facing down.
			IV. Extension Type	Disc-shaped objects with a thickness-to-diameter ratio are more than 1/20. 4-finger grip under one side of the Disk. Horizontal object orientation.

			V. Parallel Extension	Objects shaped like a disk or prism, with a thickness-diameter ratio greater than 1/20. 5-finger grip, pressure on both sides of the disc. The orientation of the object parallels the fingers downwards.
		Medium and Light Wrap	VI. Medium wrap	Cylindrical or prismatic object with a diameter less than 50 mm and greater than 100 mm. 4-finger grip and thumb on the same surface. Portrait object orientation
			VII. Adducted thumb	Cylindrical or prismatic object with a diameter of less than 50 mm and greater than 100 mm. 5-finger grip. Thumb in a vertical orientation, pointing up. Portrait object orientation.
			VIII. Light tool	Cylindrical or prismatic object with a diameter between 10 and 15 mm. 5-finger grip. Thumb in a vertical orientation, pointing up. Portrait object orientation.
			IX. Ring	Cylindrical or prismatic object with a Diameter between 30 mm and 70 mm. The grip of 2 fingers, index, and thumb, in the form of a ring around the object. Horizontal object orientation.
	Circular	Disk	X. Disk	Disc-shaped object with an approximate radius-diameter ratio of 1/8. Diameter between 90 and 120 mm. 5-finger grip with the palm on one of the flat surfaces of the object. Horizontal object orientation, downwards.
		Sphere	XI. 5 Fingers sphere grab	Sphere-shaped object with an approximate diameter of 60mm. 5-finger grip.
			XII. 4 Fingers sphere grab	Sphere-shaped object with an approximate diameter of 60mm. Four finger grip.
			XIII. 3 Fingers sphere grab	Sphere-shaped object with an approximate diameter of 60mm. 3-finger grip.
Intermediate	-	Lateral	XIV. Pinch	A Flat, rectangular prism-shaped object. Grip with two fingers, index and thumb, squeezing both flat faces

				of the object—orientation of the object: parallel to the thumb.
		stick	XV. Stick	A cylinder-shaped object of small diameter. 4-5 Finger Grip, Object Orientation Parallel to Thumb, Vertical.
			XVI. Ventral	A cylinder-shaped object of small diameter. 4-finger grip, object orientation parallel to the thumb, horizontal orientation.
		Writing	XVII. Writing Tripod	A cylinder-shaped object of small diameter. 3-finger grip with an object resting on the palm, Portrait Orientation.
			XVIII. Lateral Tripod	A cylinder-shaped object of small diameter. 3-finger grip with the object resting on the palm, Object orientation: horizontal.
Presicion	Prismatic	4-fingers	XIX. Thumb-4 fingers	Cylindrical or prismatic-shaped object with a small diameter; 4-finger grip along the object's surface and the thumb on top of the surface. Portrait object orientation.
		3-fingers	XX. Thumb-3 fingers	A cylindrical or prismatic-shaped object of small diameter; 3-finger grip and thumb on top of the surface. Portrait object orientation.
		2-fingers	XXI. Thumb-2 fingers	Cylindrical or prismatic-shaped object with a small diameter; 2-finger grip along the object's surface and the thumb. Portrait object orientation.
		1-finger	XXII. Tip Pinch	A cylindrical or prismatic-shaped object, such as a needle. The grip of 2 fingers, index, and thumb, in the form of a ring holding the object. Orientation of the object perpendicular to the thumb.
			XXIII. Thumb-1 finger	A flat, rectangular, cylindrical, or prismatic object. The grip of 2 fingers, index, and thumb, in the form of clamps holding the object. Orientation of the object parallel to the thumb.
			XXIV. Inferior pincer	Prismatic object. The grip of 2 fingers, index, and thumb, in the form of clamps holding the object around its

				surface. Orientation of the object parallel to the thumb and index finger.
	Circular	Disk	XXV. Precision disk	Disc-shaped object with an approximate radius-diameter ratio of 1/8. Diameter between 70 and 100 mm. 5-finger grip with the palm on one of the flat surfaces of the object. Object orientation is horizontal and downward.
		Sphere	XXVI. Precision sphere	Object in the form of a sphere with an approximate diameter of 60mm. Grip with the tips of the five fingers. Object orientation is vertical, downwards.
			XXVII. Quadpod	Sphere-shaped object with an approximate diameter of 30mm. Grip with the tips of the three fingers and the thumb. Object orientation is vertical, downwards.
		Tripod	XXVIII. Tripod	Sphere-shaped object with an approximate diameter of 30mm. Grip with the tip of 2 fingers and the thumb. Vertical object orientation, downwards.

Based on the Grips modes classification, gripping modes are also categorized according to the shape of the object to be held, bringing them all into three large categories [15]. Those three large categories are Parallel or flat gripping mode, cylindrical gripping mode, and spherical gripping mode [16]. Other categories are derived from these three, such as Tip mode, Hooke mode, and Lateral mode, which are presented as specific cases of the main categories. For example, Lateral mode is a particular case of parallel mode, where the object's thickness is hundreds of times less than its perpendicular area.

The following image (Figure 2) shows the three main grip types:

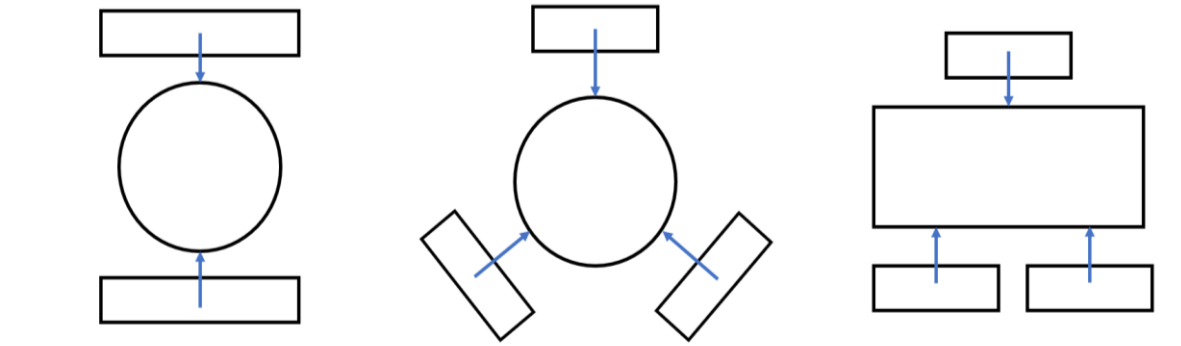

z

Figure 2 Robotic grip types

2.2 Robotic Grippers

Grippers are one of the most often utilized end-effector equipment for robots. Depending on the application, numerous kinds of robotic system grippers are required. Therefore, picking the appropriate one is a crucial component of the design process [17]. In addition, there are a variety of meanings for manipulating and grasping, depending on the context and intended use. In general, mechanical manipulation applies force or torque to an item to cause motion or deformation, while grasping is holding an object [18].

Multiple materials are used to construct grippers. Recent gripper research has focused on soft materials, microelectromechanical systems, and synthetic sheets. In addition, modern materials, such as piezoelectric, shape-memory alloys, intelligent fluids, carbon fiber, and many others, are being used to increase the functioning of grippers [19].

2.2.1 Types of Robotic Grippers

Multiple criteria may be used to classify robotics grippers. For instance, they may be classified according to their uses, actuation, mechanism type, and material. To begin with, a first categorization based on applications is made, and then other classifications are delved into to delimit all the characteristics used for the proposed design. [19]

- **Grippers for Industry:** Initially, grippers were designed for factory usage. They are grippers used in mass production coupled to a stationary platform. Regarding industrial grippers, several conditions may be investigated, such as the geometrical condition of grabbing, position and orientation of gripping, static equilibrium of grasped objects, and dynamic conditions [20].

- **Grippers for Known Environments:** Most grippers used in controlled environments are used for manipulating prefabricated parts. When the parts are in their specified orientations, it is simpler for grippers to hold the object. These grippers may employ servos, non-contact sensors, contact sensors, or a combination of the three to receive input. Hall sensors, accelerometers, ultrasonic and photoelectric detectors are examples of sensors used for this kind of grippers. This device can detect a variety of variables, including position, force, torque, speed, or/and acceleration [21].

- **Grippers for Unknown Environments:** Frequently, grippers may be assigned pick-and-place tasks without knowledge of the surrounding environment. Various designs

and methods have been developed to enhance the flexibility of grippers in unfamiliar environments, including the use of machine-vision systems, sensory feedback, and innovative grasping mechanisms with increased flexibility. Object detection is also performed using camera systems [19].

- **Grippers for Fragile Objects:** Most grippers in this category include underactuated and compliance mechanisms. These mechanisms are achieved by replacing rigid joints with a framework composed of hyper-elastic materials that flex continually in reaction to external or internal forces. Due to the structure of their mechanism, they can securely pick up and handle delicate goods such as eggs and food [22].

- **Grippers for Medical Applications:** Regarding the usage of robotic grippers in surgery, the absence of force feedback and tissue damage are two of the primary concerns. Soft-bodied grippers are well suited for use in the medical industry because of their inherent safety and self-limiting properties, which allow for safe contact with biological tissues [19].

- **Grippers for ADLs:** This type of gripper is used in assistive robots, whose primary function is to carry out daily living activities. 2 or 3 finger grippers with underactuated mechanisms are commonly used for these applications [138].

- **Micro and Nano Grippers:** Thanks to the growing field of nanotechnology, various designs, and technologies of micro and nano grippers have been developed. These grippers, used to manipulate micro assemblies and bio and nanomaterials, are

composed chiefly of semiconductor materials. Some of those can even manipulate objects smaller than 10 micrometers [23].

- **Soft Fabric Grippers:** Fabric selection remains an unresolved issue in the gripper development process. Ingressive grippers, also known as piercing grippers, have been designed for this purpose. Because suction cups cannot vacuum porous substances, they are used to maintain textiles in the textile industry. In contrast to other materials, textiles may be perforated during transport without damaging their underlying woven structure [19].

2.2.2 Nottable Grippers:

Salisbury Hand:

The Salisbury hand [33] was the first humanoid robot hand to be built successfully as a sophisticated end-effector for grasping investigations. Since then, numerous robot hands have been designed and implemented, serving in various industrial, hazardous, and remote environments, from power plants to outer space [32].

Each of the fingers has three joints in this design, allowing it to mimic the human hand's dexterous gripping somewhat. Steel wires activate the fingers via flexible tubes coated with Teflon. A DC brush-type motor, functioning through a gear reducer, provides tension to each cable (Figure 3). The actuator package may be mounted on the robot's forearm thanks to the flexible conduit that allows the wires to be routed around the wrist [33].

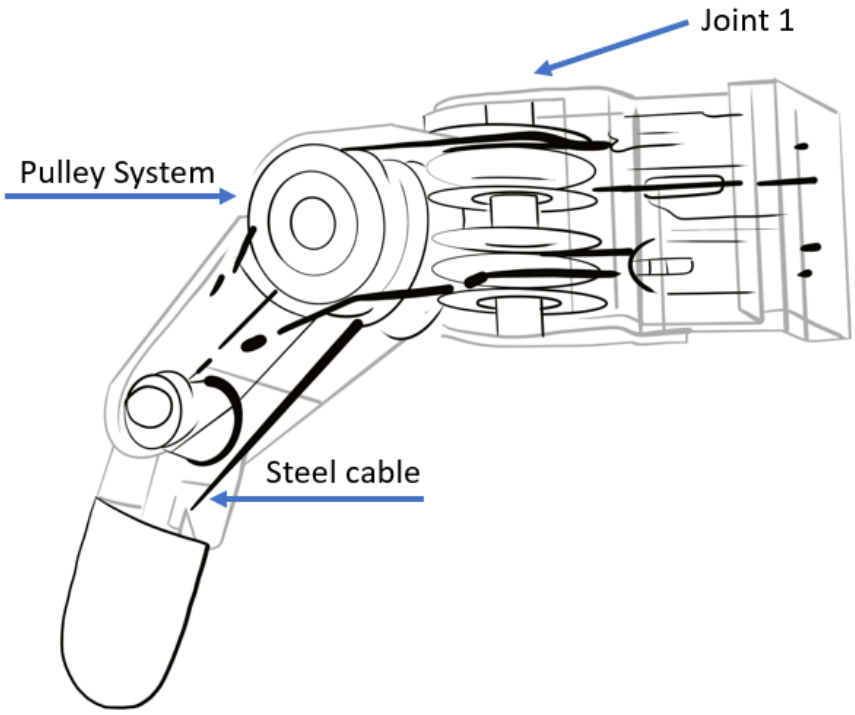

Figure 3 Salisbury hand Mechanism

Barrett Hand:

Barrett's hand is one of the most famous examples of hands used in industry and for grasping and manipulating research. In order to make the robot hand more effective in grasping tasks, this research investigates its modeling and contact control [33] inside of the hand; one motor power each finger, responsible for powering two joint axes. These joints receive torque through a TorqueSwitch mechanism (Figure 4). When a fingertip first makes contact with an object, it locks both joints, deactivates motor currents, and waits for further instructions from the microprocessors [34].

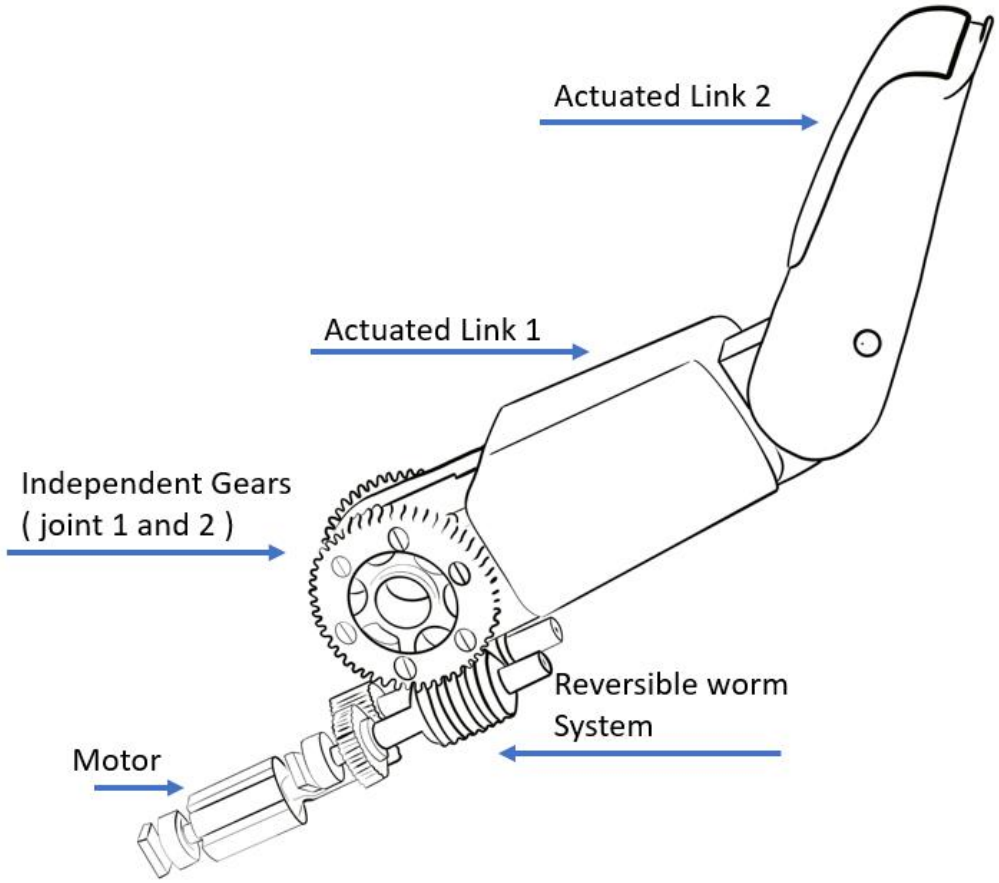

Figure 4 Barrett hand Mechanism

DLR Hand:

The DLR Hand [35] is an aluminum and steel open skeleton hand that can manipulate various objects with great dexterity and accuracy. In each finger, three separate joints are driven by their actuators. All actuation systems are built by brushless dc-motors, tooth belts, harmonic drive gears, and bevel gears at the base joint. As can be seen in Figure 5, the base joint is a differential bevel gear type, allowing for two independent motions. In addition, the two actuators may be used to their utmost potential, allowing the joint to flex or extend as needed.

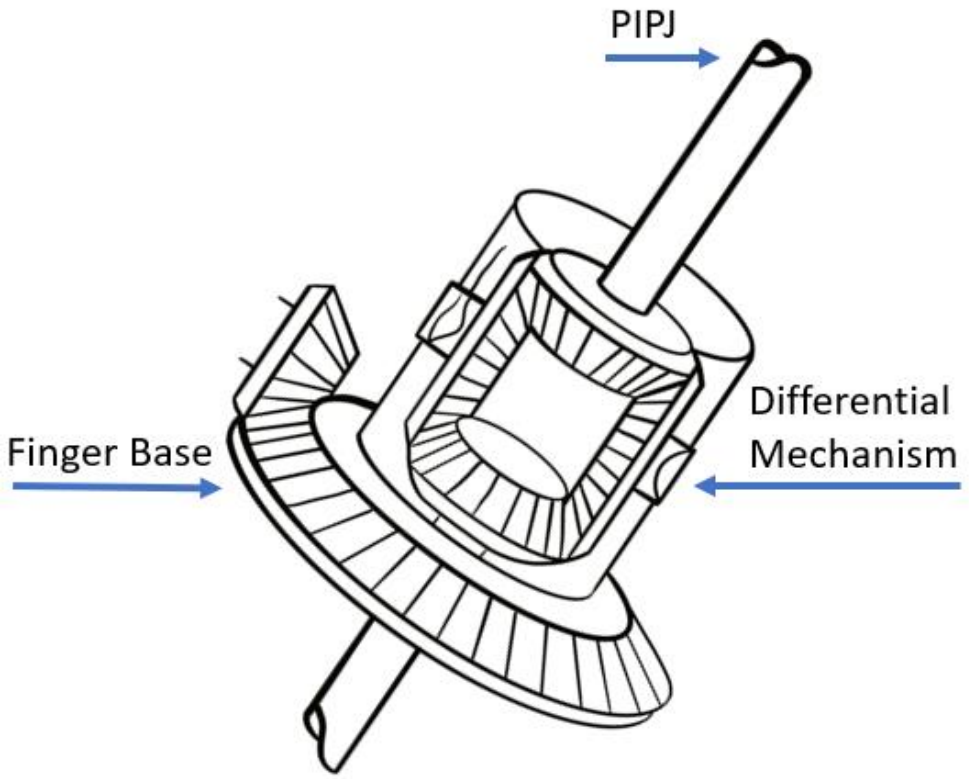

Figure 5 DHL Hand Differential Mechanism

Schunk Gripper:

The Schunk SVH hand [36] is one of the most compact designs ever. All the humanoid SCHUNK hand motors are housed in the wrist, saving a good amount of space for the mechanisms. This robotic gripper hand has 20 individual joints, and most of the SVH's joints are operated by leadscrew mechanisms that transform linear motion into rotational motion. There are a total of 22 joints. However, only nine are fully actuated, converting this hand into an underactuated mechanism (Figure 6).

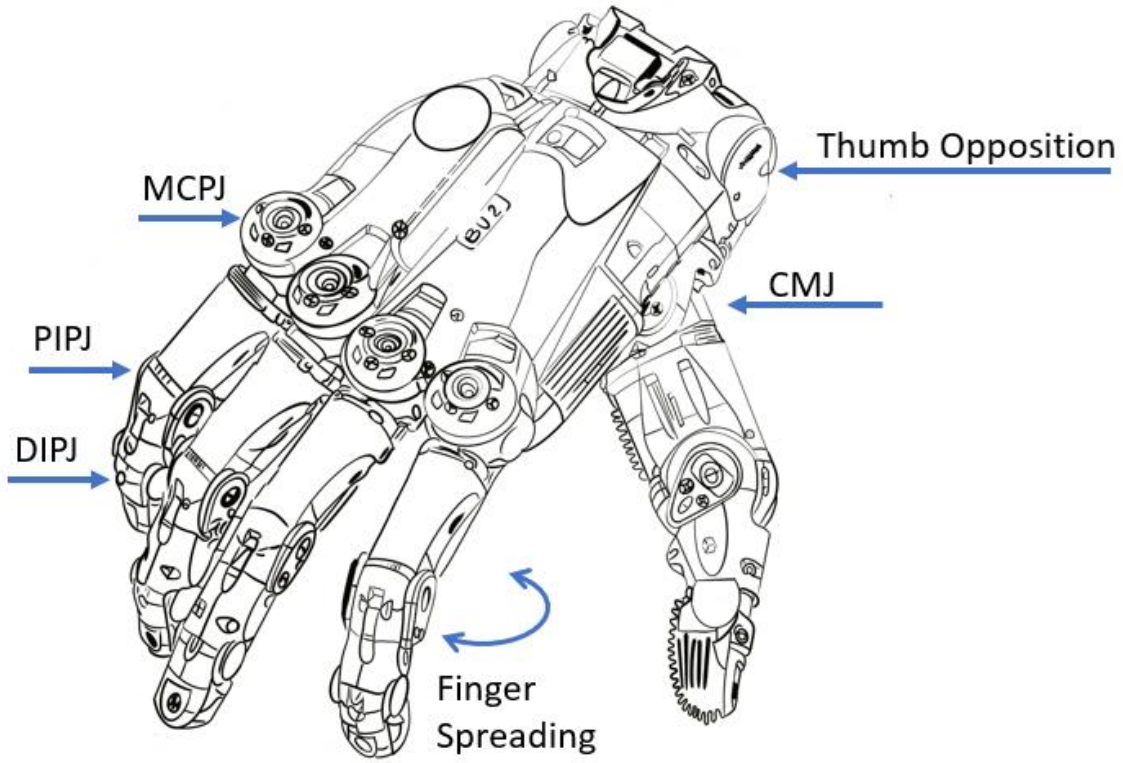

Figure 6 *SVH Hand Distribution*

2.3 Robotic Grippers in Assistive Robots:

One of the most important uses of robotics is the employment of assistive robots in healthcare settings. Assistive robotics help those who need special attention, such as people with reduced mobility, the elderly, and people with disabilities.

The field of study of assistive robots is expanding quickly. Assistive robots are generally categorized as interactive robots [24], which means that, like Co-bots, they interact directly with the users who control them. Moreover, Grippers specially designed to be used in assisted robots have their categorization. The design and materials used in these grippers vary over a wide range. For example, some grippers can handle fragile objects and grasp a wide range of

shapes, while others can carry more than 10 kilograms of weight, open doors, and grasp objects placed on tables and shelves [25]. In general, grippers designed for assistive robots should be able to perform a minimum of tasks effectively, such as those shown in Table 2:

Table 2 Minimum Task list for assistive robots

No.	Task
1	Picking/ Placing objects from Table, book, pen
2	Picking/ Placing objects from Ground, shoe
3	Picking/ Placing objects from Man reach, Upper shelf
4	Holding objects (up to 10 lbs)
5	Opening & closing drawers
6	Push-pull, Swing open-close doors
7	Holding cup near month
8	Gradual upward positioning of the cup during drinking
9	Holding spoon/fork
10	Maneuvering spoon/fork to take food from bowl to plate
11	Maneuvering spoon/fork to put food in mouth
12	Holding credit cards, Swipe credit cards at market, ATM booth
13	Putting pills/medicine in mouth
14	Holding medicine
15	Opening/ closing Refrigerator, oven Door
16	Opening/ closing lid of jar, box, paper box, cap of bottles
17	holding the phone near ear or put in speaker mode
18	Holding Pen, Maneuvering on paper or surfaces
19	Holding printed books, turning pages

2.4 Activities of Daily Living (ADLs)

activities of daily living (ADLs) are a set of essential activities that we commonly carry out in our day to day. The list of ADLs represents the minimum tasks a person should be able to perform to be independent of another person's care [26]. According to a user study with six participants, the most frequently requested activities involved personal hygiene (washing face and hands, brushing teeth, combing hair, or applying cosmetics), lying in bed (bringing goods close), in a wheelchair (eating, drinking, and bringing objects close), and in the kitchen

(opening cupboard doors and moving utensils) [27]. In that order, ADLs are classified into seven broad categories (Table 3):

Table 3 [28] Activities of daily living categories

Categories	Essential ADLs
CATEGORY 1	Picking/ Placing objects from table Holding spoon/fork Maneuvering spoon/fork to take food from bowl to plate Holding credit cards, Swipe credit cards at the shop, ATM booth Opening/ closing lid of a jar, box, paper box, cap of bottles Holding printed books, turning pages
CATEGORY 2	Picking/ Placing objects from ground
CATEGORY 3	Picking/ Placing objects from man reach, upper shelf
CATEGORY 4	Opening closing drawers
CATEGORY 5	Push-pull, Swing open-close doors Opening/ closing Refrigerator, Oven
CATEGORY 6	Holding cup near the mouth Gradual upward positioning of the cup while drinking Maneuvering spoon/fork to take food from bowl to plate Maneuvering spoon/fork to put food to the mouth Putting pills/medicine in the mouth Holding the phone near the ear or put in speaker mode
CATEGORY 7	Holding Pen, Maneuvering on paper or surfaces

A list of objects organized according to their dimensions and weights emerges from the previous categories. During the design stage, this data will be used to define the proposed gripper's parameters.

Table 4 List of objects used to design the GAR

Objects	Min Diam	Min Height	Min Length	Min Depth	Min Weight	Max Diam	Max Height	Max Length	Max Depth	Max Weight
Glass of water	41 mm	87 mm	-	-	112 gr empty	93 mm	164 mm	-	-	607 gr full
Apple	62 mm	62 mm	-	-	107 gr	92 mm	62 mm	-	-	396 gr

Pen	-	8 mm	8 mm	45	5.2 gr	-	9 mm	9 mm	235 mm	5.2 gr
Tablet	-	142 mm	115 mm	9.6 mm	286 gr	-	262 mm	159 mm	9.8 mm	504 gr
Shoe	-	74 mm	200 mm	45 mm	110 gr	-	102 mm	302 mm	58 mm	161 gr
Smart phone	-	75 mm	158 mm	9,2 mm	192 gr	-	-	-	-	-
Pill bottle	25,4 mm	61 mm	-	-	3.71 gr	-	-	-	-	-
book	-	130 mm	190 mm	14 mm	172 gr	-	205 mm	260 mm	38 mm	1072 gr
Pair of glasses	-	125 mm	140 mm	30 mm	60 gr	-	-	-	-	-
Stylus	10 mm	134 mm	-	-	6 gr	-	-	-	-	-
Single pill	8 mm	4 mm	-	-	250 mg	8 mm	17 mm	-	-	500 mg
Cereal box	-	254 mm	196 mm	88 mm	370 gr	-	-	-	-	-
Pringle	89 mm	125 mm	-	-	65 gr	89 mm	380 mm	-	-	158 gr
Coffee jar	-	254 mm	158 mm	107 mm	1088 gr empty	-	254 mm	158 mm	107 mm	2588 gr
Bread	-	52 mm	96 mm	37 mm	33 gr	-	115 mm	225 mm	85 mm	395 gr
2L Milk	-	-	-	-	-	-	152 mm	102 mm	82 mm	2120 gr
Drawers	-	145 mm	120 mm	46 mm	145 gr empty	-	230mm	143 mm	80 mm	248 gr empty
Knob	48 mm	48 mm	48 mm	48 mm	192 gr	-	-	-	-	-
Credit cards	-	88 mm	78 mm	2 mm	10 gr	-	-	-	-	-

Additionally, it is essential to understand the performance of commercial grippers and compare it with the proposed gripper regarding grasping objects from Table 4. For a better understanding, factors such as the maximum weight each gripper can support and the maximum size of the objects it can grasp is also presented in the following list (Table 5), along with the number of objects each gripper can correctly manage.

Table 5 Commercial grippers comparison

Gripper	Actuators Used	Weight [kg]	Precision [mm]	Payload [kg]	Max Stroke [mm]	Objects Can Handle	Fingers	Sensors
GAR	electrical: linear	0.67	0.50	5.00	110.00	glass of water; pill bottle, book; smart phone; pringle; shoe; cereal box; apple; bread;	3	-
Hand-E Adaptive	electrical: linear	1.00	0.40	5.00	50.00	glass of water; pen; book; pill bottle; knob	2	-
3-Finger Adaptive Robot	electrical: rotary	2.30	0.05	10.00	150.00	glass of water; pen; book; smart phone; pill bottle; Pringle; knob	3	Tactile
2F-85 Gripper	electrical: rotary	0.90	0.40	5.00	85.00	glass of water; pen; book; pill bottle; knob; shoe	2	-
2F-140 Gripper	electrical: rotary	1.00	0.60	2.50	140.00	glass of water; pen; book; smart phone; pill bottle; Pringles; knob	2	-
Vacuum Grippers EPick	pneumatic	0.71	0.00	10.00	0.00	tablet; smart phone; book; cereal box; credit cards	1	Camera; Torque
Vacuum Grippers AirPick	pneumatic	0.48	0.00	10.00	0.00	tablet; smart phone; book; cereal box; credit cards	1	Camera; Torque
HRC-01	electrical: linear	1.60	0.05	50.00	80.00	-	2	-
OnRobot 2FG7	electrical: linear	1.10	0.10	7.00	59.00	pen; stylus; knob; eyeglasses	2	-
OnRobot RG6	electrical: rotary	1.25	0.10	6.00	130.00	glass of water; pen; book; smart phone; pill bottle; Pringles; knob	2	-
OnRobot RG2-FT	electrical: rotary	0.98	0.10	2.00	100.00	glass of water; pen; book; smart phone; pill bottle; Pringles; knob	2	-
OnRobot 3FG15	electrical: linear	1.15	0.10	10.00	152.00	pen; shoe; smart phone; pill bottle; Pringles	3	-
OnRobot Soft-Gripper	electrical: linear	0.17	0.10	2.20	40.00	apple; bread	-	-
Gentle Duo Mini Soft Gripper	electrical: linear	0.80	-	1.50	175.00	apple; bread	2	-

Finally, to narrow down the scope of this thesis:

This research focuses on the mechanical development of a simple robotic gripper with a minimally feasible design that can grasp various objects of different shapes and weights. Based on Table 3 and Table 4 (The tasks/objects tables mentioned before), the design target is to perform those tasks in the range of 80% effectiveness for all the objects presented.

CHAPTER 3

LITERATURE REVIEW:

The capacity to grasp and manipulate objects has been indispensable to the development of robots [37-46]. Utilizing advancements in gripper technology, manufacturers can use end-effector tooling for picking, placing, and packing objects to gain precision, performance, and productivity [47]. Gripper's classification is based on its design, power source, and application. For instance, one of the most straightforward designs for industrial grippers is the parallel motion two-jaw gripper, commonly used to lift objects [48] – [51]. The bellows gripper, the O-ring gripper, and the needle gripper are three additional design types. Depending on the application requirements, industrial grippers can be hydraulic, pneumatic, or electric [54] – [56]. However, even though the number of grippers currently available on the market has increased over the years, there are still many complex tasks that robots cannot perform. Robotic grippers have difficulty grasping delicate items with the proper force [39, 42, 44, 46]. For instance, a gripper handling fruit or food must hold it firmly enough to prevent it from slipping out of their hands yet gently to prevent the item from being harmed. Human fingers are soft and can adapt to different situations, but this is not a characteristic of robotic grippers, which are often constructed of metal or other hard materials. To address this challenge, designers created grippers made from softer materials, enabling robotic grippers to manipulate delicate items and establishing the field of soft robotics. Soft robotics is a subfield that focuses on robots constructed from soft materials resembling those of biological animals, such as the tentacles of an octopus or a human's fleshy finger. Recent advancements in soft robotics make it possible for robots to overcome previous barriers and join new industries [57, 58].

Dexterity is another problem for gripper design. Many conventional gripper designs consist of two or three stiff fingers. While they are successful at pick-and-place tasks, they are only suitable for some simple manipulation tasks [59], [60]. In order to be practical and effective during picking and placing tasks, the gripper must adapt itself to the shape of the item grasped. Specialize in grasping and manipulating objects using ultra-sensitive touch sensors and having low power consumption, resembling a human hand [61].

This chapter investigates the most recent industrial and research designs of grippers to answer the question: which gripper design can handle the majority of items regardless of their fragility, form, or weight?

Consequently, Grippers are categorized based on their mechanical design, the degrees of freedom (DOF), the type of actuation, and the shape of the graspable objects, focusing the research on determining which gripper has the best handling capabilities.

The Chapter structure is as follows:

- The process for choosing and structuring the selected articles for the analysis is presented in Section II.

- The classification of grippers in Section III is based on their degrees of freedom and design.

- Sections IV, V, and VI successively cover the constrained gripper mechanism, the under-constrained gripper mechanism, and the deformable grippers.

- The grippers are organized in Section VII according to their uses and grabbing capacity.

- Finally, in Section VIII, the analysis's conclusions are presented.

3.1 How to Choose the Papers to Analyze?

In January 2022, a systematic electronic search was conducted in a few databases to choose studies focusing on the robotic arm gripper's current design and control methods. Furthermore, the research was restricted to the last five years to focus on the most recent advancements in this sector. In order to concentrate on the most recent developments in this sector, the research was limited to the past five years. "Robotic gripper," "robotic hand," "gripper design," "robotic manipulation," and "robotic grabbing" are search terms.

Various databases, including Google Scholar, IEEE Xplore, ScienceDirect, Engineering Village, Microsoft academic search, Google Patent Search, Scopus, Springer, PubMed, MDPI, IOS Press, Hindawi, SAGE, PLOS, Frontiers in Robotics and AI, were searched for this study.

In this search, around 235 publications are identified for evaluation. However, following a preliminary screening, 190 papers were selected for assessment. Several articles were then

rejected based on eligibility criteria (particular objectives, duplication, and review), resulting in the selection of 64 papers for a comprehensive evaluation.

All of the selected papers (n=64) were reviewed, including their abstracts, introductions, design approach, experiments, conclusions, and future work sections, in order to identify any additional pertinent information, such as the problem addressed, contribution, control theory, applications, experiments, used material, and sensors.

The inclusion and exclusion criteria are illustrated in Figure 7.

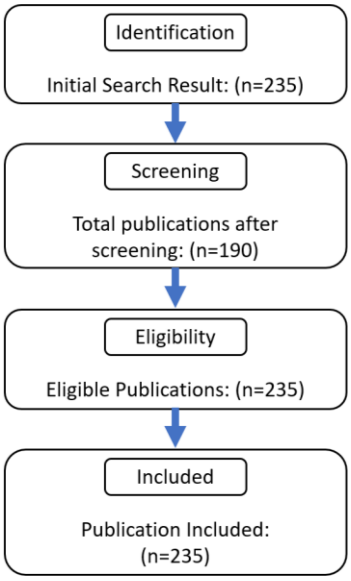

Figure 7 Papers selection method

3.2 Systems-Based Classification for Robotic Grippers

There are three basic categories for classifying the design of robotic grippers based on their mobility: completely confined, underconstrained, and deformable. Furthermore, as seen in

Table 6, several subgroups are within these categories. This research examines each categorization of robotic grippers, concentrating on their merits and limitations.

Table 6 Categorization of robotic grippers

Completely constrained	Compliant mechanism	Cable driven	[42]
		linear actuator	[37], [62]-[64]
	Rigid links	Linear actuator	[65]-[67]
		Rotary actuator	[68]-[70]
		Cable driven	[40], [71], [72]
		Unspecified	[106]
		Electromagnet	[73], [74]
Underconstrained	Compliant mechanism	unspecified	[75]
		Cable driven	[50], [76]
		Rotary actuator	[77]
		Linear actuator	[78]
		Piezo actuator	[79], [80]
	Rigid links	Linear actuator	[51], [81], [82]
		Rotary actuator	[46], [83]-[86]
		Cable driven	[41], [45], [48], [49], [87]-[94]
		Pneumatic actuation	[95]
Deformable	Single mass gripper	Vacuum	[38], [47], [96]
		Cable driven	[44], [97], [98]
	single mass finger	Pneumatic/Hydraulic actuation	[43], [99]-[105]
		Dielectric elastmer (DE) actuator	[106]
		Linear actuator	[107]
	Square continuun robot	Cable driven	[108]

3.3 Analysis of Chosen Papers:

3.3.1 Completely Constrained Gripper Mechanism

Devices with a degree of freedom equivalent to the number of actuators they include are wholly restricted mechanisms. These mechanisms allow the trajectory of the tip of the finger

to follow a route that has been predetermined. Because of this attribute, the device can create a large output torque, which enables the gripper to grasp things with a significant weight [62], [77]. The majority of these devices only have one degree of freedom (DOF) to regulate the gripper's motion, which restricts the types of complicated objects that the gripper may manipulate [65]. In order to address this problem, researchers have increased the degrees of freedom (DOF) present in the grippers, resulting in a reduction in the amount of torque that can be generated by the grippers [69]. In addition, there are two types of entirely confined finger mechanisms: compliant mechanisms and rigid links. These categories are based on the designs of the mechanisms.

3.3.1.1 Compliant Mechanism

A compliant mechanism is a flexible mechanism that transmits force and motion by deforming elastically. Compliant mechanisms feature fewer moving components, making them lightweight. Also, friction affects flexible connections less than rigid ones because flexible connections need fewer parts than other mechanisms. In addition, the reduced number of assembly components reduces undesired nonlinear effects such as backlash and noise in compliant mechanisms.

Typically, compliant mechanisms are made from 3D-printed materials, which minimizes manufacturing costs. However, because the linkages are flexible, they are significantly weaker than rigid links, diminishing the output torque capabilities [109].

A common design technique for compliant mechanisms is topological optimization, as stated in [42] for a 3-fingered gripper. The optimization's primary objective was to simplify the modeling of gripper-object interactions. Figure 8 depicts the steps of gripper design

optimization. During the author's research, the optimization model analyzes the loading pressure and traction frictions to determine the objective function in this instance. Finally, they test the mechanism activated by cables and pulleys.

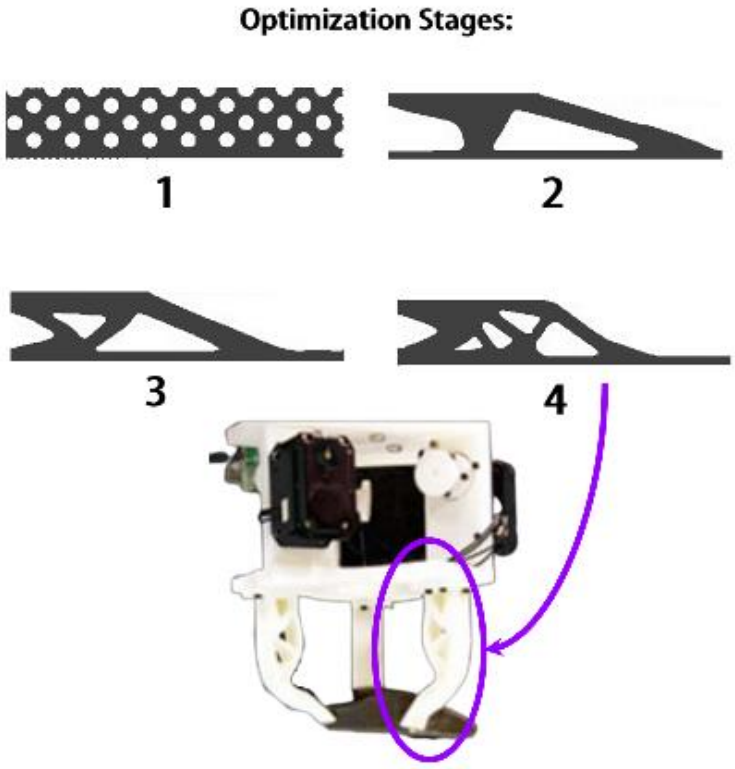

Figure 8 Topological optimization stages

Another example of a compliant mechanism is utilized for each finger of a three-finger flexible gripper [37]. The finger mechanism moves linearly, as seen in Figure 9. The finger mechanism was constructed from thermoplastic elastomer (TPE) and tuned for interactions with unexpected surroundings and manipulating delicate items of varying sizes. In addition, the gripper mechanism includes only one linear actuator to move all three fingers concurrently, resulting in identical displacement for each finger.

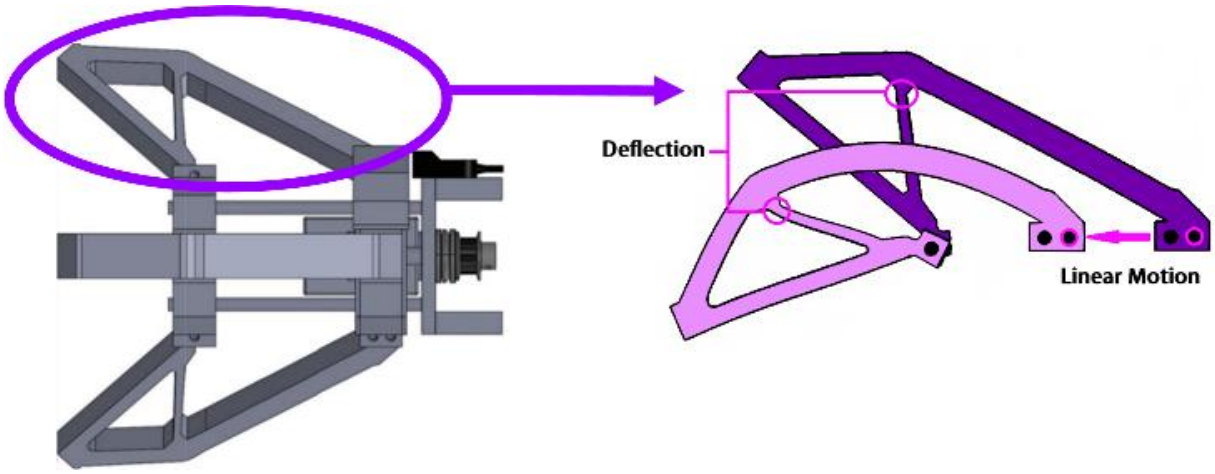

Figure 9 Flexible finger performing linear motion

A similar idea was presented in [62], which centered on the best design of a 3D-printed finger with continuous force compliance. This finger mechanism employs a force control method to manipulate fragile items rapidly. The force-regulatory strategy is described in detail in [63]. Figure 10 depicts the gripper's actuation system, which includes the jaw and FRM. The gripper mechanism is pneumatically activated and contains two spring-like complaint mechanisms.

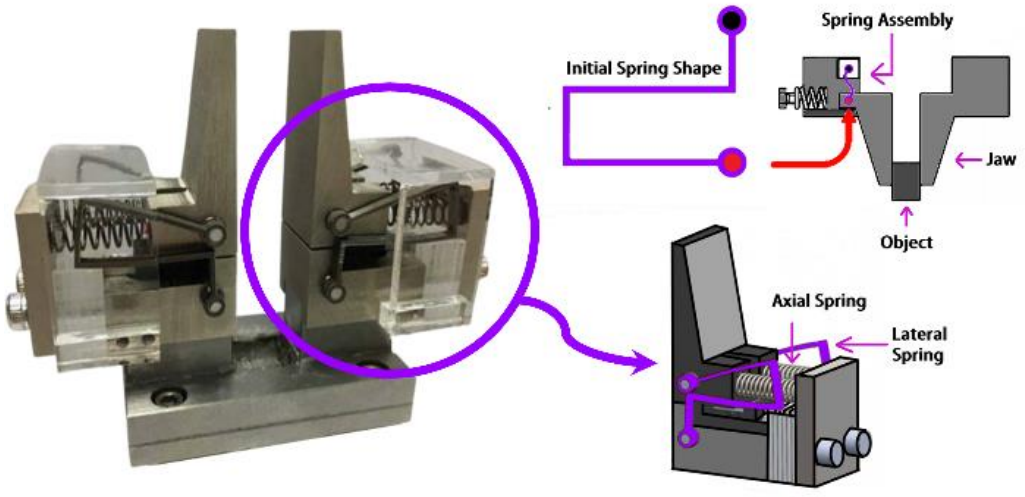

Figure 10 Actuation system of a gripper including the jaw and FRM

As demonstrated in [64], other devices incorporate sensors into the construction of the compliant gripper. This compliant gripper incorporates an integrated position and grasping/interaction force sensor for automated micro-assembly tasks. The inbuilt sensor restricts the workspace to 2.2 mm at a distance of 2.2 mm with a grasping force of 16 mN. However, this may not be an imminent feature for the planned use of this gripper. Figure 11 depicts the end-effector control mechanism with integrated force and position sensors and a piezoresistive strain gauge. This gripper mechanism uses topological optimization using finite elements as well. Comparing the optimization findings to those of an experimental environment, the author demonstrated the viability of this technique.

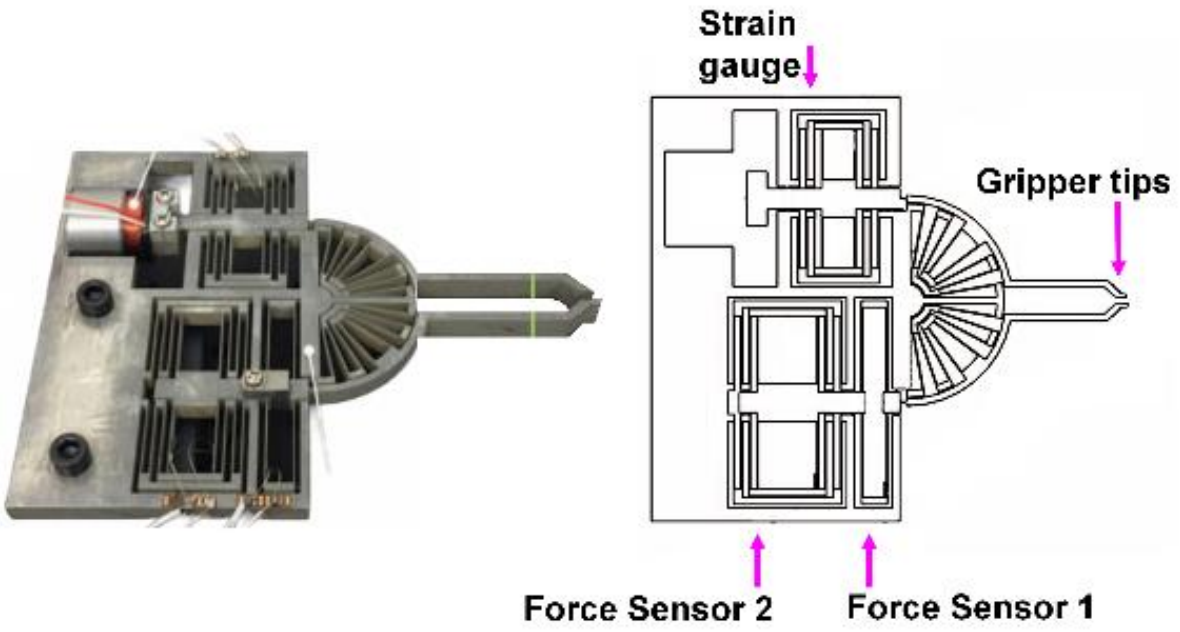

Figure 11 Structure of the complaint mechanism with integrated sensors.

3.3.1.2 Rigid Links

In contrast to flexible mechanisms, rigid linkages may provide ample output torque while maintaining rigidity. Nonetheless, force sensors are necessary for this gripper device to prevent damage to the objects being handled.

This architecture is illustrated in [71], which provides a cable-driven adaptive multi-DOF finger with an integrated mechanical sensor to control the position and output torque. This ABS finger mechanism is capable of making single-plane movements. In addition, the design of this finger mechanism maximizes output forces along a preset path, resulting in a gripper mechanism capable of grasping objects measuring 55 mm in diameter and weighing 800 grams. Figure 12 depicts the kinematic diagram of the gripper mechanism for the design trajectory.

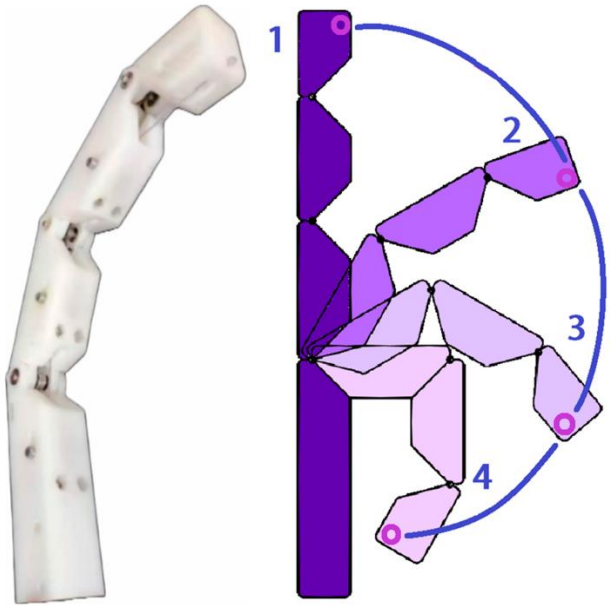

Figure 12 Kinematical diagram of the finger mechanism for the design trajectory.

The mentioned source [40] offers another example of a stiff gripper with equivalent features. The rigid gripper is a four-finger, cable-operated hand gripper, with each finger possessing three degrees of freedom. In addition, each finger on this gripper is the same length and has two phalanges.

As in the case of reference [72], some stiff grippers feature variable friction surfaces that improve the gripper's manipulability and dexterity. As illustrated in Figure 13, the friction of this gripper is modified by the operation of two pulleys coupled to DC motors. The texture of this gripper is a combination of PLA and TPU.

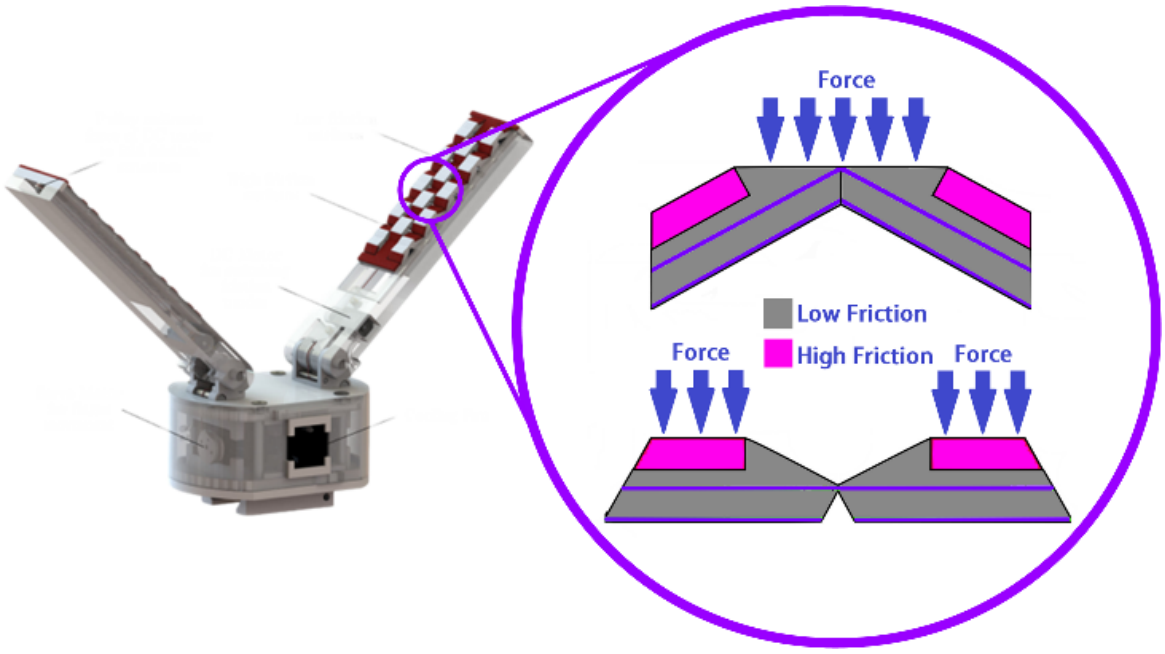

Figure 13 System of friction changing Surface.

The requirement for a precise control approach restricts the use of rigid connections. Due to the nature of the force sensor, it is impossible to achieve this accuracy. As demonstrated in reference [66], some authors approximate experimental data into an accurate control plan using a fuzzy logic controller. Figure 14 illustrates the experimental setup performed by the

author to validate the behavior of this approach. Other designs with stiff links, such as [110], employ link chains with closed loops. As seen in Figure 15, this finger gripper consists of two parallel grippers constructed from symmetric parallelograms.

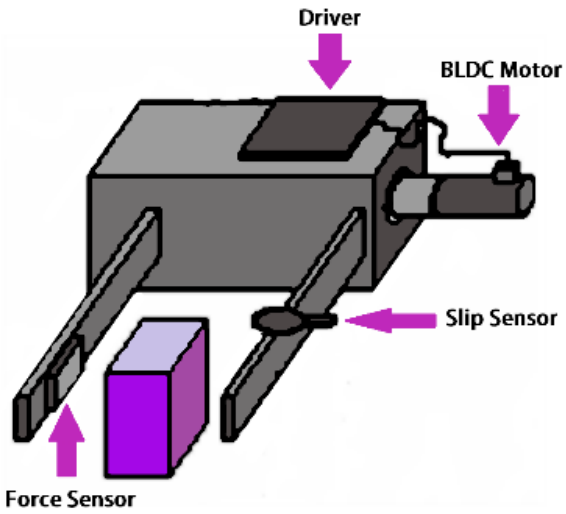

Figure 14 Gripper configuration with one movable finger (with force sensor) and one fixed finger (with slip sensor) to ease the control

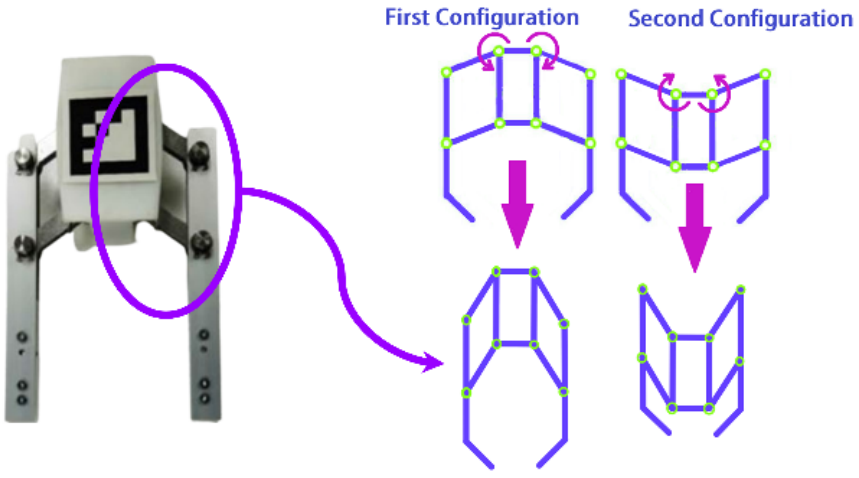

Figure 15 Finger gripper composed of two parallel grippers of symmetric parallelograms

This kinematical design has the advantage of being easier to implement, ensuring that the tool responds efficiently to the gripping forces and spring stiffness. In addition, certain rigid links grippers use lead screws to enhance precision. There are examples of this practice in references [67] and [65]. As seen in Figure 16, the former employs a gripper modeled after a chuck clamping mechanism. This gripper features a closing mechanism that positions objects. The latter employs the technique depicted in Fig. 17.

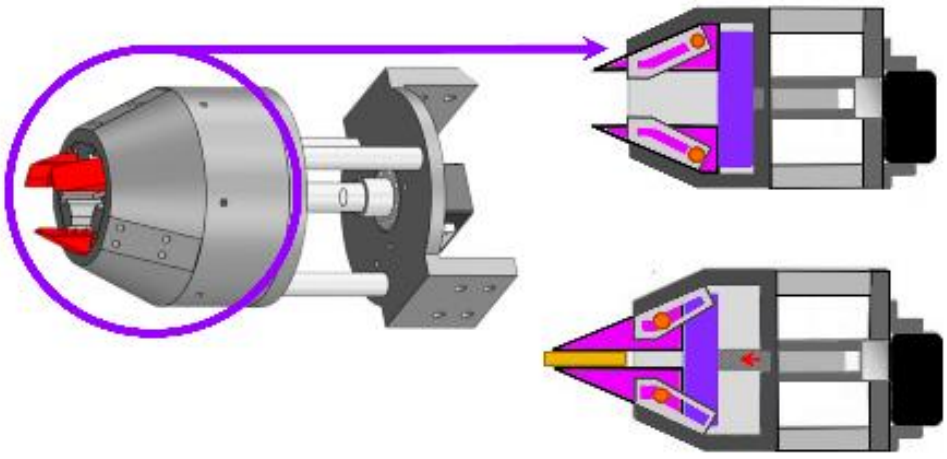

Figure 16 Assembly and operation of the chuck type system

This stiff link system can handle goods weighing up to 5 kg and delicate products such as eggs. Both gripper mechanisms are self-locking, decreasing energy usage since the motors do not need to be constantly engaged. Due to the significant mechanical advantage, however, this sort of gripper mechanism has a problem with slow motion. Other versions operate stiff linkages using electromagnets.

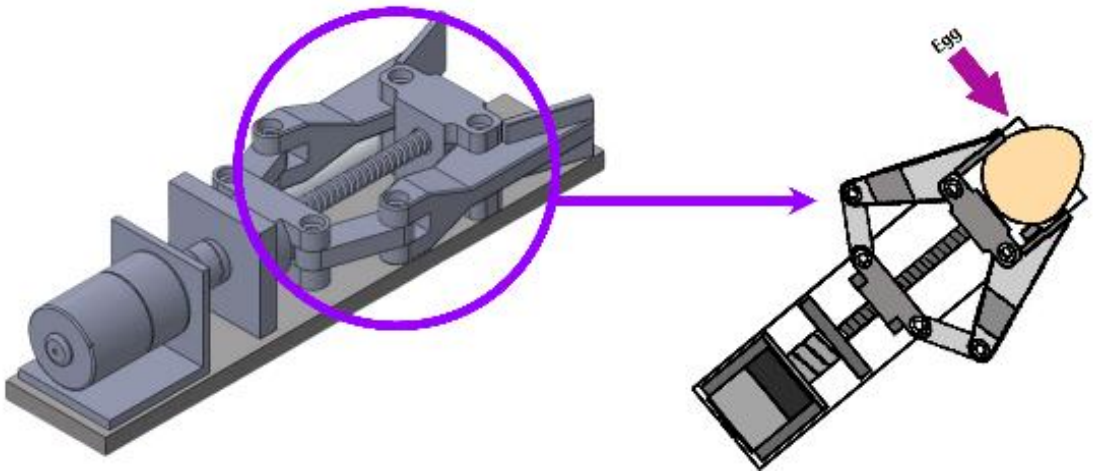

Figure 17 Representation of the gripper holding an egg without breaking it

For instance, a fabric-manipulating electromagnet-actuated gripper is shown in reference [73]. As illustrated in Figure 18, the gripper features a slider-crank mechanism. Multiobjective genetic algorithms are utilized to optimize more complex electromagnet-actuated grippers. The citation [74] provides an example of this optimization strategy. The authors modeled the actuator as a stack of series and parallel arrays of individual actuator components arranged in four possible configurations. As a result of this optimization procedure, the gripper is more precise than other grippers of the same type. However, electromagnets require substantial input energy, rendering them unsuitable for autonomous applications.

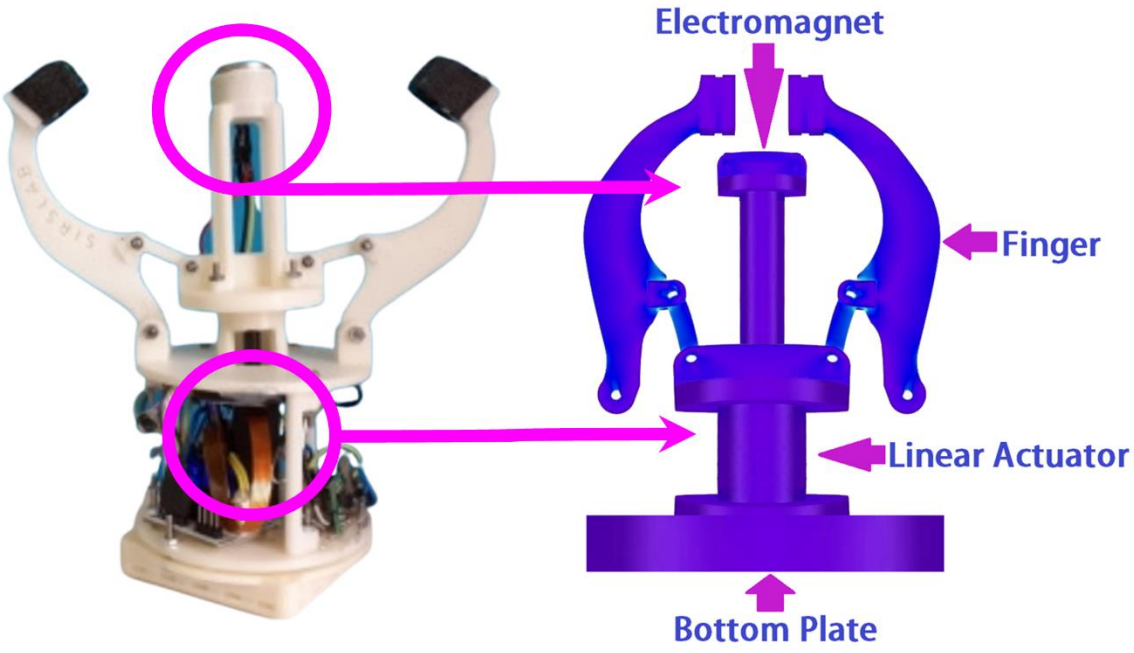

Figure 18 Electromagnet actuated gripper

3.3.2 Underconstrained Mechanism

3.3.2.1 Compliant Mechanism

In comparison to fully constrained mechanisms, underconstrained mechanisms offer a broader range of motion. The enhanced motion is due to more degrees of freedom (DOF) than actuators, allowing for greater flexibility when manipulating irregularly shaped items. Typically, springs passively activate the additional DOF to sustain the structure. However, as with underconstrained compliant systems, the geometry of the gripper may already incorporate the spring's effects. Figure 19 depicts a robotic gripper with compliant cell stacks designed for industrial component handling by the authors of reference [75].

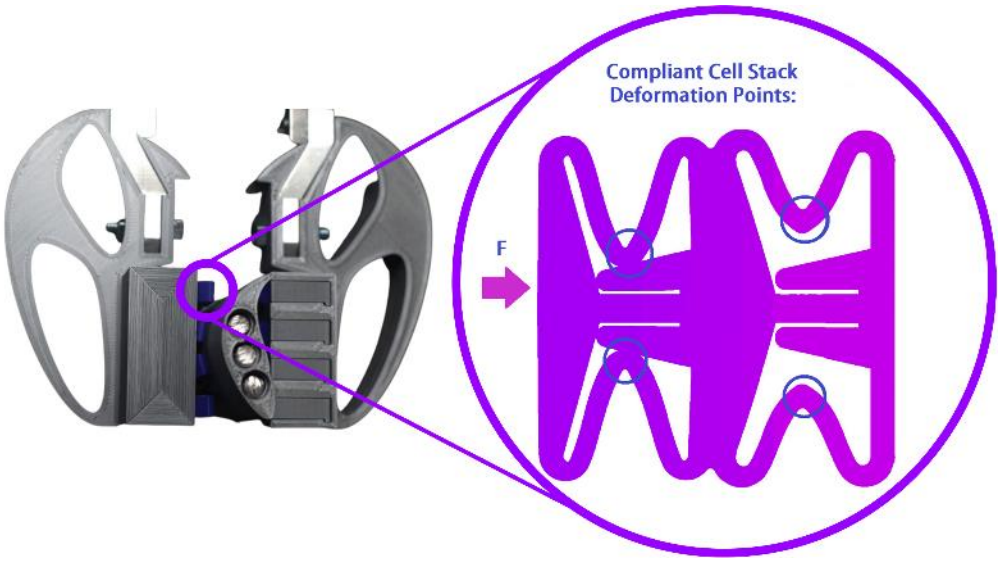

Figure 19 Robotic gripper with compliant cell stacks mechanism

Another example is offered in [76], which describes the development of a three-fingered robotic gripper inspired by the origami tower (Figure 20). A central servomotor controls the cable-driven activation of each finger of the gripper. Although the gripper mechanisms can manipulate complex-shaped items, their payload capacity is capped at 100 Nm. This type of gripper has a low carrying capacity, which is a disadvantage.

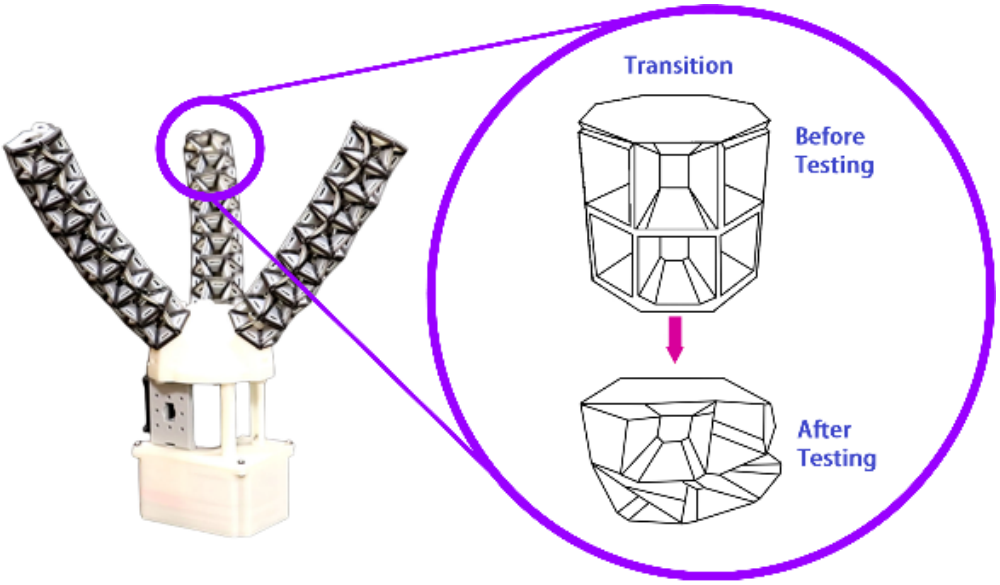

Figure 20 Underactuated robotic gripper inspired in an origami twisted tower

The authors of [82] designed a passive-compliant piezo-actuated micro-gripper (Figure 21), whereas the author of [77] offered a 3D-printed Gripper for Cloth Manipulation and position control (Figure 22). The latter, however, utilized a variable friction finger surface controlled by a micromotor that pushed the high friction surface to the tip of the top finger, thereby boosting the payload capacity.

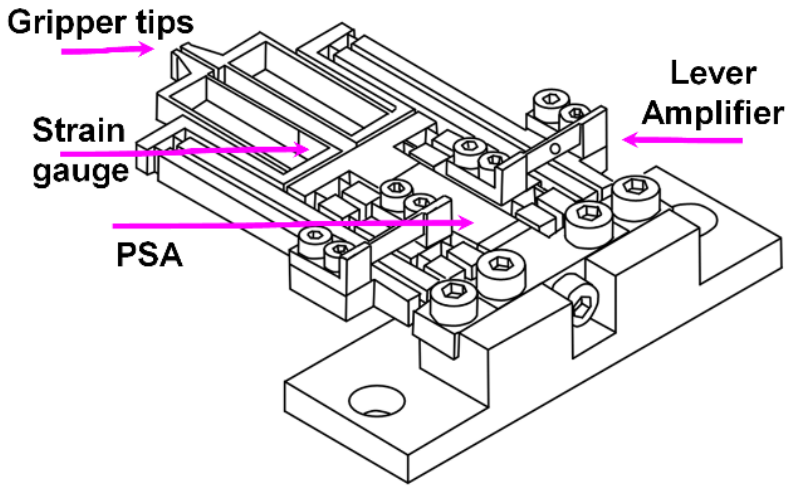

Figure 21 Passive-compliant piezo actuated micro-gripper

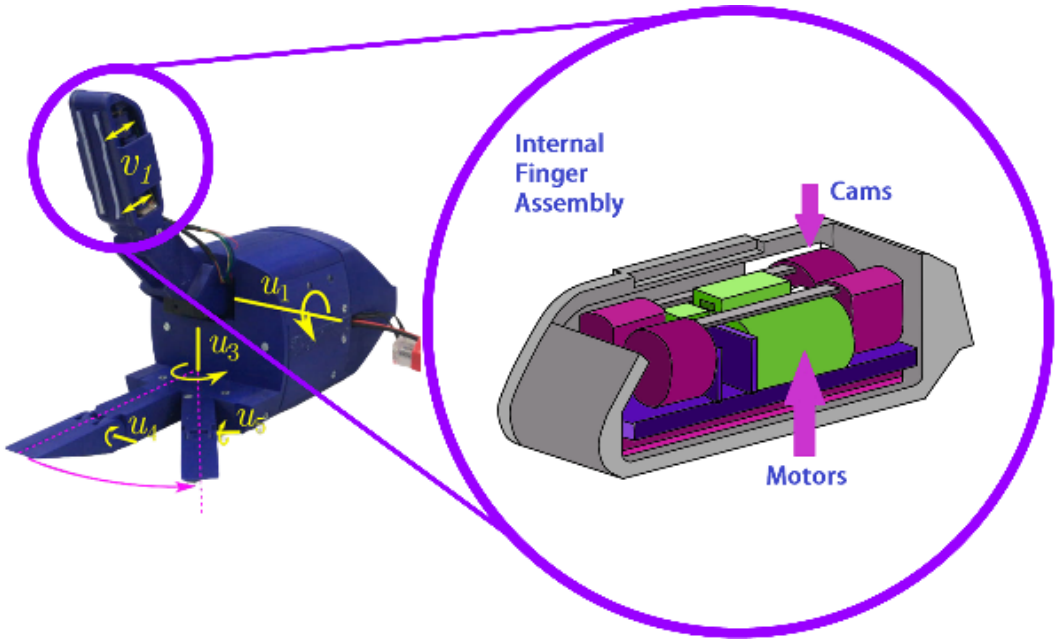

Figure 22 3D Printed Gripper for Cloth Manipulation. The figure shows the motors used to change the friction in the gripper.

The previous type of gripper is constrained by the need for a force sensor to detect the distributed forces on a surface. In order to accomplish this, the authors of the given study [119] designed a gecko-inspired gripper with a metalized ABS polyimide or mylar polyester surface for the sensors (Fig. 23). The sensor is fabricated on-site using thin adhesive films on each finger. It analyzes the change in capacitance that occurs when an adhesive area comes into contact with a surface.

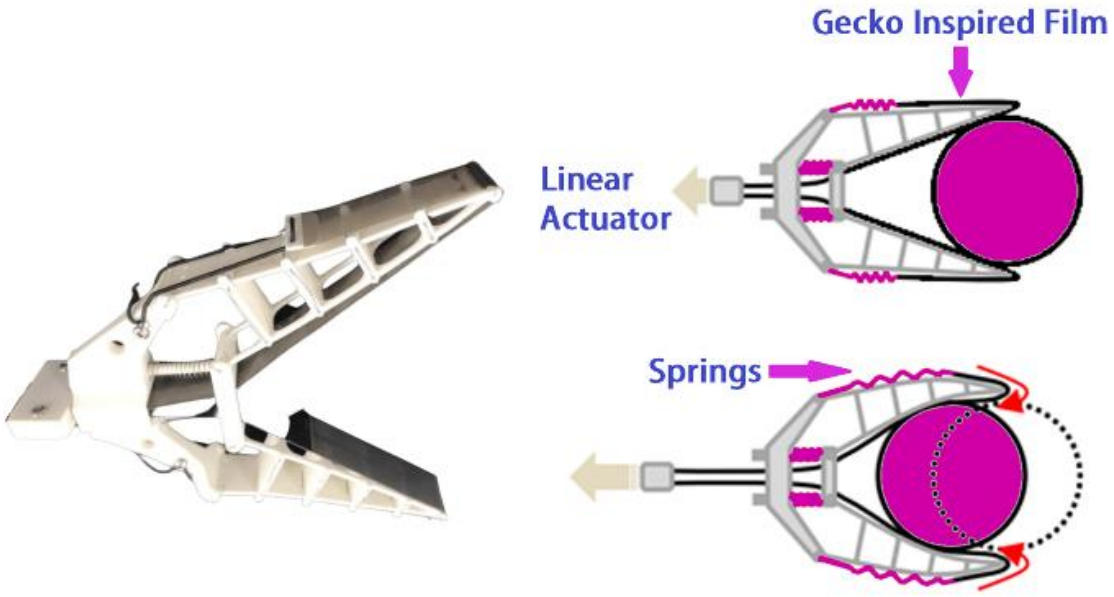

Figure 23 Movement sequence to perform a full grasping

The authors of [78] designed a second sensor for a compliant adaptive gripper with implicit force. Knowing the gripper's deformations enables the calculation of output force. The authors employed a large numerical network model to calculate the system's deformation (NTM). Using a hand-eye camera, the NTM determines the mechanism's node coordinates (Figure 24). Using the node data, the NTM then calculates the gripping force of the gripper. The proposed mechanism is the first fin-ray-based gripper capable of adaptive grabbing and intrinsic force sensing without requiring a separate force sensor.

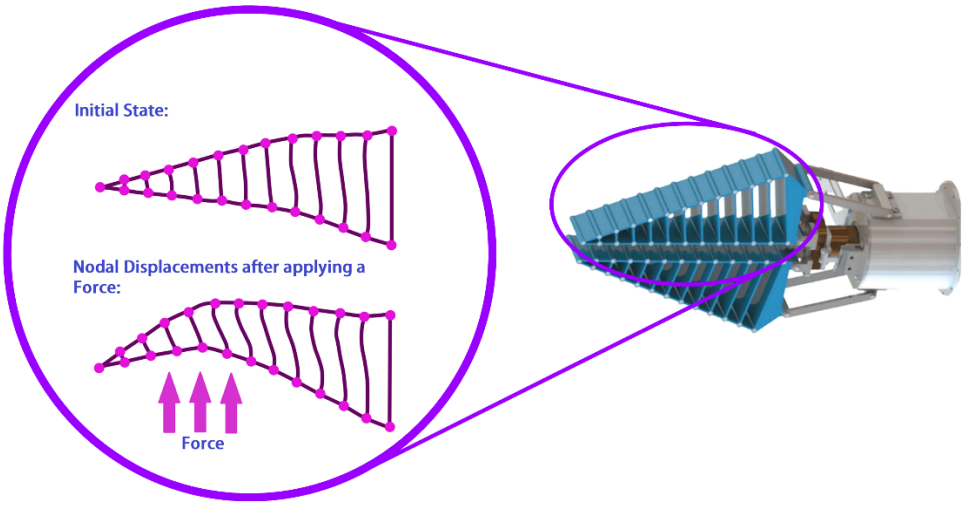

Figure 24 Representation of the theoretical deformation of the gripper given by the general numerical network model

The author of the mentioned study [80] designed a one-of-a-kind compliant constant-force gripper based on buckling fixed-guided beams with comparable properties (Figure 25). Incorporated into the gripper is a passive, compliant, constant-force mechanism. Combining positive and negative stiffness mechanisms allows the gripper to produce a constant output force. The mechanism for negative stiffness is a bidirectional, fixed-guided beam.

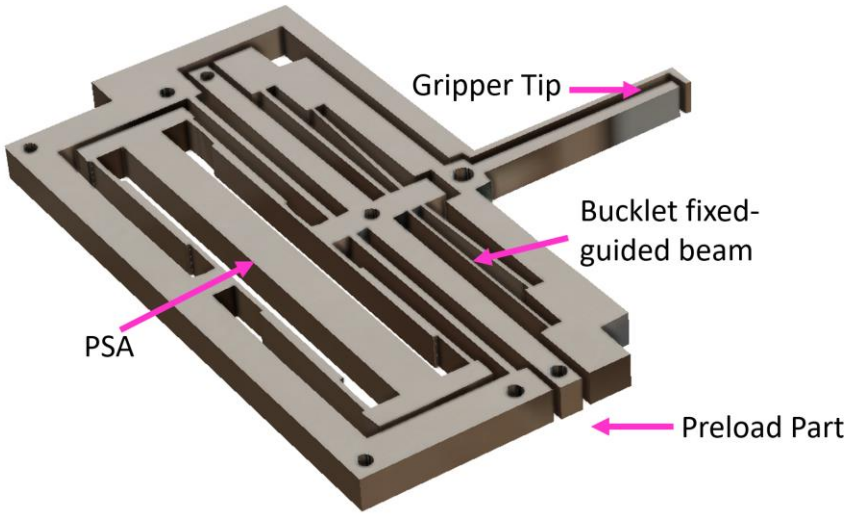

Figure 25 Compliant mechanism structure model

3.3.2.2 Rigid Links

The load capacity of underconstrained rigid gripper mechanisms is greater than that of their compliant equivalents. However, in contrast to wholly constrained gripper mechanisms with rigid links, the load capacity of these mechanisms is still reasonably moderate. Therefore, they have an average output load capacity. Moreover, the bulk of designs for underconstrained grippers incorporate optimization strategies to improve kinematic capabilities.

The reference authors [87] illustrate an optimized gripper and present a geometric design for underactuated three-phalanx fingers. This research investigates the stability of two types of cable-driven, underactuated three-phalanx fingers. In addition, the theory for the optimal design of the gripper is provided, along with an objective function that maximizes the forces normal to the contact trajectory while limiting contact loss and ejection (Figure 26).

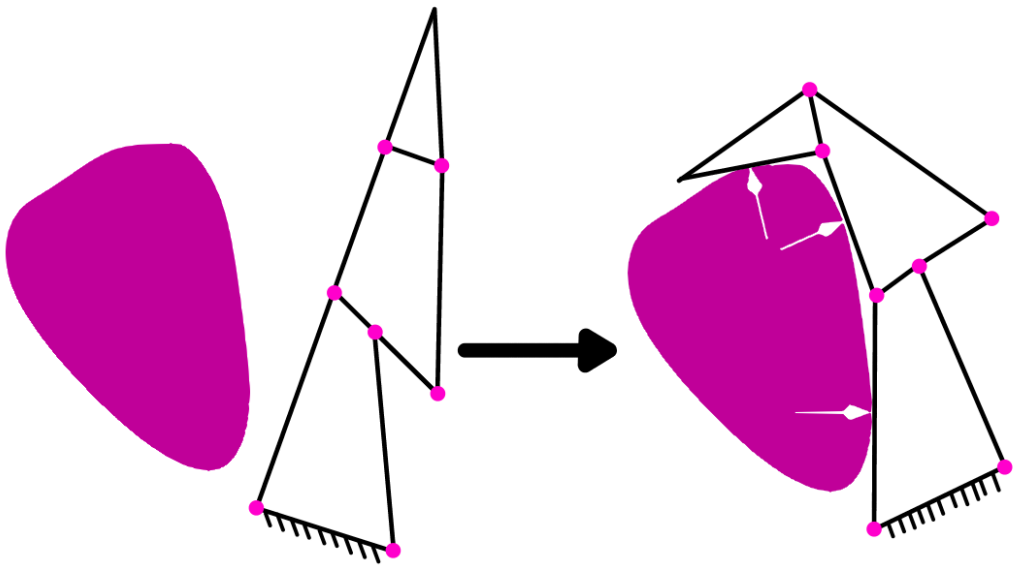

Figure 26 Clamping sequence for an object preventing ejection from the gripper design

Another illustration of optimization may be found in reference [51], which details a multimodal adaptive gripper with the ideal design of a reconfigurable finger designed to improve robotic manipulation without sacrificing gripping efficiency (Figure 27). Utilizing a simultaneous multi-start search method, the authors optimize the volume of the workspace for a range of objects. This method computes the workspace for dexterous manipulation by considering all possible item positions during in-hand manipulation. The technique builds a planar point cloud by grouping all configurations into this collection of points. The bounding volume of the point cloud is generated using the alpha-Shape method, which formalizes the abstract shape of the provided collection of points using Delaunay triangulation.

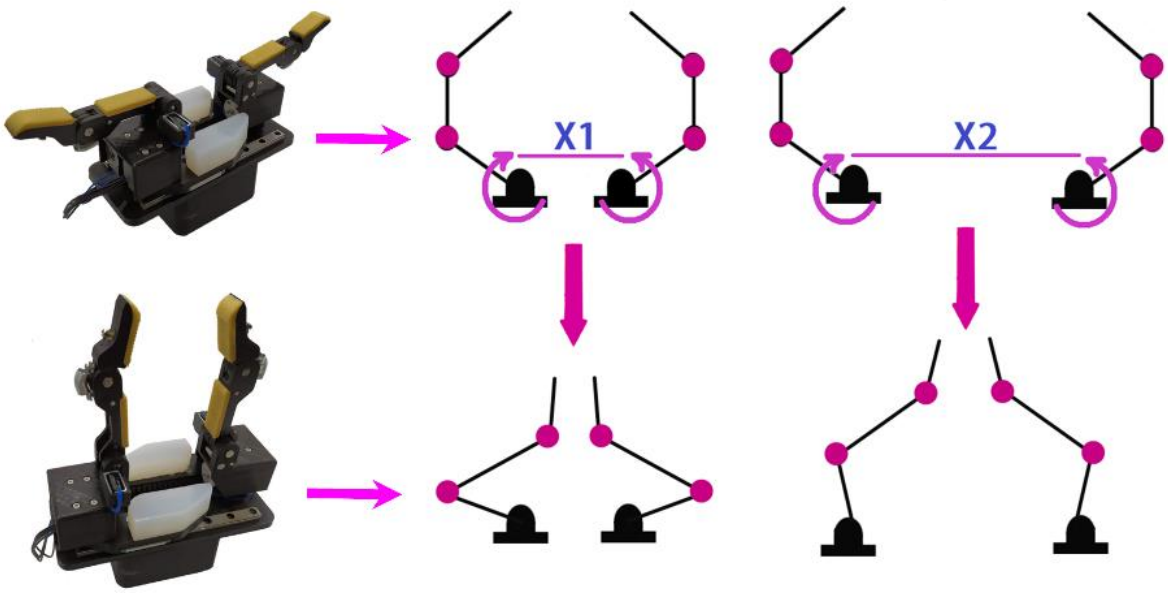

Figure 27 Multimodal adaptive gripper with the optimal design of a reconfigurable finger

Other methods boost the gripping capability of a gripper by adding spines. For instance, the authors in reference [41] offer a passive spine gripper for a climber robot that can handle hard rocky surfaces. This six-fingered gripper is excellent for space exploration in uncharted

settings. The mechanism's (Figure 28) twin spines let it clamp to various surfaces. The finger component is attached to a preload spring within the gripper. A servomotor-pulley actuator governs the finger mechanism. In addition, to release or remove the gripper from the surface, a servo motor pulls a nylon gut linked to each fingertip. The range of the gripper is 120 degrees, and it can hold 4.7 N. The author determined the spring's stiffness using energy techniques.

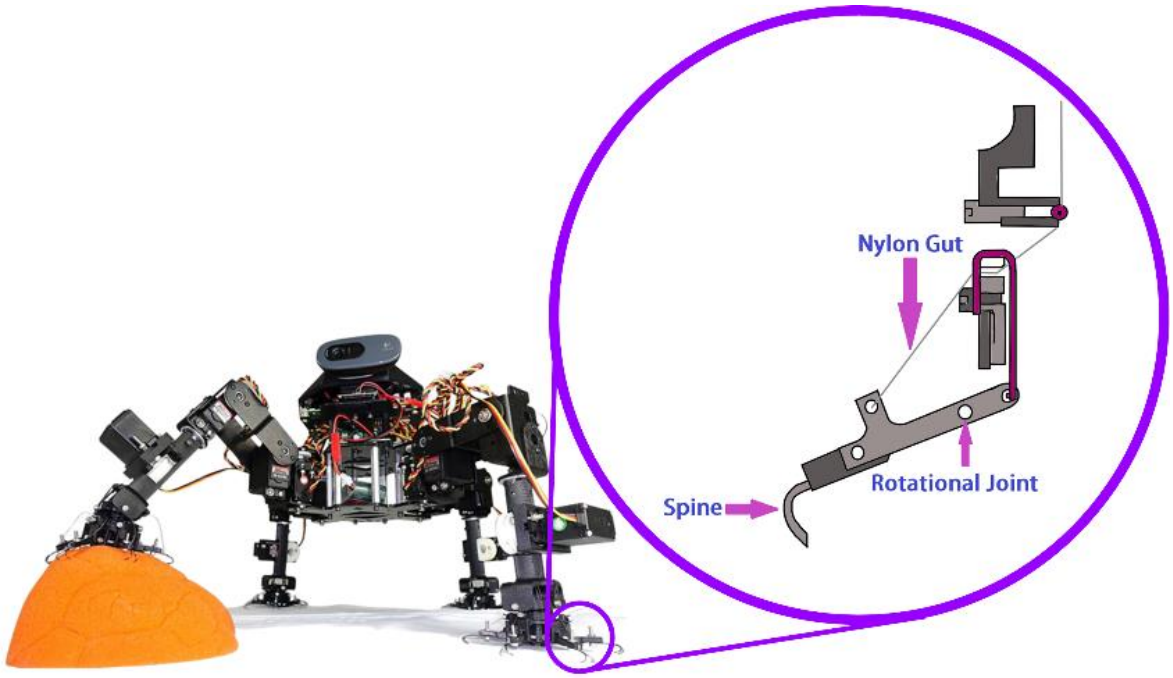

Figure 28 Dual spines that allow the mechanism to clamp to different surfaces

A shortcoming of stiff links is that they require a more significant number of rigid connections than mechanisms with complete constraints. Consequently, specific gripper systems may be bulky. Several writers have employed cable-driven actuation to circumvent this problem. Consider the concept for an open-loop gripper depicted in [48]; the device is a two-fingered, cable-driven hand with underactuated fingers (Figure 29). Each finger is

tendon-driven with a 21-mm pulley diameter and an MX-28 Dynamixel servo capable of generating a stall torque of 2.5 Nm at 12 V. The gripper can accommodate both square and round items. The author evaluated the gripper by measuring the displacement position and orientation using an Ascension trakSTAR sensor located in the gripper's core. The sensor has a spatial resolution of 0.5mm and 0.002 rad for tracking 6-DOF. In addition, the gripper has a stroke of 0 to 103 mm and a holding force of 8.9 N at the fingers. The article's scope is restricted to describing the design, not its mathematical considerations. According to the authors, however, reference [111] presents a library for creating underactuated grippers.

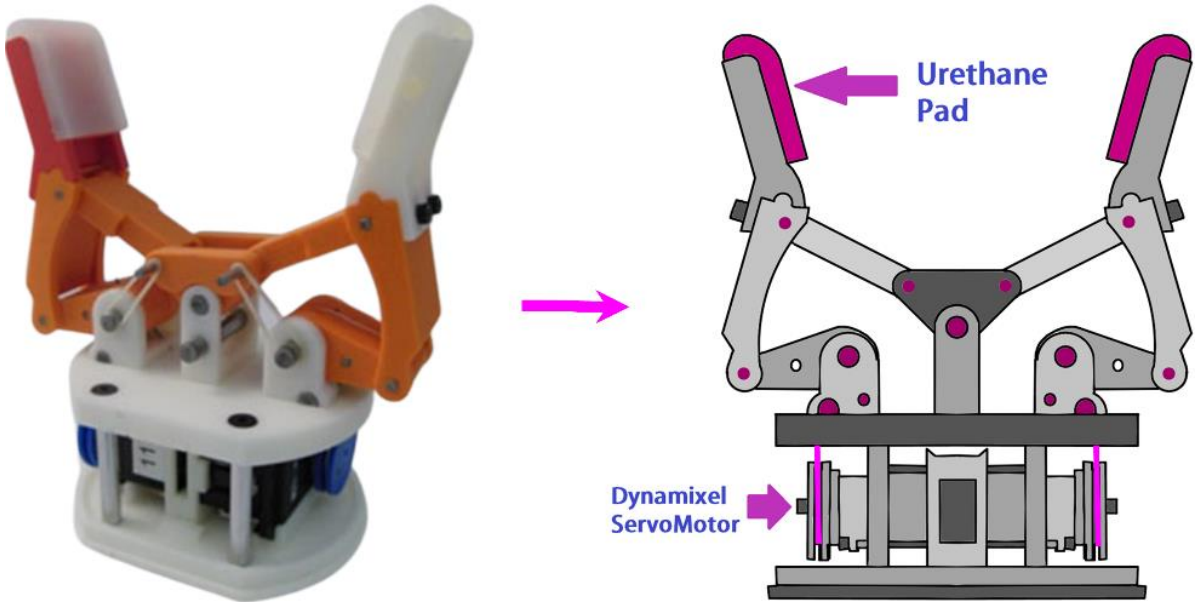

Figure 29 Internal gripper assembly

Another comparable two-fingers underactuated system with cable-driven actuation and active tactile manipulation is described in the reference [49]. The tip is a rubber-like substance with white pins (1 mm in diameter) embedded in its inner surface. The tip is 3D-printed using a multi-material 3D printer (Stratasys Objet 260 Connex), with the solid

elements produced in the Vero White material and the flexible skin created in the rubber-like TangoBlack+ material. An acrylic glass filled with RTV27905 silicon gel separates the electrical components from the tip. A circuit of six LEDs lights the protruding rubber pins inside the tip surface (Figure 30). Object size and form determine the whole range of orientations, which ranges from -34.4 degrees to 32.3 degrees for a cylinder with a 20 mm diameter to 21.8 degrees to 20.6 degrees for a cylinder with a 35 mm diameter.

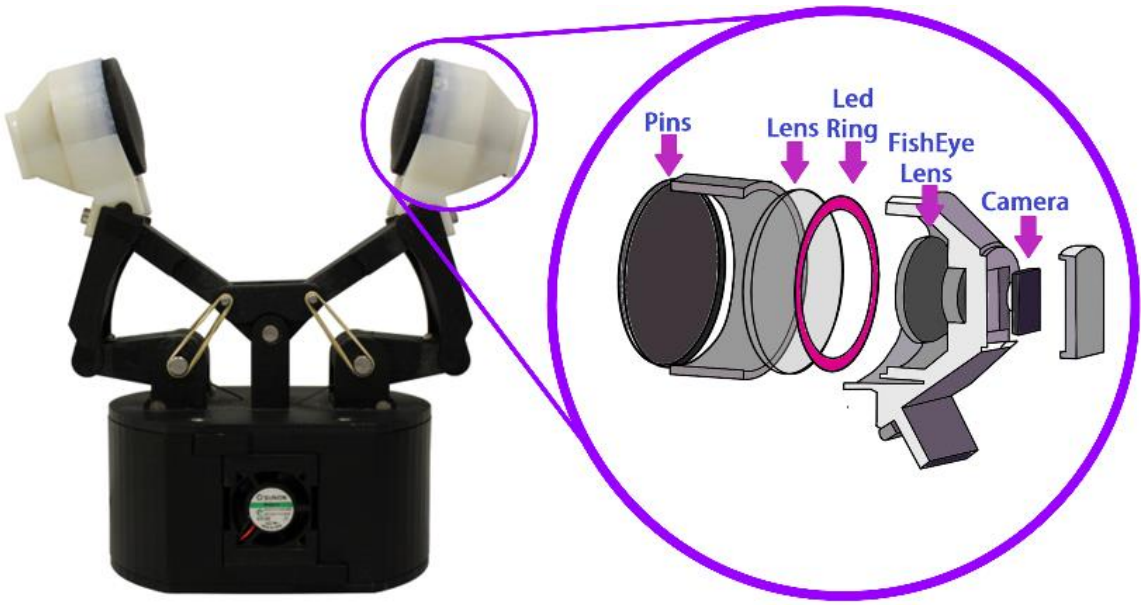

Figure 30 Layers used to use Leds as sensors at the tip of the gripper

For engagement in an unpredictable environment, the authors of [90] designed a gripper with transitional features between a precision pinch and a compliant grasp. Each finger has a minimal number of components for flexion action: one stiff link, one belt, one fingertip frame, and one motor (40 Watt ECX16 motor) (Figure 31). The structure of the fingers enables precise parallel pinching and a highly compliant, pressure-distributed, steady grip. The gripper is constructed from a high-rigidity flexible belt material, while the fingers are

composed of ABS. The gripper's grasping force is close to 13 N, and it can grasp various objects, such as a drill, baseball, hammer, cup, and tape. Kinematics improves the gripper by identifying the ideal lengths for a Compliant Grasping Pose.

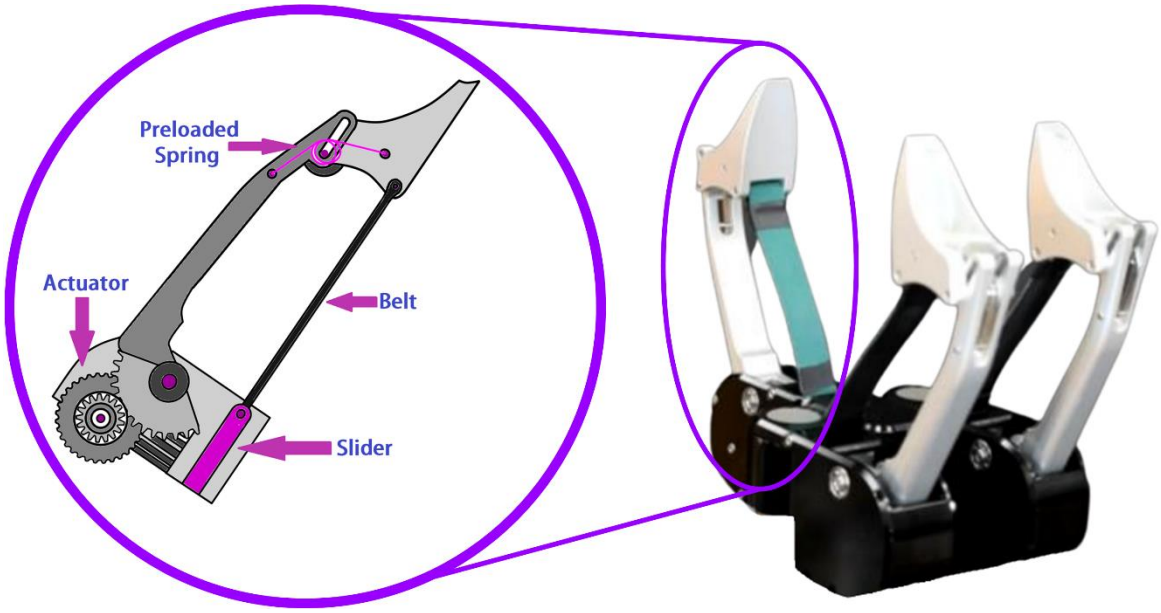

Figure 31 Double actuated gear and belt system of the gripper

In addition, the authors of reference [91] created an underactuated origami gripper for modifying the joint stiffness (Figure 32). This two-fingered gripper comprises shape-memory polymers and is controlled by a tendon-driven Robogami system with adjustable stiffness joints. Without a control method, the regulated compliance of the fingers limits contact pressures to the desired magnitude without requiring Feedback. The lack of a sensor simplifies the gripper's functioning and enables it to grasp delicate and small objects such as an egg, foam, and a penny. For example, the gripper could hold a penny with a minimum diameter of 31.5 mm and a maximum moment of 970 Nmm. By considering system energy, the authors discovered a link between tendon tension and joint angle.

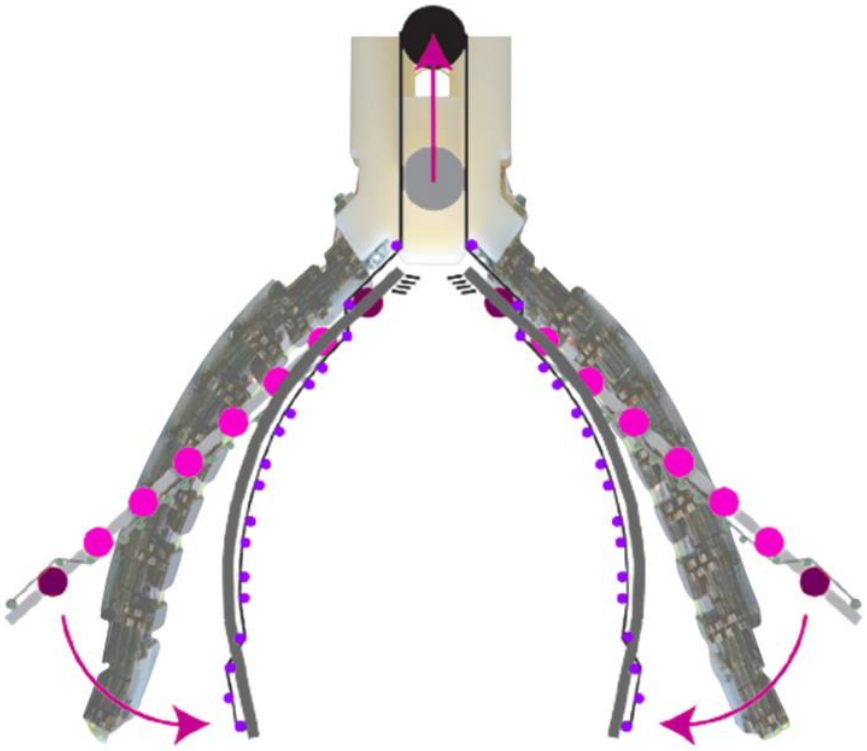

Figure 32 Underactuated origami gripper for changing the stiffness of the gripper joints

In [92], the authors present a physics simulation for the design of a cable-driven robot gripper with a passively switchable underactuated surface based on parameter optimization. The author suggested a gripper with a partially active fingertip surface (Figure 33). In response to the activation of a single motor, a spring-loaded passive switching mechanism produces three grasp modes in series: approaching the object as a standard parallel gripper, pulling items inside the hand with an actuated fingertip crawler, and power grasping the object as an underactuated gripper. The authors successfully proved that a gripper prototype for the proposed structure could pick up a 3-mm-thick sheet and a paperback book off a flat surface. In addition, the gripper's encircling grasp can lift cylinders from a flat surface. This gripper has an operating range of approximately 200 mm and a gripping force nearly linear to the size of the object and greater than 20 N.

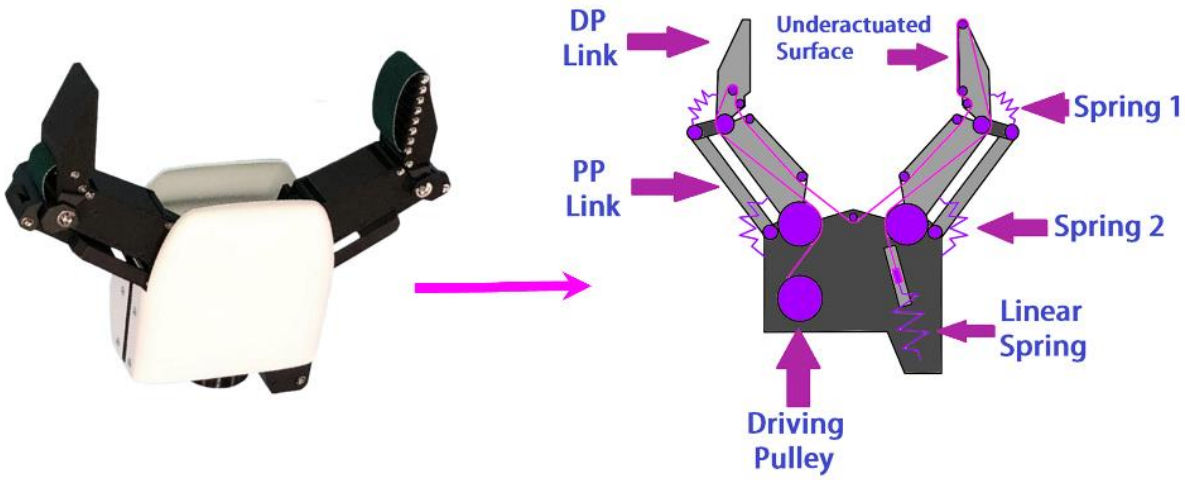

Figure 33 Cable-driven robot gripper with a passively switchable underactuated surface

[45] describes an adjustable three-fingered prismatic gripper with passive rotating joints. (Figure 34). Laser-cut 3 mm Delrin and 3D-printed ABS compose the basic structure of the hand (printed on a Fortus 250mc). Fingers are likewise 3D-printed; the finger pads are Smooth-On VytaFlex 30 urethane rubber castings. Each finger has a passively rotating joint at right angles to the palm that connects the finger's single joint to the prismatic joint. With the rotating joints in place, fingers can passively transition from a spherical to a cylindrical grasp, and the finger joint allows fingers to wrap around the object in the grasp. The article states that the gripper can grasp things with diameters ranging from 17.4 mm to 145 mm, a set of washers ranging from 9.8 mm to 50.8 mm, a credit card, and other equipment.

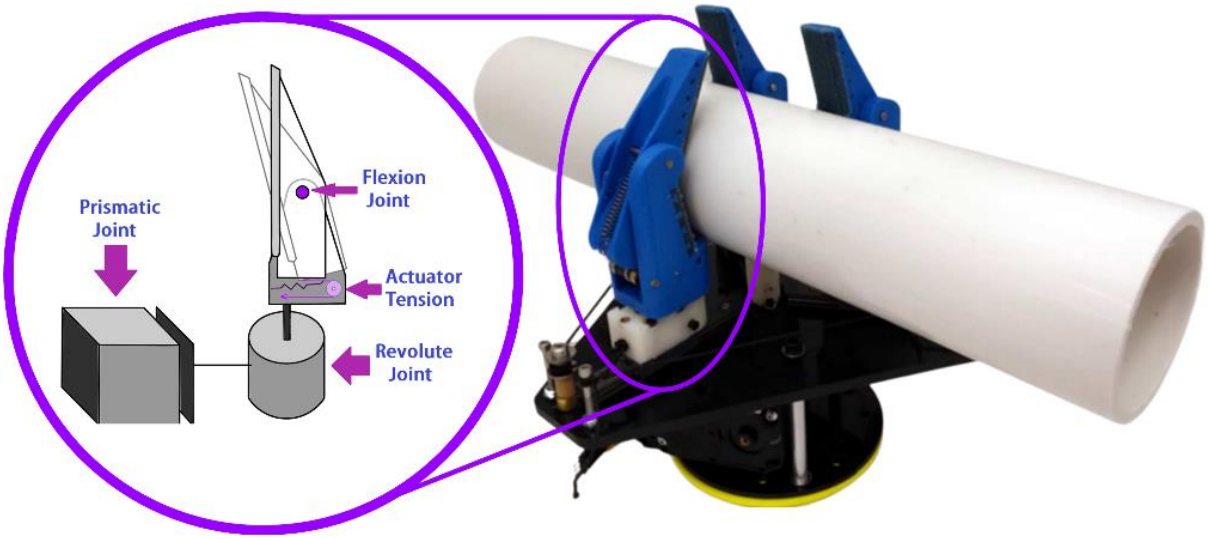

Figure 34 Adaptive three-fingers prismatic gripper with passive rotational joints

In [93], the authors provide a joint-compliant underactuated gripper based on a mathematical description of soft robotic fingers inspired by screw theory (Figure 35). Using the mentioned mathematical model, the designer of a gripper can investigate how elements such as fingertip trajectory, stiffness, contact force distribution, and others affect the gripper's performance. The gripper's 85 mm reach allows it to manipulate cylindrical and spherical objects such as a cup, tennis ball, small box, and other objects. In addition, the gripper is manufactured of ABS and has a holding capacity of 43N.

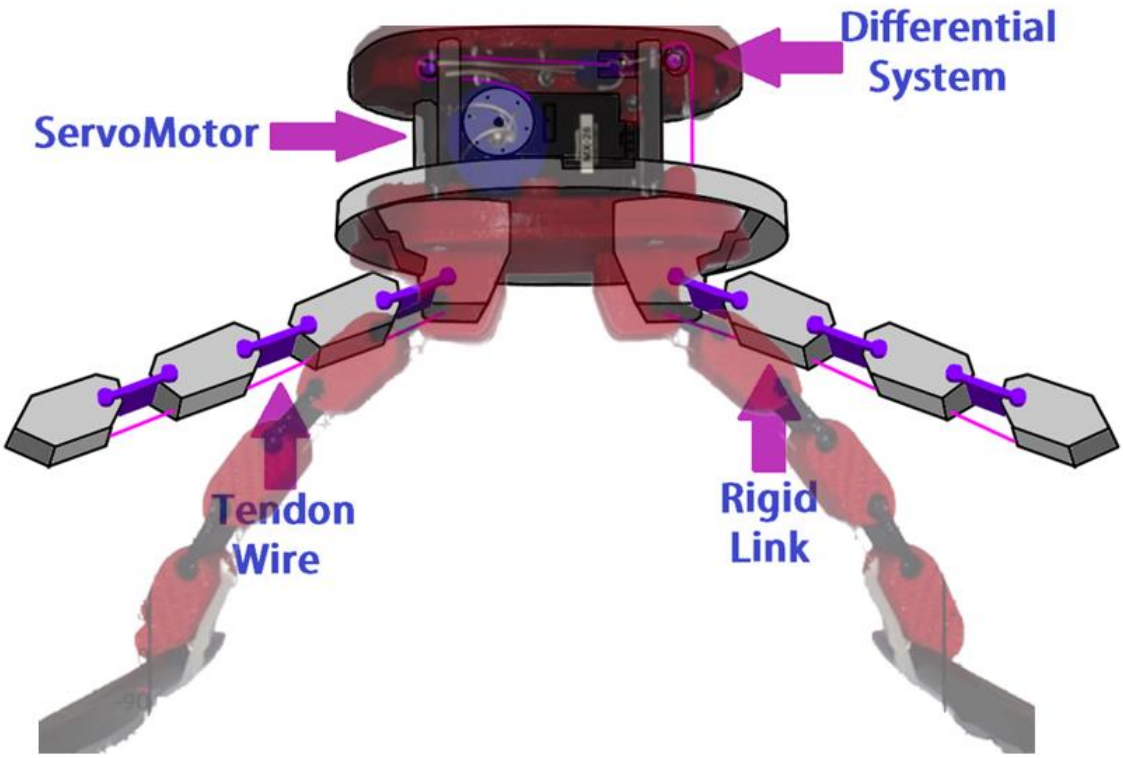

Figure 35 Underactuated gripper exploiting joint compliance

The design and study of a one-of-a-kind robotic gripper combined with a three-phalanx finger for medical applications are presented in [94]. The mechanism has a tiny gripper for picking up small objects (shown in Figure 36) and a big gripper for taking up and transporting heavy objects. This innovative enhancement broadens the application of the gripper to accommodate more routine tasks.

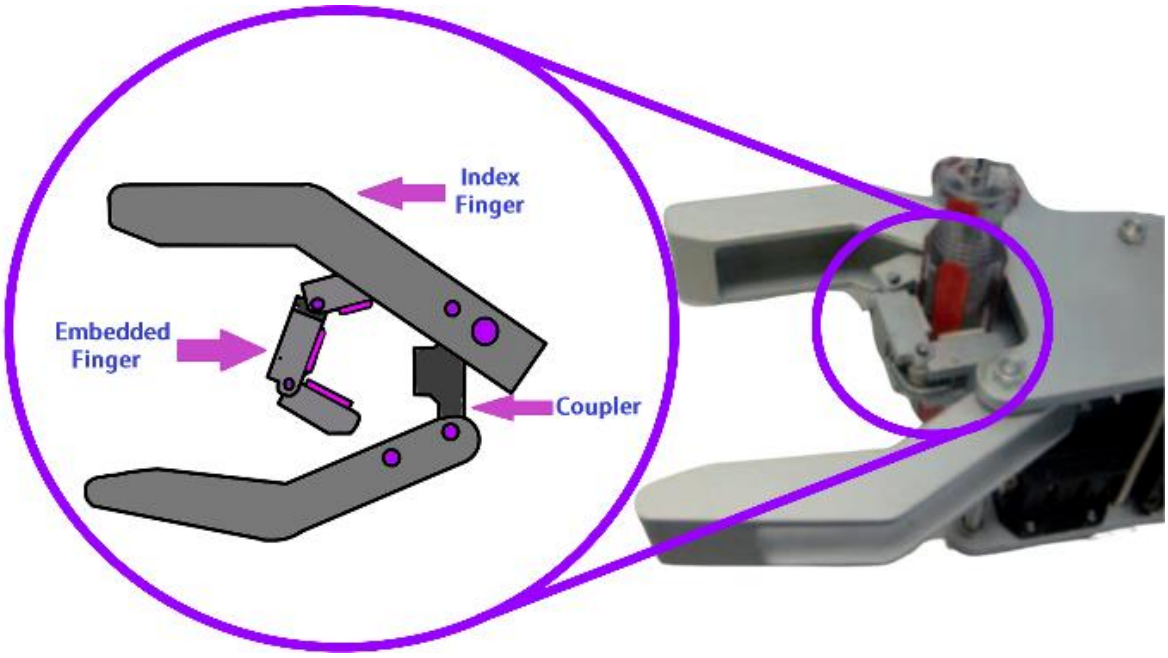

Figure 36 Novel robotic gripper integrated with a three-phalanx finger for medical applications

Other approaches employing rigid connections with linear actuators include the one seen in reference [82], a reconfigurable gripper for robotic autonomous depalletizing for supermarket logistics. The depalletizing gripper has a pair of retractable, rail-mounted prongs and two suction systems, each with suction cups and controlled by a closed-loop controller (Figure 37). The gripper has a 10kg weight capacity and can grasp objects between 15 and 50 centimeters in length.

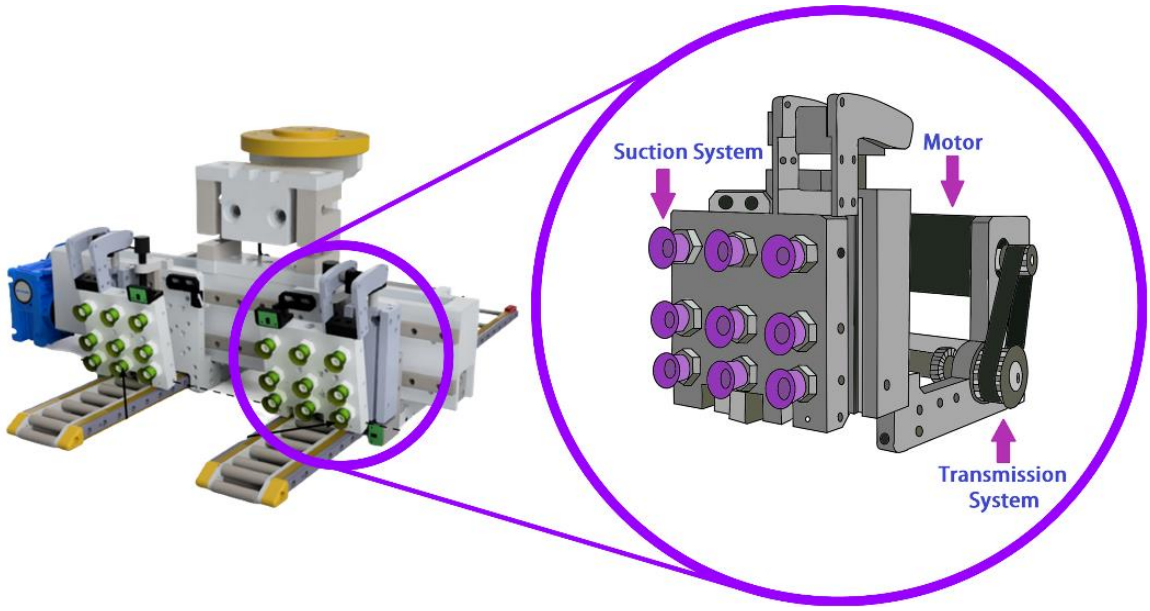

Figure 37 Depalletizing gripper with rigid links and linear actuators

In stiff links, rotary actuators are another type of actuation. [46] hints at an underactuated four-bar link (Figure 38). The gripper is activated by a single actuator (Maxon EC45 70-W) that generates a forceful squeeze regardless of the conditions. Fingertips can slide over curved surfaces with a diameter between 11 and 85 millimeters. The gripper can also manage lightweight goods. The study also includes a static and kinematic analysis in Plucker coordinates to determine the working principle of the actuator. The data were incorporated into a dimensionless link synthesis based on numerous sliding and lifting characteristics.

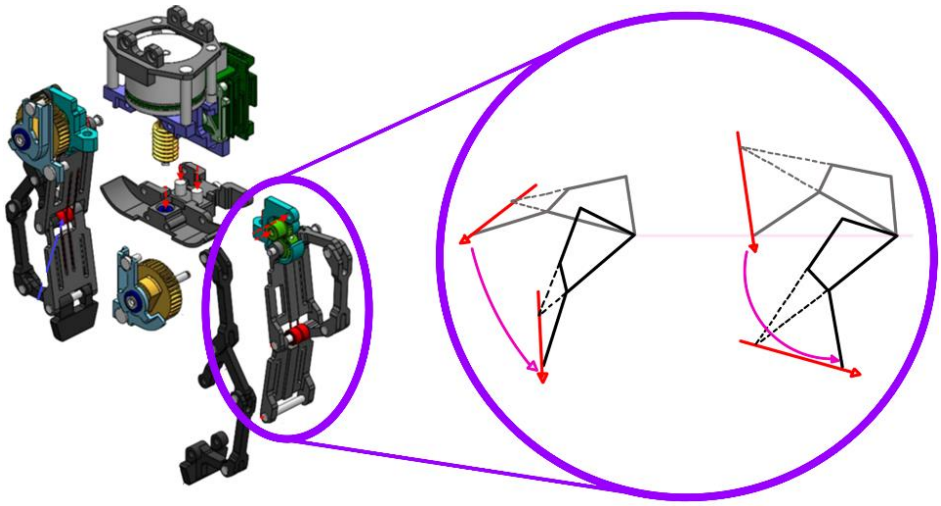

Figure 38 Underactuated four-bar linkage-based gripper

A similar concept is offered in [84] and proposes a 3D-printed robot hand with three linkage-driven, underactuated fingers that can move two or three of its digits (Figure 39). The mechanism of each finger consists of a chain of rigid links that separates into three phalanges. The design of the gripper allows it to interact with a wide range of object sizes and shapes with a consistent 15N contact force, including cylinders up to 81 mm by 19 mm in diameter and spheres up to 70 mm in diameter. In addition, the gripper is equipped with return springs that permit it to return to its original position. The size of the mechanism was determined by optimizing the grip for various objects.

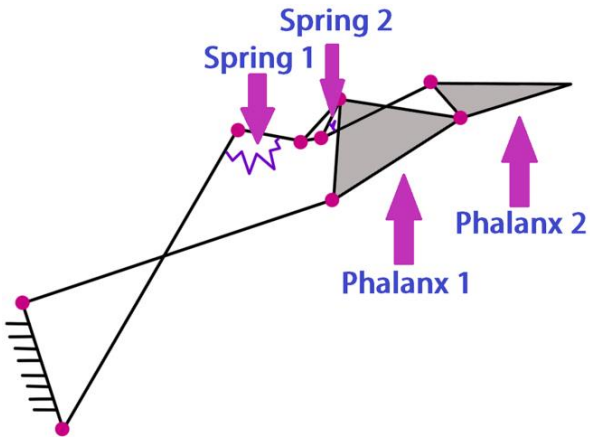

Figure 39 Kinematic representation of one of the three linkage underactuated fingers

Reference [83] provides yet another alternative for a rotational actuator gripper. This work provides a 3D-printed robotic gripper with low actuation for usage in unforeseen circumstances. Each of the gripper's fingers' underactuated mechanism comprises five joints and a single spring (Figure 40). The grippers are made from thermoplastic elastomer (TPE), polylactic acid (PLA), and acrylic block plastic (ABS). In addition, the gripper can grasp several common household goods, such as pencils, bottles, whiteboard erasers, and spherical objects, with a maximum diameter of 75 mm and a maximum weight of 2.5 kg. In order to select the spring, they also conducted a kinematic and quasi-static study of the finger [85].

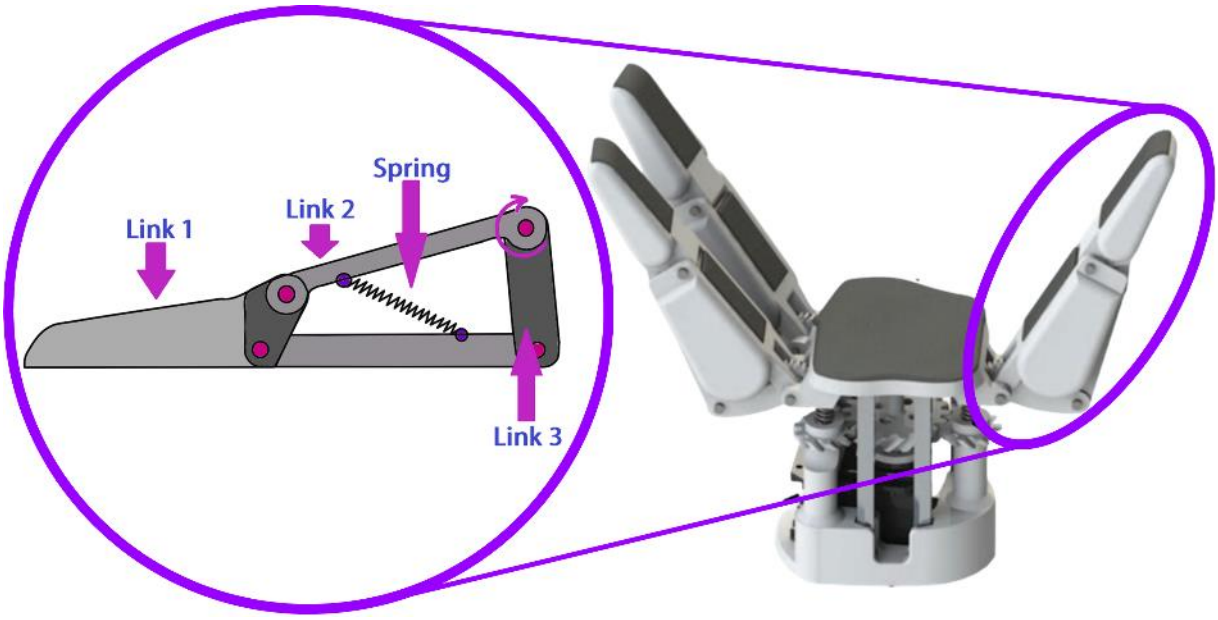

Figure 40 Underactuated adaptative 3d printed robotic gripper for interactions with unpredictable environments

In alternate designs, such as [95], pneumatic actuators are utilized. The authors describe the design of a hybrid robotic gripper capable of gripping large objects using soft origami actuators. The only degree of freedom the proposed actuator possesses is linear translation

along its axis. Due to the repetition of the trapezoid shape, it is relatively simple to construct the geometry parameters required for individualization and linear stability (Figure 41). Polypropylene rubber is used for the actuator body and the bottom cover during the molding process. In order to connect to pneumatic connections, the top of the actuator features an air vent. The gripper comprises a flexible actuator joint and rigid, motion-restricting support components. An analytical model derived from geometric characteristics describes the relationships between the actuator's output force, internal pressure, and axial displacement.

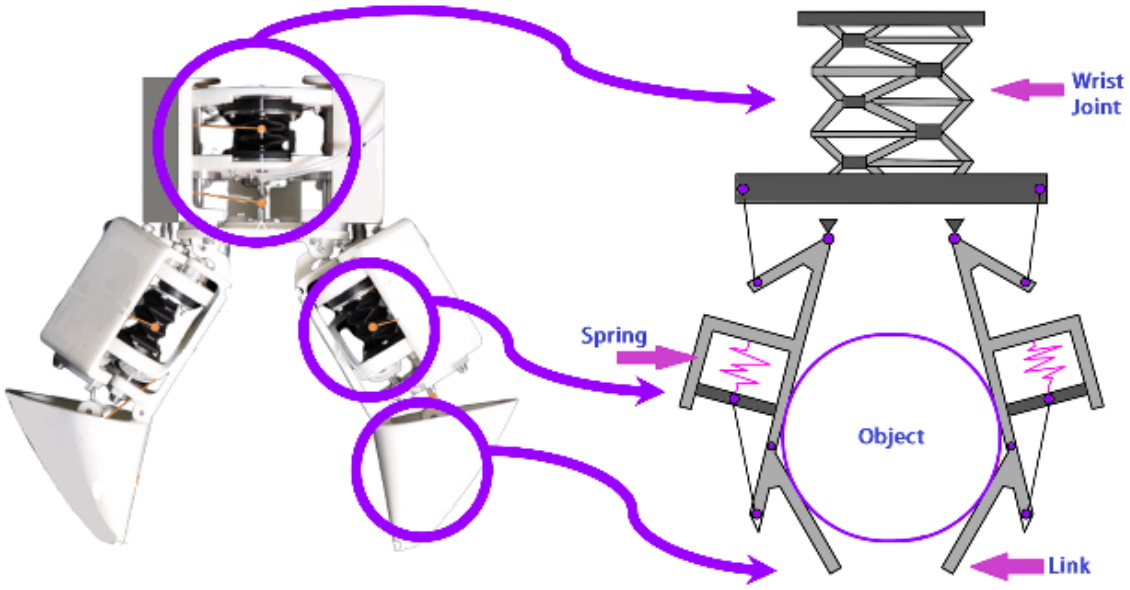

Figure 41 High-payload hybrid robotic gripper with soft origamic actuators

3.3.3 Deformable

3.3.3.1 Single Mass Gripper

Single-mass grippers manipulate objects by altering their shape. Instead of wholly constrained or underconstrained grippers, there is no straightforward one-to-one relationship between deformation and actuator mechanism. Due to this, single-mass grippers can be twisted and curved to ring their target tightly. In addition, this gripper's pneumatic or cable-

driven actuation makes it ideal for a more extensive range of irregularly shaped objects. Although they can manipulate objects, pneumatic actuation may limit the gripper's range of motion, as seen in reference [44], which depicts a three-fingered, pre-tensioned soft gripper for food handling. The actuator consists of a three-dimensional printed soft chamber with a rigid connection and a sealed cover. A prestressing effect is achieved by stretching the soft chamber and then adhering to a non-stretched cover on top (Figure 42). Without inflating the soft actuators, the gripper can achieve a sizeable initial opening with a large contact area. The fingers of actuators are comprised of a rubbery material. The authors utilized a JUN-AIR 3- 4 air compressor and an SMC ITV2030 electro-pneumatic regulator to pressurize the actuator. The 87-mm long soft actuator has a success rate of 80% while picking up 75.2 g objects. To identify the optimal measurements, the author used a finite element simulation.

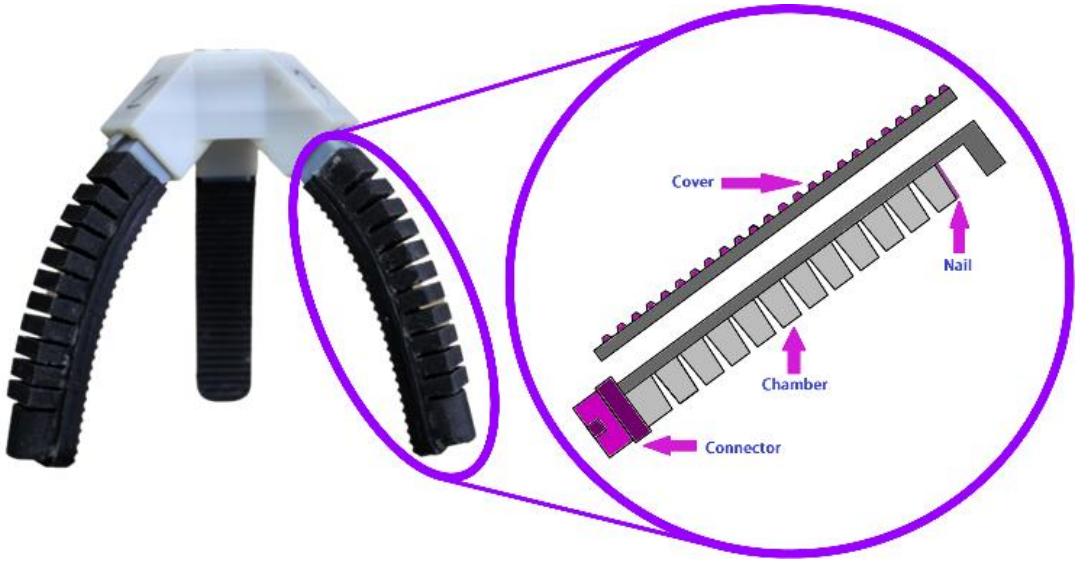

Figure 42 The prestressed soft gripper with three fingers for food handling has a soft chamber with a rigid connector and a sealed cover

Similar issues are experienced by other writers, such as in reference [96], which describes a soft robotic gripper with Microneedles for manipulating fragile textiles. The gripper is composed of an elastomer. The gripper is equipped with four microneedles for securing delicate materials. Once the textile-handling gripper is positioned, a vacuum pump serves as the actuator, deforming the elastomer (Figure 43). While the author does not use a pressure sensor, one alternative is to place a soft pressure sensor into the end of the gripper. However, not only is the vacuum pump bulkier than a typical air compressor, but it also consumes more energy.

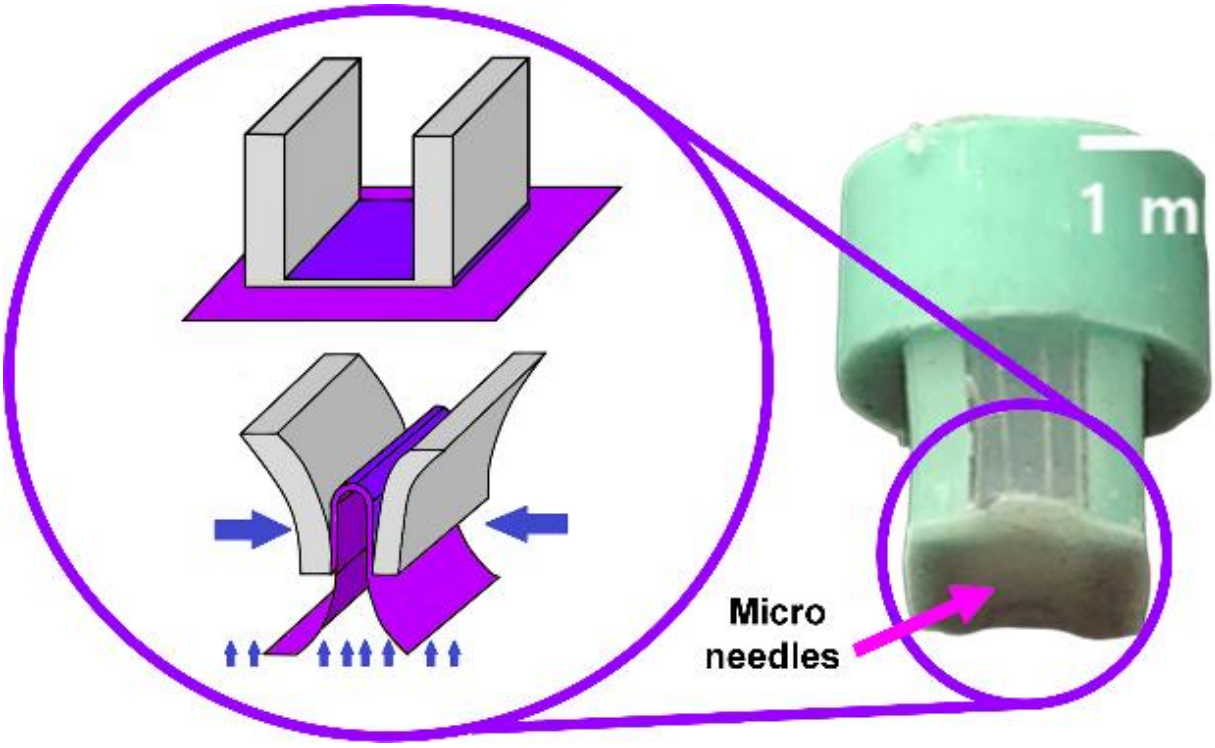

Figure 43 Single mass soft robotic gripper embedded with Microneedles for handling delicate fabrics

Similarly, an origami-inspired SMA actuator-controlled gripper [47] is designed to grasp and carry objects of various sizes and shapes. The design of the gripper was influenced by a flexible suction gripper (Figure 44). The gripper is powered by small shape memory alloy actuators and composed of hard and soft components, allowing it to self-fold into three different forms. The primary objective is to select objects with diameters ranging from 2 mm to 43 mm and weighing less than 5.2 N, encompassing large and small, flat and thin, cylindrical, triangular, and spherical shapes.

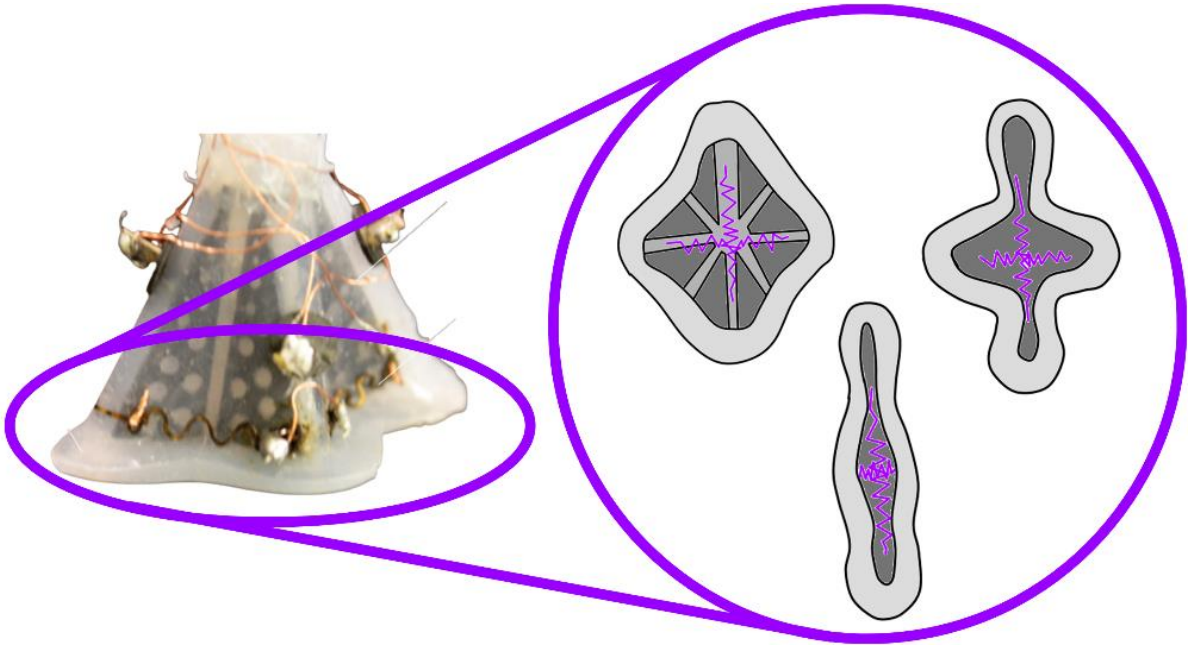

Figure 44 origami-inspired gripper controlled by an SMA actuator and the possible forms that the gripper can take due to the SMA actuators that it has inside

Other approaches use cable-driven actuation to reduce power requirements and increase versatility. However, due to the complexity of the deformation model, managing the gripper's motion becomes difficult.

The writers of [97] present an excellent example of this approach. The Author built a multi-legged gripper with an adjustable adhesion value that resembles a gecko. The dry adhesive technology of the gripper is self-adjusting, so it can easily handle both flat and curved objects.

The system consists of four symmetric adhesive components controlled by one of two adaptive locking mechanisms for compression, rotation, or both. Both adaptive locking mechanisms are height- and curvature-adjustable, enabling them to provide a secure hold on objects of various sizes and forms (Figure 45). The configuration for lock adaption enables shared load bearing for a secure grasp. In addition, the peeling process allows for rapidly separating the adhesive surfaces from the substrate.

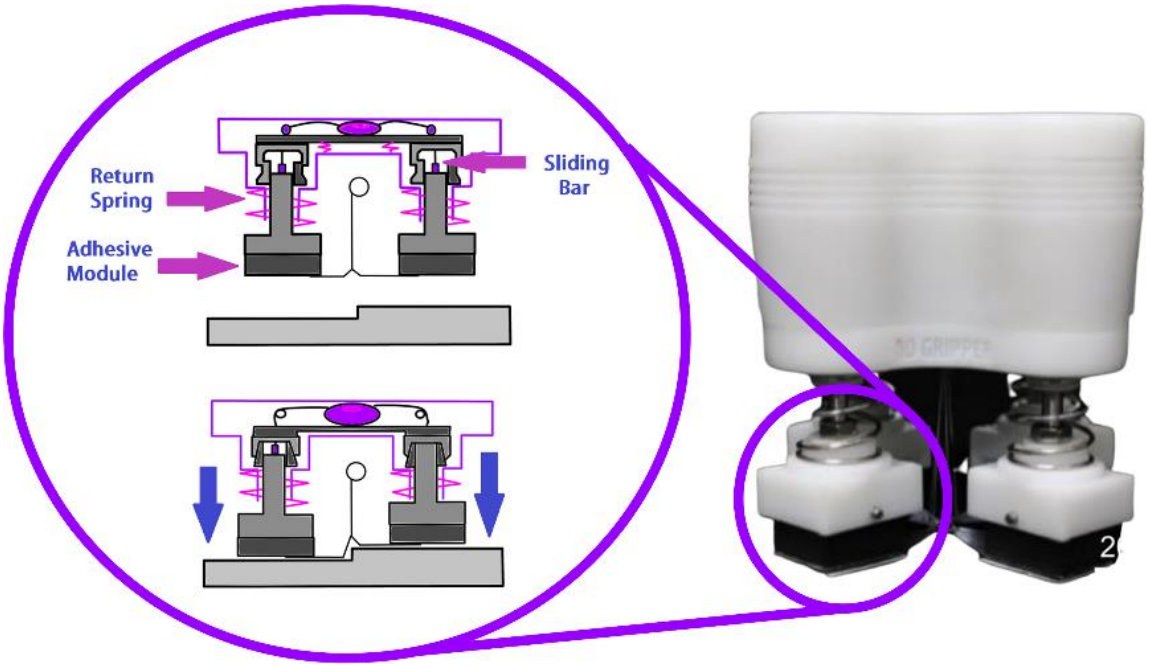

Figure 45 Multi-legged gripper inspired by a gecko with a controllable adhesion parameter generating a firm grip thanks to the adaptability of the gripper

Another instance of a flat dry sticky soft gripper is presented in [98], which draws inspiration from the gecko and cat's foot to construct a soft actuator, micro spine, and bioinspired structure. The redesigned design of the soft gripper makes it more effective overall, whether utilized on a flat or uneven surface. The design models both the proximal and distal phalanges using SMA coils (Figure 46). SMA coils are situated opposite an adhesive layer on the underside of the base layer. Between the two layers is a flexible force sensor that measures

the internal pressure of the finger. As a result, Microneedle fingertips increase the user's gripping strength. The adhesive preloading approach is established using the viscoelastic mechanics model, which links the adhesive's stress with the considered contact area.

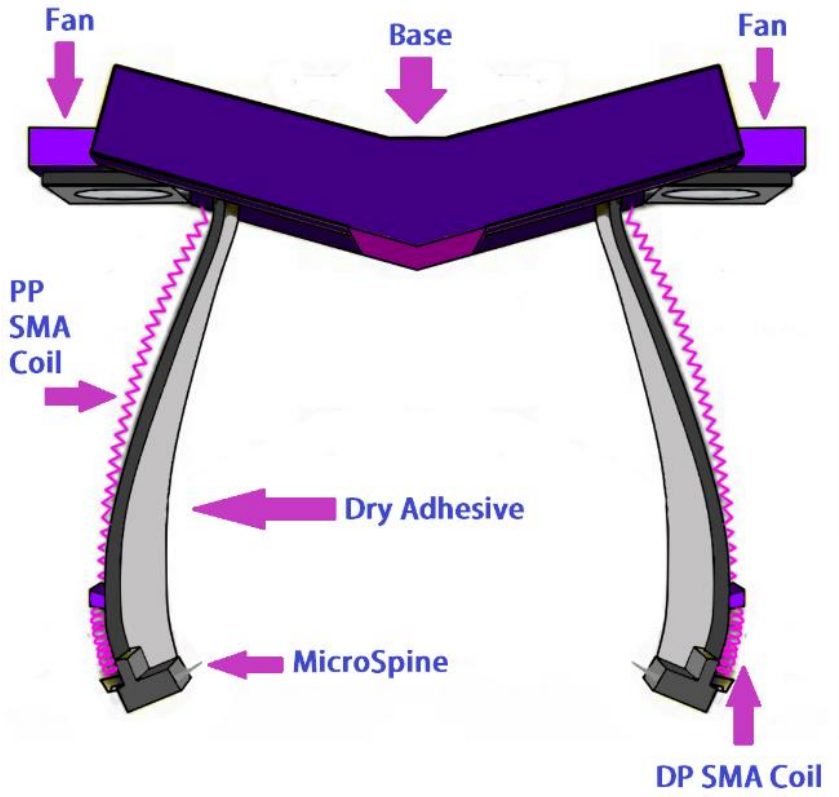

Figure 46 System composed of the SMA actuators, the structure and the cooling system for the soft gripper

3.3.3.2 Single Mass Finger

Individual mass fingers alter their structure to move each finger independently. This gripper mechanism has the same advantages and disadvantages as single mass grippers, including its ability to hold items of various shapes due to the action of the fingers. In addition, the use of many grippers aids gripper control since an increase in the number of grippers permits a more even distribution of the generated forces, reducing the need for a precise control approach.

However, the issue of bulkiness is more pronounced for these types of grippers because the actuator must bend multiple fingers as opposed to a single structure.

A few examples include: The three-fingered soft robotic gripper seen in [43] utilizes particle transmission. A pair of nipper pliers, a roll of tape, a haptic device, and an electric screwdriver can be gripped securely with the fingers. The gripper is fitted with a vertical force sensor that predicts a fingertip-holding force of 20 N. The system was modeled using mass conservation and the concept of incompressible homogeneous neo-Hookean materials [R66–70]. To further enhance the actuators, the authors utilized molded silicone rubber reinforced with woven fiberglass thread and polylactic acid (PLA) (Figure 47). With minimal modifications, the proposed actuator design is based on the extensively investigated fiber-reinforced soft pneumatic actuator [R61->66].

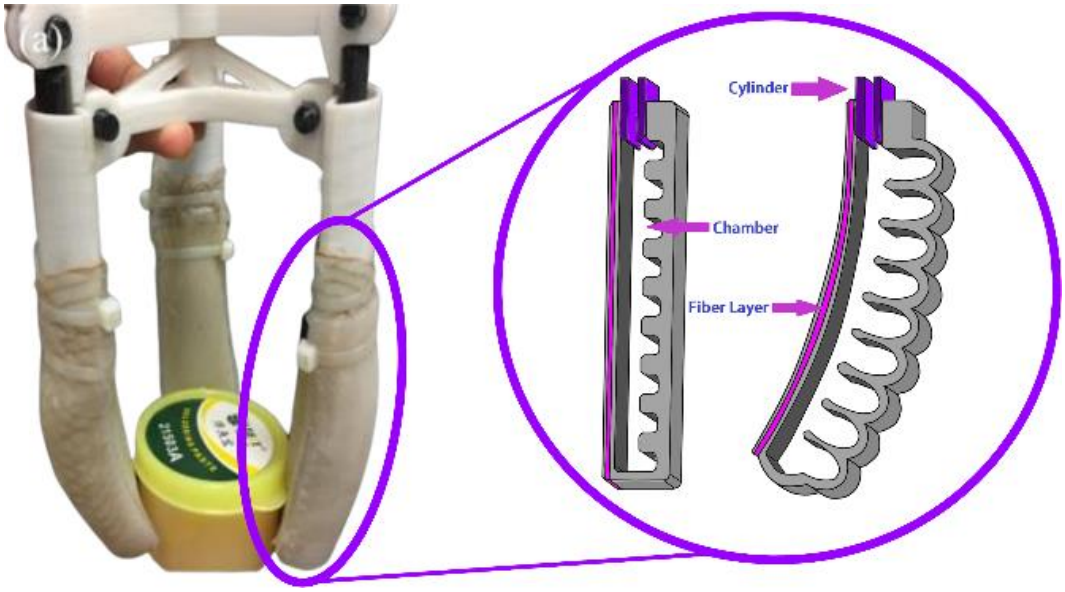

Figure 47 Soft robotic gripper actuated by particle transmission

In addition, [100] demonstrates a soft robotic gripper with an active palm and programmable fingers capable of complex activities such as rolling a pen or filling a glass of water. The robotics application of the gripper includes manipulation, medicine, mobility, rehabilitation, and assistance robots. EcoFlex silicone elastomers are utilized for the fingers of the gripper. Stepper motors, micropumps, and solenoids (Figure 48) are used to control the finger's placement. Each finger contains three independent pneumatic chambers, allowing for extraordinary dexterity. There is a brief mention of optimizing previous incarnations, but no specifics are supplied. However, after doing a workspace analysis, the author calculates the total useable space.

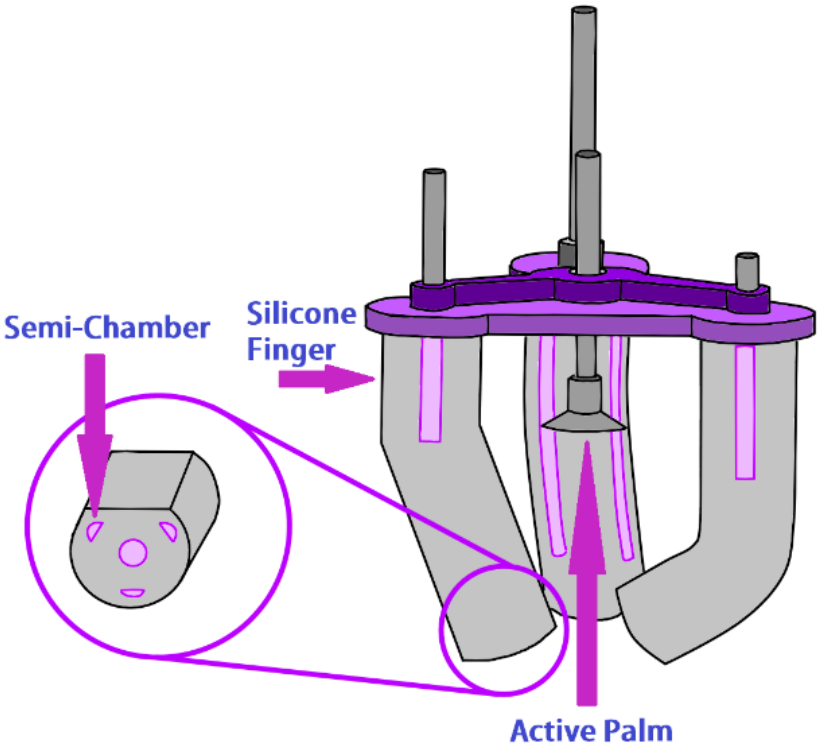

Figure 48 Soft robotic gripper with an active palm and reconfigurable fingers

In addition, the soft pneumatic actuators in the soft gripper illustrated in [99] are pre-charged. A silicone chamber and a single air tube constitute the pre-charged pneumatic (PCP) system of the PCP gripper (Figure 49). The silicone casing has a pressure-regulating check valve. Under strain, fingers with tensile cables or tendons can be reshaped. The body of the actuator is made of silicone rubber, and an inextensible layer is added to the bottom of the actuator with a 150 mm range so that it can grasp fragile objects such as tomatoes or eggs.

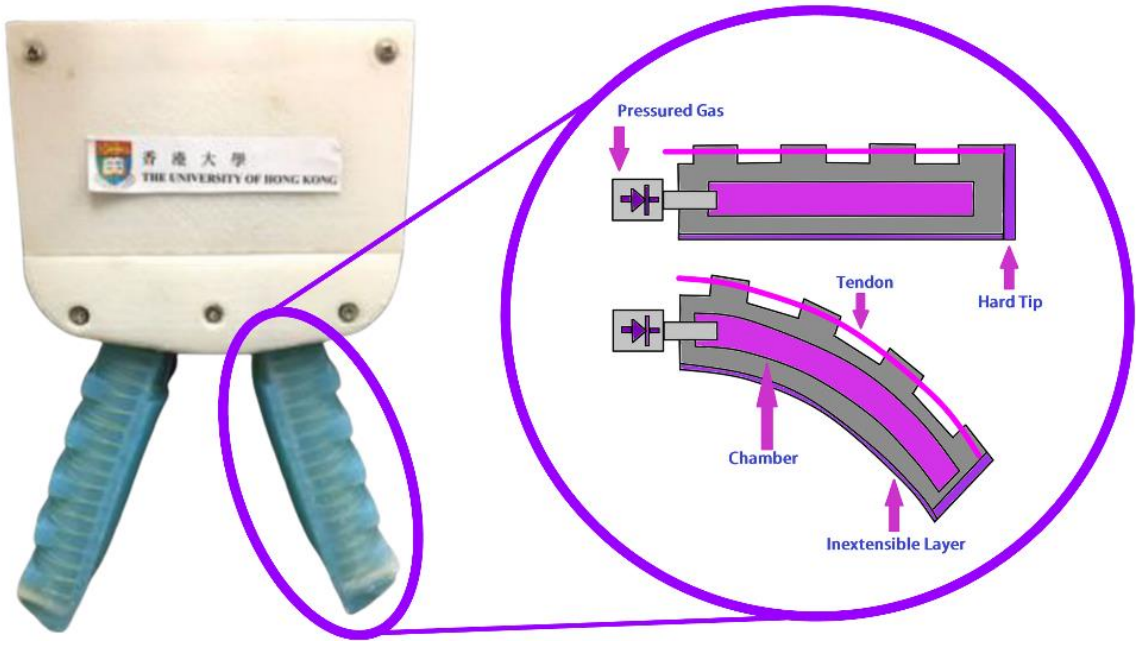

Figure 49 Soft gripper using a tendons to pre-charge the pneumatic soft actuators

In [101], the second type of gripper composed of rigid and malleable materials is found. The position of the gripper is controlled by a single pressure chamber within. This design improved parameters such as the degree of bending, the ratio of the rigid structure, the longitudinal strain by adjusting the chamber's geometry, and the relationship between soft and rigid materials in the same finger to concurrently improve fingertip force and actuation

speed (Figure 50). In addition, the gripper is operated by two pneumatic pumps (DAO-370A), offering a sizeable operational envelope suitable for remote control. The gripper has a capacity of 28.7N, allowing it to handle objects such as a banana, coffee cup, or drill driver. The design parameters were optimized using the finite element technique (FEM) and a simulation based on the hyperrealistic Mooney-Rivlin model.

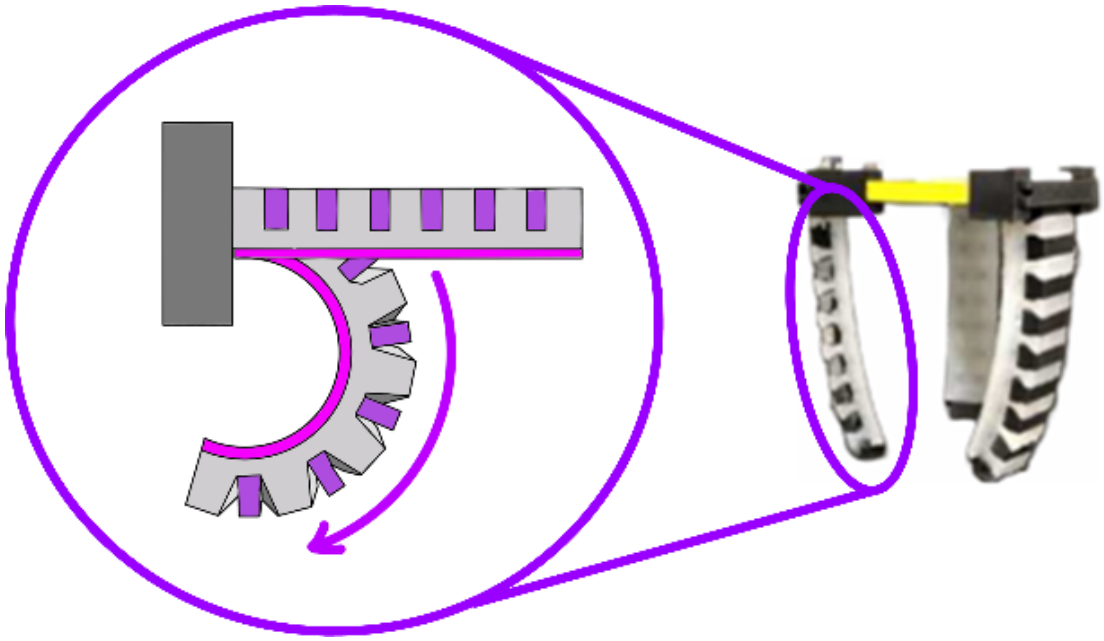

Figure 50 Representation of the circular path that the fingertip travels when pressure is applied in its chamber for the soft gripper

Several versions have been developed for medical applications, such as the pneumatically propelled gripper with retractable, telescoping fingers described in [102]. Two tiny air pumps with low pressure activated this silicone rubber gripper. In addition, an eight-camera optical motion capture system was utilized to detect gripper angular displacement (Figure 51). For increased precision, the upper surface of the actuator, where the gripper includes retroreflective markings, is accurately measured. The range of motion of the soft actuator is

adjustable from 0 to 135 degrees. The maximum grabbing power of the gripper is 14.53 Newtons, which is sufficient for holding a medium mustard bottle, water bottle, egg, or drill driver. An FEA model of the soft actuator deformation was developed to comprehend the structure's inflation behavior.

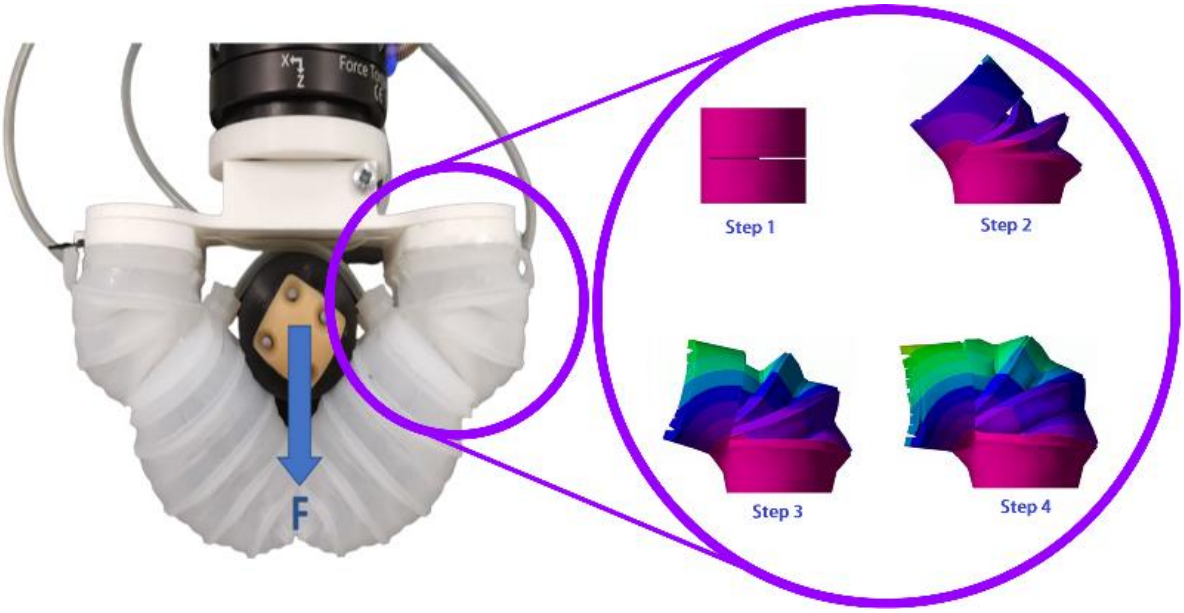

Figure 51 Deformation sequence captured by a camera to track movement at specific points on the gripper

The pneumatic two-finger soft robotic gripper illustrated in [103] is also capable of enveloping and pinching gripping modes, allowing it to manipulate a wide range of objects (Figure 52). This gripper consists of several chambers and passages. In addition, the gripper comprises a rigid elastomer main body and a base. It combines a height-adjustable chamber with two pneumatic actuators that employ two distinct modules each. The most significant bend radius of the gripper's working zone is 250 degrees, although it can only support a maximum load of 4 Newtons. Internal to the finger is a computerized force gauge that measures the force within the chamber. Predominantly, FE analysis and testing were performed to analyze the pinching-grabbing mode.

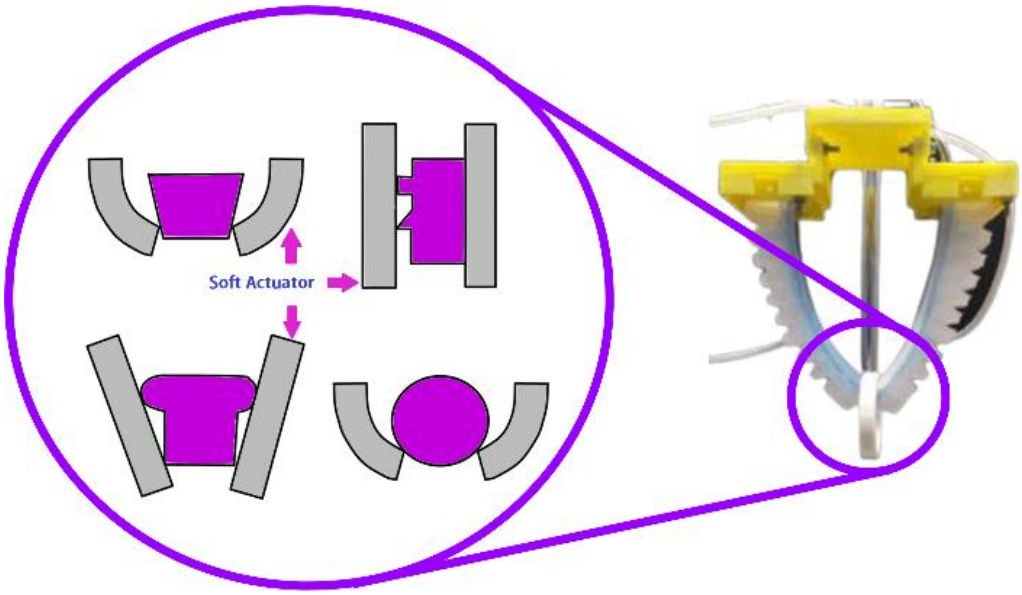

Figure 52 Different grip modes for the pneumatic two-finger soft robotic gripper and different shapes and objects

Alternative techniques, such as the one reported in [104], combine a soft robotic gripper with a Gecko-inspired adhesive to deal with rough or dirty surfaces with low adhesion. Gecko-inspired grippers use fluidic elastomer actuators with a circular cross-section as the actuation mechanism (Figure 53). Actuators made of gecko elastomer augment the control authority of manipulation tasks. More significant ultimate grip strengths on various objects allow for the manipulation of larger objects and faster accelerations of moving objects. This characteristic is particularly advantageous for time-sensitive operations such as picking and placement. The gecko elastomer actuator requires little input energy and may be activated rapidly despite its use of adhesion-enhanced friction for stronger grips.

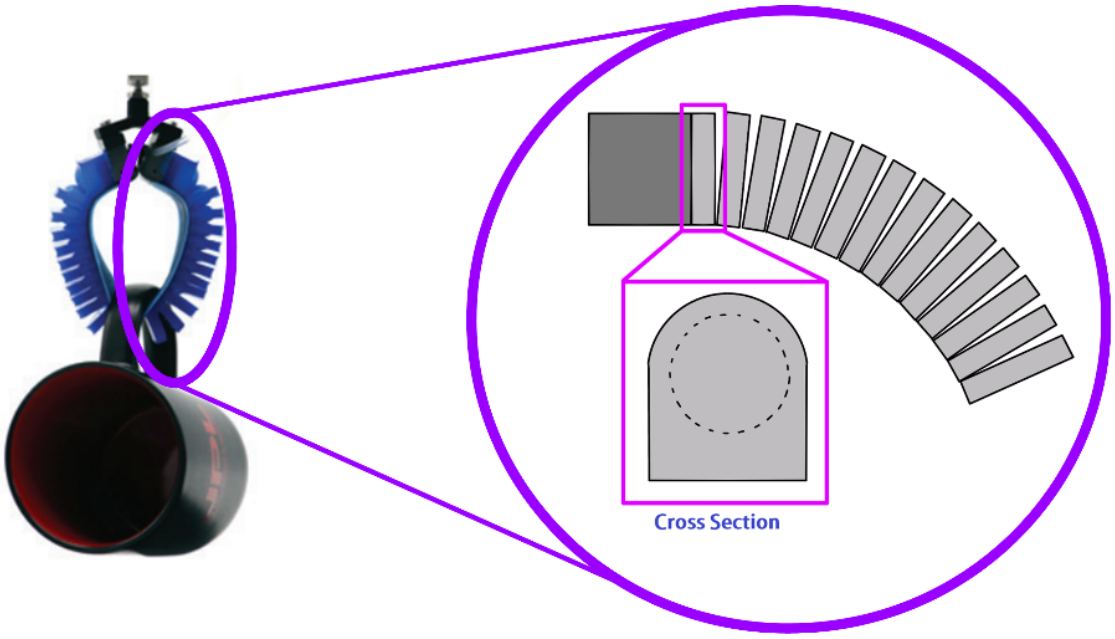

Figure 53 Cross-sectional area used for elastomer actuation of gecko-inspired gripper

In [105], the deformation properties of water hydraulic flexible actuators are investigated alongside an underwater gripper. The pliers are fitted with three fingers for a secure grip. The inner skeletons of each finger are composed of 3J1, 3J21, TC4, and Carbon fiber, with 1 mm wall thickness and 30 mm and 80 mm lengths for the first and second knuckles, respectively. The representation of the workspace is a nonlinear equation. When the inlet pressure is 0 MPa and 10 MPa, the equation states that the minimum and maximum deformation of the flexible actuator are 0 mm and 0.20213 mm, respectively. The author examined how varying the intake pressure, knuckle length, wall thickness, inner skeleton, and exterior surface material affected the deformation properties of the flexible actuator using simulations. Figure 54 depicts the theoretical deflection of the gripper's internal bar and the subsequent impact on the gripper's surface coating. According to the authors, gripper deformation is mainly determined by wall thickness and distance between knuckles.

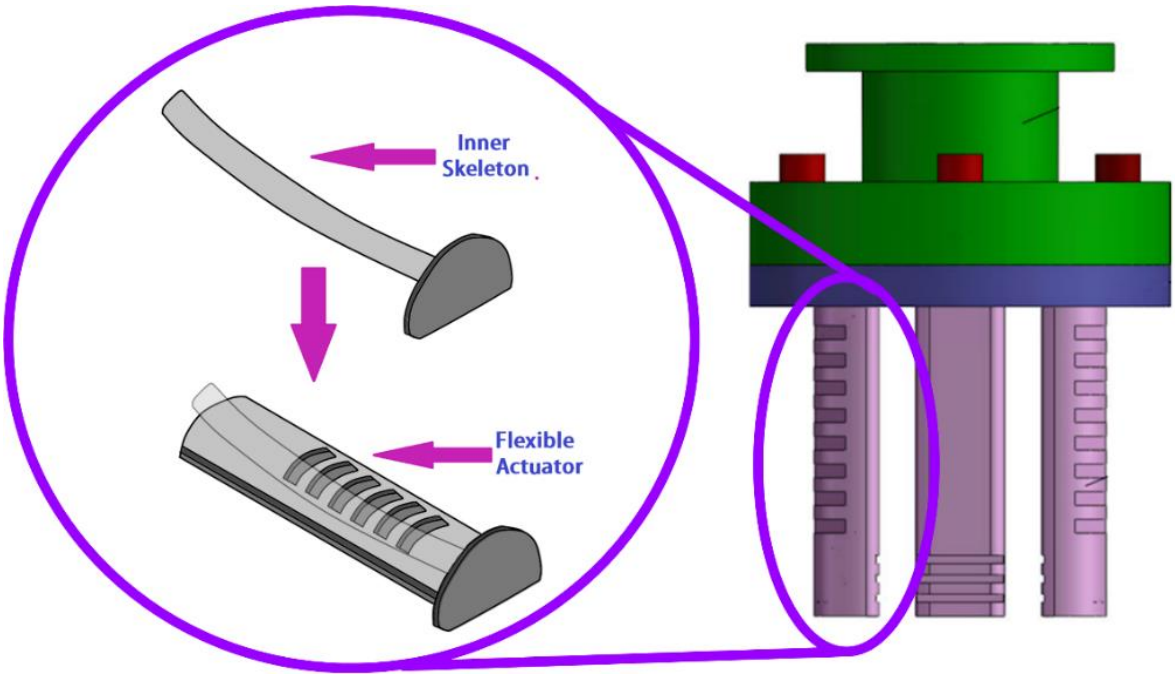

Figure 54 Theoretical deflection of the internal bar of the underwater gripper and its repercussion on the external coating

3.4 Application and Object-Based Classification of Grippers

3.4.1 Grasped Objects

Table 7 illustrates the variety of sizes and materials that robotic grippers have gripped. This category includes textiles, electronics, pebbles, delicates, and even food. The subcategory Daily Objects includes items such as pencils, books, baseballs, and coffee mugs. In addition, the graph demonstrates that the most frequently utilized testing bits are of medium size, irregular shape, and delicate composition.

Table 7 Variety of sizes and materials that robotic arms have gripped

Main	Sub	Papers
Size	Small	[68], [75], [79], [91], [112]–[114]
	Medium	[37], [38], [42], [43], [47], [49], [89], [106], [107], [115]
	Large	[82], [116]
Shape	Circular	[39], [49], [63], [65], [67], [71], [81], [98], [103]
	Squared	[82], [117]
	Irregular	[44], [47], [48], [51], [66], [78], [87], [88], [91], [97]–[100], [105], [107], [115]
Material	Delicate	[37], [43], [44], [63], [65], [75], [76], [80], [107], [114], [118]
	Fabric	[72], [73], [79], [77], [96]
	Electronic	[64], [112], [114]
	Rocks and Soils	[41], [104]
	Food	[44]
Daily Objects		[39], [46], [50], [51], [69], [84]–[86], [90], [93], [95], [101], [102]

3.4.2 Gripper Applications

Table 8 lists the most important uses of robotic grippers from the texts analyzed. Pick-and-place object manipulation is the most common application, followed by force- and position-based feedback control for handling fragile objects. The applications cover a wide range of disciplines, from industry and medicine to space exploration and prosthetics, with fewer pages devoted to each topic.

Table 8 Most important uses of robotic grippers

Application	Papers
Pick and place	[42], [47], [50], [65], [67], [68], [101], [106], [112]
Holding objects	[114]–[116]
Precision force and position control	[48], [63], [66], [73], [90], [113], [115], [117]
Grasping	[39], [51], [71], [81], [107], [117]

Manipulation	[37], [42], [44], [48], [49], [69], [77], [79], [83]–[85], [87], [88], [100] , [45], [46], [63], [64], [67], [72], [75], [92], [95]–[97], [103]
Robotics	[43], [44], [75], [96], [98], [100], [101], [103], [104], [106]
Underwater robotics	[105]
Industrial	[65], [67], [75], [82], [114]
Medical	[100], [102]
Unknown environment	[37], [69], [76], [83]–[85], [87], [88], [90], [93]
Prosthetic hand	[69], [71]
Space exploration	[41]
Teleoperation	[101]

3.5 Review Summary and Selected Mechanism

The majority of robotic grippers released in the previous five years are analyzed in this chapter:

Different grippers are categorized differently depending on factors, including the number of degrees of freedom (DOF), the type of actuation used, the design philosophy, and the item being grasped.

The benefits and drawbacks of each categorization criterion are compared and contrasted to shed light on which gripper design offers the most versatility.

Now, to sum up this chapter's key findings:

First, the grabbing forces need to be accurately sensed. Engineers utilize deformable grippers to prevent the breakage of delicate goods.

Second, object gliding is a problem since it complicates the control technique. Gecko-inspired grippers, which have changeable friction, are one answer to this problem.

Finally, passive-compliant mechanisms are another alternative for deformable grippers since they provide an additional degree of freedom (DOF) that may be used to improve the gripper's maneuverability. In addition, the output force of passively compliant mechanisms, particularly those constructed with stiff connections, is sufficient for manipulating items of modest weight.

According to our findings, a rigid link underactuated mechanism with a gecko-inspired surface is the most versatile gripper design for a wide range of item weights and forms. The only disadvantage of this use is that the gecko-inspired surface's friction-gradient abilities may degrade if exposed to environmental pollutants.

Next, is presented Table () that shows a summary of this chapter:

Table 9 Grippers categories summary

Type	Description	Max Force	Max Range	Object
Completely constrain	This type of mechanism can exert greater forces, which is why it is especially used in applications where heavy objects must be moved. However, it cannot be attached to different shapes with ease.	These mechanisms can support very heavy objects (more than 10 kg).	The ranges depend on the application, but being rigid, they have geometric limitations due to their mechanism, so they have a range of movement between 2.2 mm and 170mm	They are excellent at holding rigid objects. They can also hold more fragile objects if they have a force sensor. However, they are not recommended for this application.
Underconstrain	These mechanisms offer a balance between flexibility and strength. Possessing rigid joints, it can support heavy weights while adapting to most objects' shapes. As a result, it is ideal for applications where the environment is uncontrolled or unpredictable.	They have a maximum descending load, up to 5 kg.	They have a descending range from a few millimeters to 120 mm. But, again, this range will depend on your design and application.	This mechanism can grab a wide range of objects such as a glass of water; pill bottle, book; smartphone; pringle; shoes; cereal boxes; apples; bread, among many others.

Deformable	In contrast to the two previously mentioned mechanisms, this one cannot exert large amounts of force. This could be an advantage or a disadvantage, depending on the application. However, being flexible, they can adapt to all shapes, and their lack of strength is a positive factor when holding fragile objects.	They have little carrying capacity, ranging from grams to a few kilograms.	By being able to deform, they can twist their fingers backward, giving a much greater range than previous mechanisms. Some of these grippers can hold as much as a pill, up to a soccer ball (between 8mm and 200mm).	It practically conforms to the contour of the object you want to hold, no matter how irregular it is. This includes amorphous objects, such as rocks or any complicated surface.

CHAPTER 4

GAR DESIGN

4.1 Design Methodology

This chapter detailed the development process and design of the intelligent Robotic Gripper (GAR). With a simple, minimal viable design, this robotic gripper can grasp various items in form, size, and weight. First, initial design objectives were formulated, focusing on grasping concepts. For the same reason, the research prototype has been updated with a few changes to the original goals to give it the robustness it will need throughout the testing phase. Next, the design requirements were locked down, and a CAD prototype was prepared. Next, the robotic gripper was manufactured using conventional machining and fast prototyping techniques. Finally, the UWM-BioRobotics Lab's current robot arm system was prepared to accommodate the gripper, connected through a custom circuit board.

4.2 Design Goals

Design constraints were set to build GAR as a minimum viable solution for a functional robotic gripper, including limiting each finger to only one active degree of freedom (DoF) and one passive degree of freedom. These DOF limits will allow the finger to accommodate itself depending on the type of object it is grasping. It also makes the gripper’s mathematical modeling simple, allowing more focus on the mechanical design. The design objectives selected are listed below:

a. An underactuated mechanism with one active degree of motion
b. The range of motion of the entire robotic hand should cover most of the objects declared in Table 4
c. Should be able to perform the 3 Robotic Grip Types from Figure 2
d. Should hold objects up to 5-kilograms weight in horizontal mode and 1 kilogram weight in vertical mode.

Additionally, some modifiers to the above goals are included for the research prototype. These modifications are added to ensure a rigid and robust finger while operation mode is performed during the testing phase. The modifiers are:

a. Use of relatively thick and wide links in the internal mechanism of each finger, fabricated with aluminum alloy to ensure low deflection and high rigidity.
b. Use high torque capacity linear motors to reach the forces required to grab objects in vertical mode.
c. A high factor of safety in fasteners and mounting mechanisms.

These enhancements reinforce the system sufficiently such that even a large motion failure, deflection, or elasticity during testing does not threaten the integrity of the fingers. However, considering the time and materials involved, plastic will be used to create some components. Therefore, the plastic parts are not directly connected to the primary mechanism, nor will they bear most of the mechanical load during the tests.

4.3 Design Specifications and Component Selection

The following components and component specifications have been finalized based on the aforementioned design objectives:

a. ***Materials***: The mechanical components are made of Aluminum 6061 alloy. This material allows the gripper to hold objects up to 5kg weight, while quick prototyping plastic parts are used for the shell and the outer surface of the gripper. In order to recreate a CAD model into a functional prototype, the 3D printing process was selected. Polycarbonate is the chosen material to print because of its mechanical properties. However, some other parts were made by the tank photopolymerization process because of the complexity and the great detail needed. Moreover, to resist the loads inside of the mechanism, steel screws were selected and tested, from 2mm diameter to 4 mm diameter for the connection points.

b. ***Motors:*** For the actuation of each finger, we employed a set of Coreless DC Motors with an integrated lead screw mechanism to convert the rotational motion into a linear actuation that allows a maximum applied force of 200N at under 20% Duty Rate. The selected motor for each finger's active degree of freedom is The MightyZap 12Lf-100-30. Detailed specifications for these motors can be found in Appendix A. In addition, a Built-in potentiometer (absolute position sensor) is integrated inside the motor to ensure high-resolution sensing of the lead screw position. Table 10 shows all the motor’s sensor specifications:

Table 10 Motor's sensor specifications

Position Sensor		**Absolute Position 10kΩ Linear Potentiometer Unidirectional**		
Mechanical Backlash		0.03mm (30µm)		
Rod Type		Metal Alloy Rod		
Motor	Motor Type	12DC Coreless Motor / 33.6W (Stall)		
	Input Voltage Range	DC6V -13.0V		
	Motor Speed	26500±10%rpm (At Rated Voltage & No Load) / 23500±10%rpm (At Rated Voltage & Rated Load)		
	Stall Torque	≥95g.cm		
	Motor Current	At No Load	At Rated Load	Max(Stall)
		≤ 50mA	≤350mA	2.5A
Recommended Duty Cycle		At Rated Load	At Max Applicable Load	
		Max 50%	Max 20%	
Audible Noise		Approx. 50db at 1m		
Current Accuracy		IP-54 (Dust & Water Tight)		
Position Sensor				
Size / Weight		57.4(L)x29.9(W)x15(H)mm / 48g		
(Excluding rod-end & hinge)				
Operating Temperature		-10℃ ~ 60℃		
Cable		0.08×60 (AWG 22), 30cm (2 from Motor, 3 from Potentiometer)		

c. ***Electronic control system and motor driver:*** A custom circuit board was designed to enable the possibility of connecting the robotic gripper to the UWM-BioRobotics Lab's current robot arm with a minimum number of modifications. This Board contains an ATmega328 microcontroller embedded into an Arduino board that allows communication with the existing robotic arm systems. The circuit board also contains

ultra-small DC-DC 4R7 converters that step down the power supply voltage from 24V to 12V and 5V, depending on the current necessity.

Table 11 Motor specifications

Fabrication	
Material	Aluminum 6061 alloy with Plastic (Polylactic-acid & Polycarbonate/Nylon)
Fabrication process	CNC machining and FDM 3D printing
Actuators	
Location	Joint-1
	Coreless DC Motors MightyZap 12Lf-100-30
Operating voltage	12V
Motor Nominal Speed (rpm)	26500±10%rpm
Nominal Current	<350mA
Nominal Motor Torque (gr.cm)	95g.cm
Weight (g)	48g
Control System	
Control main board	Arduino Nano Atmega328
Input/Output GPIO	5v TTL Digital Logic inputs/ 0v - 5v PWM pin Output
Communication	GPIO 4 digital signals

4.4 CAD Model and Mechanical Design

All of the GAR components were modeled in CAD software called SOLIDWORKS to make it a minimum feasible solution for a robotic assistive system. Figure 55 and Figure 56 display some rendered pictures extracted from the CAD model. Fabrication instructions for the CNC toolpaths and 3D printing files were generated directly from the CAD model. The CAD

model is also helpful in identifying future problems, such as interferences and mechanism failures, and calculating the internal forces in every system element.

Figure 55 Gar CAD Model.

4.4.1 Finger Design

As discussed in the previous chapter, the best mechanism to perform most daily activities is a rigid link underactuated mechanism. With the underactuated finger design, fewer actuators are needed in the gripper. As a result, it can handle more weight than similar tendon-driven systems with a wide range of motion for different shapes and objects.

In that order, the first step is designing the underactuated mechanism based on the current available grippers founds during the state-of-the-art review. The authors of reference [87] provide an optimized gripper and offer a geometric design for a three-phalanx underactuated finger. To organize the steps to follow, the following flowcharts are presented:

Flowchart 1

During this section, we will use flowcharts to better understand design development.

To perform the three grip types properly, estimating the normal force exerted by the objects on the gripper's finger surfaces is necessary.

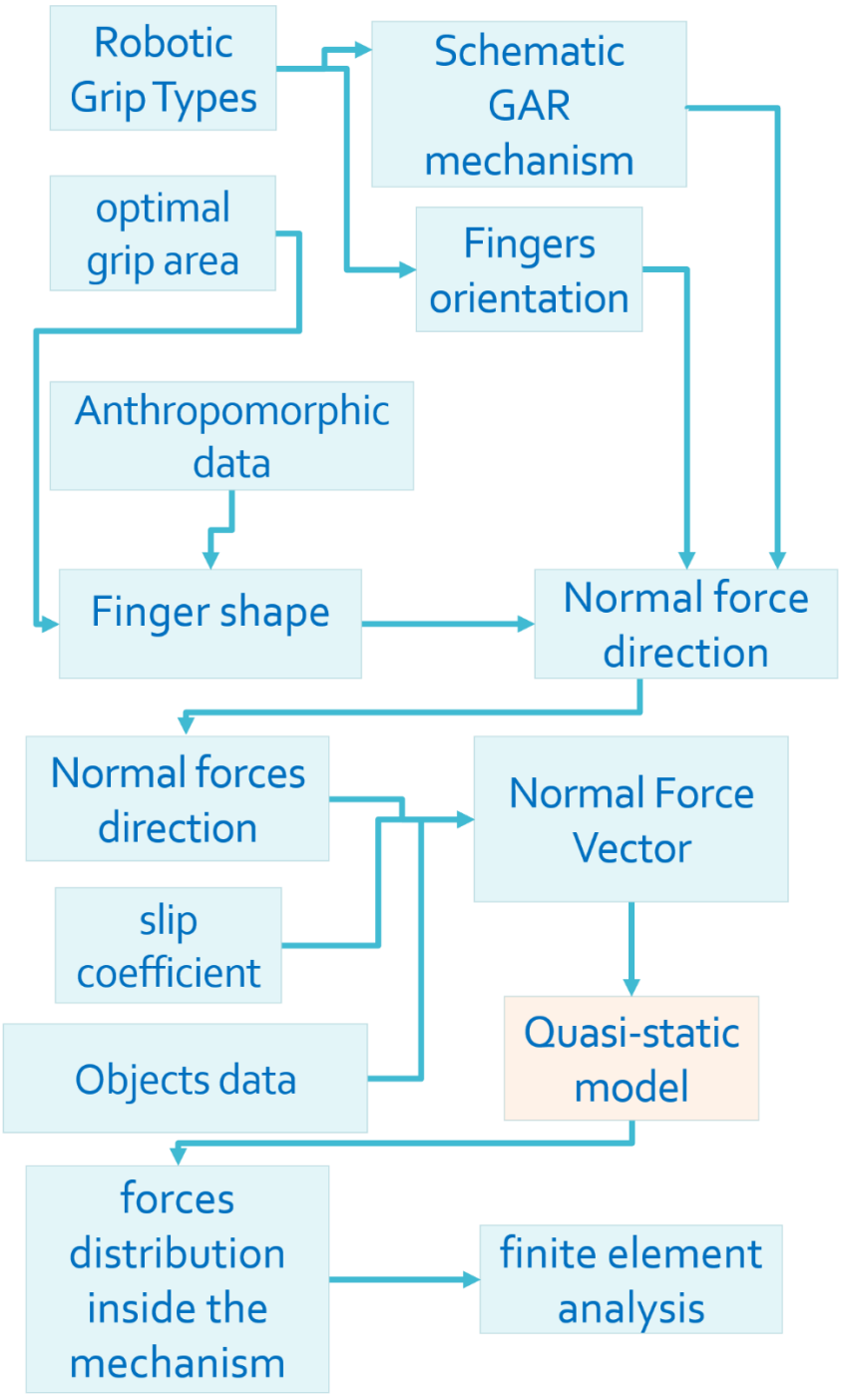

Flowchart 2

In order to simulate a finite element analysis, the magnitude and direction of the normal forces exerted by the objects on the gripper flanges must be combined.

Figure 56 shows the final distribution of the mechanism used in this thesis. This version is generated after completing each step described in the above flowcharts.

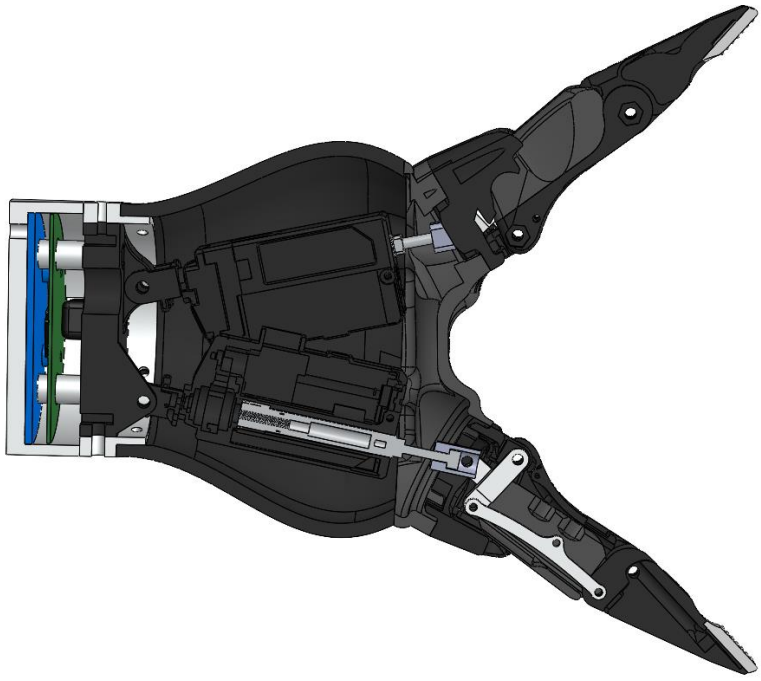

Figure 56 GAR Internal Mechanism CAD Model

For the GAR design, a Two phalanx mechanism is selected due to the model's simplicity. Similar to Reference [83], Each underactuated finger mechanism in the proposed gripper has two degrees of freedom. A passive element (a spring) is employed between the first and second finger phalanges to activate the second DOF. The schematic design of the finger is shown in Figure 57; it comprises two phalanges, two links, a spring, and a third-grade connector element that convert linear motion from the motor into rotary motion as input for the mechanism.

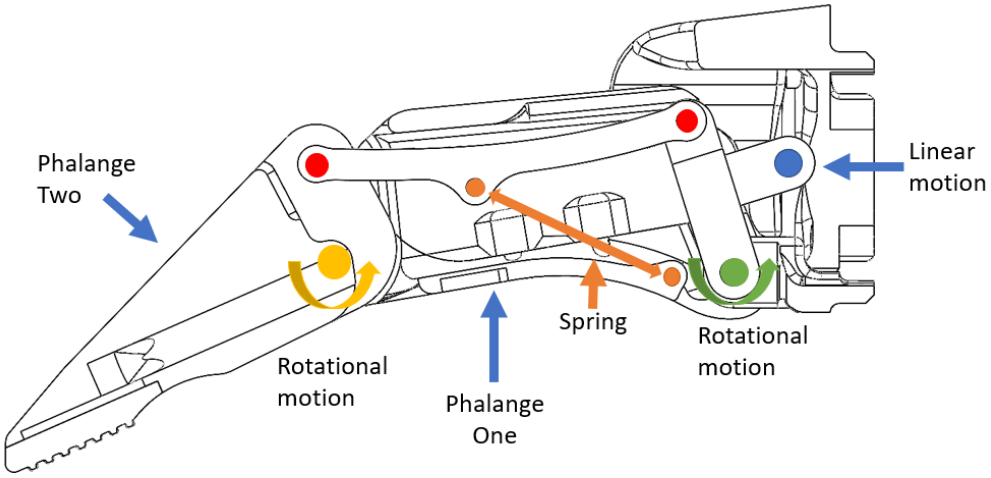

Figure 57 Schematic design of the GAR Mechanism

Due to the spring, the finger may rotate around a fixed pivot like a single rigid body. The actuator's force stretches the spring when the first phalanx touches a surface, transmitting motion only to the second phalanx. When two phalanges come together to grip an item, the motion ends, and the object is fully grasped.

A complete finger design is shown in Figure 58, representing all the system's elements.

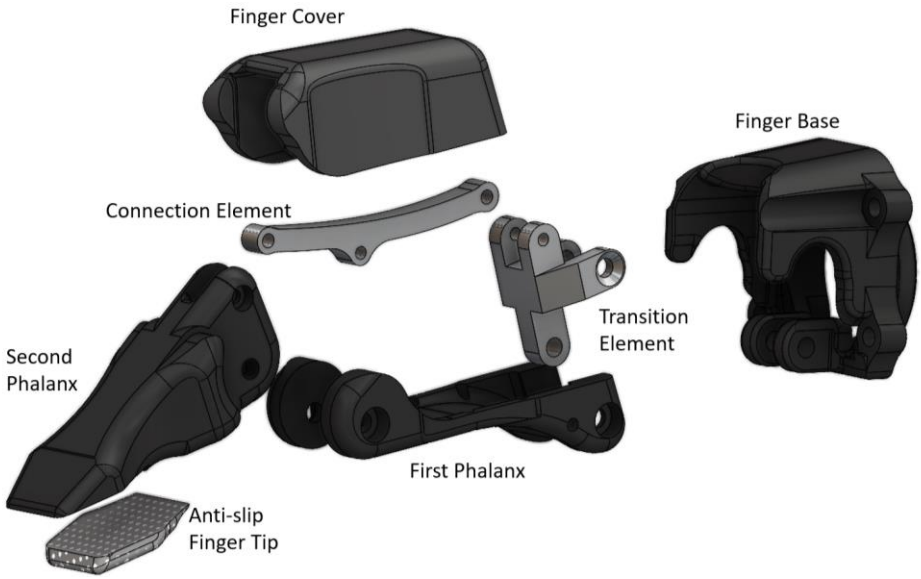

Figure 58 Exploded view of the mechanism

Considering the objects this gripper must be able to handle (Table 4), GAR must be capable of performing the following three types of grips:

I. Spherical Grip

II. Parallel Grip

III. Cylindrical Grip

Here, it is essential to examine four questions:

a. How few fingers are required to accomplish these tasks?

b. What is the proper technique for performing these grips?

c. Which contact areas between the object and the gripper are optimal?

d. What lengths are optimal for each phalanx?

According to the author of [120], human grasping is typically performed by only three fingers: the index, middle, and thumb. Moreover, based on the initial analysis conducted in Chapter 2 (Table 1), the author's assertion is accurate. Three fingers are sufficient for all three types of grips.

To perform the three grip types properly, estimating the normal force exerted by the objects on the gripper's finger surfaces is necessary. These contact surfaces vary based on the size of the object being grasped [121]. Therefore, understanding the direction of the normal forces is essential, as the direction in which these normal forces point will determine whether the object is successfully grabbed or ejected from the gripper.

A study in [121] illustrates how the contact surfaces change concerning the object's diameter changes (Figure 59).

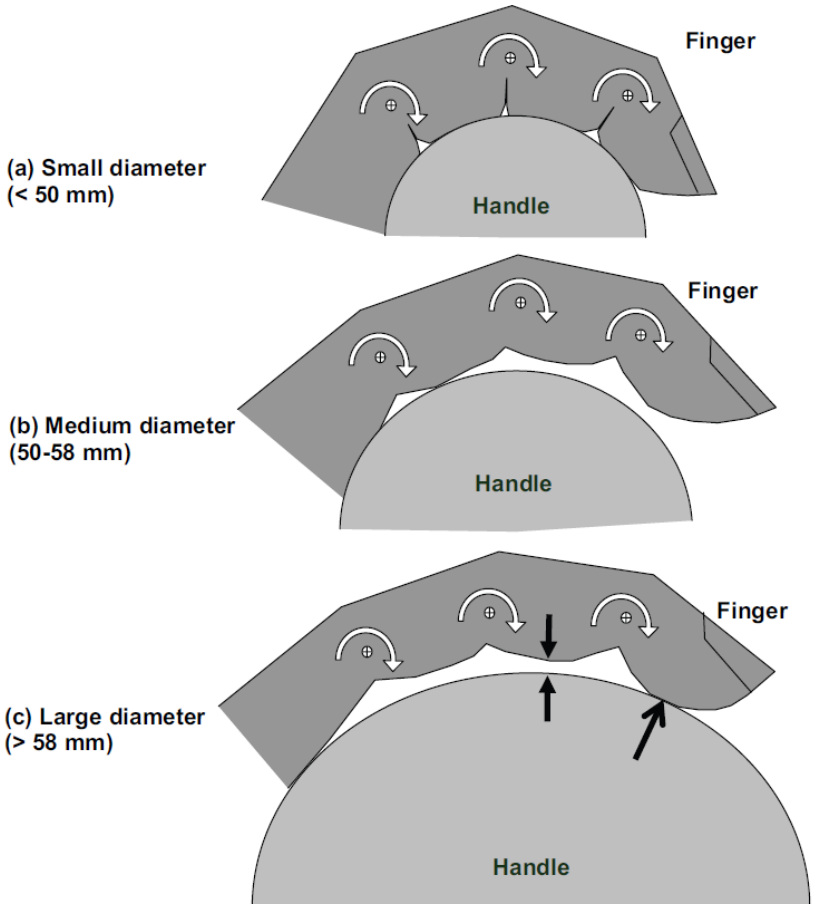

Figure 59 The relation between the contact area and the object's diameter.

Consequently, the investigation average normal force on cylindrical handles increased proportionally by 2.3 times the grip force measured using a split cylinder for handle diameters ranging from 51 to 83 mm. There is also the conclusion that there is an optimal grip diameter, a variable factor in our research. Since this diameter is a variable that depends on the object's shape, its influence on the contact surface must be taken into account to determine the optimal area for each phalanx (Figure 60) [121].

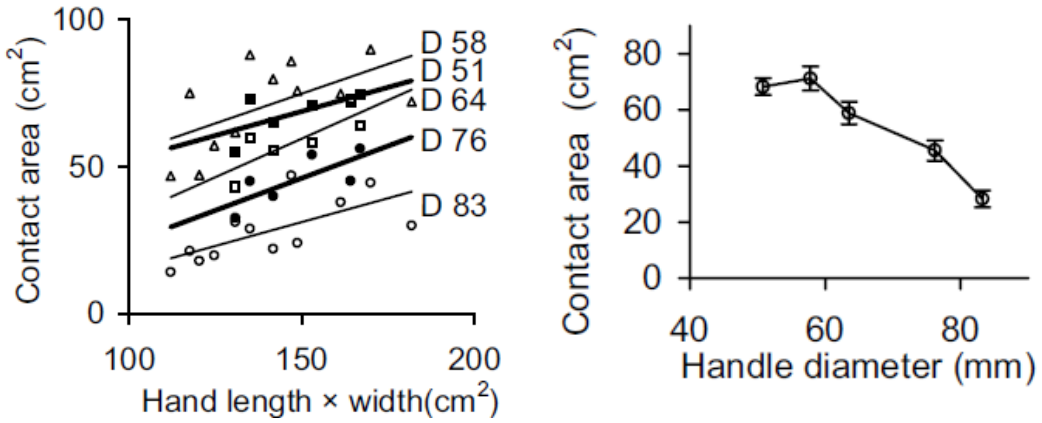

Figure 60 Relation between the contact area and the object's diameter.

The contact area presented in the previous figure represents the average total area of a human hand. Since our robotic gripper does not have five full fingers, we will use only 50% of the area of the palm and only the area of three fingers. This selected seed value for the optimum grip area will be the base for all calculations made during the next section.

The author of [120] analyzed finger lengths based on anthropomorphic data from several individuals' direct measurements. The lengths of the mechanism's internal links are then determined, considering the average lengths of a human hand capable of performing the three types of grip.

The average finger measurements[120] are depicted in the image below (Figure 61):

	Thumb		Index			Middle		
Person	Lt1 [mm]	Lt2 [mm]	Li1 [mm]	Li2 [mm]	Li3 [mm]	Lm1[mm]	Lm2 mm]	Lm3[mm]
1	37.7	30.5	25.7	22.5	24.1	28.1	24.9	25.8
2	40.3	34.9	27.4	23.5	22.1	32.5	25.7	28.4
3	39.0	34.7	26.2	19.4	28.8	29.6	23.5	28.8
4	38.3	32.6	27.1	19.2	25.1	29.6	22.2	26.0
5	39.4	33.5	28.3	23.1	25.3	31.7	25.1	27.0
Average	**38.9**	**33.2**	**26.9**	**21.5**	**25.1**	**30.3**	**24.3**	**27.2**

Figure 61 Average finger lengths

Due to the nature of the mechanism developed in this study, only two phalanges are considered, so the total finger length will be distributed as follows: 53% for the first (proximal) phalanx and 47% for the second (distal).

The following image (Figure 62) illustrates the dimensions (length and width) of each phalanx and its optimal contact area. These measurements were utilized for the CAD model's design and the gripper's kinematic and dynamic analyses.

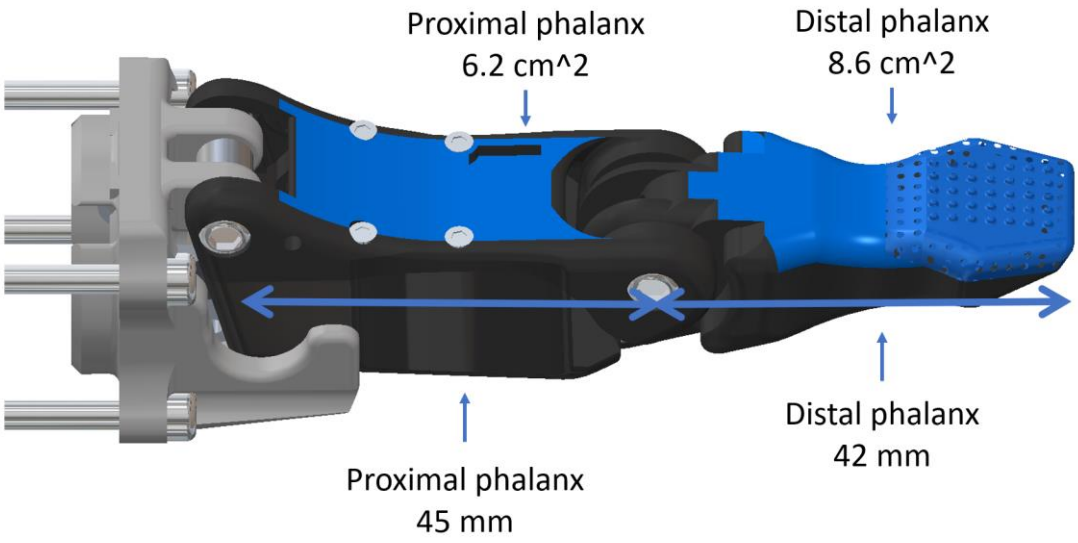

Figure 62 Dimensions of each phalanx and its optimal contact area

Finally, the internal mechanism of the finger is designed to have a range of motion that allows the gripper to grasp all objects from Table 4. Since the lengths of the phalanges have already been determined, the dimensions of the mechanism's internal components will be a function of those lengths. As this relationship is linear, the values for each component of the mechanism can be obtained from the following Figure 63 and Table 12.

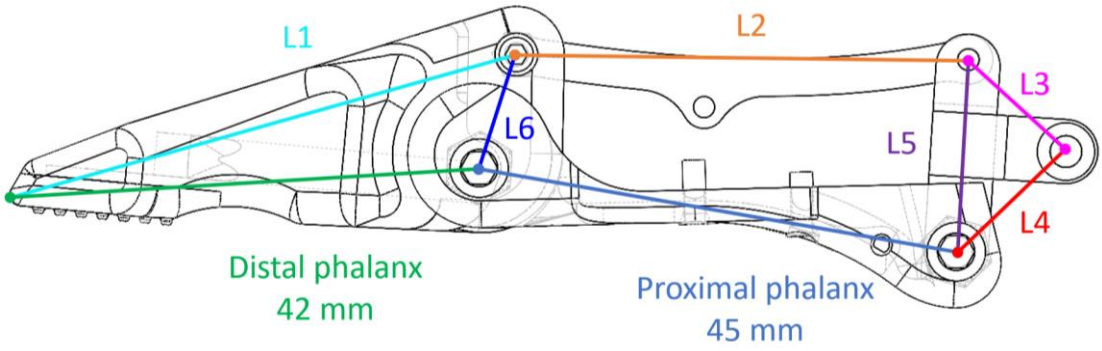

Figure 63 internal mechanisms lengths distribution

Table 12 Linear relation between the internal mechanism's parts.

Mechanism Part	Part Length (mm)	Length/Total Finger Length
Proximal Phalanx	45	0.51724138
Distal Phalanx	42	0.48275862
L1	48.21	0.55413793
L2	42.31	0.48632184
L3	12.54	0.14413793
L4	13.9	0.15977011
L5	18	0.20689655
L6	11.17	0.1283908

Fixed Angles Between Links	Value
L1 - Distal	12.45
Distal - L6	111.5
L6 - L1	56.05
L3 - L4	85.62
L4 - L5	44.01
L5 - L6	50.37

4.4.2 Palm Design

As stated previously, the GAR design employs three fingers capable of completing the three primary types of grips: spherical grip, parallel grip, and cylindrical grip. Therefore, the object's diameters and weights listed in Table 4 are also considered in these three grip

categories. The diameters in this table range from 8 mm to 93 mm; therefore, a maximum diameter of 100 mm will be considered when designing.

The spatial arrangement of these three fingers should produce a gripper capable of grasping objects with a diameter between 4 mm and 100 mm and a load capacity between 10 and 8000 grams according to the optimal lengths and contact areas established in the previous chapter. Therefore, the palm's design is essential, as it determines the angles between the fingers and their interactions when grasping an object.

Fingers angles:

The arrangement chosen for the GAR design is similar to the one the human hand employs for most activities [14], but the difference is that GAR has the thumb, the index, and the middle finger fixed. In a human hand, the thumb and middle finger naturally touch when closing, resulting in a parallel grip. However, to hold cylindrical objects, all three fingers are utilized simultaneously, with the thumb positioned between the index and middle fingers. Similarly, spherical objects are grasped by joining the tips of the fingers to form an imaginary triangle. This is because the human hand has an extra degree of freedom called abduction and adduction.

Due to the fixed position of the fingers in the proposed design, an intermediate position between the Cylindrical Grip and the Spherical Grip is chosen, which allows the thumb to grasp both cylindrical and spherical objects without movement. To locate the finger's position, an iterative procedure is employed in which the relative angles of the fingers

concerning the palm rotate, and the amount of contact area between the finger surface and some test objects designed for this simulation are measured.

These test objects represent the minimum and maximum diameter length and diameter requirements for each type of grip. For example, Figure 64 depicts the direction cosine definition for a finger:

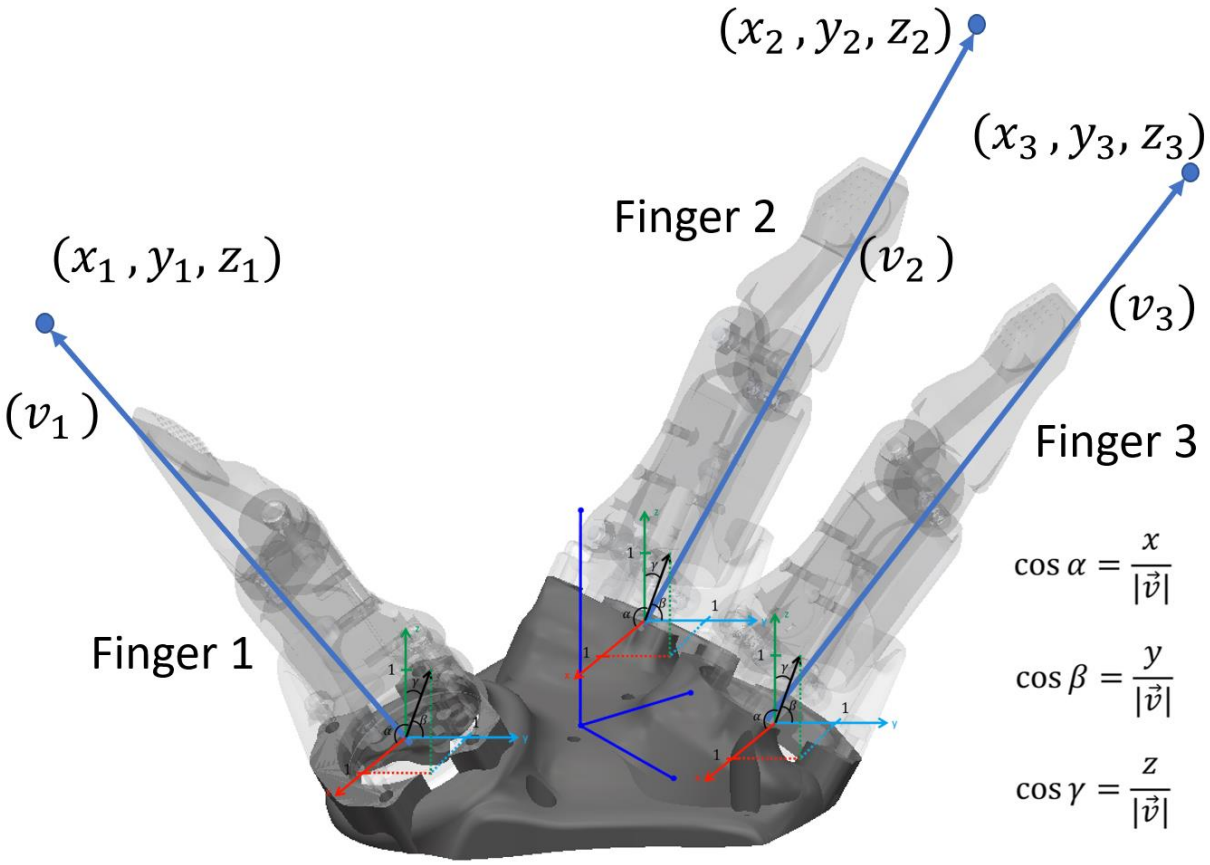

Figure 64 Direction cosine definition for all the finger

After obtaining the final coordinates of the vectors representing each finger, the direction cosines are computed using the equation depicted in Figure 65. The following steps are repeated for each finger.

Finger 1

$$|\bar{a}| = \sqrt{a_x^2 + a_y^2 + a_z^2} = \sqrt{34^2 + (-1.3)^2 + 45.3^2} = \sqrt{1156 + 1.69 + 2052.09} = \sqrt{3209.78} = 0.1 \cdot \sqrt{320978}$$

$$\cos\alpha = \frac{a_x}{|a|} = \frac{34}{0.1 \cdot \sqrt{320978}} = \frac{170}{160489} \cdot \sqrt{320978} \approx 0.6001243985383905$$

$$\cos\beta = \frac{a_y}{|a|} = \frac{-1.3}{0.1 \cdot \sqrt{320978}} = -\frac{13}{320978} \cdot \sqrt{320978} \approx -0.0229459328852914$$

$$\cos\gamma = \frac{a_z}{|a|} = \frac{45.3}{0.1 \cdot \sqrt{320978}} = \frac{453}{320978} \cdot \sqrt{320978} \approx 0.799577507464385$$

Finger 2

$$|\bar{a}| = \sqrt{a_x^2 + a_y^2 + a_z^2} = \sqrt{(-35.5)^2 + (-6.5)^2 + 41.8^2} = \sqrt{1260.25 + 42.25 + 1747.24} = \sqrt{3049.74} = 0.3 \cdot \sqrt{33886}$$

$$\cos\alpha = \frac{a_x}{|a|} = \frac{-35.5}{0.3 \cdot \sqrt{33886}} = -\frac{355}{101658} \cdot \sqrt{33886} \approx -0.6428311968483159$$

$$\cos\beta = \frac{a_y}{|a|} = \frac{-6.5}{0.3 \cdot \sqrt{33886}} = -\frac{65}{101658} \cdot \sqrt{33886} \approx -0.11770148674687475$$

$$\cos\gamma = \frac{a_z}{|a|} = \frac{41.8}{0.3 \cdot \sqrt{33886}} = \frac{209}{50829} \cdot \sqrt{33886} \approx 0.7569110993875944$$

Finger 3

$$|\bar{a}| = \sqrt{a_x^2 + a_y^2 + a_z^2} = \sqrt{(-41.9)^2 + 7.1^2 + 49.3^2} = \sqrt{1755.61 + 50.41 + 2430.49} = \sqrt{4236.51} = 0.1 \cdot \sqrt{423651}$$

$$\cos\alpha = \frac{a_x}{|a|} = \frac{-41.9}{0.1 \cdot \sqrt{423651}} = -\frac{419}{423651} \cdot \sqrt{423651} \approx -0.6437391245117053$$

$$\cos\beta = \frac{a_y}{|a|} = \frac{7.1}{0.1 \cdot \sqrt{423651}} = \frac{71}{423651} \cdot \sqrt{423651} \approx 0.10908228601510997$$

$$\cos\gamma = \frac{a_z}{|a|} = \frac{49.3}{0.1 \cdot \sqrt{423651}} = \frac{493}{423651} \cdot \sqrt{423651} \approx 0.7574305212035102$$

Figure 65 Numerical Orientation for all GAR's Fingers

Figure 66 is a representation of the iterative process described above:

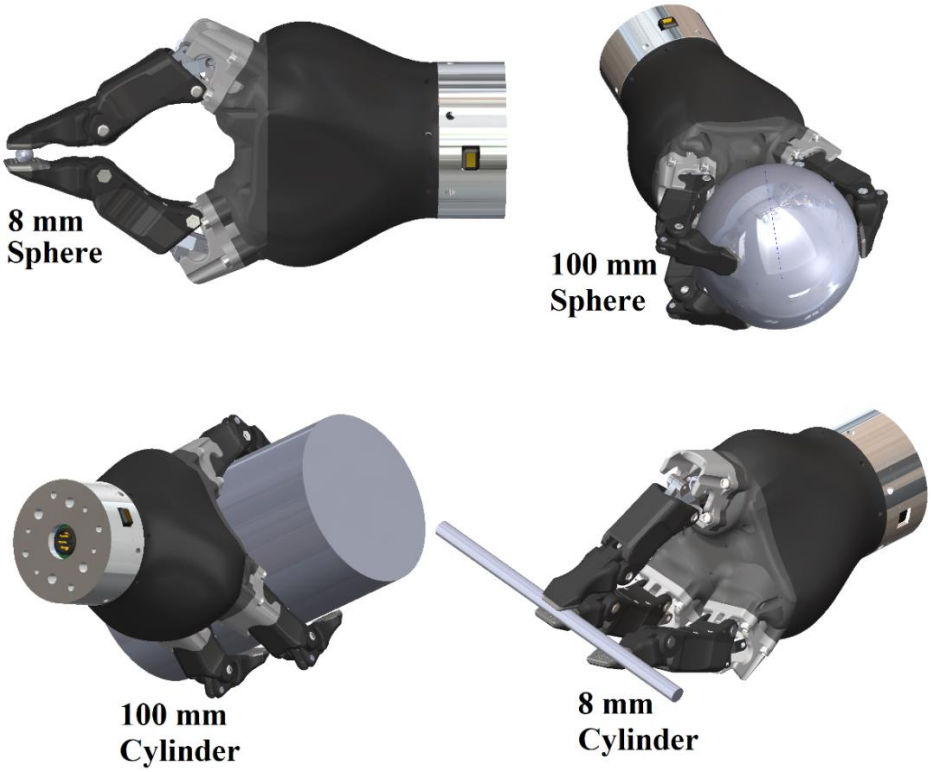

Figure 66 Objects used during the iterative process

And the subsequent Table 13 displays the final coordinates of each vector as well as the direction cosines for each finger relative to the palm:

Table 13 Final coordinates of each direction cosine vector

coordinate list		
Finger	X Y Z positions for each vector (mm)	Global Angle (Rad)
1	X1 = 34	Cos α1 = 0.6
	Y1 = -1.3	Cos β1 = -0.022
	Z1 = 45.3	Cos γ1 = 0.799
2	X2 = -35.5	Cos α2 = -6.64
	Y2 = -6.5	Cos β2 = -0.11
	Z2 = 41.8	Cos γ2 = 0.75
3	X3 = -41.9	Cos α3 = -0.64

	Y3 = 7.1	Cos β3 = 0.10
	Z3 = 49.3	Cos γ3 = 0.75

According to [129], knowing the weight and diameter of the object, the normal forces required to hold that object can be calculated using the friction between the object and the gripper and dividing the result by the number of contact points.

Thus, we can estimate the stresses experienced by the mechanism's internal components. This information is extremely valuable, as it is necessary to determine if the thicknesses of the internal components are correct and will withstand the tension, compression, and shear loads during laboratory testing. To obtain the normal forces' directions on the gripper's phalanges, a series of simulations are performed. During the simulations, GAR grasps various objects of variable sizes and shapes from Table 4. With the equations extracted from reference [129], the magnitudes of the normal forces based on the object's weight and the number of contact points the gripper has while gripping the object can be computed.

Then, combining the direction of the normal forces and their direction, we proceed to solve the dynamic system (explained during the second part of chapter 5) to obtain the vector forces in all the elements of the mechanism. Using these vector forces, a finite element simulation is executed to verify that all the elements of the mechanism support the desired loads during the experiment phase. In order to perform the finite element simulations, the cross-sectional areas of the machine elements are seeded with initial values. These seed values are considered larger than those required, so a factor of safety greater than one is anticipated from the first finite element simulation. If this is not the case, the cross-sectional areas would be recalculated, and the simulation would be rerun to determine its validity. The simulations for the sixteen objects selected from Table 4 are (Figure 67 – 70):

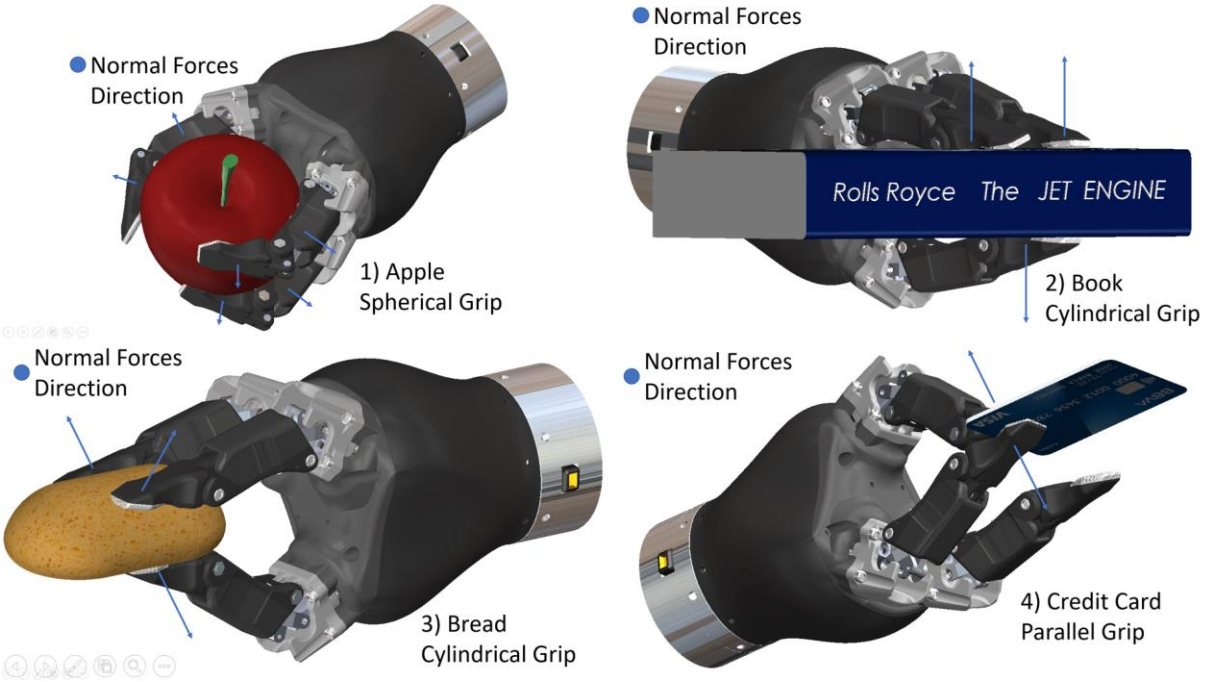

Figure 67 Normal Forces Directions - Simulation 1.

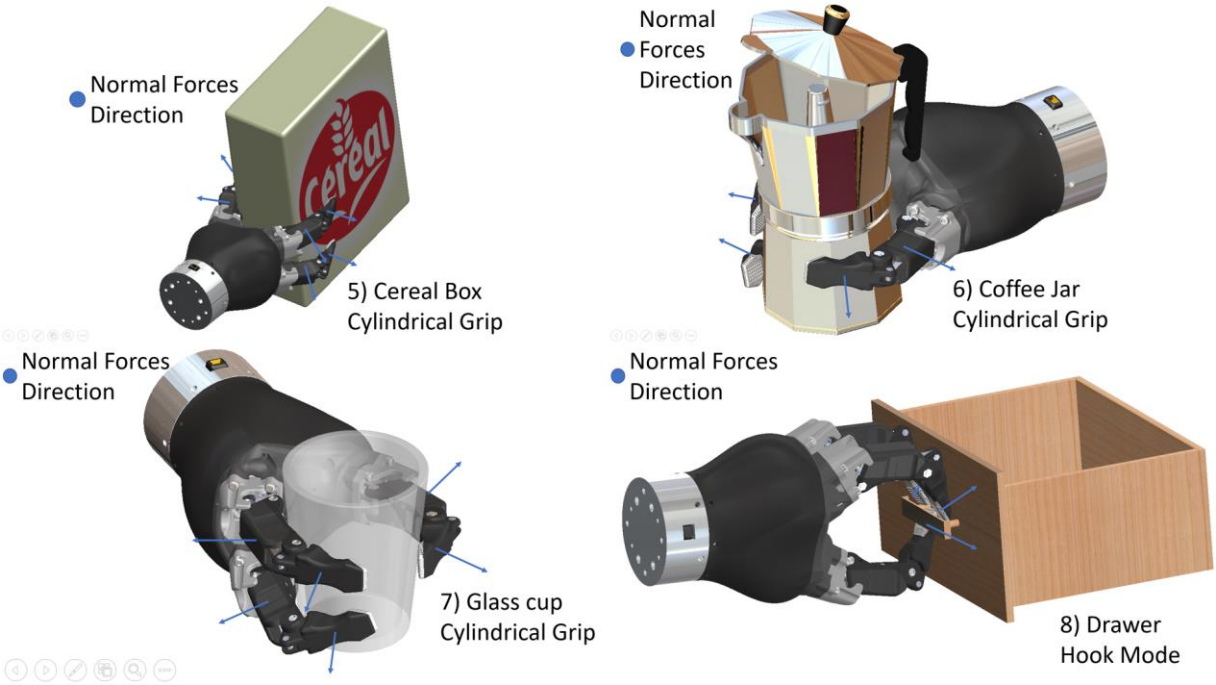

Figure 68 Normal Forces Directions - Simulation 2.

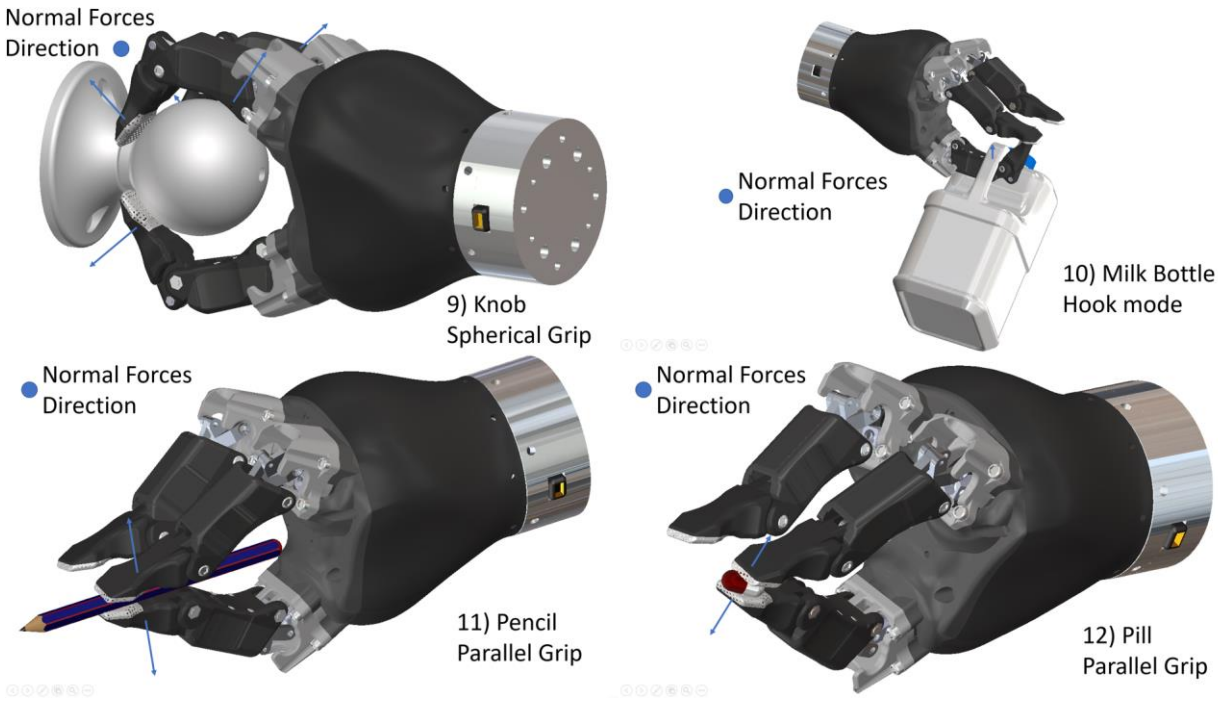

Figure 69 Normal Forces Directions - Simulation 3.

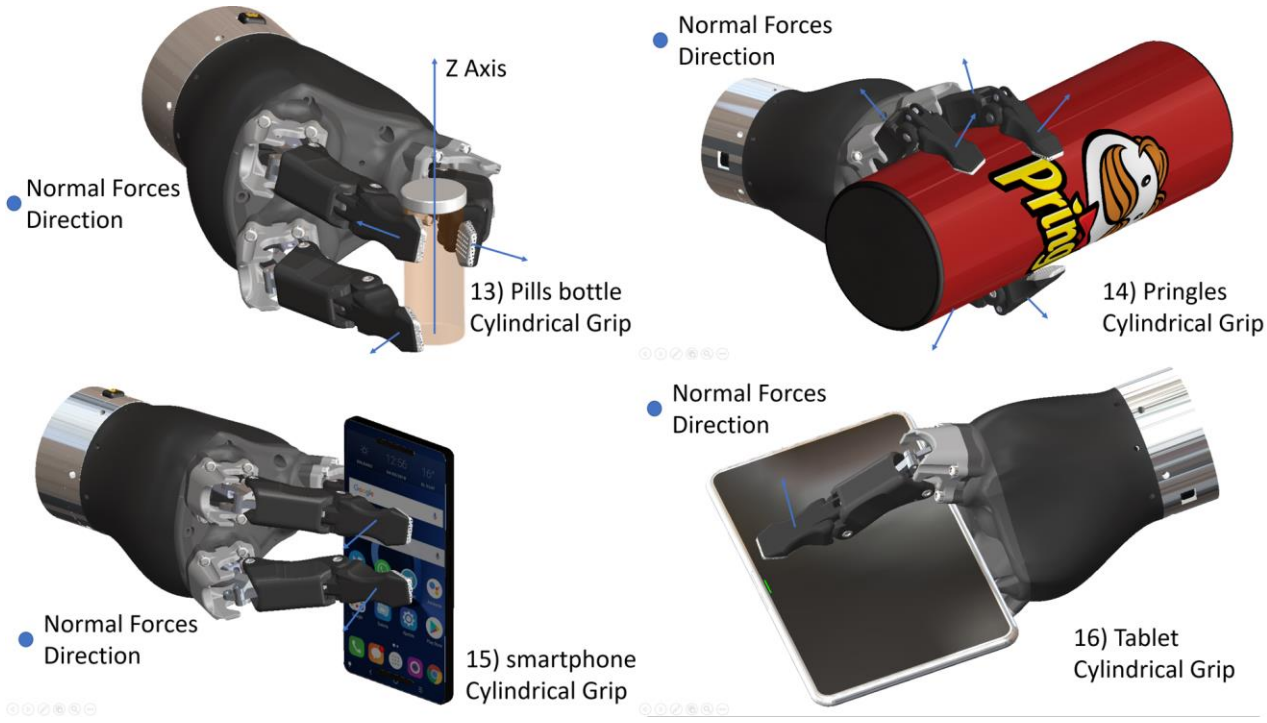

Figure 70 Normal Forces Directions - Simulation 4.

For each item in the objects list, the friction force values are computed according to the following friction equation:

$$Fr = \mu * N$$

Where μ is the coefficient of friction between surfaces. This coefficient is a function of both surfaces' roughness. Since the phalanges are coated with rubber, the average slip coefficient for this material is utilized, which can be found in [129] and is shown in Table 14.

Table 14 Average rubber slip coefficient

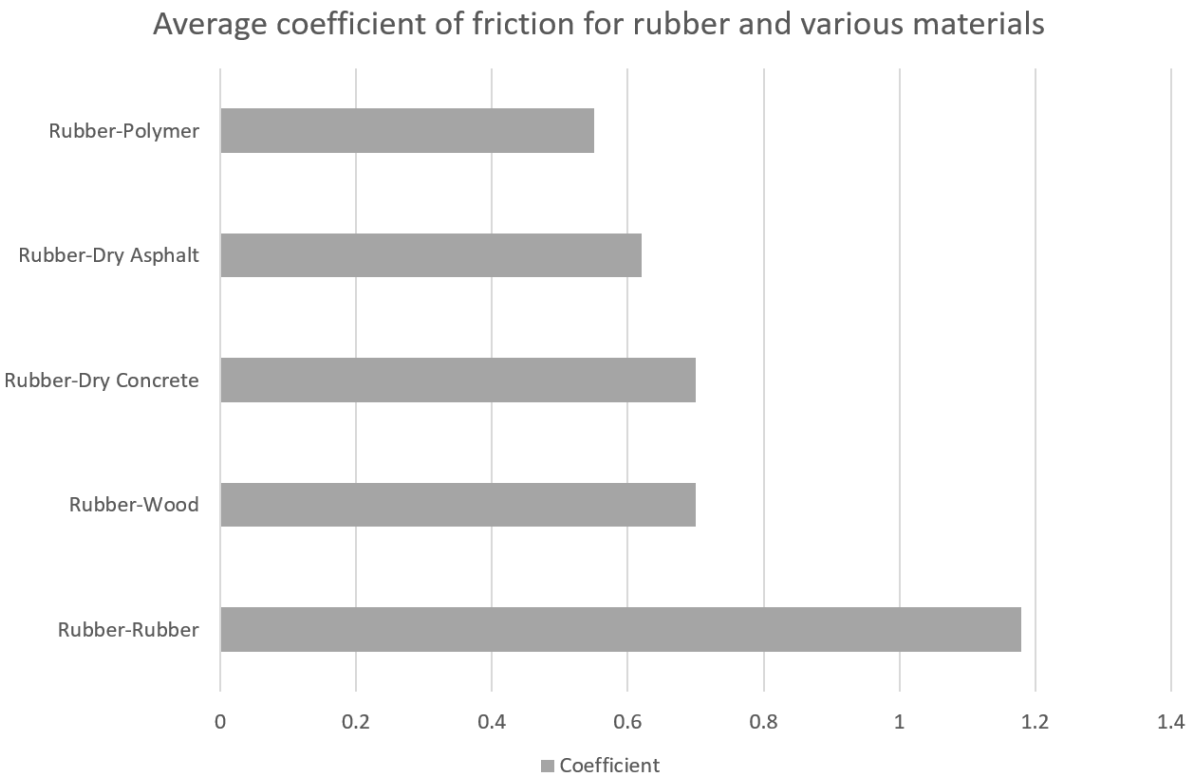

Since GAR exerts at least two contact points on the item, the object's weight is spread throughout the number of contacts and, therefore, across the normal forces created by each contact point. In this sequence of thought:

$$W = n(Fr) = n(N * \mu)$$

$$N = \frac{W}{\mu * n}$$

Where *n* is the number of gripping contact points. Also, design safety factor is added for this equation, and the average normal force is calculated and shown in Table 15:

Table 15 Average normal force

Objects	Min Diameter	Max Diameter	Min Weight	Max Weight	Mean Weight gr	Mean Normal Force [N]:
Glass of water	41 mm	93 mm	112 gr	607 gr full	495	48.51
Apple	62 mm	92 mm	107 gr	396 gr	289	28.322
Pen	-	-	5.2 gr	5.2 gr	5.2	0.5096
Tablet	-	-	286 gr	504 gr	218	21.364
Smart phone	-	-	192 gr	-	192	18.816
Pill bottle	25,4 mm	-	3.71 gr	-	3.7	0.3626
Book	-	-	172.39 gr	1072 gr	899.61	88.16178
Single pill	8 mm	8 mm	250 mg	500 mg	0.25	0.0245
Cereal box	-	-	370 gr	-	370	36.26
Pringle	89 mm	89 mm	65 gr	158 gr	93	9.114
Coffee jar	-	-	1088 gr	2588 gr	1500	147
Bread	-	-	33 gr	395 gr	362	35.476
2L Milk	-	-	-	2120 gr	2120	207.76
Drawers	-	-	145 gr	248 gr	103	10.094
Knob	48 mm	-	192 gr	-	192	18.816
Credit cards	-	-	10 gr	-	10	0.98

The normal forces value varies for each item since its geometric form governs how each object is gripped. Therefore, it should ideally be grasped according to one of the three categories described above (spherical grasp, cylindrical grasp, parallel grasp).

A finite element analysis can be computed for each finger using the critical design case from the performed simulation, the directions of the normal forces, and the normal forces calculated magnitudes.

The critical case will have the highest magnitude of normal force and the fewest number of support points. For example, in Table 16 we can get the Normal force values for each phalanx for each tested object:

Table 16 Force values for each phalanx

Objects	Normal Force Distal Phalanx 1 [N]	Normal Force Proximal Phalanx 1 [N]	Normal Force Distal Phalanx 2 [N]	Normal Force Proximal Phalanx 2 [N]	Normal Force Distal Phalanx 3 [N]	Normal Force Proximal Phalanx 3 [N]
Glass of water	8.09	8.09	8.09	8.09	8.09	8.09
Apple	4.72	4.72	4.72	4.72	4.72	4.72
Pen	0.25	0	0	0	0.25	0
Tablet	7.12	0	7.12	0	7.12	0
Smart phone	6.272	0	6.272	0	6.272	0
Pill bottle	0.12	0	0.12	0	0.12	0
Book	22.04	22.04	0	22.04	22.04	0
Single pill	0.012	0	0	0	0.012	0
Cereal box	6.04	6.04	6.04	6.04	6.04	6.04
Pringle	1.519	1.519	1.519	1.519	1.519	3.56
Coffee jar	57.5	57.5	57.5	57.5	57.5	57.5
Bread	5.91	5.91	5.91	5.91	5.91	5.91
2L Milk	34.63	34.63	34.63	34.63	34.63	34.63
Drawers	3.36	0	3.36	0	3.36	0
Knob	3.76	0	3.76	3.76	3.76	3.76
Credit cards	0.49	0	0	0	0.49	0

After getting the normal force exerted by the items on each phalanx, these data are utilized to test the design's stability. Next, the critical case from Table 16 is selected, where the system is subjected to a force of roughly 207 Newtons. To err on the side of caution, we will estimate this number to be 220 N and perform a static finite element study on the internal mechanical components of the gripper, which support the loads and stresses of the whole system.

The following steps are required to carry out the finite element analysis:

• Initially, forces are transferred from the contact point of each phalanx to the mechanism's internal components.

• Connection points are chosen and fixed for each part of the mechanism to estimate the strain and stress inside the specified element. This is shown in Figure 71

• Loads are then applied according to the predicted directions for each element.

• Later, a triangular mesh is applied. In that order, the finite element analysis would be performed node by node. The chosen mesh is a fine mesh to provide more accurate simulation results.

• Finally, the simulation is executed, and the stress data are retrieved to determine the safety factors for each element.

The findings of the finite element simulation were successful, as anticipated. The cross-sectional areas of the internal mechanism elements sustain the forces created by holding the items from the preceding list, which relate to things used during activities of daily living.

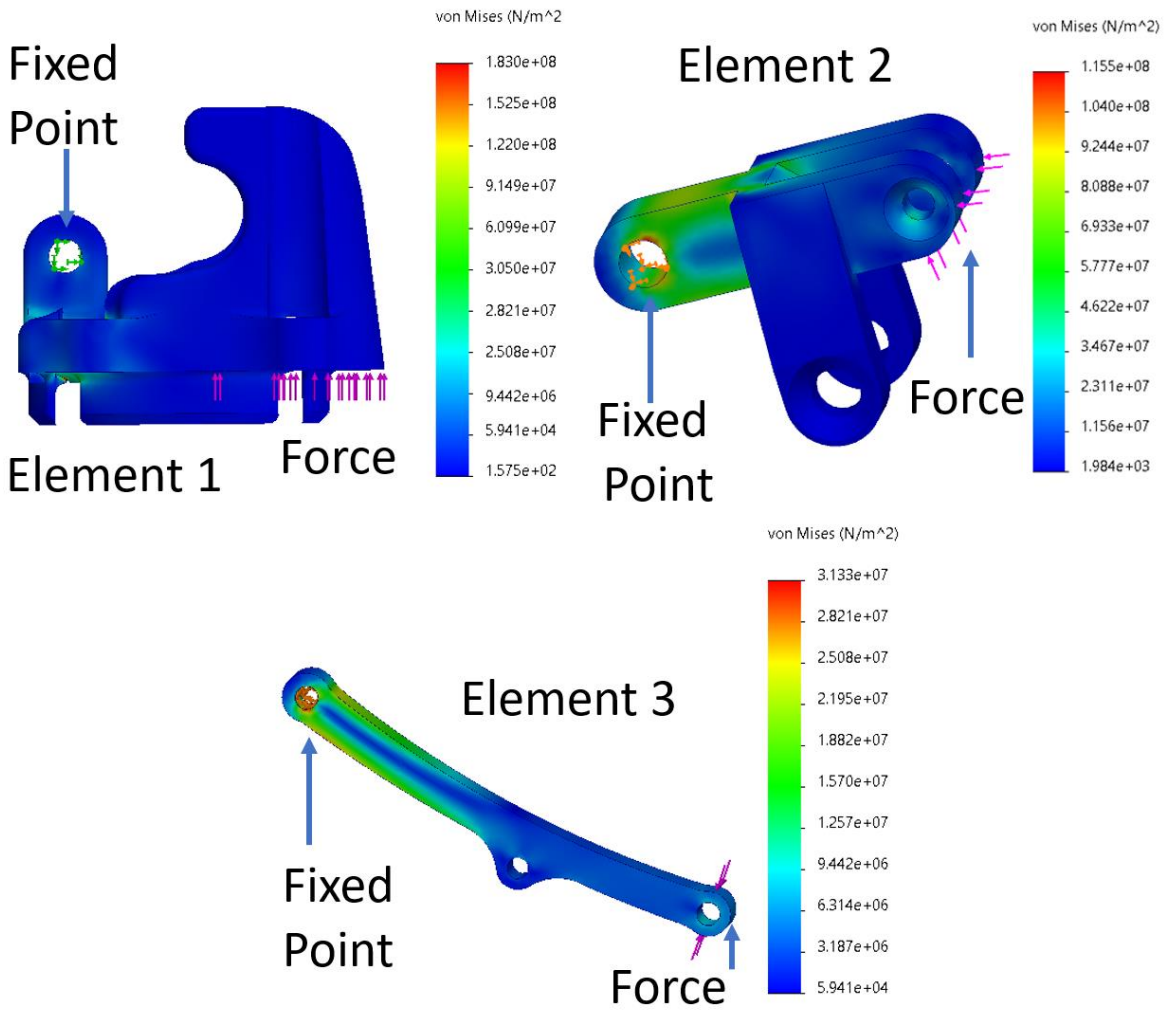

Figure 71 Finite element simulation for critical mechanism components

Next, we determine the safety factor for each component of the system. For this, we will apply the solid mechanics' equations from the book "Mechanical Engineering Design" [122], in which the factor of safety (FS) is directly proportional to the Yield stresses and the system's maximum stress. Our system's maximum stress will correspond to the von Mises stress obtained in the finite element simulation. Below, the equation to compute the FS is presented, while the Table 17 displays the calculated values and safety factors for each element.

$$\boldsymbol{FS = \sigma Y / \sigma VM}$$

The material utilized for the mechanism's internal components is commercial 6061 aluminum with a yield stress of 276 Mpa, according to the previously specified material standards. Using this theoretical information, the Factor of safety is determined for each element:

Table 17 Factors of safety for each mechanism component

Element	Von Mises Stress [Mpa]	Yield Stress [Mpa]	Factor of Safety
Element 1	183	276	1.50
Element 2	115.5	276	2.38
Element 3	31.33	276	8.80

4.4.3 Palm and Motor Base

Given that we determined the direction cosines in the preceding segment, this section searches the ideal location for the motors and their bases, given the constraints previously mentioned for the mechanism.

To determine the ideal position, the following constraints will be considered:

• The finger should not exceed its limit position to prevent uncalculated stresses inside the mechanism.

• The motor axis's zero position must match the hand's zero position (totally open).

• There must be sufficient space between the motors to move without clashing or causing friction.

• Motors must be able to pivot and rotate, as they may be reconfigured without breaking in unanticipated circumstances.

• The base must be sufficiently rigid to sustain the motors' response forces.

• The base must also have a housing attachment for the motors since they cannot be exposed during laboratory testing.

Initially, the zero location for each phalanx must be established. This zero location has previously been implicitly established, given that the diameter range of items to be handled is 8mm to 100mm. This allows us to evaluate four cases:

• Case 1: What are the relative angles between the phalanges when fully opened?

• Case 2: What are the relative angles between the phalanges when they hold an 8mm item?

• Case 3: What are the relative angles between the phalanges when a 100 mm item is being held?

• Case 4: What are the relative angles between the phalanges when grasping an item with a diameter within the specified range?

The first question can be answered through a CAD examination of a phalanx. As depicted in the illustration below (Figure 72), the relative angles are measured for each case by positioning the objects at the center of the palm.

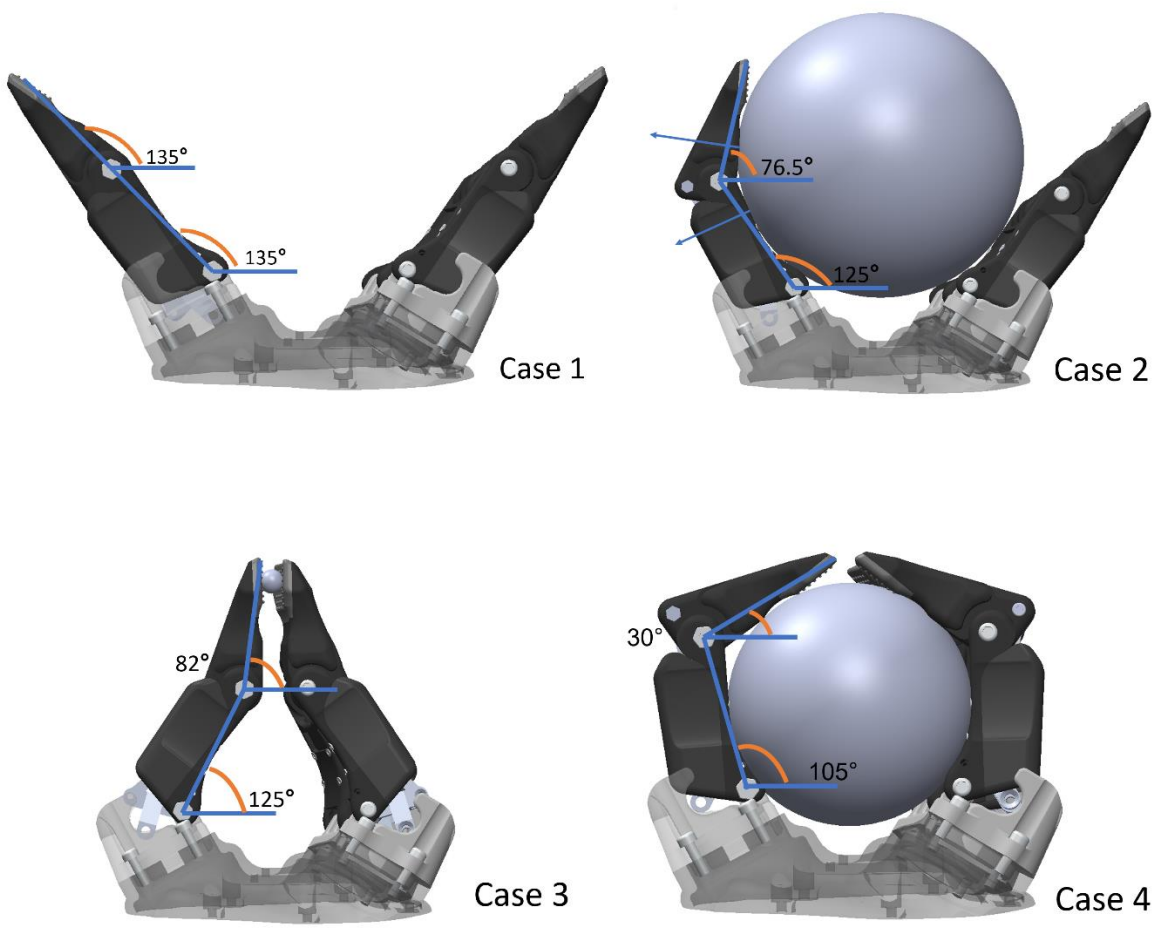

Figure 72 Relative angles measured for each limit case.

Once the GAR boundaries are determined, it is straightforward to position the engines such that they take as minimal space as feasible while adhering to the security constraints that we previously established for our mechanism.

For this, the motor shaft's maximum and minimum lengths are used. The motor used for this design has a stroke length of 27mm. The extended length is specified as 0 when the motor's shaft is completely retracted and as 27 mm when the shaft is extended to its maximum stroke.

Since the first safety restriction is that the zero position of the motor is the same as the zero position of GAR, the motor is attached to the machine when its shaft is fully retracted. The

gripper is positioned with the fingers fully extended to calculate the distance from the palm to the motor-holding base.

The determined direction cosines center the shaft axis in the same direction as each cosine vector. This ensures that the applied force is aligned with the mechanism, allowing forces to be passed from the motor to the phalanges more effectively.

This is particularly significant because if the motor shaft is misaligned, the mechanism's internal components will be exposed to pressures and stresses in directions they were not intended, which might cause the mechanism to bind or break the links.

The next step is to orient the base at the same angle as the linear motors. Therefore, their anchor points must be perpendicular to the direction cosines and parallel to the side view of the phalanges. To further clarify this notion, Figure 73 is used, which depicts the motor assembly and base concerns.

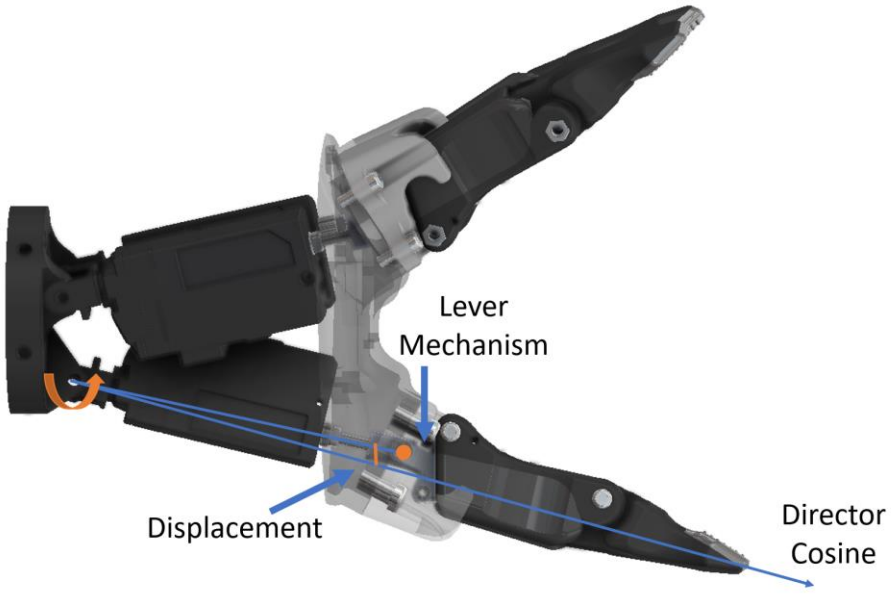

Figure 73 Relative Motor orientation

To connect the motors' base to the palm, a casing must be created to enclose the motors and provide structural support for the tension stresses produced by limiting movement between the base and the palm. Since 3D printing is utilized to construct the shell, the material's (Nylon) characteristics are first examined under stress. The maximum stress values obtained from experimental samples of various 3D-printed plastic materials can be estimated thanks to research published in [123] (Figure 74).

Material	Nozzle (°C)	Bed (°C)	Layer height (mm)	Speed (mm/s)	Build orientation	Infill (%)	σ (MPa)	E (GPa)
PLA ULTRA	200	55	0.1	40	xy	75	39.92 ± 0.74	3.00 ± 0.11
Carbon PA xz	240	80	0.1	25	xz	75	97.15 ± 1.64	7.85 ± 0.44
Carbon PA xy	240	80	0.1	25	xy	75	93.29 ± 3.41	6.39 ± 0.27
Strong ABS xy	240	80	0.1	25	xy	75	28.97 ± 0.53	2.76 ± 0.05
Strong ABS xz	240	80	0.1	25	xz	75	33.53 ± 2.84	2.96 ± 0.08
PMMA	240	90	0.1	25	xy	75	56.25 ± 1.95	2.75 ± 0.05
PEEK	420	110	0.1	20	xy	75	69.04 ± 7.01	3.53 ± 0.01
Nylon12	245	98	0.1	25	xy	75	43.08 ± 1.54	0.757 ± 0.194
Nylon12	245	98	0.1	25	xz	75	41.08 ± 1.39	0.921 ± 0.095

Figure 74 [123] 3D-printed plastic properties

Again, a seed value for the case's transverse area is used. Since the case has an irregular form along its Z-axis, the critical plane with the lowest cross-sectional area is used as a reference. Figure 75 depicts the chosen plane and the critical cross-sectional area that will be used to determine the stresses in the case. We will also consider the maximum load the gripper must sustain, which is 5 kg according to the design specifications.

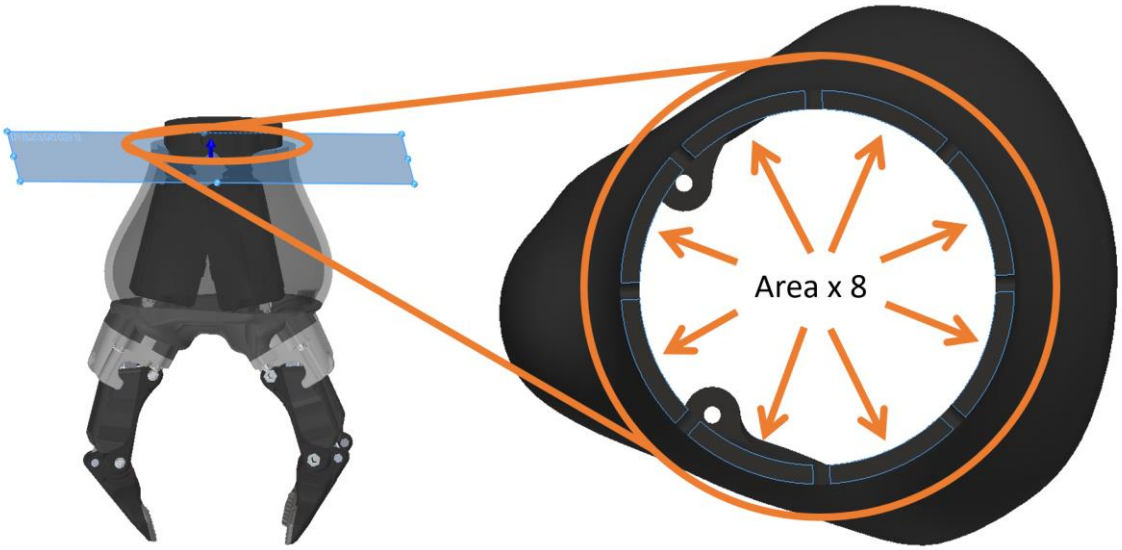

Figure 75 Chosen plane and the essential cross-sectional area

The estimated size of each section is 91.5 mm2, making the total area to be examined 730 mm2. With this data, the equations derived in [122] are used to perform a stress analysis:

$$F = 8\ kg * 9.8\frac{m}{s^2} = 78.4\ N$$

$$Area = 730mm^2$$

$$\sigma = \frac{Mc}{I}$$

$$\sigma = \frac{64F\left(F_{weight} + F_{Mech} * d\right)\frac{d_{max}}{2}}{\frac{\pi}{2} * \left({d_{max}}^4 - {d_{min}}^4\right)}$$

Where d_{max} is the distance from the center of the casing to the periphery, which in this case, is the outside diameter. d_{min} is the inside diameter of the casing in the selected plane. F_{weight} is the maximum weight exerted by an object, and d is the perpendicular distance from the object to the critical section. The weight could be placed at the farthest end of the gripper

(the distal phalanx) in the most critical case. Note that in addition toF_{weight}, a number referred to as F_{mech} is also included to include the maximum force that the mechanism might exert on the casing. A design Factor of safety *F* is also incorporated to err on the side of caution.

$$\sigma = \frac{64(2(78.4\,N + 200N) * 0.221m)\frac{0.07m}{2}}{\frac{\pi}{2}(0.070m^4 - 0.069m^4)}$$

$$\sigma = 24.22\ MPa$$

$$FS = \frac{\sigma_y}{\sigma} = \frac{41.08\ MPa}{24.22\ Mpa} = 1.69$$

The base, palm, and casing are joined with 3mm and 4mm steel screws, the gripper is adjusted to the zero position, and an aluminum piece is added to the base to complete assembly. Figure 76 presents the system's mechanical design as a conclusion for this stage.

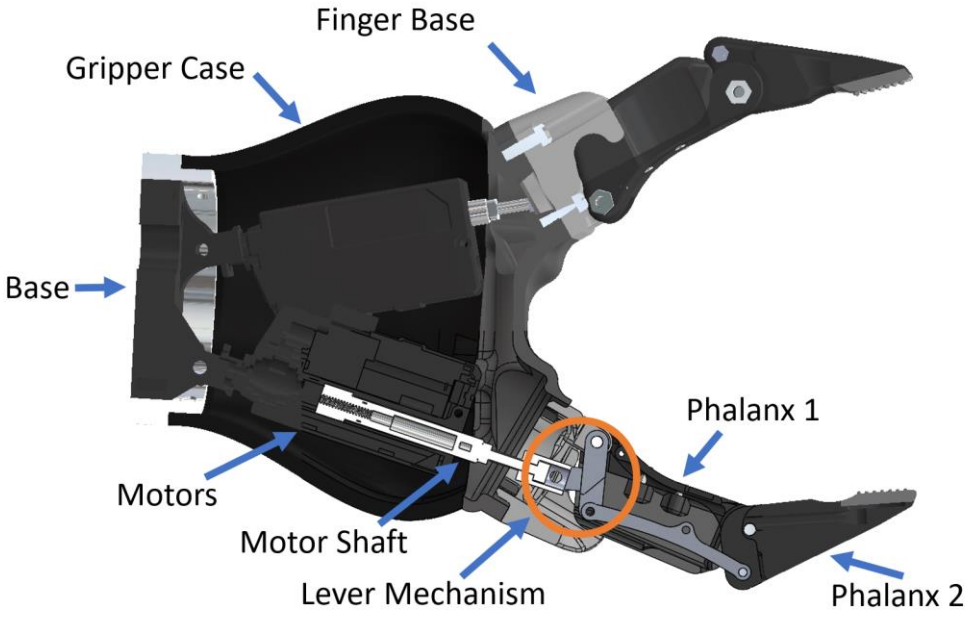

Figure 76 System's mechanical design

4.4.4 Circuit Board

Although the emphasis of this study is on the mechanical design of GAR, the next part contains information on the design of the circuits, the custom circuit board built for this application, a description of its components, and a connection diagram.

This section of the research clarifies the following issues:

• Electrical connections for chosen motors

• Driver type

• Voltage and current regulators included in the system

• Connection diagram for all system components

• Design of the circuit board

As mentioned in the preceding section, this design used MightyZap 12Lf-100-30 motors. This kind of linear motor consists of a rotating DC motor and a gear system (with a 1:100 reduction ratio) that multiplies the torque needed to move the shaft, which consists of a lead screw and an anchor point.

In this part, it is vital to note that the preceding system is controlled by an integrated circuit board with a position sensor that lets the board know where the shaft is located. This board operates at 12V and can receive PWM or TTL signals needed to regulate the position of the shaft.

Particularly advantageous is that these motors can be controlled collectively through an ID. Because each motor has its identifier, fewer cables are necessary to transfer signals to these motors. In conclusion, three motors can be linked in parallel to the same power source and controlled using pulse width modulation (PWM), requiring three connections.

The following diagram (Figure 77) shows the connections used between the motors:

Figure 77 Motor's connections

To generate PWM signals, a microcontroller that can understand instructions from the robot is required. The AtMega328 microcontroller, which has a wide variety of input and output digital and analog pins (GPIO) (Figure 78), is the most versatile in terms of the functionalities it provides for this application.

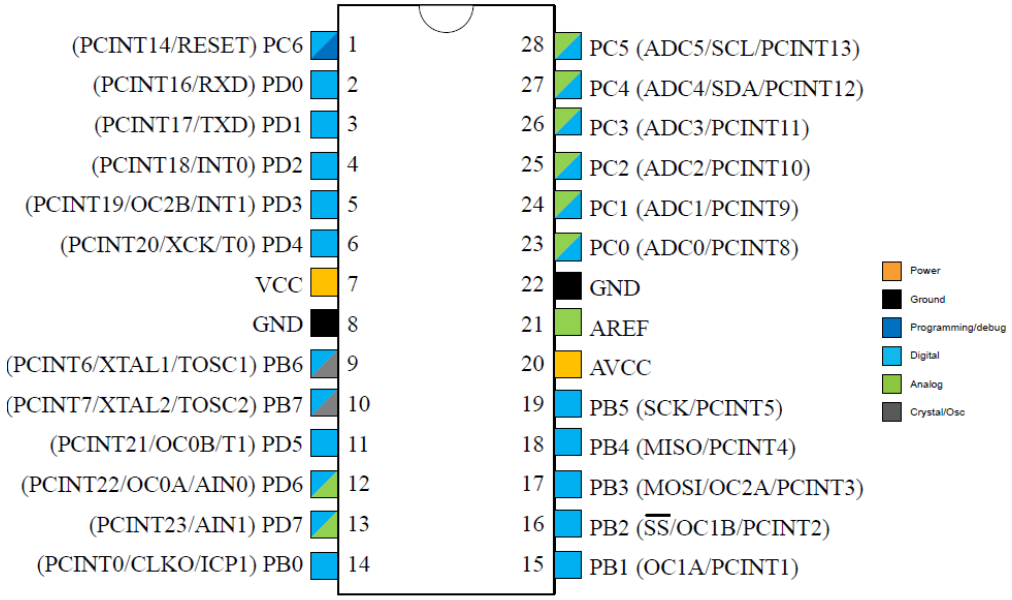

Figure 78 AtMega328 GPIO layout

This controller is used extensively on embedded boards such as the Arduino Uno and Arduino Nano. However, the GAR must be a compact, modular gripper for assistive robots; thus, the smallest version of this integrated board (Arduino Nano) was chosen to adhere to size constraints.

This integrated board operates at a maximum voltage of 5V instead of the motor system's 12V (Figure 79).

In order to deal with various voltages inside the same system, voltage reducers using the MP1584EN chip, which can modulate voltages from 28V to 4.5V, are used. The schematics used to create the motherboard are shown below (Figure 80). These diagrams match the Arduino Nano and the MP1584EN voltage regulator (Appendix B):

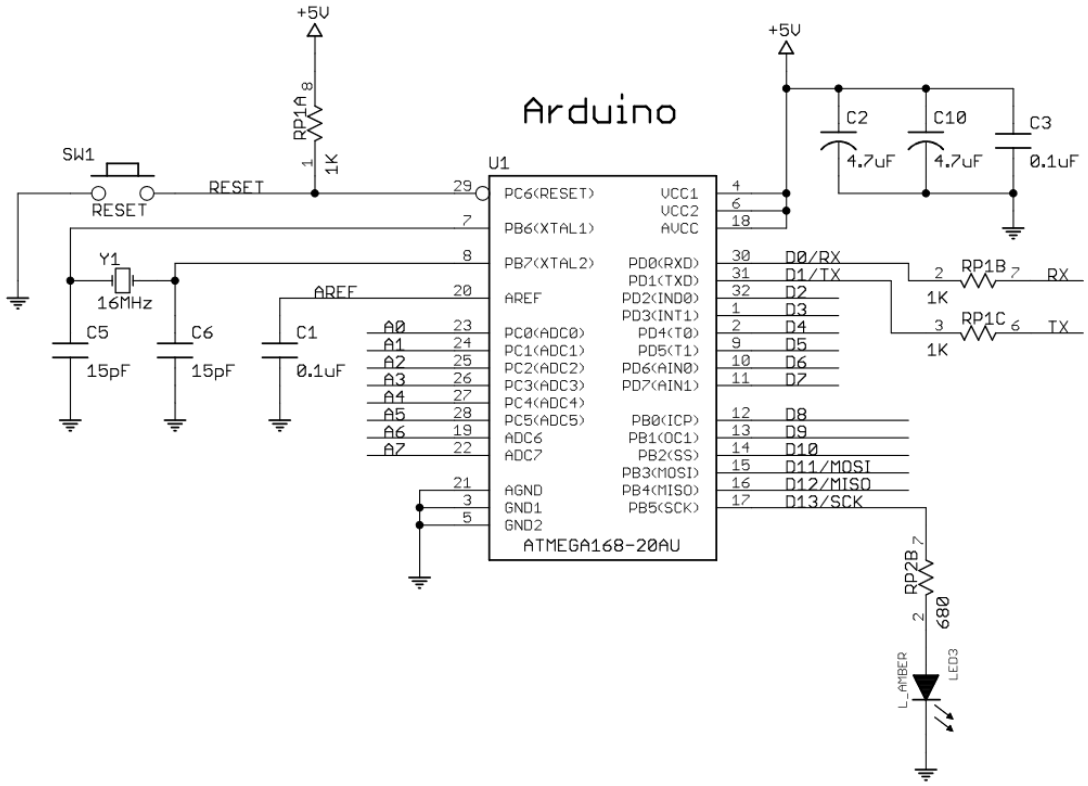

Figure 79 Arduino Nano layout

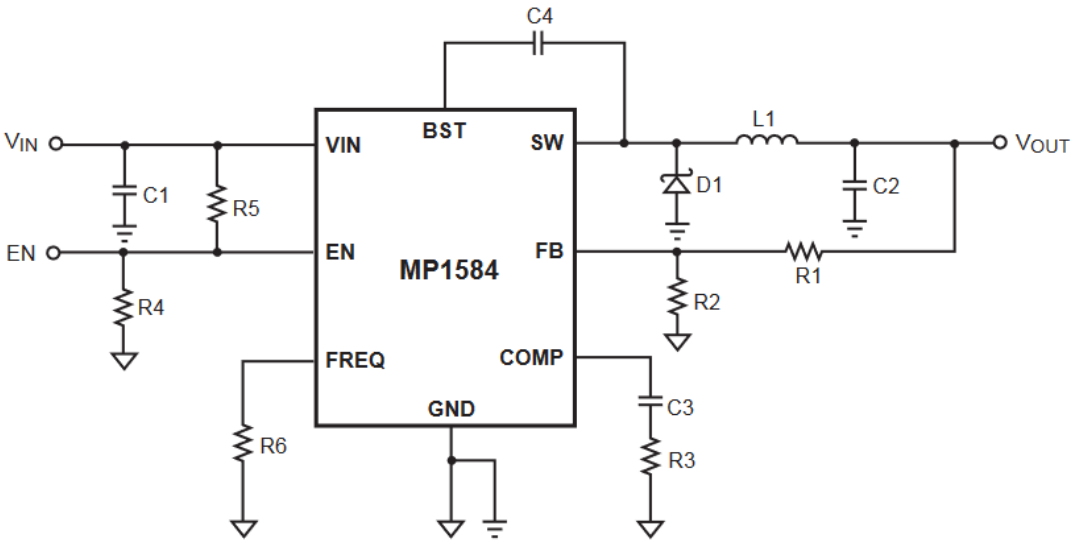

Figure 80 MP1584 circuit layout

Knowing how the components above interact, the circuit board is designed. A connection diagram is first shown in Figure 81, where 2 MP1584EN, 1 AtMega328, and three at 12 V controlled by PWM signals are connected.

Two digital pins will be utilized to send and receive signals from the robot to the Gripper. These two pins will subsequently be utilized during the programming. Consequently, the circuit's schematic is shown in Figure 82:

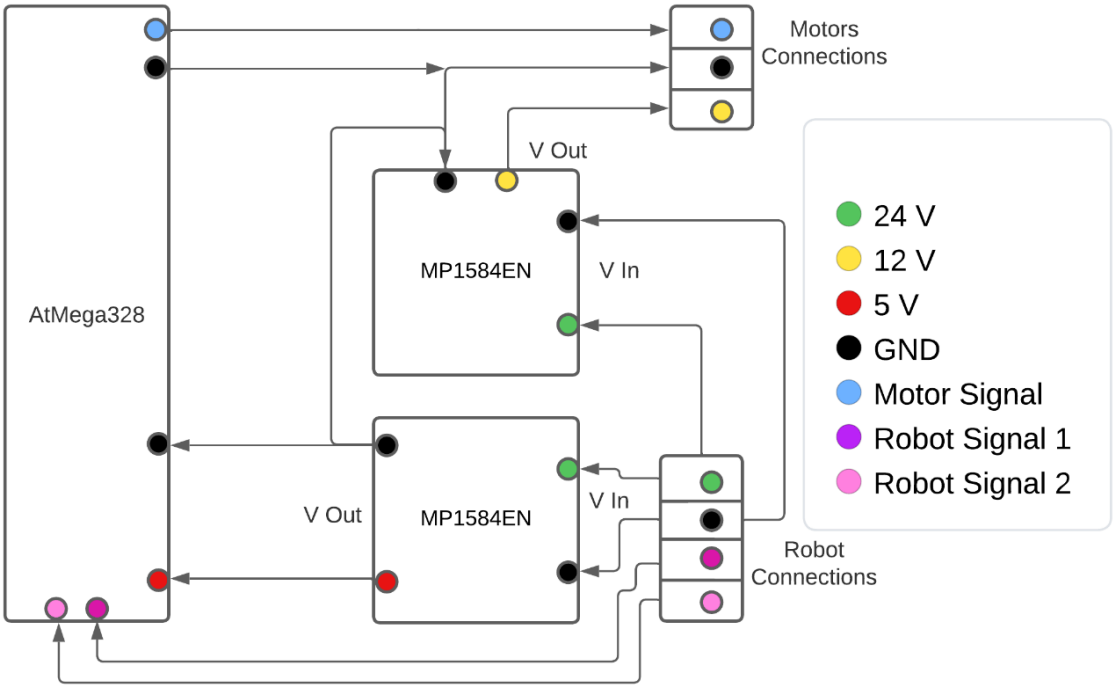

Figure 81 GAR's connection diagram

In summary, the voltage (24V) enters the gripper from the robot and is reduced by the MP1584EN chips to 5V for the microcontroller and 12V for the motors, respectively.

In summary, the voltage (24V) is reduced by the MP1584EN chips to 5V for the microcontroller and 12V for the motors, respectively. The Robotic arm supplies this voltage. The input signal of the motors is coupled to the microcontroller, which also gets two digital inputs from the Robot.

Before beginning the design of the motherboard, it is crucial to keep in mind that despite the system's appearance as three independent "islands," All the systems must be connected via a common node (GND) so that all voltages in the system are absolute voltages. Using this information, the circuit board layout is designed (Figure 82):

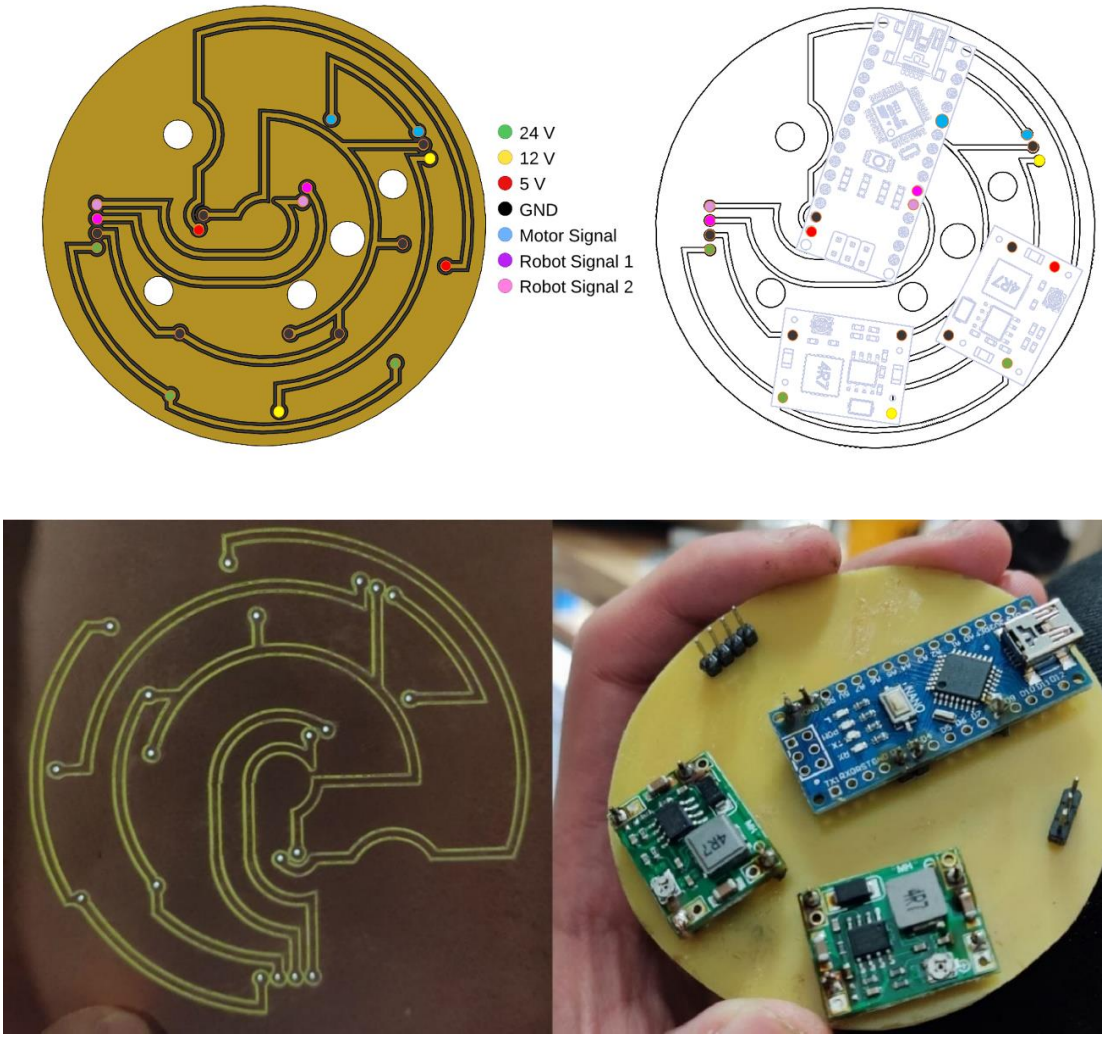

Figure 82 Gar's circuit board

To effectively cover the circuit and integrate it with the gripper, a plastic and aluminum box is built to fix, isolate, and protect the circuit from dust, shocks, and direct contact. This concludes the circuits section.

4.5 Manufacturing and Prototyping

After determining the lengths of the links, determining their cross-sectional areas, and doing a stress analysis, The next step is constructing the prototype using the following manufacturing processes:

- Metal CNC Machining
- Polymers Filament-based 3D printing
- Formation by photosensitive resin

Initially, photosensitive forming is used to evaluate the dimensions. This technology is similar to 3D printing, with the difference that it uses an ultraviolet-sensitive resin. A panel of numerous UV light pixels that can be precisely switched on or off is used for this technique. With these pixels, dimensional tolerances as small as 22 micrometers can be attained. This study used the ELEGOO 2 pro resin printer, which delivers a dimensional stability of 0.05 mm.

When printing components in resin, we must be mindful of their low mechanical resistance. These components will not be used in the final prototype because they cannot withstand the shear and tensile stresses. After verifying the mechanism's dimensions and ensuring that no interferences were missed during the design process, the aluminum components are fabricated (Figure 83 - 86).

Figure 83 Metal parts fabrication - 1

As anticipated, the resin component failed under the calculated loads. After confirming the dimensions, the metal components are fabricated. During the experiment, metal parts may be fabricated thanks to the University of Wisconsin-Biorobotics Milwaukee's laboratory's machinery and equipment. Due to the extremely tight tolerances and the small size of the components, some of them had to be manufactured many times. Mentioned below are some phases of the manufacturing procedure:

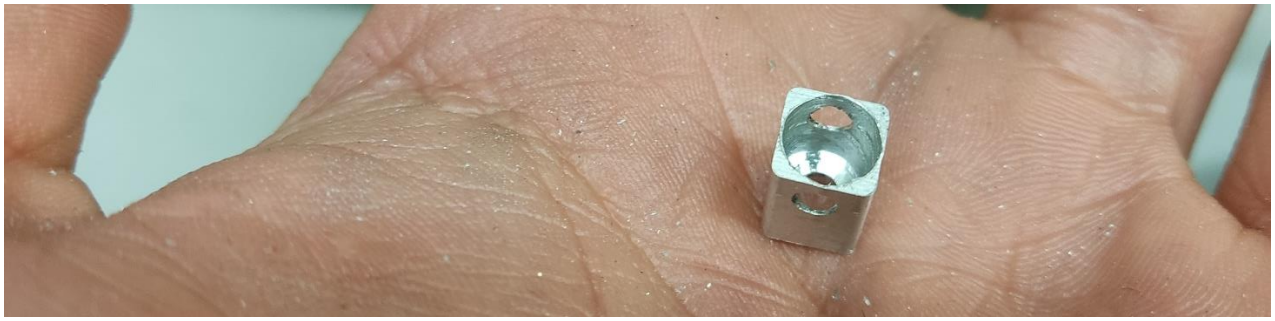

Figure 84 Metal parts fabrication - 2

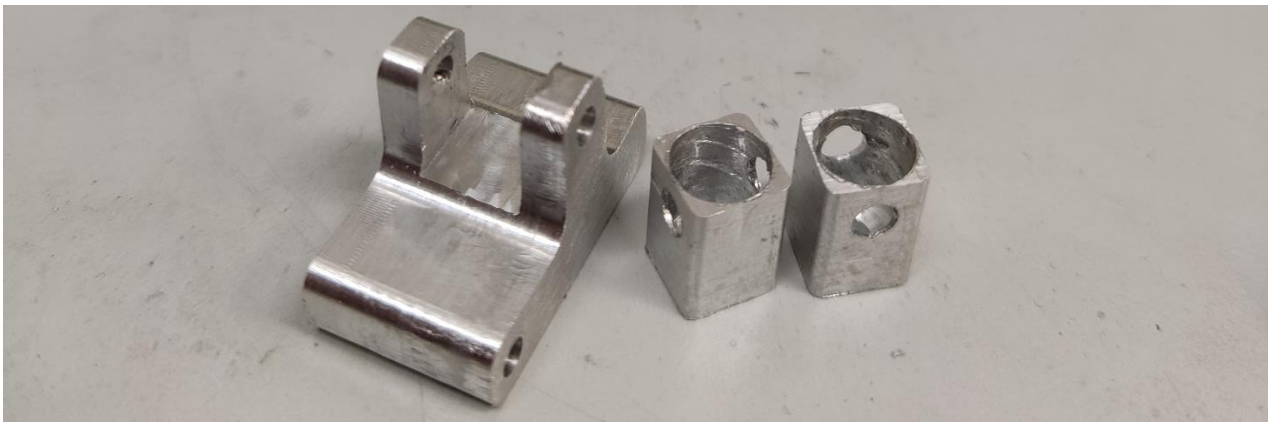

Figure 85 Metal parts fabrication - 3

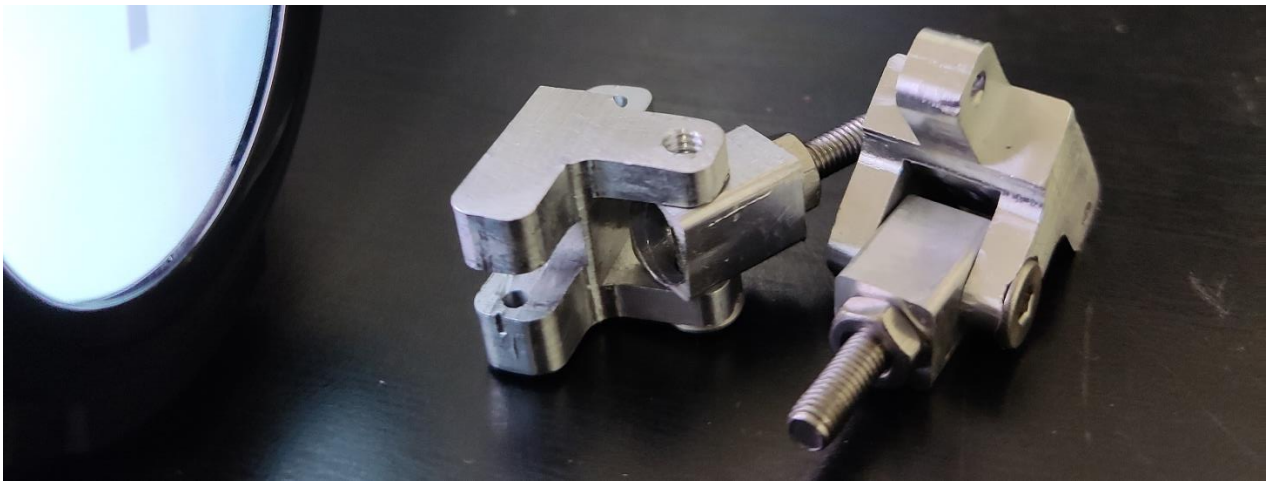

Figure 86 Metal parts fabrication - 4

After printing all the 3D components and fabricating the required metal parts for the mechanism, the gripper was built under the initial conditions: the fingers wholly extended, the gripper in the zero position, and the motors in the zero position. Throughout this research phase, the CAD model served as a guide for assembly. The following photographs (Figure 87 – 89) depict a step of the gripper construction procedure. Next, In Chapter 6, some tests are conducted to validate the gripper's efficacy while grasping items of varying weights and sizes.

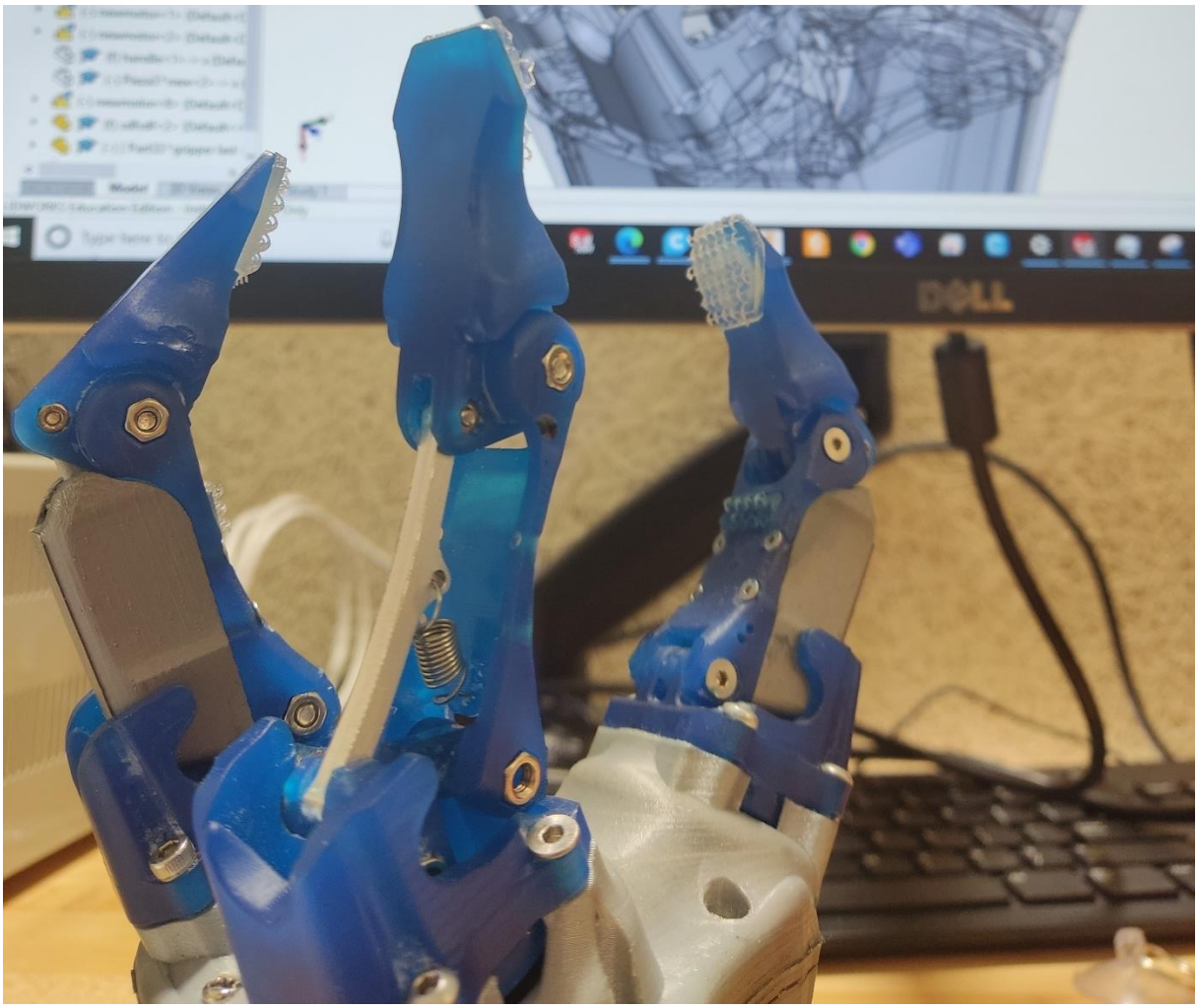

Figure 87 Gar assembly

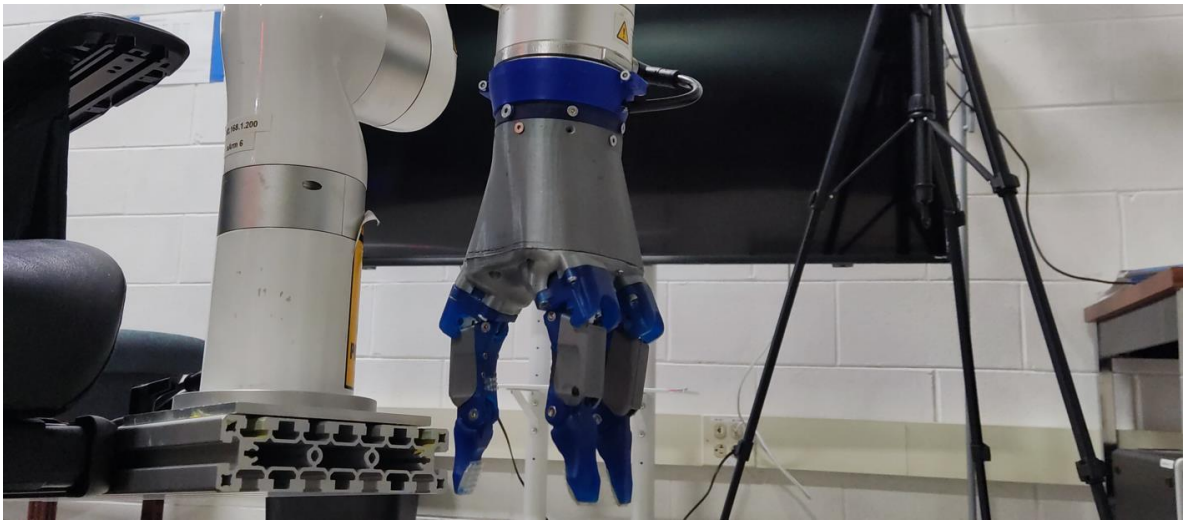

Figure 88 Gar mounted on a robotic arm

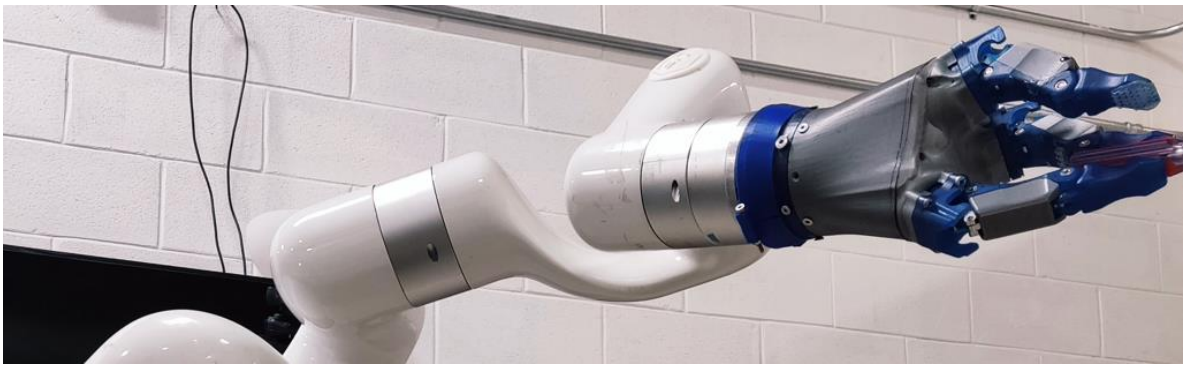

Figure 89 Gar assembled, performing its first task

4.6 Control

As stated previously, motors support two communication protocols: TTL and PWM. TTL, unlike PWM, requires an additional circuit to function. Hence PWM was chosen to control the mechanism.

PWM is the abbreviation for Pulse Width Modulation.

Analog or digital, to send a signal, it must be modulated so that it may be transferred without power loss or distortion due to interference. PWM is a method for transmitting analog signals with a digital carrier signal. In this method, the duty cycle of a periodic signal (such as a sinusoidal or square waveform) is altered to convey data across a communications channel or manage the amount of energy supplied to a load. The duty cycle of a periodic signal is the duration of the signal's positive portion relative to its period. It is stated as a percentage; consequently, a 10% duty cycle represents a high level of 10 out of 100.

$$Duty\ cycle\ =\ t\ /\ T$$

$$T = \mathrm{T}ime\ Period$$

Essentially, it involves activating a digital output for some time and deactivating it for the remainder, creating continuously repeating positive pulses. Therefore, the frequency (i.e., the

duration between pulses) remains constant, but the pulse width, or duty cycle, varies. Over time, the average of this output voltage will equal the required analog value (Figure 90).

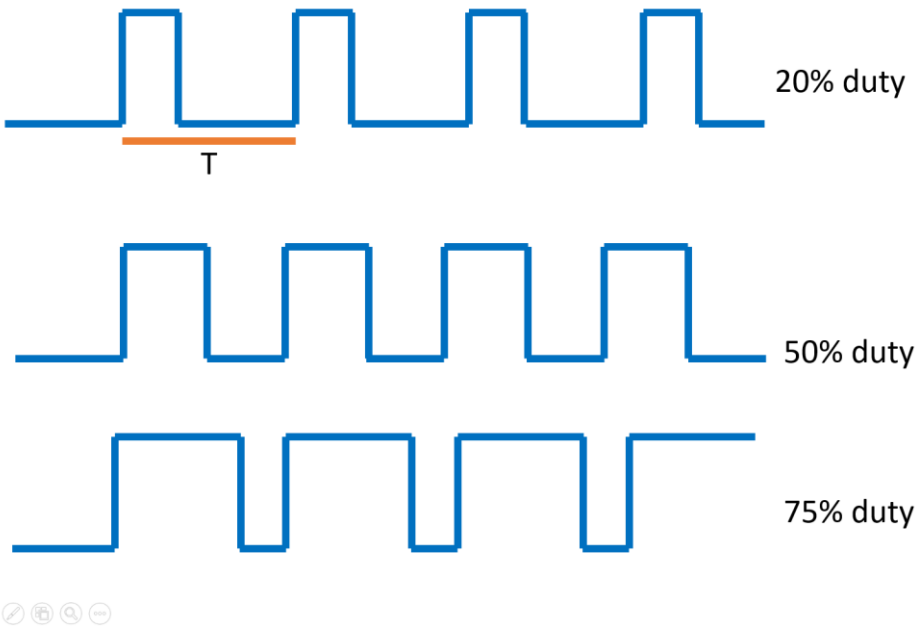

Figure 90 PWM duty cycles representation

It means that the mean voltage will be equal to:

$$V_{mean} = V_{Max} \frac{Duty\ Cycle}{100}$$

The MightyZap 12Lf-100-30 motor is classified as a servo motor. A Servomotor is a DC-powered device that can control position (0mm to 27mm stroke) or linear speed with incredible precision. As indicated earlier, it has three connecting pins: power, GND, and signal. For the latter, this PWM signal will be sent thru the control system to inform the servomotor about the desired position or speed.

The manufacturer-specified servo control signal has a period of 20 milliseconds, while the pulse width ranges from 1 millisecond to 2 milliseconds between the lowest and maximum servo positions.

With this in mind, the C++ code was written to be loaded into the microcontroller. Next, The code was tested to ensure that all system components function correctly. As an advantage, the Arduino development platform is used, which enables the loading of libraries that simplify the coding process:

The VarSpeedServo library is supplied initially.

Var Speed servo is a modified version of the Servo.h library, which allows more control over duty cycles and periods.

#include <VarSpeedServo.h>

Then, a VarSpeedServo object type, named "myservo" in the code, is created. The creation of this object enables the execution of all VarSpeedServo class methods. The following is a list of the class's methods that will be used in this code:

- Obj.attach(): This function initializes a previously constructed object of type VarSpeedServo and parents it to a microcontroller pin.
- Obj.write(): This method uses the previously assigned pin to generate a PWM with the desired Duty Cycles and period. This command can control the location and velocity of GAR's fingers.

If the desired position is not equal to the measured position, the motor's integrated circuit board readjusts the axis position until the desired point is reached.

VarSpeedServo myservo;

Next, a counter is defined, and the microcontroller's pin eight motor signal is initiated. Additionally, the communication pins linked to the robot (pins 11 and 12) and a Led attached to pin 13 to indicate system settings are also initialized. Finally, since most industrial robots emit current signals, the integrated PULLUP resistors on the Arduino nano board are initialized. Like a voltage divider, a voltage change is monitored each time the gripper receives a signal.

int cont = 0;

void setup() {

myservo.attach(8);

pinMode(11, INPUT_PULLUP);

pinMode(12, INPUT_PULLUP);

pinMode(13, OUTPUT);

The following line of code is provided to guarantee that the gripper always begins in the zero position, as well as the motors:

myservo.write(0,15,true);

delay(5000); }

The primary loop that will perform all microcontroller operations involves two steps. In the first phase, the microcontroller awaits inputs from the robot in order to update the motors' locations and speeds:

void loop() {

int sensorVal1 = digitalRead(11);

int sensorVal2 = digitalRead(12);

During each cycle of processing, it is then determined if the robot has transmitted a signal to the gripper. These cycles occur at a rate of around 16 MHz; therefore, this might be considered a real-time readout. Upon receiving a signal, the gripper responds by opening or closing the fingers, depending on the robot's command:

if (sensorVal1 == LOW) {

if (cont <= 60){

digitalWrite(13, HIGH);

cont = cont + 2;

myservo.write(cont,15);

delay(150);}}

else {

digitalWrite(13, LOW);}

if (sensorVal2 == LOW) {

if (cont >= 4){

digitalWrite(13, HIGH);

cont = cont - 2;

myservo.write(cont,15);

delay(150); } }

else {

digitalWrite(13, LOW);}}

Since the motor shaft's maximum length is above the mechanism's requirements, the fingers might be exposed to loads for which they were not built. For that reason, Note that the value of the counter is restricted between 5 and 60. This is done to establish a maximum limit for the GAR fingers.

A semi-open loop control is used for GAR. Since the location of the mechanism's phalanges is known. However, the forces to which the system is exposed during contact with objects are unknown, and the mechanism's behavior cannot be predicted. Literature suggests the development of strain-sensitive materials that release a very low voltage each time they are stretched.

A less complicated and widely used method is putting piezoelectric or tensiometric gauges inside each finger.

Not mentioned in the chapter on design is that GAR includes an internal mechanism that enables the addition of piezoelectric sensors inside the phalanges. However, piezoelectric sensors need a signal amplification system and fuzzy logic-based control algorithms that are incompatible with the capabilities of the microcontroller used in this study.

As demonstrated in Figure 91, the idea of adding these sensors is kept open for future study.

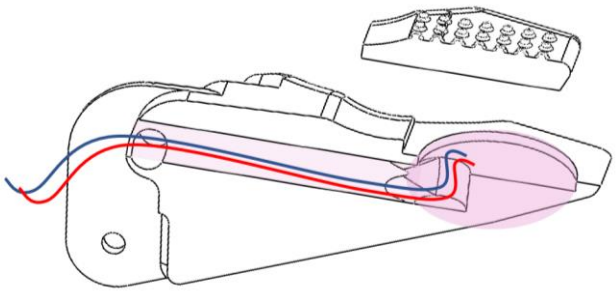

Figure 91 Integrated piezoelectric sensors system

4.7 Troubleshooting

There were a total of three physical editions and ten digital variants created during the GAR development stage. Unfortunately, design flaws and unforeseen mechanical problems were discovered during these iterations, including the following:

The gripper broke quickly in the initial prototype because all the pieces were 3D printed and resin.

By remaking the same pieces in aluminum and varying their thickness, this problem was resolved.

The original set of motors used (Actruonix PQ12) also had issues since they provided poor feedback despite having sufficient strength to hold the majority of objects. In addition, they were not self-locking, necessitating their replacement.

During the third revision, the following issues were discovered:

1) The finger screws must be adjusted to rotate without moving out of place.

2) Compared to earlier versions, the springs used in that version were weaker.

3) Because the new motors are larger, there needs to be more space within the case to accommodate them all.

4) The previous model driver proved ineffective because more current was required to drive the motors.

5) because this version of the mechanism is so strong, the plastic phalanges of the fingers shattered during testing when they were pressed too firmly against one another.

To solve these problems, the following solutions were proposed and executed satisfactorily:

The gripper screws were tightened with enough Loctite thread locker to allow rotation without misalignment.

The springs were replaced inside the mechanism to guarantee complete finger withdrawal when releasing an object.

The coupling points of the motors were relocated to prevent interference to tackle the problem of the motors colliding inside the casing.

Several circuits were put together inside and outside the gripper to quickly conduct the tests even though the final form of the circuit still needed to be designed.

Maximum restrictions have been programmed for the ranges that the fingers can move to prevent the fingers from fracturing when pressed firmly together.

CHAPTER 5

KINEMATICS AND DYNAMIC MODELING

For the GAR design, an underactuated mechanism was selected. It indicates that the DOF is more than the number of degrees of actuation. Furthermore, the internal mechanism is preloaded by a spring, which means that forces are acting on some joints even when the gripper is in its starting position.

The mechanism features a closed kinematic chain, a crucial factor to consider. Open chain kinematic systems consist of elements or links connected by joints that provide relative motion between each pair of constituent links [125].

In the case of GAR, its mechanism more closely resembles that of a parallel kinematics mechanism, distinguished by the fact that several of the mechanism's links are interconnected, generating closed kinematic chains.

Methods widely applied to open kinematic chains, such as the Denavit-Hartenber parameters [126], are inapplicable to closed kinematic chains because they cannot be correlated in the region shared by two or more links. Another common approximation is the virtual work method, which must be supplemented with the theory of bolts to operate on non-actuated joints, thereby significantly complicating the kinematic and dynamic approach [127].

The underactuated nature of the mechanism automatically transforms its kinematics into a quasi-static problem, yet another reason not to employ the abovementioned methods. Some writers [124] have developed approaches predicated on assumptions such as all phalanges having contact and the knowledge of the usual forces acting on the phalanges. Other, more

daring authors have adopted the notions of screw theory and modified them for an underactuated n-phalanges mechanism [128].

This research provides its own approach to solving the system's kinematics and dynamics based on the last two methods described. The assumptions presented in [124] will serve as a starting point for the kinematic analysis, along with simulation data such as the magnitudes and directions of the normal forces applied on the phalanges.

The methodology proposal will be founded on the following bullet points:

- Generate a vectorial representation of the mechanism using the measurements discovered in Chapter 4 (Figure 92).
- Specify the system's beginning conditions, such as the usual forces in the phalanges and the force exerted by the spring on the mechanism.
- Present the mechanism's vector loops and locate all of its angles geometrically.
- Use the determined angles to distribute the forces throughout the entire mechanism.
- Finally, the torque the motor exerts and the linear force the motor must exert to meet the quasi-static condition is determined.

Due to the numerous assumptions and equations presented by this methodology, this chapter will be divided into three sections:

• Methodology for the quasi-static case and beginning conditions

• Development of the vector ties geometrically and determining the angles of the system

• Transport of the forces to the place of interest and calculation of the needed torque for the motor

5.1 Kinematics

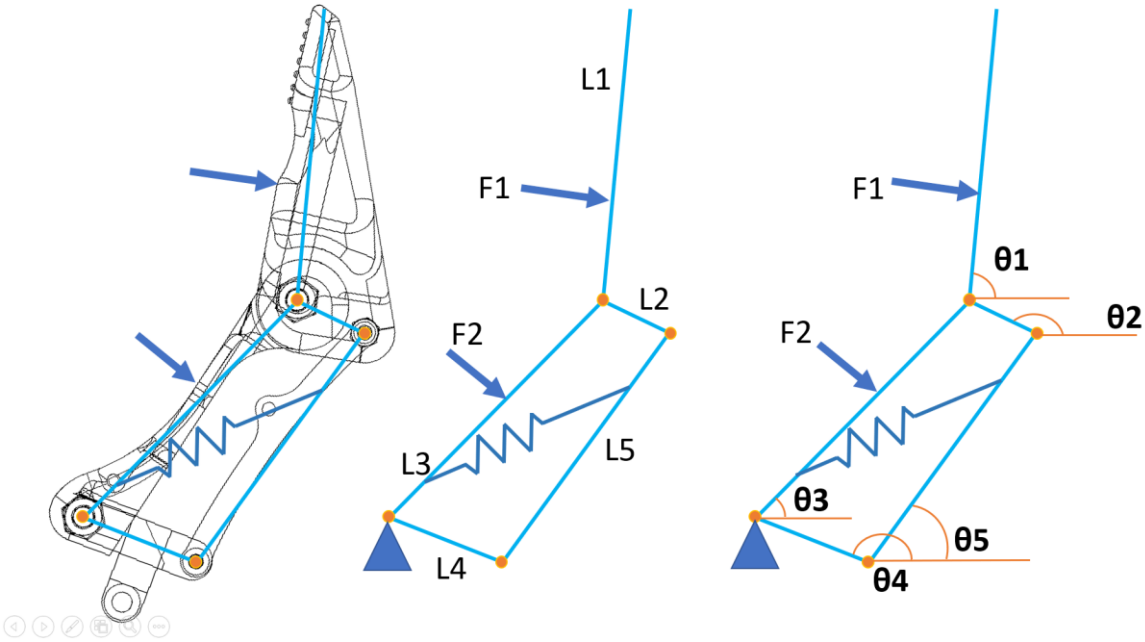

Figure 92 Vectorial representation of Gar's mechanism

As previously stated, since the system is an underactuated mechanism with a preloaded spring, forces and positions must be analyzed simultaneously, as opposed to separately, as is the case with most of the methods described on the preceding page.

Since the objective is to determine the minimum torque of the motor, we will begin by assuming that both phalanges are in contact with an object's surface [124].

We will accomplish this using an object that represents the critical design case. This object is a 5kg cylinder with a 100mm diameter for which the normal and perpendicular directions are calculated and simulated (Figure 93).

$$F = \frac{W}{\mu * n} = 16.33\ N$$

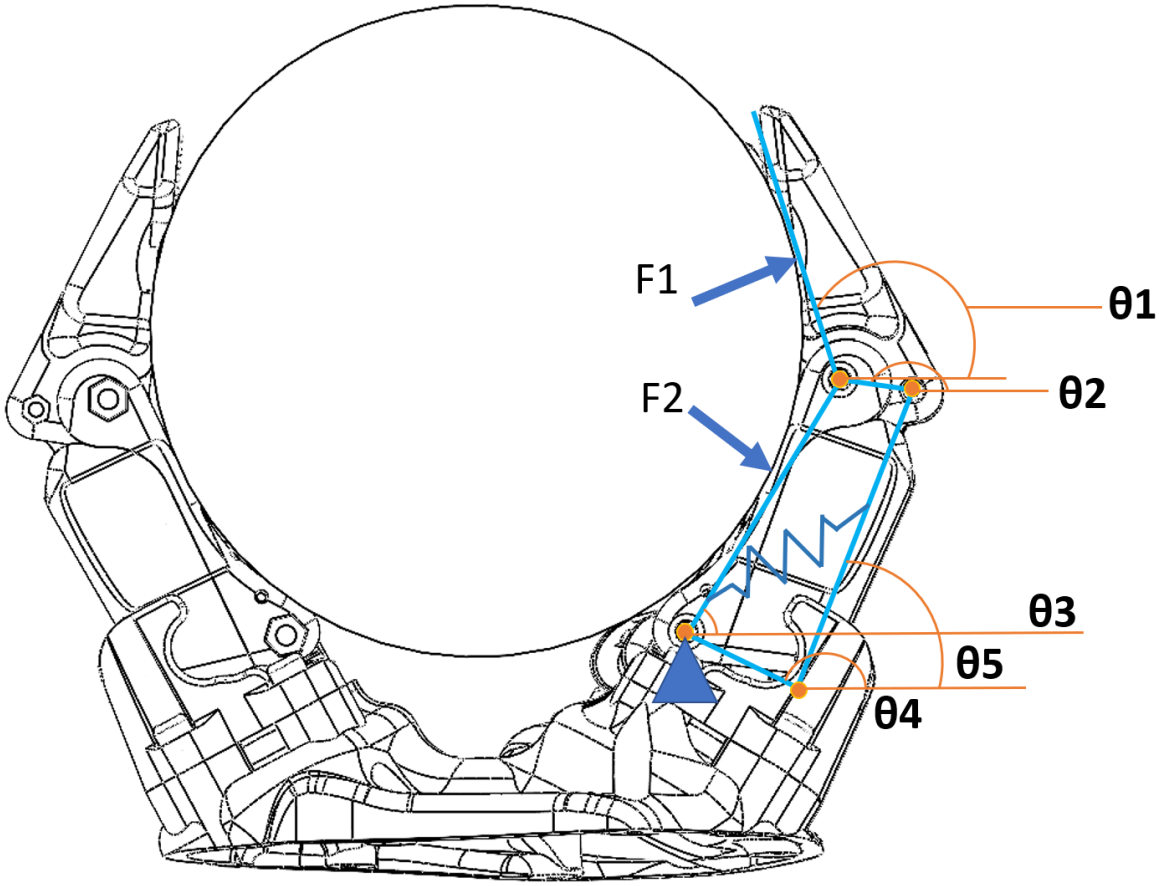

Figure 93 Critical case representation

First, the forces' directions are simulated, which are as follows (Figure 94):

$$\Theta_{F1} = 14.56°$$

$$\Theta_{F2} = 331.57°$$

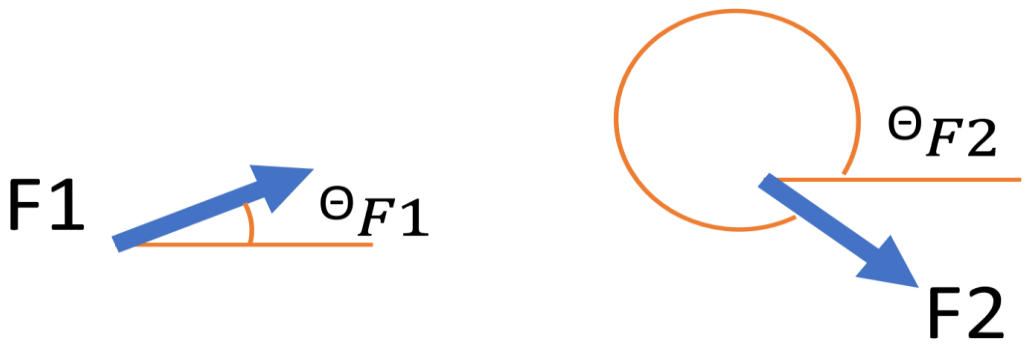

Figure 94 Frame of reference of normal force vectors.

Step 1:

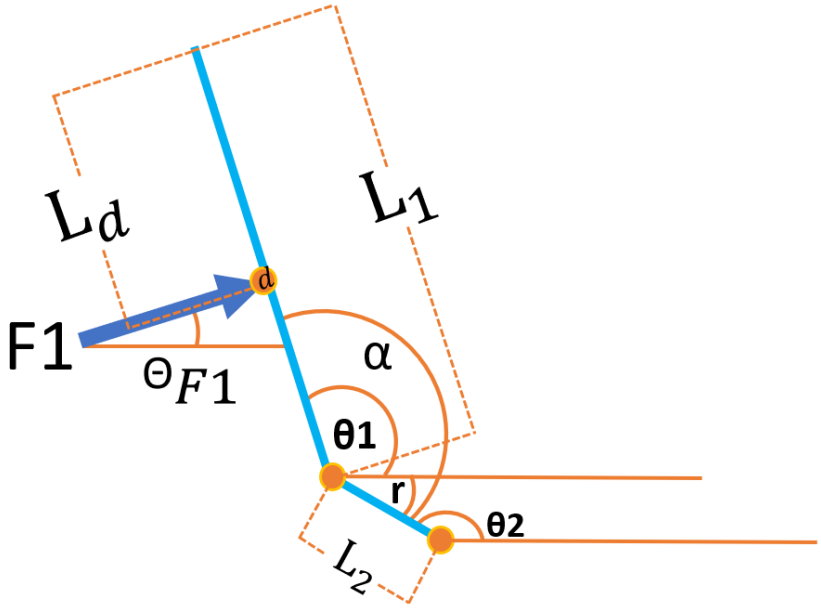

Figure 95 Angles distribution in the first phalanx

The point of contact of the first force with the distal phalanx is defined (Figure 95). This point of contact is called d, and from the angle generated by the force *F1*, we can define the angle *θ1* from the following equation:

$$\theta 1 = 90° + \theta_{F1} \quad (1)$$

Analogically, we seek to solve the angle *θ2*, knowing that there is a fixed angle between *L1* and *L2* called *α*. Given that, the distal phalanx is a ternary link (which means that the same body has two rotation points, and therefore, the internal angles between the joints

that compose it are fixed angles). To find α an auxiliary angle called *r* is used, as shown in Figure 96

$$r = \alpha - \theta 1 \quad (2)$$

$$\theta_2 = 180 - r \quad (3)$$

Again, this same method is used to find $\theta 3$, which is equal to:

$$\theta_3 = 90° + \theta_{F2} \quad (4)$$

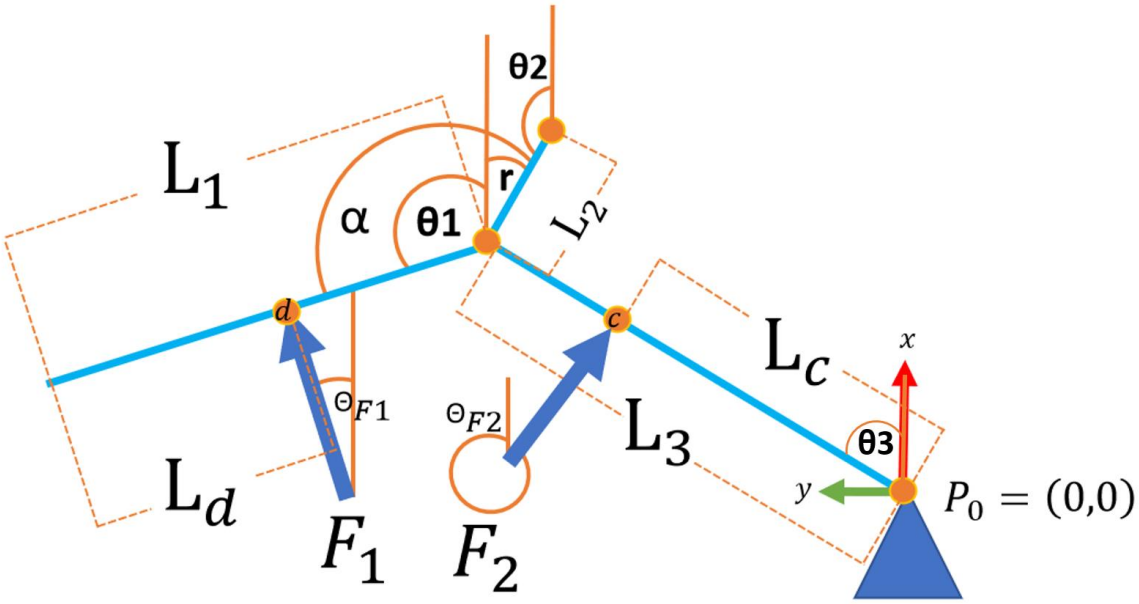

Figure 96 Angles distribution in the second phalanx - 1

Since the entire mechanism is pivoting concerning a fixed point, the point *P0* is defined, from which the relative positions of the links are determined.

Step 2 :

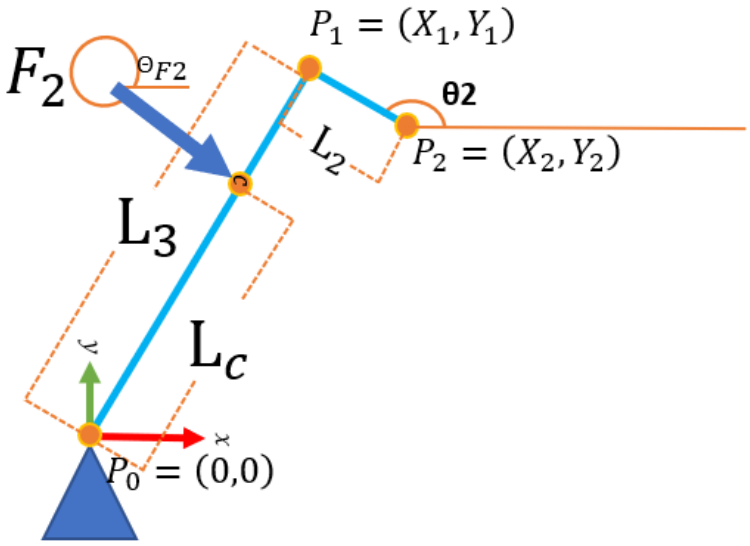

Figure 97 Angles distribution in the second phalanx – 2

On the basis of the link measurements and the angles of *L1* and *L2*, we proceed to determine *P2 (Figure 97)*, which will be utilized later. To locate *P2*, a vector loop extending from the origin (*P0*) to *P2* is generated and traversed as follows:

$$V_{0-1} + V_{1-2} = P_2 \quad (5)$$

$$X_2 = L_3 Cos_{\theta 3} - L_2 Cos_{\theta 2} \quad (6)$$

$$Y_2 = L_3 Sin_{\theta 3} - L_2 Sin_{\theta 2} \quad (7)$$

$$P_2 = \begin{bmatrix} L_3 Cos_{\theta 3} - L_2 Cos_{\theta 2} \\ L_3 Sin_{\theta 3} - L_2 Sin_{\theta 2} \end{bmatrix} \quad (8)$$

Step 3:

Now, with the coordinates (X_2, Y_2), we find the norm of the vector that goes from $P_{0(0,0)}$ to $P_{2(x2,y2)}$ and also its direction, given by the angle β:

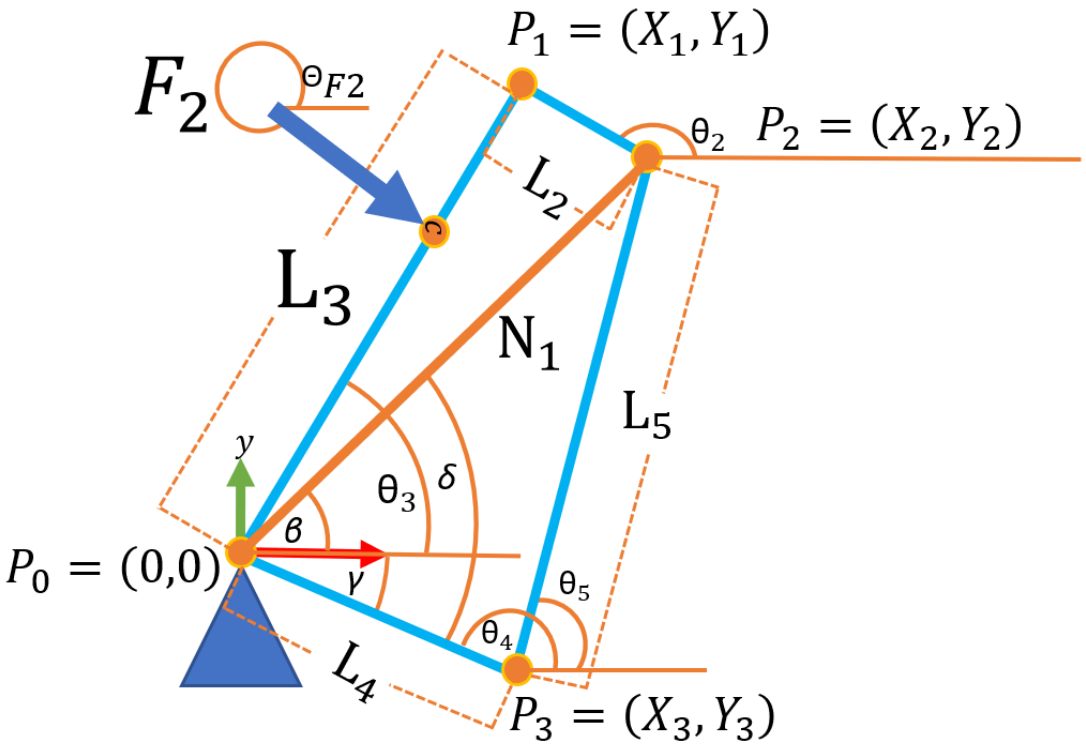

Figure 98 Angles distribution between the proximal phalanx and the mechanism

$$N_1 = \sqrt{({X_2}^2 + {Y_2}^2)} \quad (9)$$

$$\beta = \tan^{-1}\frac{X_2}{Y_2} \quad (10)$$

Furthermore, with the value of β, we proceed to find the value of γ, δ and the angle of the active joint θ_3 (Figure 98). But, first, cosine law is used to find the angle δ from the length of N, L_4, and L_5:

$${L_5}^2 = \left(N^2 + {L_4}^2\right) - 2N(L_4 Cos_\delta) \quad (11)$$

$$\delta = \cos^{-1}\frac{-{L_5}^2 + \left(N^2 + {L_4}^2\right)]}{2NL_4} \quad (12)$$

$$\gamma = \delta - \beta \quad (13)$$

$$\theta_4 = 180 - \gamma \quad (14)$$

Step 4:

To complete the kinematic analysis, θ_5 (Figure 98) is found using the γ angle:

$$X_3 = L_4 Cos_\gamma \quad (15)$$

$$Y_3 = -L_4 Sin_\gamma \quad (16)$$

$$P_3 = \begin{bmatrix} L_4 Cos_\gamma \\ -L_4 Sin_\gamma \end{bmatrix} \quad (17)$$

$$\theta_5 = \tan^{-1}\left[\frac{L_3 Cos_{\theta 3} - L_2 Cos_{\theta 2} - L_4 Cos_\gamma}{L_3 Sin_{\theta 3} - L_2 Sin_{\theta 2} + L_4 Sin_\gamma}\right] \quad (18)$$

Finally, the system's kinematics is obtained, which results in all the angles of the mechanism calculated from the direction of the contact forces.

With these angles described, we analyze forces in the mechanism.

5.2 Dynamics

To solve the dynamics of complex systems, numerous approaches have been developed. To name a few examples, The well-known Newton-Euler approach [131] applies to most dynamic systems. Moreover, the Lagrange–D'Alembert [132] is a more sophisticated method that combines a Jacobian and Hessian formulation to solve the dynamics of nearly any mechanical model.

Since the kinematics was solved geometrically, we have used a traditional method for this research, which attempts to project the forces of the mechanism in its nodes and transport them to the points of interest through unit vectors that are pointing in the parallel and perpendicular direction of the links (Figure 99) [130].

We will begin by specifying critical characteristics such as:

• Where is the force positioned relative to the phalanx?

• What force does the spring apply to the mechanism?

• How do forces travel from one node to the next?

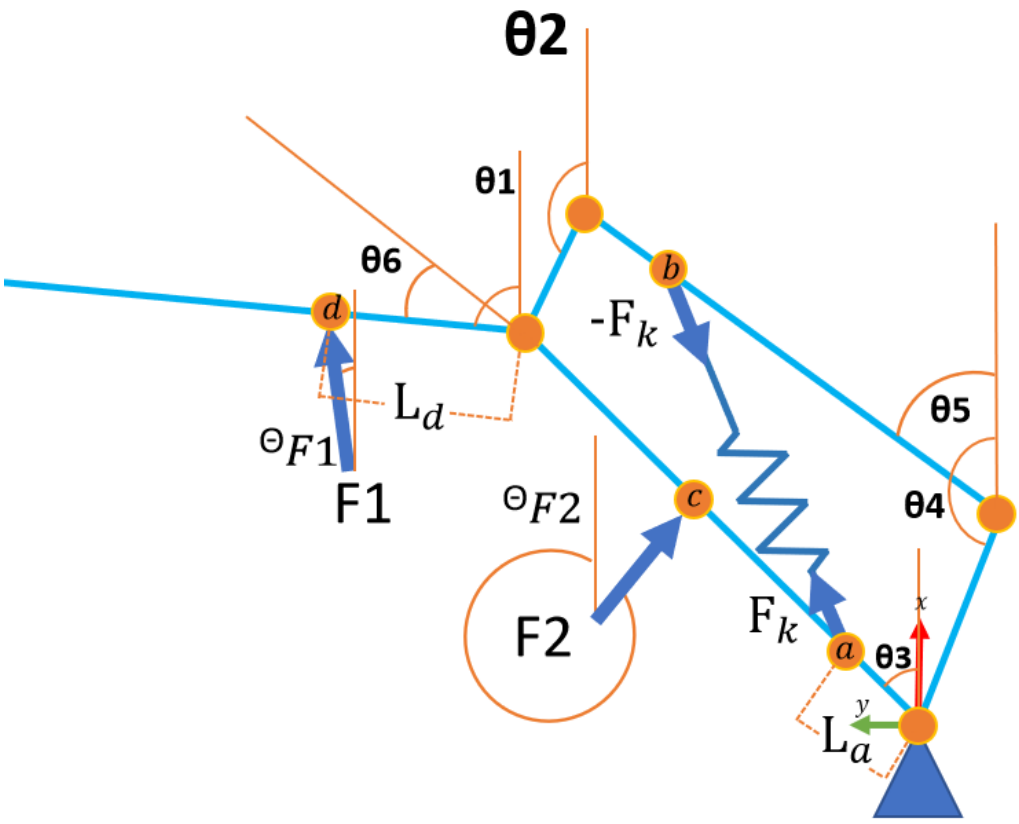

Figure 99 Diagram illustrating the system's input forces

Prior to answering these questions, specific terms must be defined and the mechanism's joints must be identified/classified.

We will begin by defining the spring's stiffness using a dynamic model based on [133].

The following equation is produced by setting the input virtual power equal to the output virtual power:

$$t^T \omega a = f^T T v \quad (19)$$

Where: (t = vector of input torque | a = vector of velocity | f = vector of contact wrenches | v = vector of contact point twist)

$$t = \begin{bmatrix} T_a \\ F_k - K\Delta\theta_6 \end{bmatrix} \quad (20)$$

$$\omega_a = \begin{bmatrix} \dot{\theta}_4 \\ \dot{\theta}_6 \end{bmatrix} \quad (21)$$

$$f = \begin{bmatrix} \zeta_1 \circ \\ \zeta_2 \circ \end{bmatrix} \quad (22)$$

$$v = \begin{bmatrix} \xi_1 \\ \xi_2 \end{bmatrix} \quad (23)$$

The actuation wrench is denoted by *Ta*, the spring stiffness is denoted by *K*, and the first derivative of the joint angles at the phalanges is denoted by $\dot{\theta}_\iota$

By adding the moment *mz* from the force axis around the platform center to the force unit vector $f = [f_i^x, f_i^y]$ for i= 1, 2, we can derive the corresponding row vectors $\zeta i \circ = [mz, f_i^x, f_i^y]$.

Also, the three-dimensional vector for planar twist is $\xi_i = [\omega_z \, v_i^x, v_i^y]$.

Then, substituting into the equations, we get:

$$F_k - K\Delta\theta_6 \begin{bmatrix} \dot{\theta}_4 \\ \dot{\theta}_6 \end{bmatrix} = [\zeta_1 \circ \quad \zeta_2 \circ] \begin{bmatrix} \xi_1 \\ \xi_2 \end{bmatrix} \quad (24)$$

And that's equal to:

$$T_a\dot{\theta}_4 - K\Delta\theta_6\,\dot{\theta}_6 = \zeta_1 \circ \xi_1 + \zeta_2 \circ \xi_2 \quad (25)$$

Now all that remains is to solve for the spring constant based on the desired torque. Since the torque is still unknown, the spring constant will be expressed.

$$K = \frac{T_a\dot{\theta}_4 - \zeta_1 \circ \xi_1 - \zeta_2 \circ \xi_2}{\Delta\theta_6\,\dot{\theta}_6} \quad (26)$$

The next step will define how forces and torque are transmitted between the joints.

There are two types of revolute joints: actuated revolute joints and passive (non-actuated) revolute joints [130].

Actuated revolute joints have a degree of actuation linked to them or rotational restriction. On the other hand, passive revolute joints join links together but do not transmit any torque. One example of this kind of joint is: two bars joined with a ball bearing between the two bars. This implies that when exerting a force at any point of a link that has passive volute joints, when displacing this force to the nodes of the link, only the corresponding component of the force will be transmitted. However, the moment generated by this will not be transmitted.

Let's take as an example the following link, which is inclined an angle θ_2 concerning the horizontal and receives a force F_1 with an angle θ_1 at a distance d_1 (Figure 100).

First, the objective will be to transform the force F_1 into nodal forces. These nodal forces must be perpendicular or parallel to the element to transmit them to the next element.

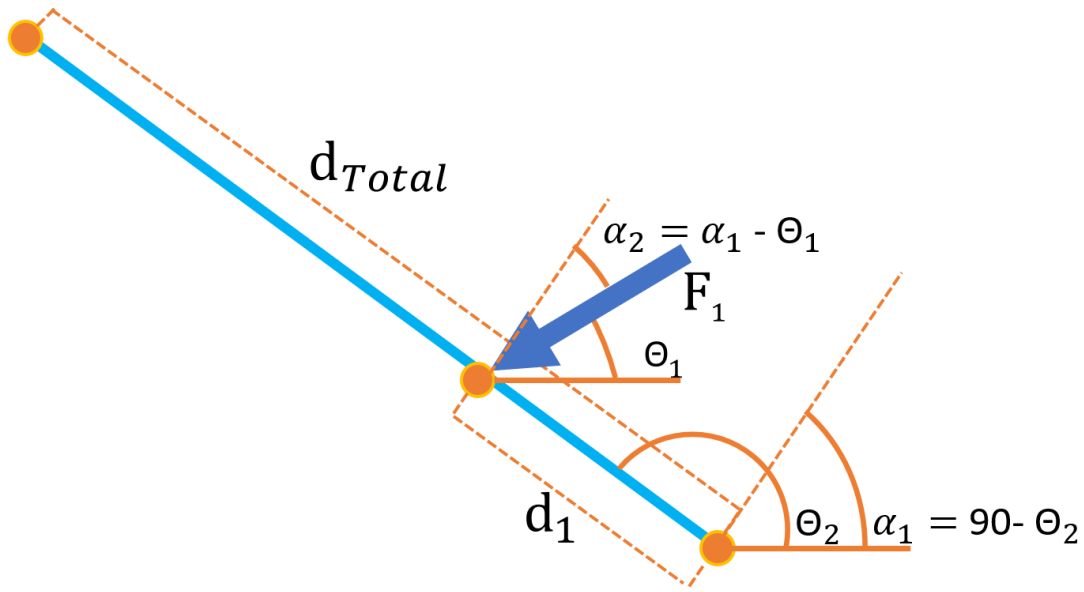

Figure 100 Transformation of forces into nodal forces – example

For this, the force F_1 is transformed into two components: a perpendicular component and an axial component.

The perpendicular component is transported to the nodes as a function of the distance d_1 , while the axial component is shared equally between the two nodes. As a result, given (F_1, d_1, θ_1 y θ_2), the following two equations are obtained that describe the perpendicular and axial component of the force F_1:

$$\alpha_1 = 90 - \theta_2 \quad (27)$$

$$\alpha_2 = \alpha_1 - \theta_1 \quad (28)$$

Now the problem is divided into two cases:

The first case can be analyzed when two joints are fully active, which means that the torque generated by the perpendicular force to the bar will also be transmitted to both nodes with different magnitudes. For this case, we will have a set of equations that will define the magnitudes and directions of the nodal forces and the moments (Figure 101).

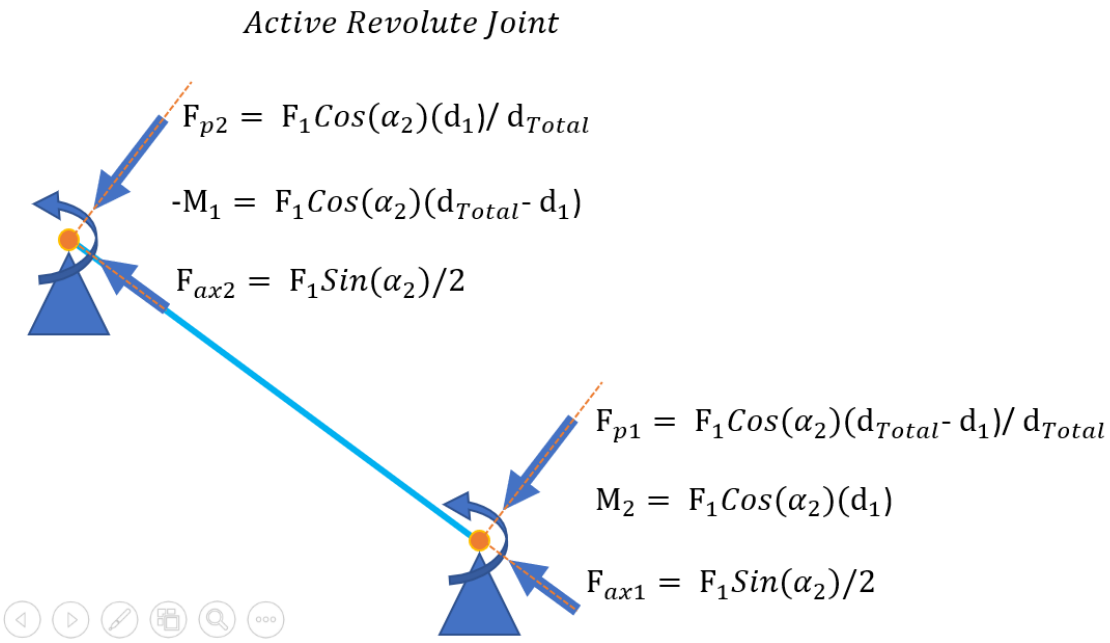

Figure 101 Transformation of forces into nodal forces – case 1

$$F_{\perp 1} = F_1 \cos(\alpha_2)\frac{(d_{total} - d_1)}{d_{total}} \quad (29)$$

$$F_{\perp 2} = F_1 \cos(\alpha_2)\frac{d_1}{d_{total}} \quad (30)$$

$$F_{ax1} = F_{ax2} = F_1 \frac{\sin(\alpha_2)}{2} \quad (31)$$

$$-M_1 = F_1 \cos(\alpha_2)(d_{total} - d_1) \quad (32)$$

$$M_2 = F_1 \cos(\alpha_2)(d_1) \quad (33)$$

The second case is when one or two of these links are passive; that means they do not have a degree of action or a rotational restriction. In this case, the links can have a relative motion, implying that the moment is not transmitted between the links. Therefore, only four equations are generated (Figure 102):

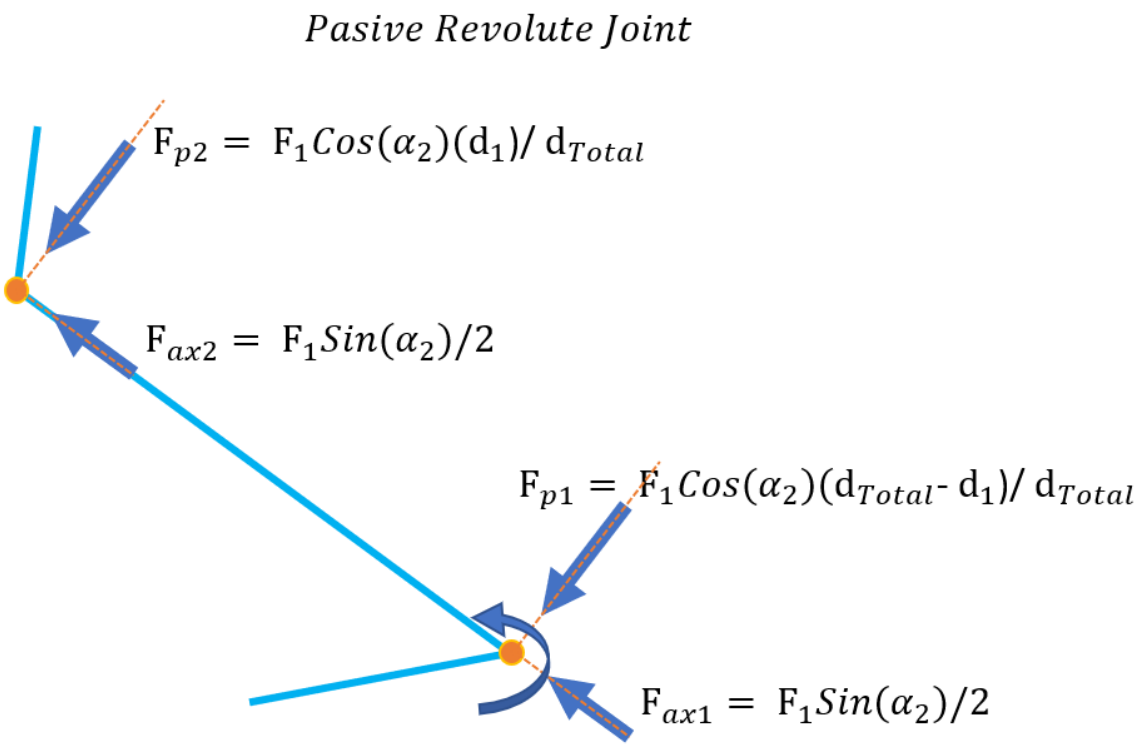

Figure 102 Transformation of forces into nodal forces – case 2

$$F_{\perp 1} = F_1 \cos(\alpha_2)\frac{(d_{total} - d_1)}{d_{total}}$$

$$F_{\perp 2} = F_1 \cos(\alpha_2)\frac{d_1}{d_{total}}$$

$$F_{ax1} = F_1 \frac{\sin(\alpha_2)}{2}$$

$$F_{ax2} = F_1 \frac{\sin(\alpha_2)}{2}$$

Finally, the motor torque can be estimated vectorially from the transmission of all forces to the active revolute of the finger mechanism because of these equations.

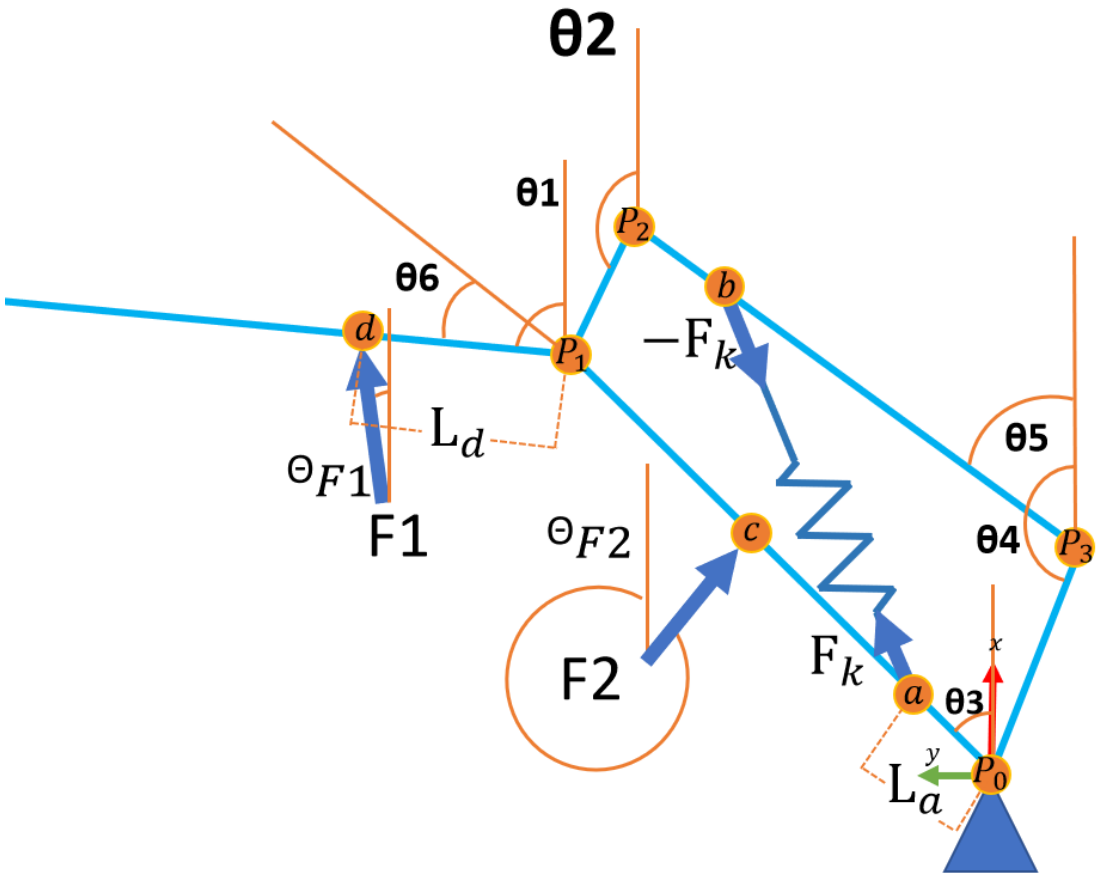

Figure 103 Location and orientation of forces in the mechanism

First, each force's influence on the bar nodes (P_0P_1) must be computed.

For this, the position of the perpendicular component relative to the bar is checked. It will determine how much of this force is absorbed by node P_0 and how much by node P_1 (Figure 103). Note that nodes P_0 *and* P_1 are nodes with passive revolutes, as the degree of actuation is not located directly on the revolute but is communicated from a lever mechanism anchored to link 4.

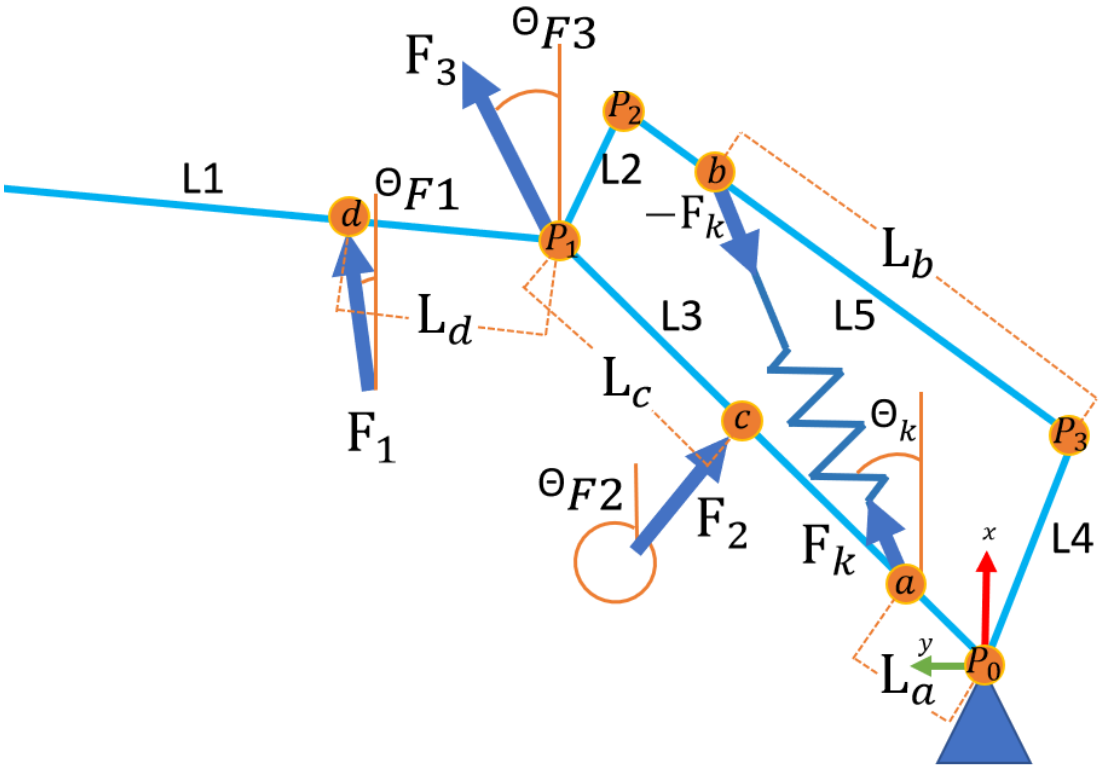

Figure 104 Location and direction of F3 force

Thus (Figure 104):

$$F_3 = \begin{bmatrix} \frac{(L_3 - L_c)}{L_3} F_2 Cos(\theta_{F2}) + \frac{L_a}{L_3} F_k Cos(\theta_k) + \frac{L_d}{L_1} F_1 Cos(\theta_{F1}) \\ \frac{L_a}{L_3} F_k Sin(\theta_k) + \frac{(L_3 - L_c)}{L_3} F_2 Sin(\theta_{F2}) + \frac{L_d}{L_1} F_1 Sin(\theta_{F1}) \end{bmatrix} \quad (34)$$

Noting that the force F_1 also causes a moment at poinP_1t (due to the fixed angle between $L_1$and L_2), point P_2 receives a perpendicular force respect to L_2 with magnitude $F_{\perp 4} = L_d(F_1)$ (because $F_1$is, by definition, perpendicular to L_1).

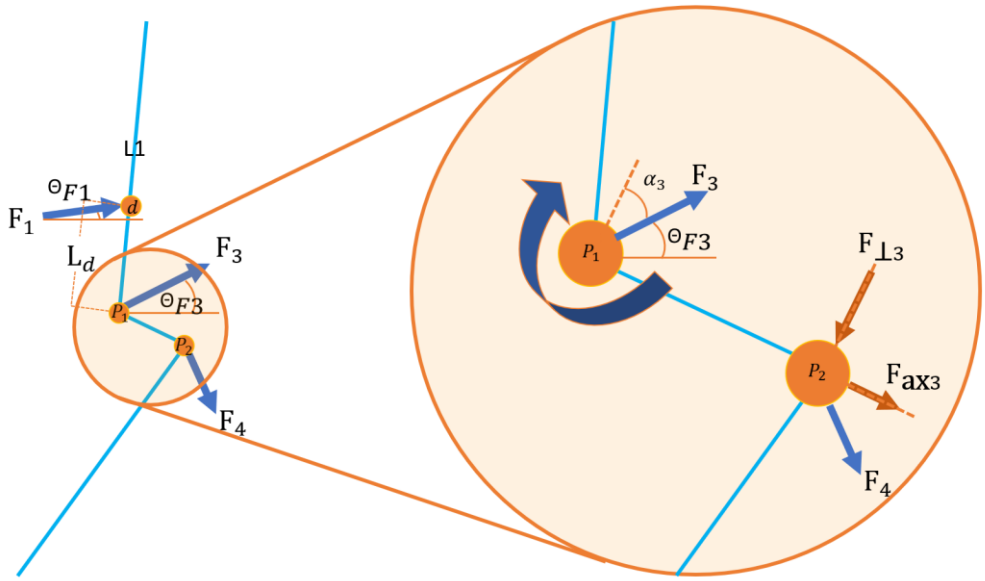

Figure 105 Transformation of F3 into nodal forces in P2

To transmit F_3 efficiently to P_2, we must apply the equations (Eq-29 – Eq-33).

F_3, reflected in P_1, consists of two components: one perpendicular force with respect to L_2 and one parallel force concerning the same element (Figure 105).

F_{ax3} is the only component transferred from P_1 to P_2 because the perpendicular force generated respect L_2 by F_3 is wholly absorbed in node P_1.

P_2 also shows a perpendicular force concerning L_2, resulting from the moment M_1 produces in P_1 by F_1. Consequently, F_4 is located as follows:

$$F_4 = \begin{bmatrix} F_{\mathbf{ax4}} \\ F_{\perp 4} \end{bmatrix} \quad (35)$$

$$F_{\mathrm{ax4}} = F_3 \frac{\sin(\alpha_3)}{2} \quad (36)$$

$$F_{\perp 4} = \frac{F_1 L_d}{L_2} \quad (37)$$

Where α_3 is the angle formed between the force F_3 and a unit vector perpendicular to L_2. Similarly, the forces are transferred from P_2 to P_3 using the same principle and adding the tension exerted by the spring on L_5 (Figure 106).

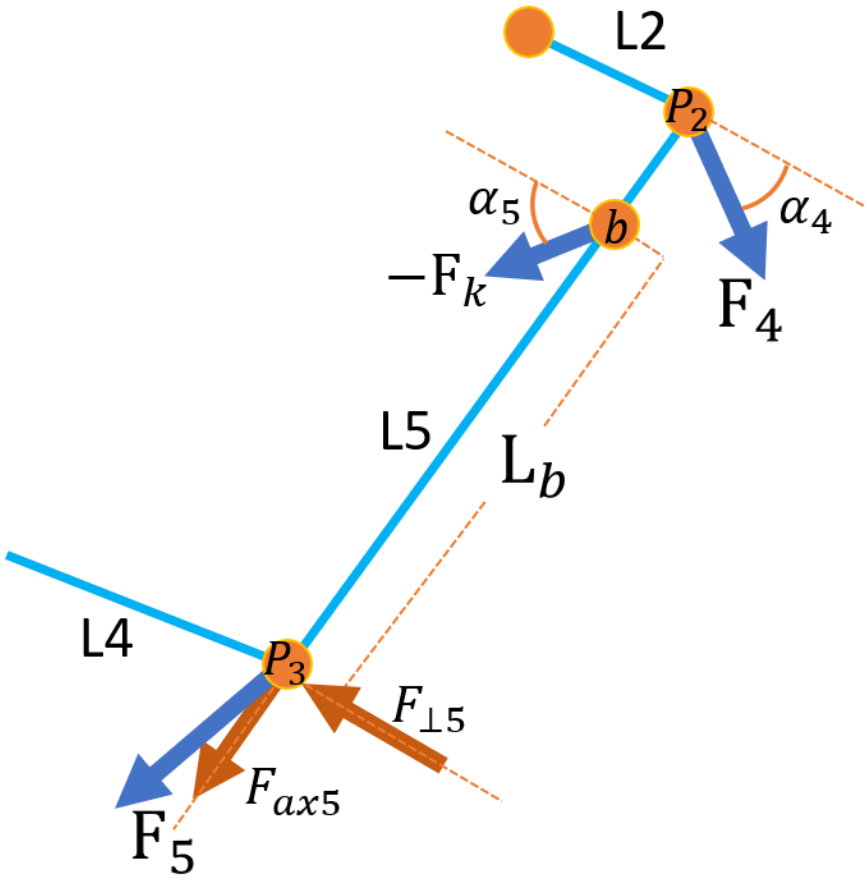

Figure 106 transformation of F3 into nodal forces in P3

$$F_5 = \begin{bmatrix} F_{\mathbf{ax5}} \\ F_{\perp 5} \end{bmatrix} \quad (38)$$

$$F_{\text{ax5}} = -F_k \frac{\sin(\alpha_5)}{2} + F_4 \frac{\sin(\alpha_4)}{2} \quad (39)$$

$$F_{\perp 5} = \frac{-(L_5 - L_{\mathbf{b}})\text{Cos}(\alpha_4)(F_{\mathbf{k}})}{L_5} \quad (40)$$

Finally, it only remains to find the motor's torque based on the perpendicular force generated by F_5. For this, P_0 will be treated as an active revolute joint, only during this step, since the motor is connected as follows (Figure 107)

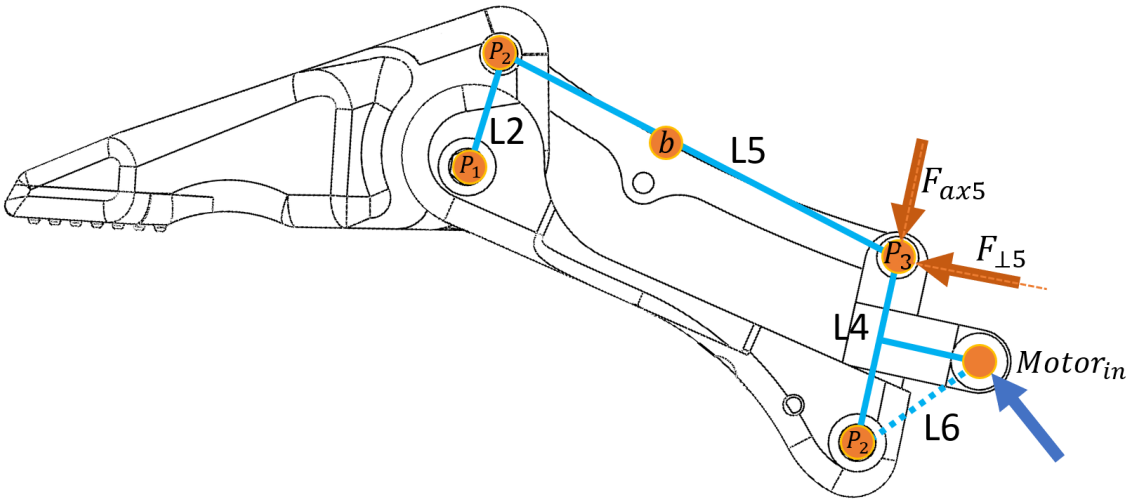

Figure 107 Actual mechanism's force input

It is also added an imaginary length called L_6 which will be the perpendicular distance between the force exerted by the motor and the pivot point P_0. As can be seen, L_6 is a fixed measure that does not vary with respect to the other angles, so the linear force of the motor can be expressed as:

$$M_{(\mathbf{0},\mathbf{0})} = L_4 F_{\perp 5} = L_{\mathbf{4}} \frac{-(L_5 - L_{\mathbf{b}})\mathrm{Cos}(\alpha_4)(F_{\mathbf{k}})}{L_5} \quad (41)$$

$$F_{\mathbf{Motor}} = L_{\mathbf{4}} \frac{-(L_5 - L_{\mathbf{b}})\mathrm{Cos}(\alpha_4)(F_{\mathbf{k}})}{L_5 L_6} \quad (42)$$

Below is a list of angles, forces, and torques, calculated for the critical condition raised (Table:18 - 20):

Table 18 Auxiliar variables and Input parameters

Input	
Parameter	Value
Normal Forces	16.33 N
Θ_{F1}	14.56°
Θ_{F2}	323.6°
α	112.76°
auxiliar variables	
Parameter	Value
r	8.2°
X_2	38.37°
Y_2	34.64°
P_2	(38.97,34.64)
N_1	51.5 mm
β	42.12°
δ	49.77°
γ	7.65°
X_3	17.84
Y_3	-2.4 mm

Table 19 Output Angular variables

output 1	
Parameter	Value
Θ_1	104.56°
Θ_2	171.8°
Θ_3	53.6°
Θ_4	177.8°
Θ_5	61.7°

Table 20 Output Force variables

output 2	
K	9.45 N/mm
F_{3x}	17.27 N
F_{3y}	-1.24 N
F_{ax4}	8.6 N
$F_{\perp 4}$	30.96 N
F_{ax5}	38.93 N
$F_{\perp 5}$	-12.43 N
M	-223 Nmm
F_{motor}	17.85

In conclusion, to carry a weight of 50 Newtons, approximately 53.55 N should be applied by the gripper. This force is distributed across the three gripper fingers.

This difference in the force is because the motors must also overcome the internal forces of the mechanism generated by the springs. This spring can be manufactured with the following specifications: Wire Diameter, wd: 1/32" ; Outer diameter, OD: 13/64" ; Length Inside Hooks, Lih: 1/2" ; Music Wire ASTM A228 [151].

The manufacturer's specifications (Appendix A-2) indicate that the average force that the motor can exert along its axis is 100N (Figure 108), therefore:

Data Sheet_12Lf-XXF-27_R.2.0

Load / 부하

Parameter	Limit Values / 한계값		Unit 단위	Remarks / 비고
	Rated/정격	Max/최대		
Load at 12.0V 부하 at 12.0V	12.0	24	N	12Lf-12F-27
	2.69	5.39	lbf	
	1.22	2.44	kgf	
	20.0	40	N	12Lf-20F-27
	4.49	8.98	lbf	
	2.04	4.08	kgf	
	35.0	70	N	12Lf-35F-27
	7.87	15.73	lbf	
	3.57	7.14	kgf	
	55.0	110	N	12Lf-55F-27
	12.37	24.72	lbf	
	5.61	11.22	kgf	
	100.0	200	N	12Lf-100F-27
	22.48	44.94	lbf	
	10.19	20.40	kgf	

* 1 kgf = 9.8N , 1lbf

Figure 108 Average motor force by models

Therefore, we can conclude that, for the critical design case, the dynamic Factor of Safety is:

$$\text{FS} = \frac{F_{Max}}{F_{Motor}} = \frac{100\ N}{17.85\ N} = 5.6$$

CHAPTER 6

EXPERIMENTS AND RESULTS

This chapter presents the results of the tests carried out with the objective of measuring the performance and GAR.

For this, the gripper was installed in a U-factory brand robotic arm called xArm-6, which has six active degrees of freedom to place the gripper in different positions and orientations. This robotic arm, in turn, is anchored to a motorized wheelchair that has been adapted to control the robotic arm and the gripper using only the joystick from the wheelchair. This joystick gives a great advantage when carrying out the tests since it will be possible to choose between moving the gripper, orienting it, and opening or closing it to grab objects, all with a single relatively easy-to-use control.

To verify that GAR works for all the objects proposed during its design, it was considered to classify them in 3 different workspaces.

This categorization is proposed to make the gripper grab objects from different orientations, depending on the object's position. For example, the green (Figure 109) workspace is close to the individual, so the gripper will need to hold or maneuver objects more safely and accurately than when lifting objects from the yellow space. On the other hand, For the yellow space, the preferred location will be with the z-axis perpendicular to the ground, and for the red space, the preferred orientation will be with the z-axis aligned forward.

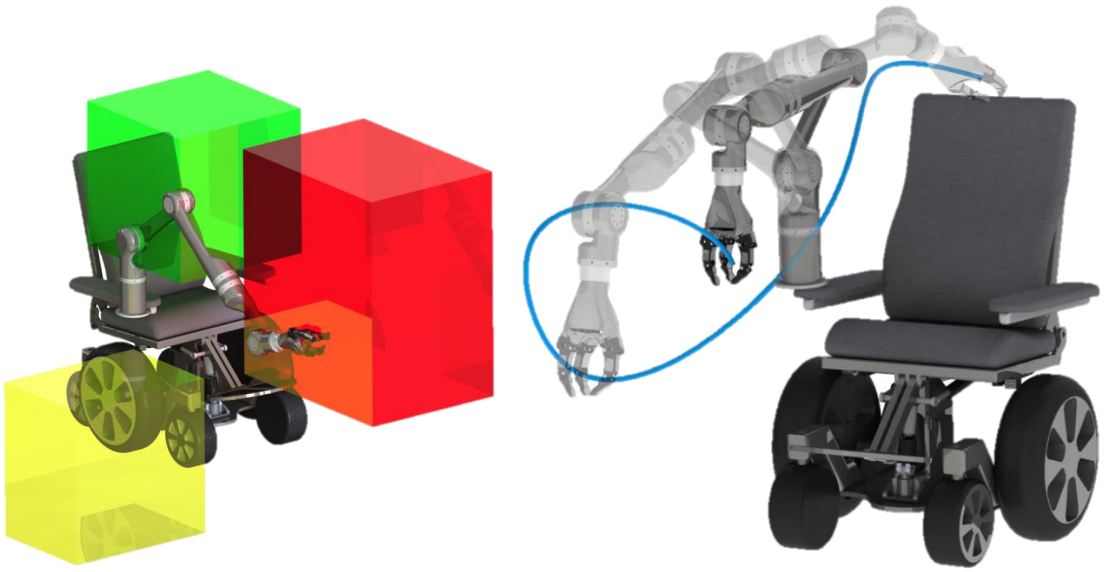

Figure 109 Tested workspace and robotic arm motions

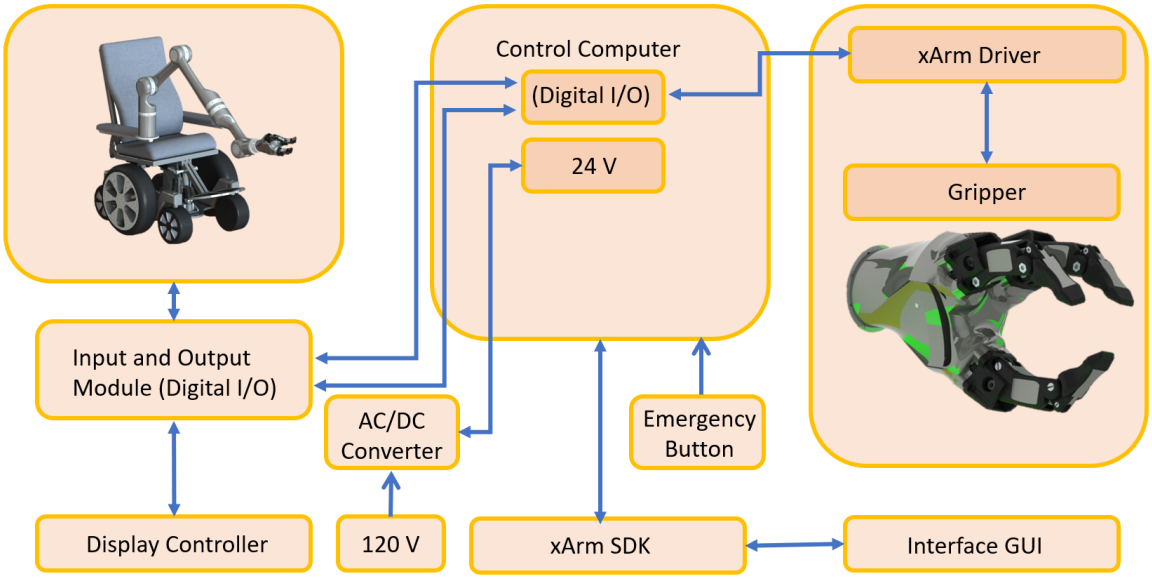

Figure 110 Wheelchair's control architecture

The components and linkages of the robotically assisted power wheelchair's control architecture are shown in Figure 110 [134]. The first section consists of the electric wheelchair and its electronics, which are managed by the R-net control system to regulate and share the wheelchair's variables. The Input–Output Module (IOM) obtains the joystick

values using R-net. It transmits logical values (0 or 1) through a D-Sub 9 Pin for each direction supplied by the chair's input device. The wheelchair may also accept logical values from an external computer. The robotic assistive arm is a device comprised of its drivers, motors, actuators, and sensors. A power cable receives control signals and transmits status information to an external computer. The user application layer allows developers to write codes for controlling and connecting new devices like GAR. This layer's applications are written in Python and use a Software Development Kit (SDK) that comes with the robotic assistance arm. It also transmits the control signals for the arm and power wheelchair and can also read the system's variables to perform the necessary control.

With the list of activities of daily life proposed in Table 2, the gripper is tested based on the three types of grip: Parallel Grip, Cylindrical Grip, and Spherical Grip.

Table 2 Minimum Task list for assistive robots

No.	Task
1	Picking/ Placing objects from Table, book, pen
2	Picking/ Placing objects from Ground, shoe
3	Picking/ Placing objects from Man reach, Upper shelf
4	Holding objects (up to 10 lbs)
5	Opening & closing drawers
6	Push-pull, Swing open-close doors
7	Holding cup near month
8	Gradual upward positioning of the cup during drinking
9	Holding spoon/fork
10	Maneuvering spoon/fork to take food from bowl to plate
11	Maneuvering spoon/fork to put food in mouth
12	Holding credit cards, Swipe credit cards at market, ATM booth
13	Putting pills/medicine in mouth
14	Holding medicine
15	Opening/ closing Refrigerator, oven Door
16	Opening/ closing lid of jar, box, paper box, cap of bottles
17	holding the phone near ear or put in speaker mode
18	Holding Pen, Maneuvering on paper or surfaces
19	Holding printed books, turning pages

Below are some images (Figure 111 – 119) of the gripper performing these tasks:

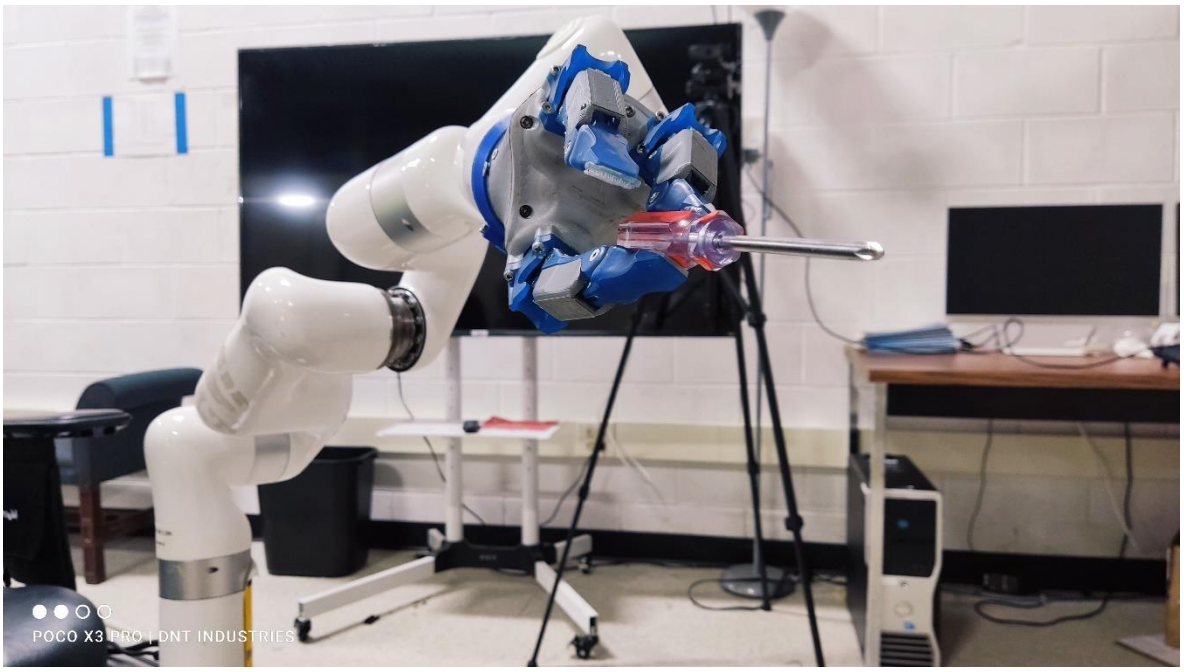

Figure 111 Gar holding a screwdriver in parallel grip mode

Figure 112 Gar lifting a shoe from the ground

GAR shows great maneuverability when grabbing objects from the ground or a table when performing a parallel grip, as shown in the images above (Figure 111 – 112).

Figure 113 Sequence: grabbing a glass from a table - orientation

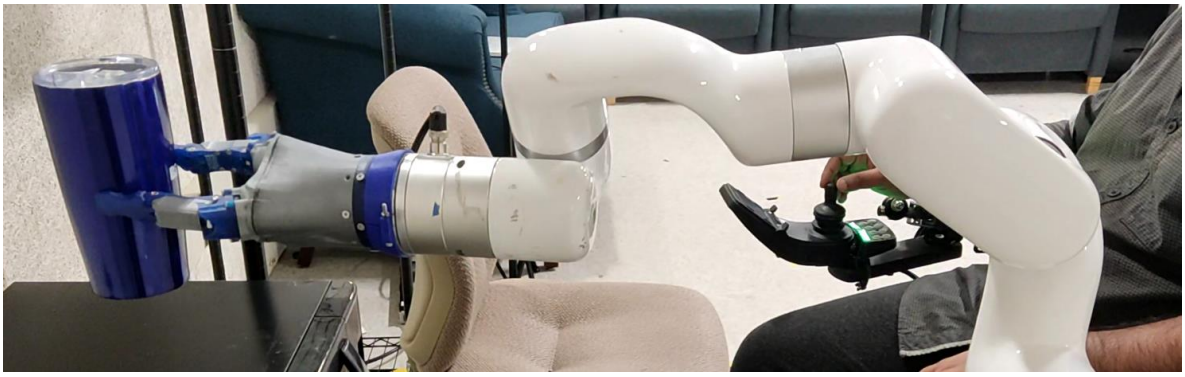

Figure 114 Sequence: grabbing a glass from a table - holding

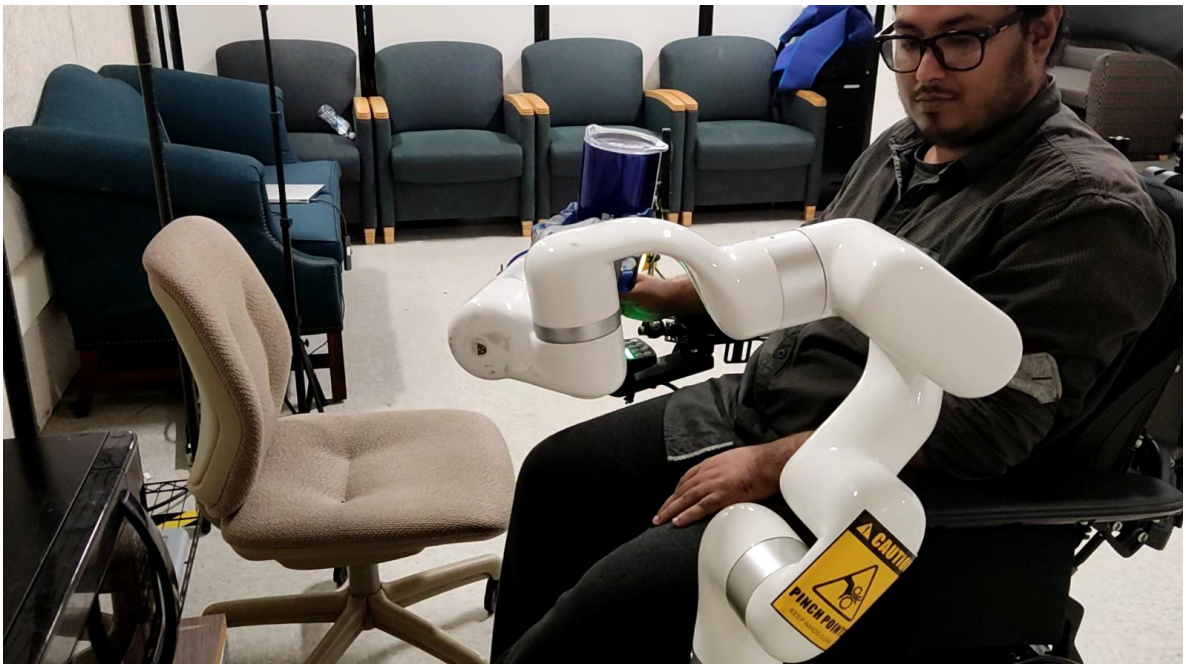

Figure 115 Sequence: grabbing a glass from a table - displacement

It can also perform tasks such as holding glasses using the cylindrical grip (Figure 113-115). This type of grip is the most used by GAR since most objects can be efficiently held with three fingers.

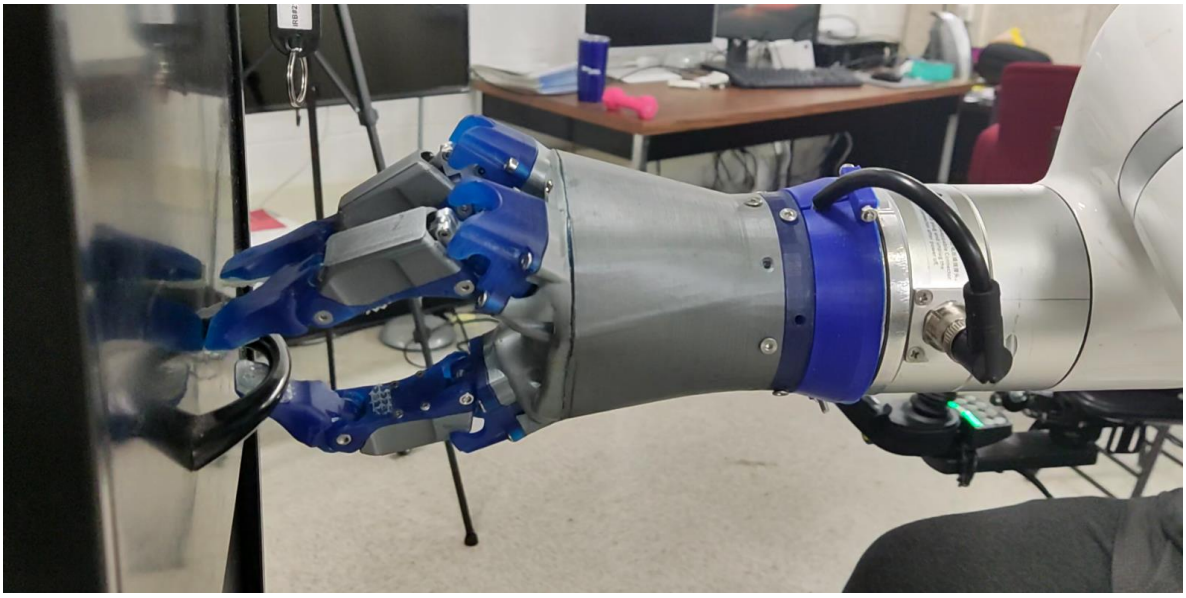

Figure 116 sequence: Opening a drawer - finger positioning

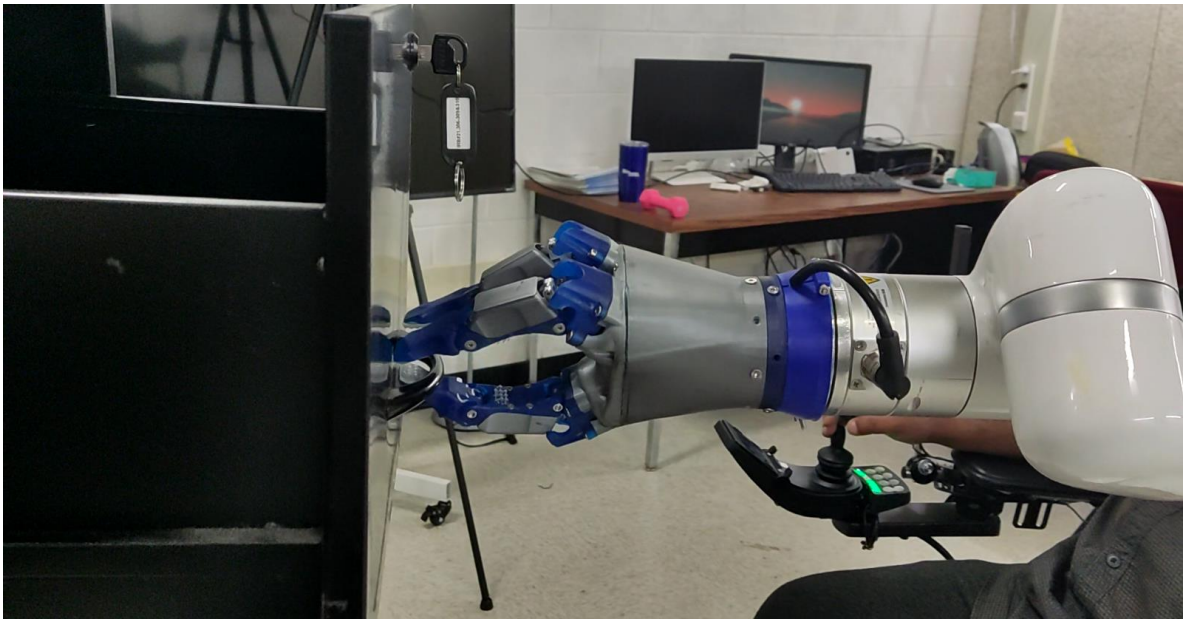

Figure 117 sequence: Opening a drawer – gripper displacement

Opening and closing drawers is a recurring activity among the ADLs list. Despite not being an easy task due to the large force that must be applied to open the drawer, GAR manages to complete this task satisfactorily (Figure 116 – 117).

Figure 118 Hook mode and cylindrical grip

During testing, it was discovered that the gripper could also be used as a grappling hook (Figure 118). Despite not being designed for that purpose, it works pretty well with particular objects and situations. For example, grabbing a 1-gallon bottle of milk by the handle or opening the microwave oven using only two fingers as hooks.

This grip mode is not included among the three official modes the gripper was designed for, but it is an interesting proposition to explore.

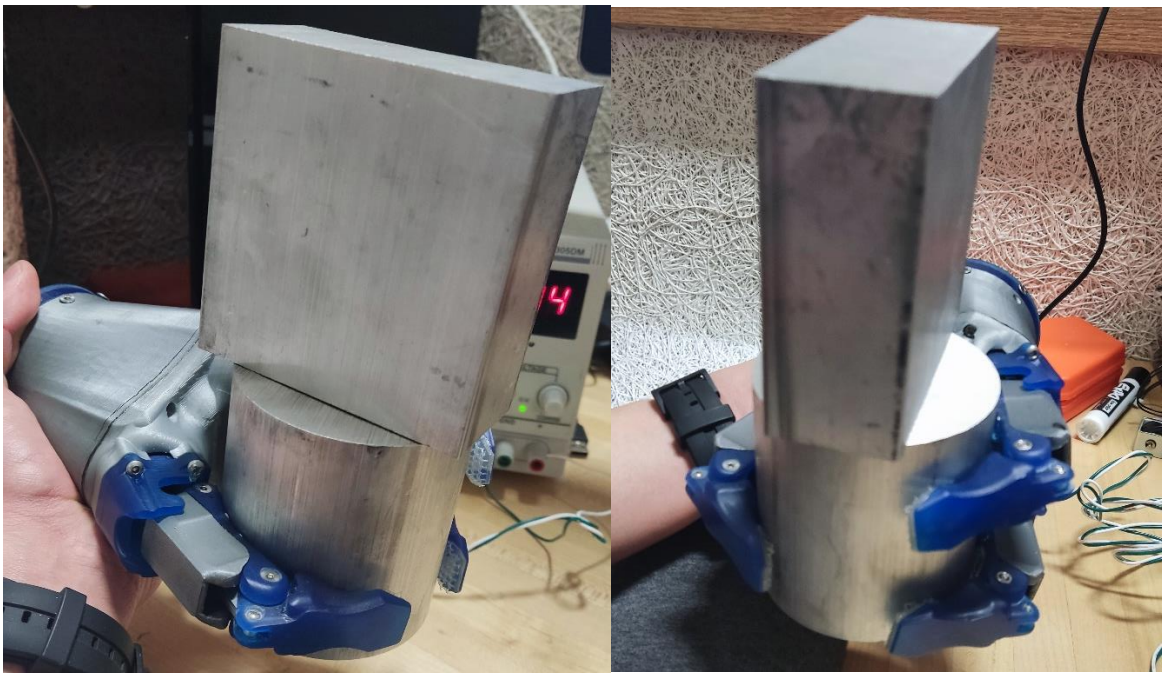

Figure 119 Gar holding approximately 5 kg of weight

Finally, solid metal blocks were used as test objects to check the motors' torque and the resistance of the mechanism.

The cylinder (Figure 119) has a radius of 50.08 mm and a height of 135.1 mm, weighing approximately 2542 grams. The rectangular aluminum block measures 127 mm x 127 mm x 50.08 mm with a weight of 2,177 grams, for a total of 4,719 grams.

Because the proposed robotic arm cannot support this weight, this test was done with the gripper disconnected from the robotic arm, as seen in Figure 119.

For all tests, a rating was made based on how stable the grip was for each object (Table 21). Some of the tests could not be taken or had a lower grade due to multiple factors such as:

Reason 1: Moving the gripper to the desired position and orientation can take time and effort. Since the inverse kinematics of the robotic arm only allows it to move back and forth and

perform some rotations to change the gripper's orientation, it is hard to orientate the gripper concerning the object. Despite not being a problem directly related to the gripper design and outside the scope of this investigation, it is a factor that affects the system's overall performance.

Reason 2: Some objects have a little surface area and require much force to move them. Because they have a little surface area, the gripper must apply a greater force to hold them without slipping. This is a particular case since it only occurred with the drawer handles, but it could be repeated with other objects not yet evaluated.

Reason 3: When an object's surface area is much bigger than its thickness. Holding credit cards on the table is the perfect example to explain this case; since it has almost no thickness, it is very difficult to grab them from that position. During the testing stage, several people inside the lab were asked to grab a credit card on the table, and they all unconsciously slid it to the edge of the table and then picked it up. Everyone was then asked to lift the card without bringing it to the edge, which was extremely difficult for everyone, even using their fingernails. This case provides two very important branches to study: the correct way to grasp very thin objects and what mechanisms could be used.

Reason 4: Since this gripper was designed to help people with reduced mobility, a single robotic arm with a single gripper could perform all the tasks on the list of activities of daily living. However, some situations cannot be solved with only one hand, even for people without reduced mobility. Opening a bottle of water or medication, for example, implies that the bottle is fixed and the cap rotates concerning the Z axis of the bottle (Figure 70). However,

since we cannot fix the bottle with our hands and our robotic arm cannot perform rotations only in joint 6, this test was not carried out, even though GAR can perfectly support the bottle caps.

Table 21 All objects used to experiment with GAR and their scores

No.	Task	Object	Score	Reason
1	Picking/ Placing objects from Table, book, pen	Book	9/10	-
		Pen	7/10	1
2	Picking/ Placing objects from Ground, shoe	Shoe	10/10	-
3	Picking/ Placing objects from Man reach, Upper shelf	Coat Hook	8/10	1
4	Holding objects (up to 10 lbs)	Aluminum Block	10/10	-
5	Opening & closing drawers	Drawers	7/10	2
6	Push-pull, Swing open-close doors	Doors	8/10	-
7	Holding cup near month	Cup	10/10	-
8	Gradual upward positioning of the cup during drinking	Cup	10/10	-
9	Holding spoon/fork	Spoon	7/10	1
10	Maneuvering spoon/fork to take food from bowl to plate	Spoon	7/10	1
11	Maneuvering spoon/fork to put food in mouth	Spoon	7/10	1
12	Holding credit cards, Swipe credit cards at market, ATM booth	Credit Card	5/10	3
13	Putting pills/medicine in mouth	Pills	10/10	-
14	Holding medicine	Pills Bottle	10/10	-
15	Opening/ closing Refrigerator, oven Door	Oven Door	7/10	1
16	Opening/ closing lid of jar, box, paper box, cap of bottles	Water Bottle	Unrealized	4 and 1
17	Holding the phone near ear or put in speaker mode	Phone	9/10	-
18	Holding Pen, Maneuvering on paper or surfaces	Pen/ Market	9/10	-
19	Holding printed books, turning pages	Holding Book	9/10	-
		Turning pages	Unrealized	3

Thanks to Table 21, we can highlight the performance of the GAR design, with 83.6% effectiveness for all the proposed activities. For the most part, the performance was affected by the low manipulability of the robotic arm used. However, in general, the results are very satisfactory and show a solid, compact, and replicable design based on a low manufacturing cost.

CHAPTER 7

CONCLUSIONS AND FUTURE WORKS

7.1 Conclusion

A robotic gripper with an underactuated mechanism, GAR (Gripper for Assistive Robots), based on how humans grasp objects, was developed to provide greater effectiveness when manipulating objects with an assistive robotic arm intended for people with reduced mobility. This thesis has produced GAR's modeling, mechanical and electrical design, components, development, and control.

The GAR kinematic model was developed based on a geometric approach and quasi-static modeling, while the dynamics were modeled from the mechanic's nodal theory. Also, the mechanism’s lengths and torques were calculated for the motor selection through simulations.

GAR is a robotic gripper that can adjust to various items of varying sizes and weights. In addition, this technology can successfully serve as a starting point for future research on grippers for assistive robots. The GAR design employs a new approach utilizing an underactuated mechanism to better adapt to unanticipated scenarios while preserving a lifting capacity of up to 5 kg. All while keeping the device's compactness and portability.

As GAR is still in the research phase, manufacturability via conventional machines was given the highest priority during its design. Therefore, daily life activities were utilized during the experiments to evaluate the design.

Those experimental results show that the GAR can effectively grab more than 80% of the objects humans grab during activities of daily living.

7.2 Recommendations & Future Scopes

GAR shows promise in providing a gripper capable of increasing assistive robots' effectiveness when performing daily tasks. However, the potential for this research could be reached to a new level through further development of the current version.

7.2.1 Improvements:

• Being a prototype version, this gripper was built with plastic materials through additive processes. However, most of these materials were replaced during the experiments multiple times, so manufacturing all the parts in aluminum or PEG by injection process would increase the durability of all the components.

• The experimental setup of GAR is currently based on a robotic arm controlled by an external computer. This robotic arm lacks many functionalities when it comes to controlling it. An upgrade to this robotic arm would considerably increase the results of these experiments. For example, moving some joints of the robot independently to orient the tool or to execute smoother movements and not just in straight lines would be a perfect upgrade.

• Even though the mechanism has limits programmed in the microcontroller, a force sensor is necessary to experiment with fragile objects. Holding a fragile object, such as an egg, is possible at the current state of research, but knowing how much force is being applied to the object is not possible now.

• Finally, anonymous data can be collected from GAR for machine learning to standardize grip patterns and required grip forces. This would help solve the problem of generating trajectories by creating a database on the orientation and the perfect force needed for different objects.

REFERENCES

[1] Jarque-Bou, N. J., Sancho-Bru, J. L., & Vergara, M. (2021). A Systematic Review of EMG Applications for the Characterization of Forearm and Hand Muscle Activity during Activities of Daily Living: Results, Challenges, and Open Issues. Sensors, 21(9), 3035. doi:10.3390/s21093035

[2] Gelder, B. L. van. (2012, 14 abril). Grip Strength Tools. Dynamic Principles. https://dynamicprinciples.wordpress.com/2012/04/05/grip-strength-tools/

[3] Samadikhoshkho, Z., Zareinia, K., & Janabi-Sharifi, F. (2019). A Brief Review on Robotic Grippers Classifications. 2019 IEEE Canadian Conference of Electrical and Computer Engineering (CCECE). doi:10.1109/ccece.2019.8861780

[4] Lundström, G. (1974). Industrial Robot Grippers. Industrial Robot: An International Journal, 1(2), 72–82. doi:10.1108/eb004449

[5] Tai, K., El-Sayed, A.-R., Shahriari, M., Biglarbegian, M., & Mahmud, S. (2016). State of the Art Robotic Grippers and Applications. Robotics, 5(2), 11. doi:10.3390/robotics5020011

[6] Langhorne P, Bernhardt J, Kwakkel G. Stroke rehabilitation. Lancet. 2011 May 14;377(9778):1693-702. doi: 10.1016/S0140-6736(11)60325-5. PMID: 21571152.

[7] Collen, F. M., & Wade, D. T. (1991). Residual mobility problems after stroke. International Disability Studies, 13(1), 12–15. doi:10.3109/03790799109166270

[8] Dodson, C. C., & Cordasco, F. A. (2008). Anterior Glenohumeral Joint Dislocations. Orthopedic Clinics of North America, 39(4), 507–518. doi:10.1016/j.ocl.2008.06.001

[9] Hersh, M. (2015). Overcoming Barriers and Increasing Independence – Service Robots for Elderly and Disabled People. International Journal of Advanced Robotic Systems, 12(8), 114. doi:10.5772/59230

[10] Alqasemi, R., Mahler, S., & Dubey, R. (2007). Design and Construction of a Robotic Gripper for Activities of Daily Living for People with Disabilities. 2007 IEEE 10th International Conference on Rehabilitation Robotics. doi:10.1109/icorr.2007.4428461

[11] Nguyen, P. H., Sridar, S., Amatya, S., Thalman, C. M., & Polygerinos, P. (2019). Fabric-Based Soft Grippers Capable of Selective Distributed Bending for Assistance of Daily Living Tasks. 2019 2nd IEEE International Conference on Soft Robotics (RoboSoft). doi:10.1109/robosoft.2019.8722758

[12] Taheri, O., Ghorbani, N., Black, M.J., Tzionas, D. (2020). GRAB: A Dataset of Whole-Body Human Grasping of Objects. In: Vedaldi, A., Bischof, H., Brox, T., Frahm, JM. (eds) Computer Vision – ECCV 2020. ECCV 2020. Lecture Notes in Computer Science(), vol 12349. Springer, Cham. https://doi.org/10.1007/978-3-030-58548-8_34

[13] Cini, F., Ortenzi, V., Corke, P., & Controzzi, M. (2019). On the choice of grasp type and location when handing over an object. Science Robotics, 4(27), eaau9757. doi:10.1126/scirobotics.aau9757

[14] Feix, T., Bullock, I. M., & Dollar, A. M. (2014). Analysis of Human Grasping Behavior: Object Characteristics and Grasp Type. IEEE Transactions on Haptics, 7(3), 311–323. doi:10.1109/toh.2014.2326871

[15] Prakash, J., & Ilangkumaran, M. (2019). An investigation of various actuation mechanisms in robot arm. Measurement and Control, 002029401986685. doi:10.1177/0020294019866854

[16] Song, Eun & Lee, Jung & Moon, Hyungpil & Choi, Hyouk & Koo, Ja. (2021). A Multi-Curvature, Variable Stiffness Soft Gripper for Enhanced Grasping Operations. Actuators. 10. 316. 10.3390/act10120316.

[17] Samadikhoshkho, Z., Zareinia, K., & Janabi-Sharifi, F. (2019). A Brief Review on Robotic Grippers Classifications. 2019 IEEE Canadian Conference of Electrical and Computer Engineering (CCECE). doi:10.1109/ccece.2019.8861780

[18] "8 Types of End of Arm Tooling Devices - Grippers | Keller Technology". Keller Technology Corporation. https://www.kellertechnology.com/blog/8-types-of-end-of-arm-tooling-devices-for-automation-projects/ (november 5 2022).

[19] Tai, K., El-Sayed, A.-R., Shahriari, M., Biglarbegian, M., & Mahmud, S. (2016). State of the Art Robotic Grippers and Applications. Robotics, 5(2), 11. doi:10.3390/robotics5020011

[20] Chen, F.Y. (1982), "Force analysis and design considerations of grippers", Industrial Robot, Vol. 9 No. 4, pp. 243-249. https://doi.org/10.1108/eb004533

[21] Ellwood, R.J., Raatz, A., Hesselbach, J. (2010). Vision and Force Sensing to Decrease Assembly Uncertainty. In: Ratchev, S. (eds) Precision Assembly Technologies and Systems. IPAS 2010. IFIP Advances in Information and Communication Technology, vol 315. Springer, Berlin, Heidelberg. https://doi.org/10.1007/978-3-642-11598-1_14

[22] Zhang, B., Xie, Y., Zhou, J., Wang, K., & Zhang, Z. (2020). State-of-the-art robotic grippers, grasping and control strategies, as well as their applications in agricultural robots: A review. Computers and Electronics in Agriculture, 177, 105694. doi:10.1016/j.compag.2020.105694

[23] Cagliani, A., Wierzbicki, R., Occhipinti, L., Petersen, D. H., Dyvelkov, K. N., Sardan Sukas, Ö., … Bøggild, P. (2010). Manipulation andin situtransmission electron microscope characterization of sub-100 nm nanostructures using a microfabricated nanogripper. Journal of Micromechanics and Microengineering, 20(3), 035009. doi:10.1088/0960-1317/20/3/035009

[24] Meng, Q., & Lee, M. H. (2006). Design issues for assistive robotics for the elderly. Advanced Engineering Informatics, 20(2), 171–186. doi:10.1016/j.aei.2005.10.003

[25] Munoz E, Sunny MSH, Rulik I, Sanjuan De Caro JD, Rahman MH. Kinematics and Workspace Analysis of xArm6 Robot for Activities of Daily Living. Proc Int Conf Ind Mech Eng Oper Manag. 2021;4(4):885-894. PMID: 35719427; PMCID: PMC9201617.

[26] Brose, S. W., Weber, D. J., Salatin, B. A., Grindle, G. G., Wang, H., Vazquez, J. J., & Cooper, R. A. (2010). The Role of Assistive Robotics in the Lives of Persons with Disability. American Journal of Physical Medicine & Rehabilitation, 89(6), 509–521. doi:10.1097/phm.0b013e3181cf569b

[27] PEÑA GONZÁLEZ, A. I.; GIL-AGUDO, A. M.; JARDÓN, A. H. Functional evaluation of asibot, a portable robot to aid disabled persons. En International Congress on Domotics, Robotics and Remote-Assistance for All, Madrid, Spain. 2007.

[28] DONG, Wenbo, et al. GA-based modified DH method calibration modelling for 6-DOFs serial robot. En 2016 31st Youth Academic Annual Conference of Chinese Association of Automation (YAC). IEEE, 2016. p. 225-230.

[29] Nejat, G., Yiyuan Sun, & Nies, M. (2008). Assistive Robots in Health Care Settings. Home Health Care Management & Practice, 21(3), 177–187. doi:10.1177/1084822308325695

[30] MANNAM, Pragna, et al. A Low-Cost Compliant Gripper Using Cooperative Mini-Delta Robots for Dexterous Manipulation. En Robotics: Science and Systems. 2021.

[31] Bélanger-Barrette, M. (s. f.). Which Robot Gripper is Easier to Integrate? Part 4 - Return on Investment. https://blog.robotiq.com/which-robot-gripper-is-easier-to-integrate-part-4-return-on investment

[32] BEZAK, Pavol; BOZEK, Pavol; NIKITIN, Yuri. Advanced robotic grasping system using deep learning. Procedia Engineering, 2014, vol. 96, p. 10-20.

[33] PELLERIN, Cheryl. The salisbury hand. Industrial Robot: An International Journal, 1991.

[34] Townsend, W. (2000). The BarrettHand grasper – programmably flexible part handling and assembly. Industrial Robot: An International Journal, 27(3), 181–188. doi:10.1108/01439910010371597

[35] Butterfass, J., Grebenstein, M., Liu, H., & Hirzinger, G. (n.d.). DLR-Hand II: next generation of a dextrous robot hand. Proceedings 2001 ICRA. IEEE International Conference on Robotics and Automation (Cat. No.01CH37164). doi:10.1109/robot.2001.932538

[36] Ruehl, S. W., Parlitz, C., Heppner, G., Hermann, A., Roennau, A., & Dillmann, R. (2014). Experimental evaluation of the schunk 5-Finger gripping hand for grasping tasks. 2014 IEEE International Conference on Robotics and Biomimetics (ROBIO 2014). doi:10.1109/robio.2014.7090710

[37] C.-H. Liu, F.-M. Chung, Y. Chen, C.-H. Chiu, and T.-L. Chen, "Optimal design of a motor-driven three-finger soft robotic gripper," IEEE/ASME Transactions on Mechatronics, vol. 25, no. 4, pp. 1830–1840, 2020.

[38] L. Birglen and T. Schlicht, "A statistical review of industrial robotic grippers," Robotics and Computer-Integrated Manufacturing, vol. 49, pp. 88–97, 2018. [Online]. Available: https://www.sciencedirect.com/science/article/pii/S0736584516304240

[39] B. Choi, H. R. Choi, and S. Kang, "Development of tactile sensor for detecting contact force and slip," in 2005 IEEE/RSJ International Conference on Intelligent Robots and Systems, 2005, pp. 2638–2643.

[40] G. Cannata and M. Maggiali, “An embedded tactile and force sensor for robotic manipulation and grasping,” in 5th IEEE-RAS International Conference on Humanoid Robots, 2005., 2005, pp. 80–85

[41] K. Nagaoka, H. Minote, K. Maruya, Y. Shirai, K. Yoshida, T. Hakamada, H. Sawada, and T. Kubota, “Passive spine gripper for free-climbing robot in extreme terrain,” IEEE Robotics and Automation Letters, vol. 3, no. 3, pp. 1765–1770, 2018.

[42] F. Chen, W. Xu, H. Zhang, Y. Wang, J. Cao, M. Y. Wang, H. Ren, J. Zhu, and Y. F. Zhang, “Topology optimized design, fabrication, and characterization of a soft cable-driven gripper,” IEEE Robotics and Automation Letters, vol. 3, no. 3, pp. 2463–2470, 2018.

[43] Y. Li, Y. Chen, Y. Yang, and Y. Li, “Soft robotic grippers based on particle transmission,” IEEE/ASME Transactions on Mechatronics, vol. 24, no. 3, pp. 969–978, 2019

[44] Z. Wang, Y. Torigoe, and S. Hirai, “A prestressed soft gripper: Design, modeling, fabrication, and tests for food handling,” IEEE Robotics and Automation Letters, vol. 2, no. 4, pp. 1909–1916, 2017.

[45] S. B. Backus and A. M. Dollar, “An adaptive three-fingered prismatic gripper with passive rotational joints,” IEEE Robotics and Automation Letters, vol. 1, no. 2, pp. 668–675, 2016.

[46] D. Yoon and Y. Choi, “Analysis of fingertip force vector for pinch-lifting gripper with robust adaptation to environments,” IEEE Transactions on Robotics, vol. 37, no. 4, pp. 1127–1143, 2021.

[47] Z. Zhakypov, F. Heremans, A. Billard, and J. Paik, “An origami-inspired reconfigurable suction gripper for picking objects with variable shape and size,” IEEE Robotics and Automation Letters, vol. 3, no. 4, pp. 2894–2901, 2018.

[48] N. Rojas, R. R. Ma, and A. M. Dollar, “The gr2 gripper: An underactuated hand for open-loop in-hand planar manipulation,” IEEE Transactions on Robotics, vol. 32, no. 3, pp. 763–770, 2016.

[49] B. Ward-Cherrier, N. Rojas, and N. F. Lepora, “Model-free precise in- hand manipulation with a 3d-printed tactile gripper,” IEEE Robotics and Automation Letters, vol. 2, no. 4, pp. 2056–2063, 2017.

[50] J. Hashizume, T. M. Huh, S. A. Suresh, and M. R. Cutkosky, “Capacitive sensing for a gripper with gecko-inspired adhesive film,” IEEE Robotics and Automation Letters, vol. 4, no. 2, pp. 677–683, 2019.

[51] N. Elangovan, L. Gerez, G. Gao, and M. Liarokapis, “Improving robotic manipulation without sacrificing grasping efficiency: A multi-modal, adaptive gripper with reconfigurable finger bases,” IEEE Access, vol. 9, pp. 83 298–83 308, 2021.

[52] E. Brown, N. Rodenberg, J. Amend, A. Mozeika, E. Steltz, M. R. Zakin, H. Lipson, and H. M. Jaeger, “Universal robotic gripper based on the jamming of granular material,” Proceedings of the National Academy of Sciences, vol. 107, no. 44, pp. 18 809–18 814, 2010.

[53] Y. Makiyama, Z. Wang, and S. Hirai, “A pneumatic needle gripper for handling shredded food products,” in 2020 IEEE International Conference on Real-time Computing and Robotics (RCAR). IEEE, 2020, pp. 183–187.

[54] B. Zhang, Y. Xie, J. Zhou, K. Wang, and Z. Zhang, “State-of-the- art robotic grippers, grasping and control strategies, as well as their applications in agricultural robots: A review,” Computers and Electronics in Agriculture, vol. 177, p. 105694, 2020.

[55] L. Birglen and T. Schlicht, “A statistical review of industrial robotic grippers,” Robotics and Computer-Integrated Manufacturing, vol. 49, pp. 88–97, 2018.

[56] J. Hughes, U. Culha, F. Giardina, F. Guenther, A. Rosendo, and F. Iida, “Soft manipulators and grippers: a review,” Frontiers in Robotics and AI, vol. 3, p. 69, 2016.

[57] J. Wang, D. Gao, and P. S. Lee, “Recent progress in artificial muscles for interactive soft robotics,” Advanced Materials, vol. 33, no. 19, p. 2003088, 2021.

[58] C. Laschi, B. Mazzolai, and M. Cianchetti, “Soft robotics: Technologies and systems pushing the boundaries of robot abilities,” Science robotics, vol. 1, no. 1, p. eaah3690, 2016.

[59] A. Bicchi and V. Kumar, “Robotic grasping and contact: A review,” in Proceedings 2000 ICRA. Millennium Conference. IEEE International Conference on Robotics and Automation. Symposia Proceedings (Cat. No. 00CH37065), vol. 1. IEEE, 2000, pp. 348–353.

[60] Z. Samadikhoshkho, K. Zareinia, and F. Janabi-Sharifi, “A brief review on robotic grippers classifications,” in 2019 IEEE Canadian Conference of Electrical and Computer Engineering (CCECE). IEEE, 2019, pp. 1–4.

[61] M. Mukhtar, “Design, modelling, and control of an ambidextrous robot arm,” Ph.D. dissertation, Brunel University London, 2020.

[62] C.-H. Liu, F.-M. Chung, and Y.-P. Ho, “Topology optimization for design of a 3d-printed constant-force compliant finger,” IEEE/ASME Transactions on Mechatronics, vol. 26, no. 4, pp. 1828–1836, 2021

[63] C.-C. Chen and C.-C. Lan, “An accurate force regulation mechanism for high-speed handling of fragile objects using pneumatic grippers,” IEEE Transactions on Automation Science and Engineering, vol. 15, no. 4, pp. 1600–1608, 2018.

[64] Q. Xu, “Design and development of a novel compliant gripper with integrated position and grasping/interaction force sensing,” IEEE Trans- actions on Automation Science and Engineering, vol. 14, no. 3, pp. 1415–1428, 2017.

[65] A. Suebsomran, “Development of robot gripper and force control,” in 2018 13th World Congress on Intelligent Control and Automation (WCICA), 2018, pp. 433–437.

[66] A. M. Zaki, O. A. Mahgoub, A. M. El-Shafei, and A. M. Soliman, “Design and implementation of efficient intelligent robotic gripper,” WTOS, vol. 9, no. 11, p. 1130–1142, nov 2010.

[67] T. Nishimura, M. Tennomi, Y. Suzuki, T. Tsuji, and T. Watanabe, “Lightweight, high-force gripper inspired by chuck clamping devices,” IEEE Robotics and Automation Letters, vol. 3, no. 3, pp. 1354–1361, 2018.

[68] K. Nie, W. Wan, and K. Harada, “A hand combining two simple grippers to pick up and arrange objects for assembly,” IEEE Robotics and Automation Letters, vol. 4, no. 2, pp. 958–965, 2019.

[69] R. Mahmoud, A. Ueno, and S. Tatsumi, “Dexterous mechanism design for an anthropomorphic artificial hand: Osaka city university hand i,” in 2010 10th IEEE-RAS International Conference on Humanoid Robots, 2010, pp. 180–185.

[70] P. Wattanasiri, P. Tangpornprasert, and C. Virulsri, “Design of multi- grip patterns prosthetic hand with single actuator,” IEEE Transactions on Neural Systems and Rehabilitation Engineering, vol. 26, no. 6, pp. 1188–1198, 2018.

[71] C. Wu, T. Song, Z. Wu, Q. Cao, F. Fei, D. Yang, B. Xu, and A. Song, “Development and evaluation of an adaptive multi-dof finger with mechanical-sensor integrated for prosthetic hand,” Micromachines, vol. 12, no. 1, p. 33, 2021.

[72] Q. Lu, A. B. Clark, M. Shen, and N. Rojas, “An origami-inspired variable friction surface for increasing the dexterity of robotic grippers,” IEEE Robotics and Automation Letters, vol. 5, no. 2, pp. 2538–2545, 2020.

[73] S. Marullo, S. Bartoccini, G. Salvietti, M. Z. Iqbal, and D. Prattichizzo, “The mag-gripper: A soft rigid gripper augmented with an electromagnet to precisely handle clothes,” IEEE Robotics and Automation Letters, vol. 5, no. 4, pp. 6591–6598, 2020.

[74] R. Datta, S. Pradhan, and B. Bhattacharya, “Analysis and design optimization of a robotic gripper using multiobjective genetic algorithm,” IEEE Transactions on Systems, Man, and Cybernetics: Systems, vol. 46, no. 1, pp. 16–26, 2016.

[75] M. Netzev, A. Angleraud, and R. Pieters, “Soft robotic gripper with compliant cell stacks for industrial part handling,” IEEE Robotics and Automation Letters, vol. 5, no. 4, pp. 6821–6828, 2020.

[76] K. Lee, Y. Wang, and C. Zheng, “Twister hand: Underactuated robotic gripper inspired by origami twisted tower,” IEEE Transactions on Robotics, vol. 36, no. 2, pp. 488–500, 2020.

[77] S. Donaire, J. Borr`as, G. Aleny`a, and C. Torras, “A versatile gripper for cloth manipulation,” IEEE Robotics and Automation Letters, vol. 5, no. 4, pp. 6520–6527, 2020.

[78] W. Xu, H. Zhang, H. Yuan, and B. Liang, “A compliant adaptive gripper and its intrinsic force sensing method,” IEEE Transactions on Robotics, vol. 37, no. 5, pp. 1584–1603, 2021.

[79] F. Chen, Y. Gao, W. Dong, and Z. Du, “Design and control of a passive compliant piezo-actuated micro-gripper with hybrid flexure hinges,” IEEE Transactions on Industrial Electronics, vol. 68, no. 11, pp. 11 168–11 177, 2021.

[80] Y. Liu, Y. Zhang, and Q. Xu, “Design and control of a novel com- pliant constant-force gripper based on buckled fixed-guided beams,” IEEE/ASME Transactions on Mechatronics, vol. 22, no. 1, pp. 476–486, 2017.

[81] L. Birglen and C. Gosselin, “On the force capability of underactuated fingers,” in 2003 IEEE International Conference on Robotics and Automation (Cat. No.03CH37422), vol. 1, 2003, pp. 1139–1145 vol.1.

[82] G. A. Fontanelli, G. Paduano, R. Caccavale, P. Arpenti, V. Lippiello, L. Villani, and B. Siciliano, “A reconfigurable gripper for robotic autonomous depalletizing in supermarket logistics,” IEEE Robotics and Automation Letters, vol. 5, no. 3, pp. 4612–4617, 2020.

[83] K. Telegenov, Y. Tlegenov, and A. Shintemirov, “An underactuated adaptive 3d printed robotic gripper,” in 2014 10th France-Japan/ 8th Europe-Asia Congress on Mecatronics (MECATRONICS2014- Tokyo), 2014, pp. 110–115.

[84] X.-L. Li, L.-C. Wu, and T.-Y. Lan, “A 3d-printed robot hand with three linkage-driven underactuated fingers,” vol. 15, no. 5, p. 593–602, oct 2018. [Online]. Available: https://doi.org/10.1007/s11633-018-1125-z

[85] . Tlegenov, K. Telegenov, and A. Shintemirov, “An open-source 3d printed underactuated robotic gripper,” in 2014 IEEE/ASME 10th International Conference on Mechatronic and Embedded Systems and Applications (MESA), 2014, pp. 1–6.

[86] K. Telegenov, Y. Tlegenov, and A. Shintemirov, “A low-cost open-source 3-d-printed three-finger gripper platform for research and educational purposes,” IEEE Access, vol. 3, pp. 638–647, 2015.

[87] L. Birglen and C. M. Gosselin, “Geometric Design of Three- Phalanx Underactuated Fingers,” Journal of Mechanical Design, vol. 128, no. 2, pp. 356–364, 04 2005. [Online]. Available: https://doi.org/10.1115/1.2159029

[88] L. Birglen and C. Gosselin, “Kinetostatic analysis of underactuated fingers,” IEEE Transactions on Robotics and Automation, vol. 20, no. 2, pp. 211–221, 2004.

[89] C. Melchiorri and G. Vassura, “Design of a three-finger gripper for intra-vehicular robotic manipulation,” IFAC Proceedings Volumes, vol. 31, no. 33, pp. 7–12, 1998, iFAC Workshop on Space Robotics (SPRO’98), St-Hubert, Canada, 19-22 October. [Online]. Available: https://www.sciencedirect.com/science/article/pii/S1474667017383799

[90] Y.-J. Kim, H. Song, and C.-Y. Maeng, “Blt gripper: An adaptive gripper with active transition capability between precise pinch and compliant grasp,” IEEE Robotics and Automation Letters, vol. 5, no. 4, pp. 5518– 5525, 2020.

[91] A. Firouzeh and J. Paik, “Grasp mode and compliance control of an underactuated origami gripper using adjustable stiffness joints,” IEEE/ASME Transactions on Mechatronics, vol. 22, no. 5, pp. 2165– 2173, 2017.

[92] T. Ko, “A tendon-driven robot gripper with passively switchable underac- tuated surface and its physics simulation based parameter optimization,” IEEE Robotics and Automation Letters, vol. 5, no. 4, pp. 5002–5009, 2020.

[93] I. Hussain, F. Renda, Z. Iqbal, M. Malvezzi, G. Salvietti, L. Seneviratne, D. Gan, and D. Prattichizzo, “Modeling and prototyping of an underactu- ated gripper exploiting joint compliance and modularity,” IEEE Robotics and Automation Letters, vol. 3, no. 4, pp. 2854–2861, 2018.

[94] W. chen Lee and C.-W. Wu, “Design and analysis of a novel robotic gripper integrated with a three-phalanx finger,” Proceedings of the Institution of Mechanical Engineers, Part C: Journal of Mechanical Engineering Science, vol. 228, no. 10, pp. 1786–1796, 2014. [Online]. Available: https://doi.org/10.1177/0954406213511422

[95] Y. Su, Z. Fang, W. Zhu, X. Sun, Y. Zhu, H. Wang, K. Tang, H. Huang, S. Liu, and Z. Wang, “A high payload proprioceptive hybrid robotic gripper with soft origamic actuators,” IEEE Robotics and Automation Letters, vol. 5, no. 2, pp. 3003–3010, 2020.

[96] S. Ku, J. Myeong, H.-Y. Kim, and Y.-L. Park, “Delicate fabric han- dling using a soft robotic gripper with embedded microneedles,” IEEE Robotics and Automation Letters, vol. 5, no. 3, pp. 4852–4858, 2020.

[97] X. Li, X. Li, L. Li, Y. Meng, and Y. Tian, “Load sharing design of a multi-legged adaptable gripper with gecko-inspired controllable adhesion,” IEEE Robotics and Automation Letters, vol. 6, no. 4, pp. 8482–8489, 2021.

[98] Q. Hu, E. Dong, and D. Sun, “Soft gripper design based on the integration of flat dry adhesive, soft actuator, and microspine,” IEEE Transactions on Robotics, vol. 37, no. 4, pp. 1065–1080, 2021.

[99] Y. Li, Y. Chen, and Y. Li, “Pre-charged pneumatic soft gripper with closed-loop control,” IEEE Robotics and Automation Letters, vol. 4, no. 2, pp. 1402–1408, 2019.

[100] A. Pagoli, F. Chapelle, J. A. Corrales, Y. Mezouar, and Y. Lapusta, “A soft robotic gripper with an active palm and reconfigurable fingers for fully dexterous in-hand manipulation *,” IEEE Robotics and Automation Letters, vol. 6, no. 4, pp. 7706–7713, 2021.

[101] W. Park, S. Seo, and J. Bae, “A hybrid gripper with soft material and rigid structures,” IEEE Robotics and Automation Letters, vol. 4, no. 1, pp. 65–72, 2019.

[102] G. Gao, C.-M. Chang, L. Gerez, and M. Liarokapis, “A pneumatically driven, disposable, soft robotic gripper equipped with multi-stage, re- tractable, telescopic fingers,” IEEE Transactions on Medical Robotics and Bionics, vol. 3, no. 3, pp. 573–582, 2021.

[103] S. Liu, F. Wang, Z. Liu, W. Zhang, Y. Tian, and D. Zhang, “A two-finger soft-robotic gripper with enveloping and pinching grasping modes,” IEEE/ASME Transactions on Mechatronics, vol. 26, no.1, pp. 146–155, 2021.

[104] P. Glick, S. A. Suresh, D. Ruffatto, M. Cutkosky, M. T. Tolley, and A. Parness, “A soft robotic gripper with gecko-inspired adhesive,” IEEE Robotics and Automation Letters, vol. 3, no. 2, pp. 903–910, 2018.

[105] S. Nie, X. Liu, H. Ji, Z. Ma, and F. Yin, “Simulation and experiment study on deformation characteristics of the water hydraulic flexible actuator used for the underwater gripper,” IEEE Access, vol. 8, pp. 191 447–191 459, 2020.

[106] G. Hwang, J. Park, D. S. D. Cortes, K. Hyeon, and K.-U. Kyung, “Electroadhesion-based high-payload soft gripper with mechanically strengthened structure,” IEEE Transactions on Industrial Electronics, vol. 69, no. 1, pp. 642–651, 2022.

[107] J. M. Krahn, F. Fabbro, and C. Menon, “A soft-touch gripper for grasping delicate objects,” IEEE/ASME Transactions on Mechatronics, vol. 22, no. 3, pp. 1276–1286, 2017.

[108] L. Li, T. Jin, Y. Tian, F. Yang, and F. Xi, “Design and analysis of a square-shaped continuum robot with better grasping ability,” IEEE Access, vol. 7, pp. 57 151–57 162, 2019.

[109] S. Kim, C. Laschi, and B. Trimmer, “Soft robotics: a bioinspired evolution in robotics,” Trends in biotechnology, vol. 31, no. 5, pp. 287– 294, 2013.

[110] Z. Hu, W. Wan, and K. Harada, “Designing a mechanical tool for robots with two-finger parallel grippers,” IEEE Robotics and Automation Letters, vol. 4, no. 3, pp. 2981–2988, 2019.

[111] K. Tai, A.-R. El-Sayed, M. Shahriari, M. Biglarbegian, and S. Mahmud, “State of the art robotic grippers and applications,” Robotics, vol. 5, no. 2, 2016. [Online]. Available: https://www.mdpi.com/2218-6581/5/2/11

[112] E. Brown, N. Rodenberg, J. Amend, A. Mozeika, E. Steltz, M. R. Zakin, H. Lipson, and H. M. Jaeger, “Universal robotic gripper based on the jamming of granular material,” Proceedings of the National Academy of Sciences, vol. 107, no. 44, pp. 18 809–18 814, 2010. [Online]. Available: https://www.pnas.org/content/107/44/18809

[113] K.-C. Chan and N. Cheung, “Grasping of delicate objects by a novel two-finger variable reluctance gripper,” in Conference Record of the 2001 IEEE Industry Applications Conference. 36th IAS Annual Meeting (Cat. No.01CH37248), vol. 3, 2001, pp. 1969–1974 vol.3.

[114] L. Kuang, Y. Lou, and S. Song, “Design and fabrication of a novel force sensor for robot grippers,” IEEE Sensors Journal, vol. 18, no. 4, pp. 1410–1418, 2018.

[115] M.-J. Salami, N. Mir-Nassiri, and S. Sidek, “Design of intelligent multifinger gripper for a robotic arm using a dsp-based fuzzy controller,” in 2000 TENCON Proceedings. Intelligent Systems and Technologies for the New Millennium (Cat. No.00CH37119), vol. 3, 2000, pp. 348–353 vol.3

[116] R. Kolluru, K. Valavanis, S. Smith, and N. Tsourveloudis, “Design fundamentals of a reconfigurable robotic gripper system,” IEEE Transac- tions on Systems, Man, and Cybernetics - Part A: Systems and Humans, vol. 30, no. 2, pp. 181–187, 2000.

[117] M. Barsky, D. Lindner, and R. Claus, “Robot gripper control system using pvdf piezoelectric sensors,” IEEE Transactions on Ultrasonics, Ferroelectrics, and Frequency Control, vol. 36, no. 1, pp. 129–134, 1989.

[118] M. Honarpardaz, M. Tarkian, J. ̈Olvander, and X. Feng, “Finger design automation for industrial robot grippers: A review,” Robotics and Autonomous Systems, vol. 87, pp. 104–119, 2017. [Online]. Available: https://www.sciencedirect.com/science/article/pii/S0921889015303171

[119] Hashizume, J., Huh, T. M., Suresh, S., & Cutkosky, M. (2019). Capacitive Sensing for a Gripper with Gecko-Inspired Adhesive Film. IEEE Robotics and Automation Letters, 1–1. doi:10.1109/lra.2019.2893154

[120] Ceccarelli, M., Rodriguez, N. E. N., & Carbone, G. (2005). Design and tests of a three finger hand with 1-DOF articulated fingers. Robotica, 24(02), 183. doi:10.1017/s0263574705002018

[121] Seo, N. J., & Armstrong, T. J. (2008). Investigation of Grip Force, Normal Force, Contact Area, Hand Size, and Handle Size for Cylindrical Handles. Human Factors: The Journal of the Human Factors and Ergonomics Society, 50(5), 734–744. doi:10.1518/001872008x354192

[122] Budynas, R. (2020). Mechanical Engineering Design (11.ª ed.). New York: Mc Graw Hill Education. New York: Mc Graw Hill Education.

[123] Cicala, G., Latteri, A., Del Curto, B., Lo Russo, A., Recca, G., & Farè, S. (2017). Engineering Thermoplastics for Additive Manufacturing: A Critical Perspective with Experimental Evidence to Support Functional Applications. Journal of Applied Biomaterials & Functional Materials, 15(1), 10–18. doi:10.5301/jabfm.5000343

[124] Montambault, S., & Gosselin, C. M. (2001). Analysis of Underactuated Mechanical Grippers. Journal of Mechanical Design, 123(3), 367. doi:10.1115/1.1374198

[125] Serje-Martínez, D. A., & Pacheco-Bolívar, J. A. (2017). Cinemática paralela en la máquina-herramienta: Investigación, desarrollo y tendencias futuras. Dyna, 84(201), 17-26.

[126] P. I. Corke, "A Simple and Systematic Approach to Assigning Denavit–Hartenberg Parameters," in IEEE Transactions on Robotics, vol. 23, no. 3, pp. 590-594, June 2007, doi: 10.1109/TRO.2007.896765.

[127] Azad, F. A., Yazdi, M. R. H., & Masouleh, M. T. (2019). Kinematic and dynamic analysis of 3-dof delta parallel robot based on the screw theory and principle of virtual work. In 2019 5th Conference on Knowledge Based Engineering and Innovation (KBEI) (pp. 717-724). IEEE.

[128] Birglen, L., & Gosselin, C. M. (2004). Kinetostatic analysis of underactuated fingers. IEEE Transactions on Robotics and Automation, 20(2), 211-221.

[129] Emcgee, | (2015) 5) coefficient of friction and tumbling, Mathematics of Cheerleading. Available at: https://mathematicsofcheerleading.wordpress.com/2015/03/12/5-coefficient-of-friction-and-tumbling/ (Accessed: December 6, 2022).

[130] Shigley, J. E., Uicker, J. J., Pérez, J. H., & de Contín, H. C. (1983). Teoría de máquinas y mecanismos (No. TJ145. S54 1983.). México;: McGraw-Hill.

[131] Khalil, W. (2010, June). Dynamic modeling of robots using recursive newton-euler techniques. In ICINCO2010.

[132] Abo-Shanab, R. F. (2020). Dynamic modeling of parallel manipulators based on Lagrange–D'Alembert formulation and Jacobian/Hessian matrices. Multibody System Dynamics, 48(4), 403-426.

[133] K. Telegenov, Y. Tlegenov and A. Shintemirov, "A Low-Cost Open-Source 3-D-Printed Three-Finger Gripper Platform for Research and Educational Purposes," in IEEE Access, vol. 3, pp. 638-647, 2015, doi: 10.1109/ACCESS.2015.2433937.

[134] Sunny, Md. Samiul & Islam, Ishrak & Rulik, Ivan & Sanjuan, Javier & Rahman, Mohammad & Ahamed, Sheikh & Wang, Inga & Schultz, Katie & Brahmi, Brahim. (2021). Eye-gaze control of a wheelchair mounted 6DOF assistive robot for activities of daily living. Journal of NeuroEngineering and Rehabilitation. 18. 10.1186/s12984-021-00969-2.

[135] V.M. Parker, D. T. Wade and R. L. Hewer, "Loss of arm function after stroke: measurement, frequency, and recovery," Int Rehabil Med, vol. 8, no. 2, p. 69-73, 1986.

[136] Long, Z., Jiang, Q., Shuai, T., Wen, F., & Liang, C. (2020). A Systematic Review and Meta-analysis of Robotic Gripper. IOP Conference Series: Materials Science and Engineering, 782, 042055. doi:10.1088/1757-899x/782/4/042055

[137] Ramesh Kolluru, Kimon Valavanis, Stanfird Smith and Nikos Tsourveloudis, "Design and analysis of a reconfigurable robotic gripper for limp material handling." Proceedings of the 2000 IEEE International Conference on Robotics and Automation (ICRA 2000), pp. 1988-1993, San Francisco, CA, April 2000.

[138] GertWillem Romer, Harry Stuyt, Gijs Kramer, Malicum O'Callaghan and Jeroen Scheffe, "Alternative grippers for the assistive robotic manipulator (ARM)," Proceedings of the gth IEEE International Conference on Rehabilitation Robotics(ICORR 2005), pp. 473-476, Chicago, IL, June 2005.

[139] Robotic Arm Grippers – Cosimtech Robotics & System Control. (s. f.). https://www.cosimtech.com/robotic-arm-grippers/

[140] Kinova Gen3 lite. (s. f.). Clearpath Robotics. https://store.clearpathrobotics.com/products/gen3-lite

[141] Zhu, M., Wang, Z., Hirai, S., & Kawamura, S. (2017). Design and fabrication of a soft-bodied gripper with integrated curvature sensors. 2017 24th International Conference on Mechatronics and Machine Vision in Practice (M2VIP). doi:10.1109/m2vip.2017.8211521

[142] G. R. B. E. Römer, H. J. A. Stuyt, G. Peters and K. van Woerden, The current and future processes for obtaining a “Manus” (ARM) rehabrobot within the Netherlands, Proceedings of the 8th ICORR2003, Daejon, Korea, 2003, pp.9-12

[143] H.H. Kwee, et al. “First experimentation of the Spartacus Telethesis in a Clinical Environment.” Paraplegia 21:275, 1983.

[144] M. T. Mason and J. K. Salisbury, Robot Hands and the mechanics of Manipulation, MIT Press, Massachusetts, USA, 1985.

[145] I. Kato and K. Sadamoto. Mechanical Hands Illustrated (Revised Edition). Hemisphere Publishing Corp, NYC, 1987 (originally published in 1982).

[146] T. Laliberté, L. Birgleny and C. M. Gosseliny, Underactuation in robotic grasping hands, Machine Intelligence & Robotic Control, 4(3), pp.1–11, 2002.

[147] Disability Impacts All of Us Infographic | CDC. Updated 2022/10/28/. https://www.cdc.gov/ncbddd/disabilityandhealth/infographic-disability-impacts-all.html

[148] Disability Statistics Center UOC. Mobility Device Statistics: United States. Updated 02 October, 2022. https://www.disabled-world.com/disability/statistics/mobility-stats.php

[149] Travel Patterns of American Adults with Disabilities | Bureau of Transportation Statistics. Updated 2022/01/03. https://www.bts.gov/travel-patterns-with-disabilities

[150] Allen S, Resnik L, Roy J. Promoting independence for wheelchair users: The role of home accommodations. The Gerontologist. 2006;46(1):115-123.

[151] Spring Calculator - The Spring Store. (s. f.). https://www.thespringstore.com/spring-calculator.html

Data Sheet_12Lf-XXF-27_R.2.0

Load / 부하

Parameter	Limit Values / 한계값		Unit 단위	Remarks / 비고
	Rated/정격	Max/최대		
Load at 12.0V 부하 at 12.0V	12.0	24	N	12Lf-12F-27
	2.69	5.39	lbf	
	1.22	2.44	kgf	
	20.0	40	N	12Lf-20F-27
	4.49	8.98	lbf	
	2.04	4.08	kgf	
	35.0	70	N	12Lf-35F-27
	7.87	15.73	lbf	
	3.57	7.14	kgf	
	55.0	110	N	12Lf-55F-27
	12.37	24.72	lbf	
	5.61	11.22	kgf	
	100.0	200	N	12Lf-100F-27
	22.48	44.94	lbf	
	10.19	20.40	kgf	

* 1 kgf = 9.8N , 1lbf = 4.45N

Caution/주의

※ It is highly recommended to apply rated load under 50% duty cycle. When max applicable load (2times the rated load) is applied, goal current setting should be 1600 and duty cycle should be less than 20%. See Figure2-2 below.

※ 가급적 정격 부하 조건에서 사용하되, 최대 허용 부하 (정격부하의 2배) 적용시에는 Goal current설정을 1600(1.6A)으로, Duty cycle을 20% 이하로 낮추어야 합니다. 하단의 Figure2-2 그래프를 참고하십시오.

Self Lock Feature / 셀프-락 기능

		-	N/A(불가)	-	N	12Lf-12F-27
		-		-	N	12Lf-20F-27
		-	Available (가능)	-	N	12Lf-35F-27
		-		-	N	12Lf-55F-27
		-		-	N	12Lf-100F-27

- Self-lock feature :The feature which actuator maintains its position by mechanical friction without motor power.
- 셀프-락 기능 :액츄에이터가 전원을 통한 모터의 힘 없이, 기구마찰력만으로 위치를 고수할 수 있는 기능

Appendix A-2

Figure 1.

Figure1-1 . Voltage /Speed[m/s] – Goal current 1.6A설정 시 기준

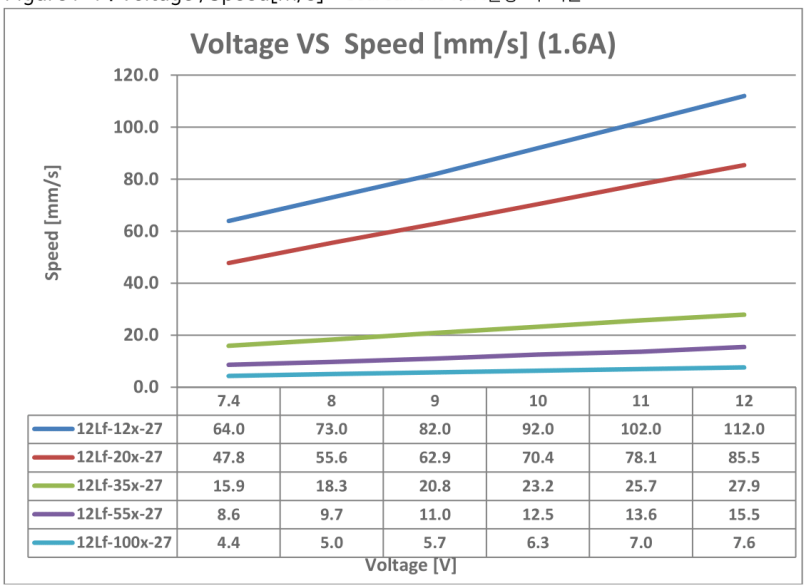

	7.4	8	9	10	11	12
12Lf-12x-27	64.0	73.0	82.0	92.0	102.0	112.0
12Lf-20x-27	47.8	55.6	62.9	70.4	78.1	85.5
12Lf-35x-27	15.9	18.3	20.8	23.2	25.7	27.9
12Lf-55x-27	8.6	9.7	11.0	12.5	13.6	15.5
12Lf-100x-27	4.4	5.0	5.7	6.3	7.0	7.6

※ Data includes tolerance. / 해당 Data는 오차를 포함하고 있습니다.

Figure1-2 . Voltage /Stall Force[N] – Goal current 1.6A설정 시 기준

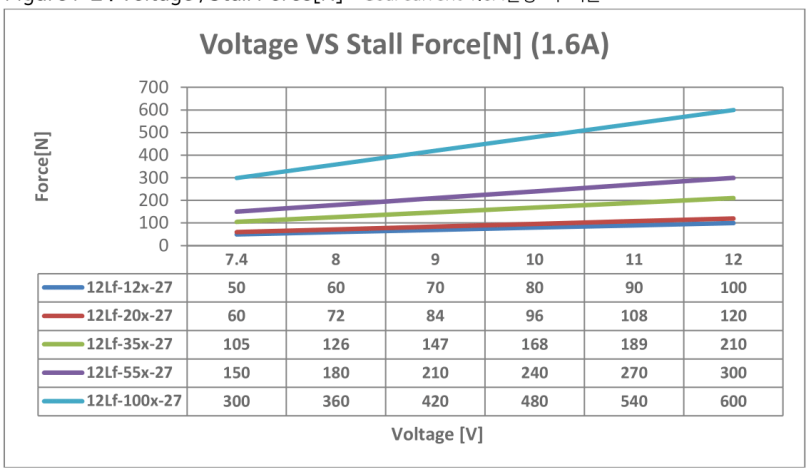

	7.4	8	9	10	11	12
12Lf-12x-27	50	60	70	80	90	100
12Lf-20x-27	60	72	84	96	108	120
12Lf-35x-27	105	126	147	168	189	210
12Lf-55x-27	150	180	210	240	270	300
12Lf-100x-27	300	360	420	480	540	600

※ Data includes tolerance. / 해당 Data는 오차를 포함하고 있습니다.

CAUTION (주의)

- Stall force는 참고용으로, 제품의 파손을 방지하기 위해 실제 application에서의 사용시에는 가급적 정격부하에 맞추어 사용하여 주십시오.
- Stall force is for reference only. In order to prevent damage of the product, please use it according to the Rated load when using in actual application.

Appendix B

MP1584

3A, 1.5MHz, 28V Step-Down Converter

The Future of Analog IC Technology

DESCRIPTION

The MP1584 is a high frequency step-down switching regulator with an integrated internal high-side high voltage power MOSFET. It provides 3A output with current mode control for fast loop response and easy compensation.

The wide 4.5V to 28V input range accommodates a variety of step-down applications, including those in an automotive input environment. A 100μA operational quiescent current allows use in battery-powered applications.

High power conversion efficiency over a wide load range is achieved by scaling down the switching frequency at light load condition to reduce the switching and gate driving losses.

The frequency foldback helps prevent inductor current runaway during startup and thermal shutdown provides reliable, fault tolerant operation.

By switching at 1.5MHz, the MP1584 is able to prevent EMI (Electromagnetic Interference) noise problems, such as those found in AM radio and ADSL applications.

The MP1584 is available in a thermally enhanced SOIC8E package.

FEATURES

- Wide 4.5V to 28V Operating Input Range
- Programmable Switching Frequency from 100kHz to 1.5MHz
- High-Efficiency Pulse Skipping Mode for Light Load
- Ceramic Capacitor Stable
- Internal Soft-Start
- Internally Set Current Limit without a Current Sensing Resistor
- Available in SOIC8E Package.

APPLICATIONS

- High Voltage Power Conversion
- Automotive Systems
- Industrial Power Systems
- Distributed Power Systems
- Battery Powered Systems

TYPICAL APPLICATION

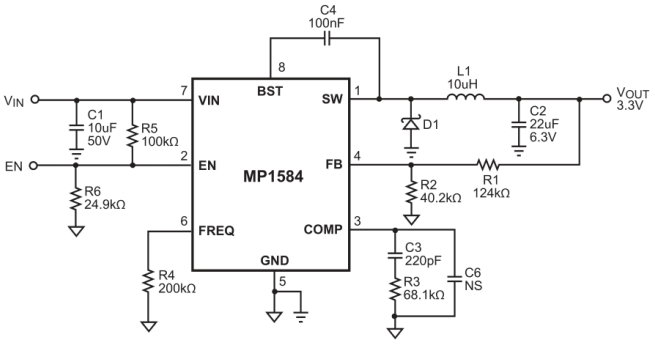

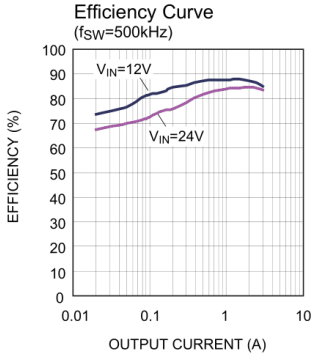

Appendix C

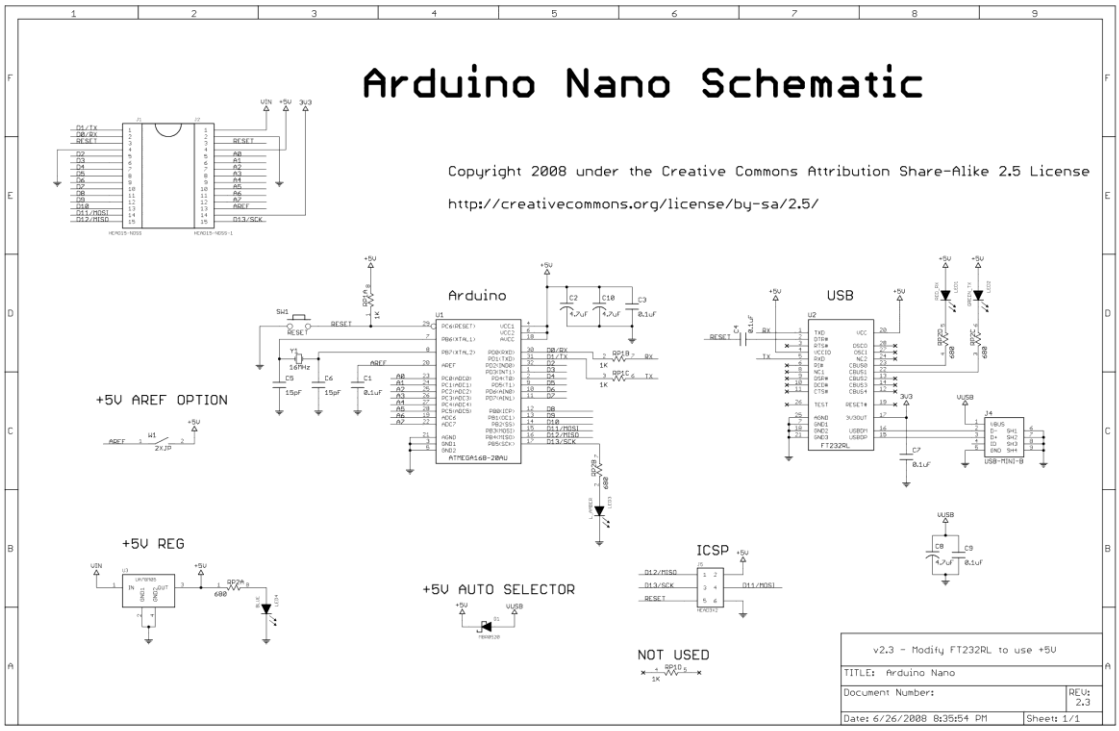
Arduino Nano Schematic
Copyright 2008 under the Creative Commons Attribution Share-Alike 2.5 License
http://creativecommons.org/license/by-sa/2.5/
Arduino
USB
+5V AREF OPTION
+5V REG
+5V AUTO SELECTOR
ICSP
NOT USED
ATMEGA168-20MU
FT232RL
v2.3 - Modify FT232RL to use +5V
TITLE: Arduino Nano
Document Number:
REV: 2.3
Date: 6/26/2008 8:35:54 PM
Sheet: 1/1

Appendix D

Arduino Nano Pin Layout

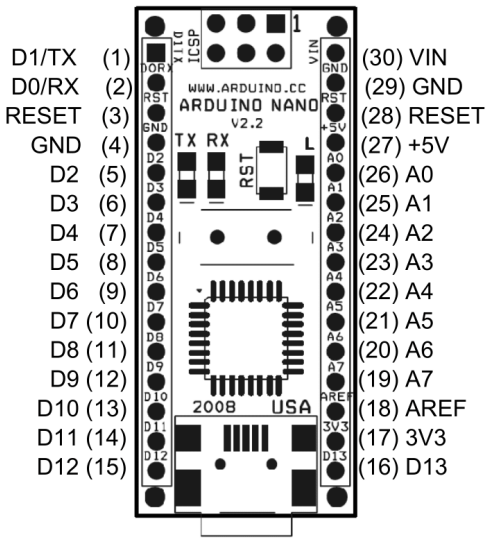

Pin No.	Name	Type	Description
1-2, 5-16	D0-D13	I/O	Digital input/output port 0 to 13
3, 28	RESET	Input	Reset (active low)
4, 29	GND	PWR	Supply ground
17	3V3	Output	+3.3V output (from FTDI)
18	AREF	Input	ADC reference
19-26	A7-A0	Input	Analog input channel 0 to 7
27	+5V	Output or Input	+5V output (from on-board regulator) or +5V (input from external power supply)
30	VIN	PWR	Supply voltage

Appendix E

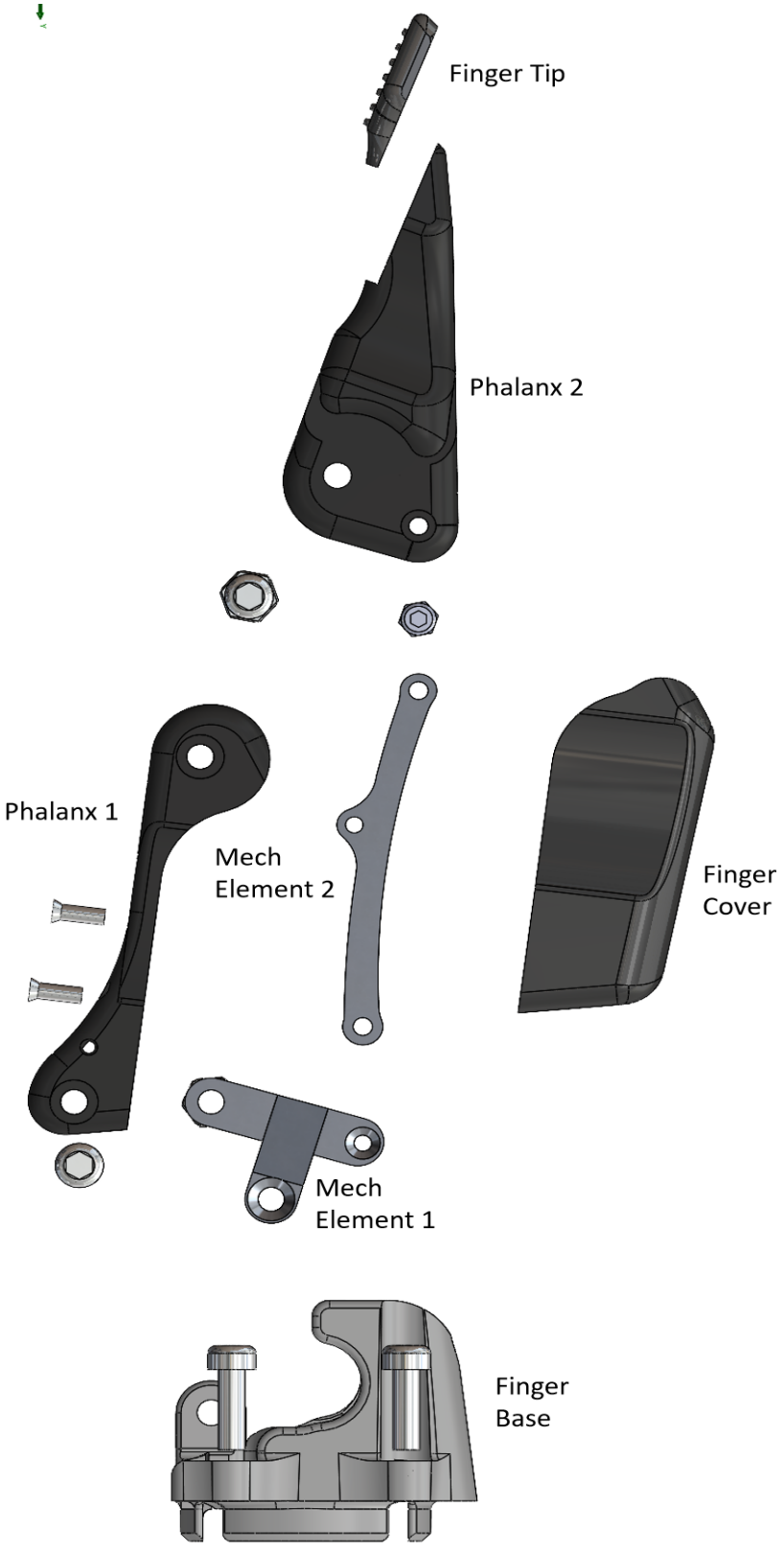
Finger Tip
Phalanx 2
Phalanx 1
Mech
Element 2
Finger
Cover
Mech
Element 1
Finger
Base

Appendix E

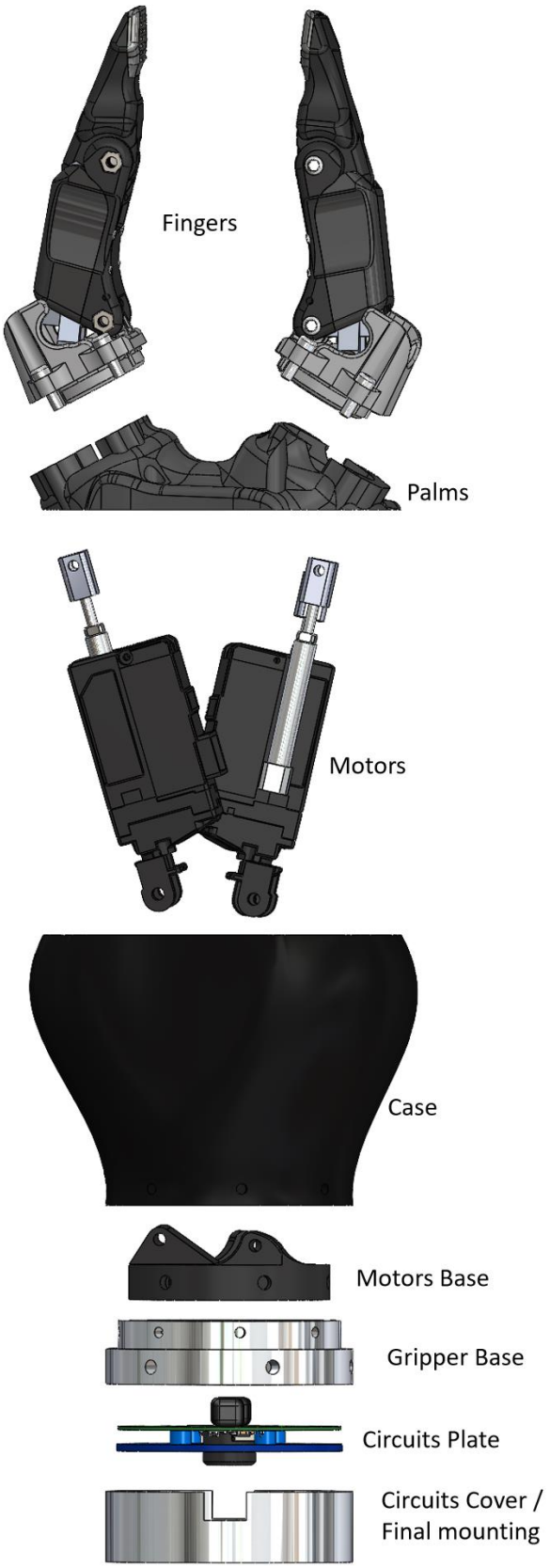
Fingers
Palms
Motors
Case
Motors Base
Gripper Base
Circuits Plate
Circuits Cover /
Final mounting